University of Southampton

FACULTY OF ENGINEERING AND APPLIED SCIENCE
INSTITUTE OF SOUND AND VIBRATION RESEARCH

ROBUST OPTIMAL DESIGN USING PASSIVE AND ACTIVE METHODS OF VIBRATION CONTROL

David Keith Anthony

A thesis submitted for the degree of
Doctor of Philosophy

February 2000

UNIVERSITY OF SOUTHAMPTON

ABSTRACT

FACULTY OF ENGINEERING AND APPLIED SCIENCE
INSTITUTE OF SOUND AND VIBRATION RESEARCH

Doctor of Philosophy

ROBUST OPTIMAL DESIGN USING PASSIVE AND ACTIVE METHODS OF VIBRATION CONTROL

by David Keith Anthony

This thesis is concerned with the design of a lightweight cantilever structure to optimise the vibrational energy transmitted from the base to the end. The methods by which this is achieved are: i) the use of geometric redesign of the structure (passive optimisation), ii) the application of Active Vibration Control (AVC) techniques (active optimisation), iii) combinations of both passive and active methods. However, even though the nominal performance of a structure may be optimal, the sensitivity of the structure to small geometric perturbations (e.g., those representing manufacturing tolerances) also needs to be considered. For some optimal structures their performance deteriorates rapidly in the face of such perturbations, and a better solution may be a structure with a slightly worse performance but that is robust to such perturbations.

Optimised structures were designed using the methods outlined above. For passively optimised structures, good reductions in vibration transmission were achieved using both classical optimisation methods and genetic algorithms (GA). The structures attained using the classical methods were not at all robust, to the extent that the nominal performance would not be realised in practice. Using GA, in general, it was found that the wider the frequency band over which the average performance was assessed, the more robust the structures produced. For active control, optimal actuator positions were sought to achieve the best reductions attainable using feedforward control. The control effort associated with an AVC system also needs to be considered when selecting an optimal solution, and as with the performance, the robustness in the face of geometric perturbations needs to be assessed. The choice of the parameter representing the vibration was also investigated and it was found that the choice of parameter can affect the success in reducing the physical vibration. Optimised structures were also produced using both passive and active methods, and the robustness of their performance and control effort evaluated. It was seen that the application of AVC with a geometrically optimised structure is more effective and more efficient than with the unoptimised structure.

Finally, optimisation was considered so as to produce structures with performance which are both optimal and robust to geometric perturbations. Different methods were used and it was found that increases in robustness can be obtained whilst maintaining similar levels of nominal performance, and with only a doubling of the required computational expense.

LIST OF CONTENTS

LIST OF TABLES

LIST OF FIGURES

ACKNOWLEDGEMENTS

The author would like to thank the following for their contributions to the research work detailed in this thesis:

Professor Steve Elliott, my supervisor, for the advice, support and time given to me throughout the duration of my Ph.D. studies.

Professor Andy Keane, effectively my second supervisor, especially for his advice on optimisation related issues and for his support with the optimisation software used.

Prasanth Nair for his help and discussions, especially relating to the FEA modelling.

Professor Tim Sluckin of the Maths Department for some technical advice on mathematical questions relating to Appendix A.

The author acknowledges support in the form of a studentship from the Faculty of Engineering and Applied Science at the University of Southampton, and also from the Institute of Sound and Vibration Research.

CHAPTER 1

Introduction

1.0 INTRODUCTION TO THE PROBLEM OF VIBRATION ON AEROSPACE STRUCTURES

Unwanted vibration in a structure can have many undesirable effects. It can cause damage to the structure itself or components to which it is connected. It may prevent the structure being used for its intended application if the vibration occurs in critical regions. The example motivating the study here is that typical within the aerospace industry: to control the vibration, originating from the main body of a satellite, at the far end of a boom arm where typically antennae are mounted. Some structures (especially those employed in space) often have inherently small amounts of damping and the transmission of vibration through the structure can be an important issue. The need is even greater in lightweight structures as the controlling inertial effects of the mass are reduced.

Traditional techniques to reduce vibration are to increase the mass and damping of the structure. The former is normally in violation with design goals, and the latter is the most regularly applied passive technique, but this can also increase the mass. It is desirable to consider the dynamic behaviour of the structure during its design and it may be possible to the optimise the inherent performance alleviating the need for any additional vibration control measures. A more recent development has been the application of Active Vibration Control systems that act to produce counter vibrations in order to reduce vibration. This may be employed together with traditional techniques, but since there is an interaction between both methods the successful application is often not a straightforward procedure. Alternatively, where applicable and practical, vibration transmission can be reduced by dynamically isolating the structure, again using the aforementioned techniques.

Previous work by Keane (1995b) has considered the optimisation of the geometry of a lightweight two-dimensional structure comprised of 40 rigidly joined beams to minimise vibration transmission. The positions of the joints were used as the optimisation variables. The design was optimised in order to produce a structure that inherently had a much greater degree of vibration isolation than the original, traditional, regular design (achieving an improvement of three orders of magnitude). The study presented in this thesis uses an identical structure model to that used by Keane.

Although the optimised designs show better performance in theory, practical design implementations with exactly the required parameters may not be feasible, due to manufacturing tolerances, for example. Even if this was not the case, the parameters might change during service due to, for example, thermal expansion and contraction. If the effect of these changes on the optimised performance is not studied then a design candidate that is predicted to be the best (under *nominal* operating conditions) in service may yield less than optimum performance. Another candidate design, although having a slightly lower optimised performance under nominal operating conditions may be less sensitive (more *robust*) to changing operating conditions, and is thus would be a more practical choice.

In aerospace structures the unwanted vibration originates from both acoustic and vibration sources. Testing on the grounds of both form key constituent parts of a spacecraft programme. Typical bandwidths are 30Hz to 10kHz for acoustic and 20Hz to 2kHz for vibration (Forgrave *et al*, 1999). Often testing for both types of excitation is necessary as the structural response is different. For vibration excitation the structure tends to acts as a high pass filter. This effect is reported and experimentally demonstrated by Bondaryk (1997). Only structural excitation is considered here.

1.1 BACKGROUND TO WORK PRESENTED IN THESIS

A brief background of several areas addressed in the thesis is presented here. The intention is to give a general overview and not report an exhaustive survey. Where such surveys exist, to the author's knowledge, these are included.

1.1.1 METHODS OF MODELLING VIBRATIONS IN STRUCTURES

The systematic analysis of vibrations is normally first accredited to Rayleigh (1894). The mathematical description of beams undergoing transverse or flexural vibration was achieved by Euler and Bernoulli, (as detailed in Bishop & Johnson, 1960, for example), although this beam model is sufficient for most cases an improved model was reported by Timoshenko (see for example, Timoshenko, 1995).

A composite structure comprising of beams can be modelled as a system in a number of ways. The three main approaches used are: Dynamic Stiffness method (Langley, 1990), Finite Element Analysis (Zienkiewicz, 1965) and more recently Statistical Energy Analysis (Lyon, 1975).

The dynamic stiffness methods model a composite structure using a dynamic stiffness matrix that describes all the degrees of freedom of the system. It uses a governing equation for each of

the elements, and thus its application is limited to structures where the components can be represented by simple beam or plate models. For complex structures whose components cannot be represented by such models, the structure may be divided into small elements (small in relation to the smallest wavelength considered) each of which is represented by a model, which depends on the element size and model order. Finite element analysis can solve the system by equating motion and forces at the interfaces between all adjoining elements. For large models or for high frequency analysis the number of elements required grows rapidly and is normally limited either by computing storage capacity or solution time.

However, as with all deterministic modelling methods, as the frequency region of interest becomes higher the response is complicated by the high modal density of the structure. The response at each frequency is strongly dependent upon many modes (whereas at lower frequencies the response at any one frequency is dominated by, at most, a few modes). Due to the sensitivity of the relative phase of the modal responses and the exact modal frequencies, the overall response becomes uncertain and sensitive to the smallest changes in the structure or its parameters. Statistical energy analysis is a probabilistic analysis method in which the structure is divided into subsystems, each of which is described by its gross properties. The properties of the connections between contiguous sub-systems, since the phase and the magnitude are relatively unpredictable, are treated as random. The parameter that is used to describe the system behaviour is the total time-averaged energy of the vibrations. Thus the 'power flow' between the subsystems, the power inputs and the external forces are used to describe the structure's response. Examples of statistical energy analysis used for beam structures are given by Shankar and Keane (1997).

Receptance analysis is closely related to the dynamic stiffness method, it was reported by Bishop and Johnson (1960). The receptance of composite systems may be determined from the receptances of individual components. This was used to form the Greens functions that were used as the basis of energy flows in a network of beams by Shankar and Keane (1995). The method is computationally more costly than for using the dynamic stiffness method for the same structure. The composite receptance matrix is of larger dimension than the dynamic stiffness matrix as the solution defines all degrees of freedom for all structural components separately. This leads to a longer solution time. One advantage is therefore that intermediate information within the structure is readily available. A major advantage with this method is that it is based on a modal solution of each element, and their modeshapes, if not readily represented by a theoretical model, can be determined experimentally or from finite element analysis. Farag and Pan (1997) also use a similar receptance method, additionally considering torsion of

beams. They state that their model 'fills the gap' between finite element analysis and statistical energy analysis, where each method has its own limitations.

1.1.2 ACTIVE CONTROL OF VIBRATION

Active Vibration Control (AVC) techniques use secondary control forces applied to the structure by a controller which uses sensory information to reduce some measure of the structural vibration caused by the originating primary vibration source. There has been a wealth of research in this area over the last three decades, made possible by advances in digital signal processing. The work has been extensively investigated and reported by Fuller *et al* (1996) and Hansen and Snyder (1997). Generally, two types of control strategy are used; feedforward and feedback. The former is the simpler control algorithm, but requires a coherent measure of the primary vibration source in the form of a reference signal. This is often available in practice, particularly for deterministic disturbances where, for example, a tachometer can provide a reference signal for rotating machinery. Figure 1.1 shows the basic scheme of a feedforward AVC system. The adaptive controller uses the reference signal and error output to continuously adjust the secondary control forces to minimise the output error. The parameter used as the output error signal is commonly an acceleration measurement but some other parameters are discussed below. The reference signal provides a measure of the primary force input, and for correct operation should not be affected the secondary force outputs. Feedback control does not require such a reference signal, but there are limitations on the performance due to causality and stability constraints. Feedback control is particularly used to control individual modes in the low frequency region, whereas feedforward control can operate on a frequency-by-frequency basis. Therefore it can be applied at frequencies where higher modal densities exist. However, von Flotow (1988) discusses the limit that is imposed as the modal density increases: the plant model will be inaccurate due to the uncertainty of such a modal based model. Another alternative, for example, is to use a travelling wave based model. Initially only feedback control was considered for broad band frequency control, however recently this has also been shown to be achievable using a feedforward strategy (Vipperman *et al* 1993). There are also practical causality constraints for feedforward AVC systems, which become increasingly more stringent with increasing frequency for flexural waves as discussed by Elliott and Billet (1993).

It is noted incidentally that genetic algorithms (which are discussed below) have also been employed in AVC control algorithms to determine the response of the controller, for simple broad band control of beam (Hossain *et al*, 1995), and also to adapt a parametric controller for active control of sound (Tang *et al*, 1996).

The success of such techniques depends on many factors including: the positioning of the sensors and actuators on the structure, the parameter which is controlled and the types of sensors and actuators used to measure each parameter. The latter is outside the scope of this thesis. The effect of the choice of parameter minimised by the control system is discussed below, and the effect of actuator position is discussed in the next sub-section.

1.1.2.1 IMPORTANCE OF THE CHOICE OF VIBRATION PARAMETER MINIMISED

The success of an AVC system depends, in part, on the particular parameter used to represent the vibration which is minimised by the controller. The most suitable parameter is sometimes compromised on practical grounds, it is easier to control a readily measurable quantity such as velocity, acceleration or force. Originally this parameter simply represented the magnitude of the vibration in the region of one or a number of strategic points, however from early on the use of a representation of energy flow (or power) was seen as a more effective practice. In general structures are lightly damped and therefore the mechanical impedance is strongly dependent upon the vibration frequency and also the positions of the sensors and actuators on a structure. Therefore, a single measurement of velocity or force is not a sufficient representation of power. Earlier use of power (Redman-White *et al*, 1987) demonstrated the advantage of using a power measurement, despite the added complexity of such systems. Howard and Hansen (1997) show that if either the force or the acceleration are minimised as a cost function for active vibration isolation, this does not necessarily lead to the minimisation of the other. Pan and Hansen (1993) demonstrate that the use of acceleration as a measurement to reduce power flow along a beam is sufficient if the sensor is placed outside the near field of any power sources. Power is used as the cost function parameter for vibration isolation by Bardou *et al* (1997), who compares different types of strategy used (to minimise power supplied by the primary source or maximise power absorbed by the secondary sources). Brennan *et al* (1995) also show that the best power measurement strategy can depend upon the nature of the problem.

1.1.2 STRUCTURAL OPTIMISATION FOR DYNAMIC PERFORMANCE

There has been much research into the areas of structural optimisation, chiefly based in the aerospace industry where lightweight lightly damped structures are abundant. Initially much of the early work evolved around the static correction of space structure, which is still a continued line of research, for example Furuya and Haftka (1995).

In terms of structural dynamic optimisation, much work has been reported by Keane. The advent of structural optimisation by passive techniques has tended to evolve later than the application of active vibration control, as the passive techniques often rely on the application of

recently developed non-classical optimisation techniques. Earlier work reported a simple structural filter between two coupled rods which was optimised using classical and the more recent evolutionary techniques (Keane, 1993). This was then extended to a two-dimensional structure similar to those employed on satellites (Keane, 1994 and 1995b), culminating in a passive design achieving values of vibration isolation comparable to that achievable using active techniques. The success was borne out experimentally (Keane and Bright, 1995), and extended to a three-dimensional structure (Keane and Brown, 1996). Another method of passive structural optimisation is to add masses to the joints of the structure, as studied by Bondaryk (1997).

The position of the sensors and actuators within the fields of both Active Control of Sound (Nelson and Elliott, 1992) and AVC is identified as being a key element to the success of such techniques; it is still the subject of much research. This area normally presents highly combinatorial, multi-modal (and often discrete) optimisation problems. Even if classical optimisation techniques can be used they need to be combined with other elements to ensure that more *global* than *local* solutions result. Benzaria and Martin (1994) used gradient method combined with a random sampling of the search space, and also noted that the problem is highly sensitive to the data. A recent survey by Padula and Kincaid (1999) summarises much of the history in this area, including its use for aerospace applications. Evolutionary algorithms are now often used for such optimisation problems. The most commonly applied techniques are genetic algorithms (Goldberg, 1989) or simulated annealing (Kirkpatrick *et al*, 1983). These techniques find very good, but not necessarily the *optimum* solutions.

In the application of lightweight structures, Chen *et al* (1991) used simulated annealing to find the optimum positions of actuators on 54 and 150 beam structures, whilst additionally the position of a number of beam dampers were simultaneously optimised. Furuya and Haftka (1996) use genetic algorithms to find optimal actuator positions for 8 actuators on a 1507 beam structure. Simpson and Hansen (1996) use a simple model of an aircraft interior, and determine optimum actuator positions using genetic algorithms, De Fonseca and Van Brussel (1999) perform a comparative study of different optimisation techniques on a similar sensor and actuator positioning problem in an aircraft trim panel. Both the latter two references had the objective of minimising the sound radiated. De Fonseca and Van Brussel found that some classical optimisation algorithms with random-based elements can sometimes perform better than genetic algorithms. In general, variations of the genetic algorithm parameters undergo trials in order to improve the convergence of the search. Furuya and Haftka (1993) use different non-binary representation of actuator positions, and later (Furuya and Haftka, 1996) used an initial population of relatively fit chromosomes together with a modified mutation

operator based on simulated annealing. However, improvement of the algorithms is likely to be problem specific. It is also important to ensure that the control energy required by the control system is realistic, this can be achieved by optimising the control system parameters as well as the actuator positions, as reported by Onoda and Haftka (1987) and Kim *et al* (1997), for example. Zimmerman (1993) showed that the consideration of the actuator mass is important, and this can result in different optimal actuator positions on lightweight structures to those if the actuators are considered mass-less.

Optimisation of both geometry or topology and actuator positioning has been reported. Liu *et al* (1997) used simulated annealing, and Liu *et al* (1998) and Furuya (1995) used both simulated annealing and genetic algorithm optimisation, in order to simultaneously optimise structure topology and the actuator positions. Here the beam cross-sections are variable and the structure geometry fixed. The work reported by Keane, above, differs in that the structure geometry is allowed to undergo changes with beams of fixed cross-section. Zhu *et al* (1999) uses sequential quadratic programming optimisation to simultaneously optimise the structure and the controller. Both parallel and serial strategies are used, and the former is found to yield better and more efficient solutions.

1.1.3 CONSIDERATION OF ROBUSTNESS TO PARAMETRIC UNCERTAINTY

Consideration of the robustness of optimal designs to structural changes began in the aerospace industry with that for the static shape correction. Adelman and Haftka (1986) provide a review of the deterministic methods used to address static and transient behaviour. More recently, and for the robust optimisation of the dynamic performance of structures, Rao *et al* (1990) considered robustness as part of a multi-objective optimisation for simple structures, and the effects of such structures to thermal distortion has been reported by, for example, Haftka and Adelman (1985) and by Farmer *et al* (1992). Hahn and Ferri (1997) evaluated the radiation and scattering properties for a structural-acoustic problem using variations in values of material properties to study the effect on the performance. Omoto and Elliott (1996) studied the effect on a feedforward Active Control of Sound system by using a set of measurements achieved from system perturbations. Furuya (1995) used the average response gained from the random perturbation of beam length in a optimum AVC actuator placement problem.

Prediction of the response of structures by using probabilistic variations on system parameters has been reported by Keane and Manohar (1993) and Manohar and Adhikar (1998). Alternatively, computer experiments can by used to measure the robustness of a system. Orthogonal arrays were used as a more efficient technique in place of Monte Carlo based parameter adjustment for evaluating the trajectory of a satellite on re-entry (Lautenschlager *et*

al, 1995) and for the optimisation of design parameters for a satellite (Erikstad *et al*, 1995). Finally, Nair *et al* (1998) report an efficient method of calculating the first-order response of a system subject to parametric perturbations.

1.2 SCOPE AND CONTRIBUTION OF THESIS

The study of the sensitivity of the performance of a structure to parametric uncertainty (robustness) is often a highly combinatorial task, and must be performed in addition to the existing computational burden of optimisation. A study of structural optimisation using both passive and active methods has been undertaken. This has been possible using the multi-processor high performance computational facilities available within the Computational Engineering and Design Centre (CEDC) at the University of Southampton. (As an indication of the computational expense required, if all the optimisation work and robustness analysis results presented in this thesis, had been run on a single processor with the hardware platforms detailed, it would have required over 1.3 years of continuous computing effort.) The robustness of the performance was investigated, with the aim of achieving optimal structure designs whose performance can be realised in practice. Specifically the scope is defined:

i) To optimise a typical aerospace structure using passive and active methods, and using both methods simultaneously, and to compare the performance and consequences of using each method.

ii) To study the robustness of optimal structures, and provide a measure of expected performance in practice.

iii) To use measures of robustness to design for structures with optimal and robust performance.

The contribution of this thesis has been: in the analysis of both passively optimised and optimally actively controlled structures; to show that considering the robustness of the optimal performance of structures is important in understanding the practical consequences of their application; that the use of classical optimisation techniques can be counter-productive in achieving robust solutions; and that it is possible to consider robustness during optimisation to produce structures with optimal and improved robustness, and without substantial increases in the computational expense required.

As well as being reported in this thesis, some of the work has also been accepted for publication in a refereed journal. For passive optimisation and robustness analysis of the structure, see (Anthony *et al*, 2000); for the application of active control with optimally placed

actuators and robustness analysis, see (Anthony and Elliott, 2000a); for the study of the success of using different parametric representations of vibration, see (Anthony and Elliott, 2000b). (Further submissions are planned reporting the results and robustness analysis of the structural optimisation using both passive optimisation and active control, an analysis of the mechanisms by which the reductions have been achieved by the optimisation and the role played by active control, and also the design of optimal and robust structures.)

1.3 OVERVIEW OF THESIS

The subsequent chapters of this thesis are structured as follows:

CHAPTER 2: The truss structure studied throughout this thesis is described, and details of the receptance theory model used to predict the vibration transmission are given. The application of Active Vibration Control techniques to the structure is described and four different cost function parameters are derived.

CHAPTER 3: The background and supporting theory to the all the optimisation methods used (both classical and evolutionary) are introduced, using supporting appendices. The adaptation of genetic algorithm optimisation to incorporate a measure of parametric variation robustness is explained. An alternative method of measuring the robustness of a system is that using computer experiments with system parameter variations governed by orthogonal arrays. The properties of such arrays are explained, and an example array is derived to demonstrate the design procedure.

CHAPTER 4: The vibration transmission of the structure studied is *passively* optimised using both classical and evolutionary algorithm methods, by allowing only the structure geometry to vary. This is performed at a single frequency, and for the average over a narrow and a broad frequency band. The robustness of all the optimal designs produced is evaluated.

CHAPTER 5: The average vibration transmission of the structure is reduced to the optimum value achievable by applying Active Vibration Control (*active* optimisation) with optimum actuator positions for one, two and three actuators, for the broad band frequency range. The use of three other cost function parameters representing vibration is assessed to determine the consequences of their use on the success of applying AVC. The robustness of the system performance and the control effort required is evaluated for the best ten actuator positions in each case.

CHAPTER 6: The average vibration transmission of the structure is optimised by using both passive and active methods: by geometric redesign of the structure and by the application of

AVC using optimal actuator positions. Two strategies are used for this, the evaluation of optimal actuator positions on a previously geometrically optimised structure, and the simultaneous optimisation of both geometry and actuator positions. The robustness of all the optimised design produced is evaluated.

A summary is then presented for all the optimised structure designs produced in this and the preceding two chapters allowing the performance achieved, and control effort to be evaluated against optimisation strategy. This was performed for both nominal performance and performance with perturbed structure geometries.

CHAPTER 7: The incorporation of a measure of robustness into the optimisation parameter is studied in order to design for optimal *and* robust structures. This is achieved by geometric redesign for the average structure performance over a narrow frequency band. Two versions of the noisy phenotype genetic algorithm and three different measures of robustness are used, each with varying levels of additional computational complexity.

CHAPTER 8: A brief summary of all the work presented and the main findings are given, and overall conclusions drawn. Recommendations for further study are also suggested.

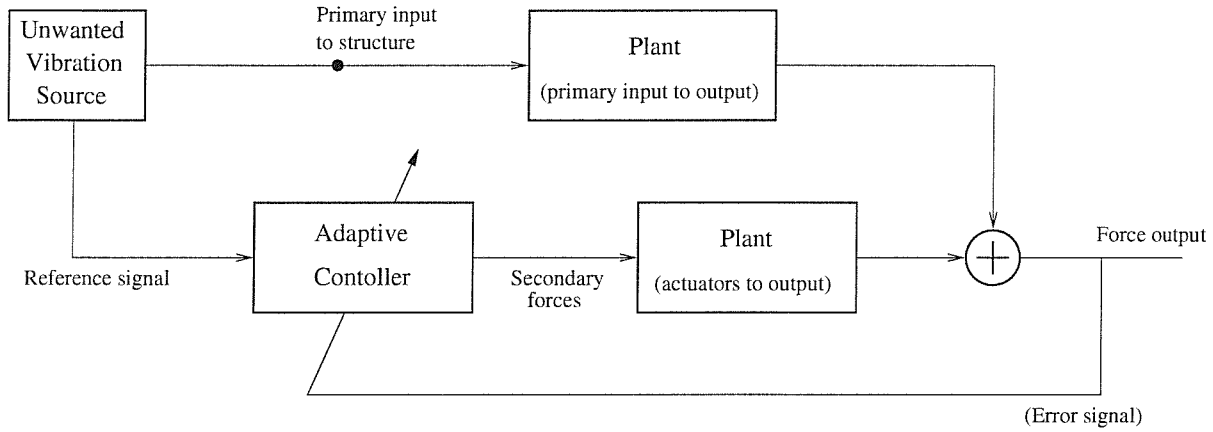

Figure 1.1: Schematic showing the basic operation of a feedforward Active Vibration Control system.

CHAPTER 2

Dynamic Model of the Structure and the Application of Active Vibration Control

2.0. INTRODUCTION

The structure whose dynamic performance is the subject of this thesis, is two-dimensional and comprises of thin rigidly joined beams in a repeated bay design. This chapter outlines the theoretical background to the mathematical models used to describe the dynamic response of such a structure. The response of the overall structure is achieved by incorporating individual beam models into a receptance analysis model which enables the coupling forces and the velocities at each joint to be resolved. From these parameters the energy level in an individual beam can be obtained. These parameters are the subject of the optimisation work which is reported in later chapters.

In this thesis the optimisation is achieved by either the redesign of the structure geometry or the application of Active Control of Vibration techniques, or by both methods. Predicting the effect of Active Control of Vibration is achieved by solving a set of simultaneous equations involving individual structure responses. The procedure for this and its application to an example structure is also given. The practical success of Active Control of Vibration depends upon the choice of cost function which is being minimised. The solutions for the minimised values of alternative three cost functions are developed in preparation for a later comparison and appraisal of the use of different cost functions in optimising the structural performance.

Finally, to enable an understanding of the mechanisms by which the vibration in the structures has been reduced by optimisation, a power analysis of the structure is described, and the constituent power components defined.

2.1 STRUCTURE SPECIFICATION AND OVERVIEW OF MODEL

The structure studied is shown in Figure 2.1 (after Keane, 1995b), in which the coordinate units are in metres. It is a lightweight cantilever structure comprising of 40 beams of lengths 1m and 1.414m. The joints at coordinates (0,0) and (0,1) are hinged, all the other joints are fixed (as if welded, for example). The structure and its vibration is considered in two dimensions; motion is only considered in the *x-y* plane. A typical application for such a

structure is that of an antenna boom arm for use on a satellite. In this scenario the aim is to reduce the vibration transmission from the base of the structure to the rightmost beam, where an antenna may be mounted in practice.

The physical properties of the beams used in the model are: the axial rigidity, EA, is 69.80MN; the bending rigidity, EI, is 12.86 kNm^2; the mass per unit length is 2.74kg/m. This is found to correspond to an aluminium beam of rectangular cross-section with approximate dimensions 50 mm by 25 mm, with the longer dimension in the x-y plane. A Proportional damping model is used for the beams (Tse, Morse and Hinkle, 1978) and all the modes of the uncoupled beams have the same bandwidth. The value used is $20 \cdot s^{-1}$ (*sic.* Shankar and Keane (1995) but may also be written as $(20/2\pi)$ $rad \cdot s^{-1}$). This corresponds to a damping ratio of 5% at 200Hz. This choice of damping parameter value is not untypical and was chosen so that a modal response was clearly evident in the structure's response, but not so low such that large resonant peaks caused noise problems due to a large dynamic range (Keane, 1998).

The flexural vibration of each beam is modelled using the Euler-Bernoulli model (Bishop and Johnson, 1960) and longitudinal vibration using a rod model, with both models using a modal series summation. The response of the structure is analysed by studying the coupling between all the individual beams. This is performed using a receptance analysis (Bishop and Johnson, 1960) in which the unknown displacements, forces and moments are solved for each beam end when driven by the external force inputs. This is achieved at all the beam ends at each joint by equating the displacements and rotations, and summing the net forces and moments to zero. From this analysis the power transmitted into or out of each beam end and externally applied forces can be calculated. This process is described in detail in the next section.

The forces and moments at each beam end are solved by incorporating the individual beam receptance relationships into a global receptance matrix, and calculating the inverse to this matrix, which then enables the displacements and rotations to be evaluated. For the structure analysed here the size of this matrix is approximately 170 by 170 elements. The optimisation parameter used in the structural design is normally averaged across a frequency band, and hence the dynamic response for each design scenario must be evaluated at a number of frequencies, which can become computationally expensive. Therefore only the use of efficient optimisation techniques is feasible, especially with regard to the size of the optimisation problem, discussed in Chapter 4.

2.2 RECEPTANCE MODEL OF STRUCTURE

Initially, consider the general case of a single beam, shown in Figure 2.2. It is inclined by angle θ_N to the x-axis of the global coordinate system, which is shown in Figure 2.1. In order to study the interaction between the beams, and therefore the response of the whole structure, the beam behaviour at two, and sometimes three points needs to be considered. Firstly the response at each end obviously needs to be analysed since this is the interface between beams or mechanical ground, which form the end conditions for the beam. If a beam has an external force input along its length, or the displacement of a beam along its length is of interest, then a third position is also required. In order to distinguish between forces and displacements specified in local coordinates (where the x-axis is along the beam length) and those specified in the global coordinates (as shown in Figure 2.1), lower and upper case symbols are used to indicate local and global coordinates, respectively. The frequency dependence is dropped in the following, except where necessary, and it is assumed that the analysis is repeated at each frequency of interest.

Three components of force acting on each point of the beam are considered. Specified in the local beam coordinates: forces acting horizontally, vertically and rotary components. The complex forces at each point are expressed in vector notation, the forces at end 1 for beam N are represented by vector $\{\mathbf{f}_N\}^1$ where,

$$\{\mathbf{f}_N\}^1 = \begin{Bmatrix} f_{xN}^1 \\ f_{yN}^1 \\ M_N^1 \end{Bmatrix}. \tag{2.1}$$

f_{xN}^1 and f_{yN}^1 are the axial and transverse forces acting on beam N at end 1 respectively, and M_N^1 is the applied moment. Following the notation used in (from Shankar and Keane, 1995), any external forces applied to the beam are applied at positions x_a, x_t and x_m for axial, transverse and rotary components respectively. Similarly the displacement and rotation at end 1 are represented by the complex vector $\{\mathbf{x}_N\}^1$, defined as,

$$\{\mathbf{x}_N\}^1 = \begin{Bmatrix} x_N^1 \\ y_N^1 \\ \theta_N^1 \end{Bmatrix}. \tag{2.2}$$

The vectors describing the forces and displacements at beam end 0, and those at the point of external force inputs, follow the same format, and are not explicitly defined, in the interest of

brevity. The displacement of the beam at end 1 is the summation of the displacement components resulting from the forces at end 0, end 1 and, if applicable, an external force applied to the beam. For example the displacement component at end 1 due to the external forces applied to the beam is given in terms of the beam's Green function by,

$$\{\mathbf{x}_N\}^1_{(external)} = [\mathbf{G}_N]^{1e}.\{\mathbf{f}_N\}^e, \tag{2.3}$$

where $[\mathbf{G}_N]^{1e}$ is explicitly,

$$[\mathbf{G}_N]^{1e} = \begin{bmatrix} G_{N,axial}(1, x_a) & 0 & 0 \\ 0 & G_{N,tran}(1, x_t) & G_{N,tran}(1, \mathrm{D}\, x_m) \\ 0 & G_{N,tran}(\mathrm{D}1, x_t) & G_{N,tran}(\mathrm{D}1, \mathrm{D}\, x_m) \end{bmatrix}, \tag{2.4}$$

and describes the displacement response at end 1 due to an external force. (Note that the superscripts represent the type of Green function, three options are available for each symbol: 0, 1 and *e*. The superscripts do not describe the positions explicitly but simply distinguish between each end of the beam and any external input. The first superscript defines the location of the displacement response, due to an excitation force whose position is defined by the second superscript). D denotes the derivative operator at either the point of response or excitation, as denoted. The non-zero elements of the matrix are Green functions which describe the displacement or rotational response to input forces or moments on the beam. Their notation is,

$$G_{N,<input\_type>}(< response >, < excitation >).$$

The type of input force,<*input_type*>, is either *axial* or *tran* (transverse), <*response*> is the position that the displacement (in local beam coordinates) produced by the input force at location <*excitation*>. All distances along the beam are referenced from end 0. Where the response or excitation is either a bending moment or rotary component then the derivative of either the force or displacement, respectively, with respect to distance along the beam at that point is used.

The individual Green functions can be thought of as complex transfer receptances, each of which is evaluated from a summation of a series of *n* modal contributions. *n* is sufficiently large so that the nth modal frequency is higher than, and makes an insignificant contribution at, the highest frequency studied. So,

$$G_{N,<input\_type>}(x, y) = \sum_{j=0}^{n} \frac{\phi_j(x)\phi_j(y)}{l_N \rho_N \left(\omega_j^2 - \omega^2 + ic_d\omega\right)}, \tag{2.5}$$

where l_N is the length and ρ_N the mass per unit length of beam N. $\phi_j(x)$ is the value of the mass normalised modeshape at position x from the end 0 of the beam, ω_j the natural frequency of the j^{th} mode. The Green function is evaluated at frequency ω, but the frequency dependence is omitted, as noted above. c_d is the beam damping, which is the same for all modes and all beams. It can be related to the damping ratio ζ such that, $c_d = 2\zeta\omega_j$ for mode j. Here proportional damping is used and c_d is specified directly, in the units of rad s^{-1}. It can be shown that for light damping (as for the value of damping used for the structure considered) that the bandwidth of each beam mode is approximately equal to the value of c_d. The modeshapes for the axial and transverse mode must be normalised according to some consistent scheme, and also rigid body motion of the beam, where permitted, must be taken into account.

The type of Green function implemented depends upon the end conditions of the beam. The two end conditions that are applicable here are hinged-free and free-free. The hinged-free Green functions are for beams that have one end jointed at the base of the structure. Although no notation is used to distinguish between the different Green functions this is achieved by a reference list for the beams which records their end conditions. On evaluating a Green function for a beam this is referenced so the correct function is evaluated by the code. The use of the different Green functions is illustrated in the example that follows.

The net displacement at the end 1 of the beam is the sum of the three displacement/rotation components due to forces acting at ends 0 and 1 and any external forces. So,

$$\{\mathbf{x}_N\}^1 = [\mathbf{G}_N]^{10}.\{\mathbf{f}_N\}^0 + [\mathbf{G}_N]^{1e}.\{\mathbf{f}_N\}^e + [\mathbf{G}_N]^{11}.\{\mathbf{f}_N\}^1, \tag{2.6}$$

represents the net displacement at end 1. Hence each component is found from the Green function matrix which gives the input force to output displacement response receptance at the points on the beam studied multiplied by the force vector detailing the forces at the input point.

From the Green function matrices, such as that shown in (2.4), it can be seen that purely axial forces only generate axial displacements, however there exists a coupling between the transverse and rotary components, and both of these are capable of producing both transverse and rotary components (both causing beam flexure). When beams are coupled together at different incident angles coupling can exist between all vibration components. In order to resolve inter-beam coupling correctly a global coordinate system must be used. This is as shown in Figure 2.1. A coordinate transformation matrix $[\mathbf{T}_N]$ for each beam is defined,

$$[\mathbf{T}_N]=\begin{bmatrix}\cos\theta_N & -\sin\theta_N & 0\\ \sin\theta_N & \cos\theta_N & 0\\ 0 & 0 & 1\end{bmatrix}, \tag{2.7}$$

which is used to define the local coordinate system for beam N, such that,

$$\begin{Bmatrix}x_N^0\\ y_N^0\\ \theta_N^0\end{Bmatrix}=[\mathbf{T}_N].\begin{Bmatrix}X_N^0\\ Y_N^0\\ \Theta_N^0\end{Bmatrix}, \tag{2.8}$$

where uppercase characters denote global coordinates. Hence in order to convert local to global coordinate systems the inverse $[\mathrm{T}_N]^{-1}$ is used.

2.2.1 APPLICATION TO SMALL STRUCTURE EXAMPLE

In order to calculate the global receptances, enabling the vibration transmission across the structure to be studied, all the displacements at each end of all beams coupled at one joint are equated together and net force at each joint are equated to zero. This results in a large number of simultaneous equations which are dealt with in matrix format. To illustrate the formation of such a matrix a small example structure is used, which consists of one bay cantilever structure which is shown in Figure 2.3. The structure consists of four similar rigidly joined beams. The two leftmost points are mechanical ground and constrain the beams end by a hinged joint (which constrains displacement but allows rotation). The other joint type is that of a 'free' end. The beam and joint indexing is shown, as is the beam end notation. An external transverse force is applied at a point along the length of Beam 1, similar to that applied to the structure in this thesis. The component displacements for the three beam end at joint A are given, in full, by

$$[\mathbf{T}_1]^{-1}[\mathbf{G}_1]^{1e}\{\mathbf{f}_1\}^e+[\mathbf{T}_1]^{-1}[\mathbf{G}_1]^{10}\{\mathbf{f}_1\}^0+[\mathbf{T}_1]^{-1}[\mathbf{G}_1]^{11}\{\mathbf{f}_1\}^1=\{\mathbf{X}_1\}^1, \tag{2.9}$$

$$[\mathbf{T}_2]^{-1}[\mathbf{G}_2]^{0e}\{\mathbf{f}_2\}^e+[\mathbf{T}_2]^{-1}[\mathbf{G}_2]^{00}\{\mathbf{f}_2\}^0+[\mathbf{T}_2]^{-1}[\mathbf{G}_2]^{01}\{\mathbf{f}_2\}^1=\{\mathbf{X}_2\}^0, \tag{2.10}$$

$$[\mathbf{T}_4]^{-1}[\mathbf{G}_4]^{1e}\{\mathbf{f}_4\}^e+[\mathbf{T}_4]^{-1}[\mathbf{G}_4]^{10}\{\mathbf{f}_4\}^0+[\mathbf{T}_4]^{-1}[\mathbf{G}_4]^{11}\{\mathbf{f}_4\}^1=\{\mathbf{X}_4\}^1. \tag{2.11}$$

As Beams 1, 3, 4 each have an end which forms a hinged joint to mechanical ground, the Green functions $\mathbf{G_1}$, $\mathbf{G_3}$, and $\mathbf{G_4}$ are of the hinged-free type, whilst $\mathbf{G_2}$ is of the free-free beam type. This determines the modeshape used, as described above. There is only an external force on Beam 1 and so the leftmost terms in (2.10) and (2.11) are zero. Similarly there is no displacement component contribution from the ends of Beams 1 and 4 that are connected to

mechanical ground. The second term on the left hand sides in (2.9) and (2.11) are therefore also zero. So in this case,

$$[\mathbf{T}_1]^{-1}[\mathbf{G}_1]^{1e}\{\mathbf{f}_1\}^e + [\mathbf{T}_1]^{-1}[\mathbf{G}_1]^{11}\{\mathbf{f}_1\}^1 = \{\mathbf{X}_1\}^1, \tag{2.12}$$

$$[\mathbf{T}_2]^{-1}[\mathbf{G}_2]^{00}\{\mathbf{f}_2\}^0 + [\mathbf{T}_2]^{-1}[\mathbf{G}_2]^{01}\{\mathbf{f}_2\}^1 = \{\mathbf{X}_2\}^0, \tag{2.13}$$

$$[\mathbf{T}_4]^{-1}[\mathbf{G}_4]^{11}\{\mathbf{f}_4\}^1 = \{\mathbf{X}_4\}^1. \tag{2.14}$$

All the beam end displacements are coupled by a rigid joint, and hence must all be equal. Since $\{\mathbf{X}_1\}^1 = \{\mathbf{X}_2\}^0$ then,

$$[\mathbf{T}_2]^{-1}[\mathbf{G}_2]^{00}\{\mathbf{f}_2\}^0 + [\mathbf{T}_2]^{-1}[\mathbf{G}_2]^{01}\{\mathbf{f}_2\}^1 - [\mathbf{T}_1]^{-1}[\mathbf{G}_1]^{11}\{\mathbf{f}_1\}^1 = [\mathbf{T}_1]^{-1}[\mathbf{G}_1]^{1e}\{\mathbf{f}_1\}^e, \tag{2.15}$$

and since $\{\mathbf{X}_1\}^1 = \{\mathbf{X}_4\}^1$ then,

$$[\mathbf{T}_4]^{-1}[\mathbf{G}_4]^{11}\{\mathbf{f}_4\}^1 - [\mathbf{T}_1]^{-1}[\mathbf{G}_1]^{11}\{\mathbf{f}_1\}^1 = [\mathbf{T}_1]^{-1}[\mathbf{G}_1]^{1e}\{\mathbf{f}_1\}^e. \tag{2.16}$$

Similarly equating the displacements for the two beam ends at joint B yields,

$$[\mathbf{T}_2]^{-1}[\mathbf{G}_2]^{10}\{\mathbf{f}_2\}^0 + [\mathbf{T}_2]^{-1}[\mathbf{G}_2]^{11}\{\mathbf{f}_2\}^1 - [\mathbf{T}_3]^{-1}[\mathbf{G}_3]^{11}\{\mathbf{f}_3\}^1 = 0. \tag{2.17}$$

Next, considering the forces at the ends of the beams at each joint (using global coordinates) the net force must be zero. Hence for joints A and B, respectively, this yields,

$$[\mathbf{T}_1]^{-1}\{\mathbf{f}_1\}^1 + [\mathbf{T}_2]^{-1}\{\mathbf{f}_2\}^0 + [\mathbf{T}_4]^{-1}\{\mathbf{f}_4\}^1 = 0, \tag{2.18}$$

$$[\mathbf{T}_2]^{-1}\{\mathbf{f}_2\}^1 + [\mathbf{T}_3]^{-1}\{\mathbf{f}_3\}^1 = 0. \tag{2.19}$$

There are five unknowns (the force vectors at each non-constrained beam end) in the five equations (2.15) to (2.19), and can, therefore be solved. This can be achieved using matrix methods by assembling the $[\mathbf{T}_N]$ and $[\mathbf{G}_N]$ terms in as global matrix and the force vectors as a concatenated force vector, using a consistent scheme,

$$\begin{bmatrix} [\mathbf{T}_1]^{-1}[\mathbf{G}_1]^{11} & -[\mathbf{T}_2]^{-1}[\mathbf{G}_2]^{00} & 0 & [\mathbf{T}_2]^{-1}[\mathbf{G}_2]^{01} & 0 \\ [\mathbf{T}_1]^{-1}[\mathbf{G}_1]^{11} & 0 & -[\mathbf{T}_4]^{-1}[\mathbf{G}_4]^{11} & 0 & 0 \\ 0 & [\mathbf{T}_2]^{-1}[\mathbf{G}_2]^{10} & 0 & [\mathbf{T}_2]^{-1}[\mathbf{G}_2]^{11} & -[\mathbf{T}_3]^{-1}[\mathbf{G}_3]^{11} \\ [\mathbf{T}_1]^{-1} & [\mathbf{T}_2]^{-1} & [\mathbf{T}_4]^{-1} & 0 & 0 \\ 0 & 0 & 0 & [\mathbf{T}_2]^{-1} & [\mathbf{T}_3]^{-1} \end{bmatrix} \cdot \begin{bmatrix} \{\mathbf{f}_1\}^1 \\ \{\mathbf{f}_2\}^0 \\ \{\mathbf{f}_4\}^1 \\ \{\mathbf{f}_2\}^1 \\ \{\mathbf{f}_3\}^1 \end{bmatrix} = \begin{bmatrix} -[\mathbf{T}_1]^{-1}[\mathbf{G}_1]^{1e}\{\mathbf{f}_1\}^e \\ -[\mathbf{T}_1]^{-1}[\mathbf{G}_1]^{1e}\{\mathbf{f}_1\}^e \\ 0 \\ 0 \\ 0 \end{bmatrix} \tag{2.20}$$

and is more succinctly expressed,

$$\mathbf{C}_s\mathbf{F} = \mathbf{E}, \tag{2.21}$$

where $\mathbf{C}_s$ is the structural coupling matrix, $\mathbf{F}$ the individual beam-end force vector and $\mathbf{E}$ the vector of displacement components from externally applied forces. The forces at each beam end are then solved from the inverse of $\mathbf{C}_s$,

$$\mathbf{F} = \mathbf{C}_s^{-1}\mathbf{E}. \tag{2.22}$$

In practice the explicit inverse is not determined directly, but instead a system of linear equations is solved. Once the force vector $\mathbf{F}$ has been resolved, together with the appropriate Green functions, the displacement or rotation at the ends of (or any point in between) a beam can be found. The resolved forces are the coupling forces at each beam end, and at each joint different forces act on each beam (though the net sum at a joint is zero).

2.2.2 CALCULATING ENERGY LEVEL WITHIN A BEAM

In order to calculate the energy level within the beam, the power dissipated in the beam must first be found. The power at the end of each beam is considered in three components (two due to linear motion and one due to rotation). Thus the power vector at end 1 of beam N (in global coordinates) is,

$$\{\mathbf{P}_N\}^1 = \begin{Bmatrix} P^1_{XN} \\ P^1_{YN} \\ P^1_{\Theta N} \end{Bmatrix}. \tag{2.23}$$

The power is derived from the conjugate product of the coupling force and the velocity at each beam end. Velocities are derived from the displacements as the system being analysed at discrete frequencies. The velocity vector representing the three velocity components at end 1 of beam N is derived from the displacement, at frequency ω,

$$\{\mathbf{V}_N\}^1 = i\omega\{\mathbf{X}_N\}^1. \tag{2.24}$$

It is re-iterated that the frequency dependence of the variables is omitted for clarity. The global joint velocity is common to the beam ends which form a particular joint. It is the different coupling forces at the end of each beam that determine the power transmitted between beams. For each power component, using the product of the complex force and the conjugate of the complex velocity the real part corresponds to the power transmitted. As the analysis is performed at discrete frequencies, the time averaged power is given by half the real part of the product;

$$\{\mathbf{P}_N\}^1 = \frac{1}{2}\mathrm{Re}\begin{Bmatrix} \mathbf{F}^1_{XN}.\mathbf{V}^{1\ *}_{XN} \\ \mathbf{F}^1_{YN}.\mathbf{V}^{1\ *}_{YN} \\ \mathbf{F}^1_{\Theta N}.\mathbf{V}^{1\ *}_{\Theta N} \end{Bmatrix}, \tag{2.25}$$

where * denotes complex conjugation. The forces have been transformed in the global coordinate system (as performed for the displacement vector in (2.8)). The sign of the real part allows the direction of power in each component to be ascertained.

The sum of all the end beam forces at a joint is zero (see (2.18) and (2.19)) and all the end beam velocities are common, so the net transmission of power into (or out of) a joint is zero. All the net energy flowing into a beam from each end, or from an external power input, must be dissipated in the beam, so

$$\{\mathbf{P}_N\}^e + \{\mathbf{P}_N\}^0 + \{\mathbf{P}_N\}^1 + \{\mathbf{P}_N\}^{damp} = 0, \tag{2.26}$$

where $\{\mathbf{P}_N\}^{damp}$ is the energy lost in the beam due to effect of damping. A positive value of power indicates power into the beam, and thus $\{\mathbf{P}_N\}^{damp}$ is negative by definition. Hence as the remaining terms in (2.26) are known, then the average power loss in a beam can be calculated. The energy level in beam N is the power dissipated in the beam divided by the damping. The beam damping specification, c_d, is given above. The energy level e_N is thus derived from the sum of the power transmitted in all planes in beam N,

$$e_N = \frac{1}{c_d}\sum_{j=X,Y,\Theta}\{\mathbf{P}_{jN}\}^{damp}, \tag{2.27}$$

and where $\{\mathbf{P}_{xN}\}^{damp}$, for example, represents the power dissipated (2.26) in the x-axis direction. In the optimisations considered in the thesis the objective function is either the energy level at a single frequency, and is thus expressed as in (2.27) with the frequency dependence

assumed, or the average energy level over a frequency band. The calculation of this average is detailed in Section 2.5.

2.3 APPLICATION OF ACTIVE CONTROL TO THE STRUCTURE

To support the work detailed in Chapter 5, a model for the application of Active Vibration Control (AVC) to the structure is described. The active control system modelled here uses double-acting axial operating actuators. For simplicity, it is assumed that the addition of an actuator to a beam does not alter the mechanical properties of that beam. The point of application of the forces from the actuators are offset (by 10mm) from the ends of the beams. It is noted that the force vector **f** used in this section is distinct to the force vector used in Section 2.2, and that only global coordinates are used in this section.

The base vibration is modelled as a single transverse force of 1N applied at the middle of one of the beams adjoined to the base (as shown in Figure 2.1). In AVC terminology this is called the *primary force*. Two vectors defining the effect of the force and velocity components (for all degrees of freedom considered) at the joints of the ends of Beam 40 in Figure 2.1, in the absence of any other forces (i.e. without active control operative) are denoted $\mathbf{f}_p$ and $\mathbf{v}_p$. AVC applies *secondary forces* to 'counter' vibrations on the structure. Their effect is determined by a vector describing the values of secondary forces of each actuator $\mathbf{f}_s$, and either a 'transformed' force or mobility transfer matrix (**C** or **Y**) which represents the resultant force or velocity components from these secondary forces at the joints at the ends of the beam. The net force and velocity vectors from the combination of both primary and secondary forces are then given by the summations of these two components, thus the net force vector, **f**, is

$$\mathbf{f} = \mathbf{f}_p + \mathbf{C}\mathbf{f}_s \,, \tag{2.28}$$

where the format of the force vector **f**, which describes the forces at the ends of Beam 40, is given by,

$$\mathbf{f} = \left[\left\{f_x^{40,0,} \quad f_y^{40,0} \quad f_\theta^{40,0}\right\} \quad \left\{f_x^{40,1} \quad f_y^{40,1} \quad f_\theta^{40,1}\right\}\right]^T. \tag{2.29}$$

The net velocity vector, $\mathbf{v}$, is

$$\mathbf{v} = \mathbf{v}_p + \mathbf{Y}\mathbf{f}_s \,, \tag{2.30}$$

where the format of the velocity vector **v** is given by,

$$\mathbf{v} = \left[\left\{v_x^{40,0} \quad v_y^{40,0} \quad v_\theta^{40,0}\right\} \quad \left\{v_x^{40,1} \quad v_y^{40,1} \quad v_\theta^{40,1}\right\}\right]^T. \tag{2.31}$$

$\mathbf{v}_p$ is the vector of the six velocity components due to the primary force only. $\mathbf{f}_s$ being common to the formulation of $\mathbf{f}$ and $\mathbf{v}$. All the net and primary force and velocity vectors ($\mathbf{f}, \mathbf{f}_p, \mathbf{v}, \mathbf{v}_p$) are of the same format.

The two 'transformed' force and mobility transfer matrices used, $\mathbf{C}$ and $\mathbf{Y}$, are themselves comprised of two terms, so (2.28) and (2.30) may be written,

$$\mathbf{f} = \mathbf{f}_p + \mathbf{C}'\mathbf{T}\mathbf{f}_s \,, \tag{2.32}$$

$$\mathbf{v} = \mathbf{v}_p + \mathbf{Y}'\mathbf{T}\mathbf{f}_s \,, \tag{2.33}$$

where $\mathbf{C}'$ and $\mathbf{Y}'$ are the force transfer and mobility transfer matrices, which define the mechanical coupling between the actuators and their effect of the force and velocity components at the ends of Beam 40. $\mathbf{T}$ is a transformation matrix which maps each axial-only secondary force onto six components in each plant matrix. This is required as force and velocity components at the end of Beam 40 in all degrees of freedom are not independent, but solely defined by the axial forces of the force vector, $\mathbf{f}_s$. (2.32) is then explicitly (shown extended to the case with two secondary force actuators, denoted f_s),

$$\begin{bmatrix} \begin{Bmatrix} f_x^{40,0} \\ f_y^{40,0} \\ f_\theta^{40,0} \end{Bmatrix} \\ \begin{Bmatrix} f_x^{40,1} \\ f_y^{40,1} \\ f_\theta^{40,1} \end{Bmatrix} \end{bmatrix} = \begin{bmatrix} \begin{Bmatrix} f_{p_x}^{40,0} \\ f_{p_y}^{40,0} \\ f_{p_\theta}^{40,0} \end{Bmatrix} \\ \begin{Bmatrix} f_{p_x}^{40,1} \\ f_{p_y}^{40,1} \\ f_{p_\theta}^{40,1} \end{Bmatrix} \end{bmatrix} + \begin{bmatrix} \begin{Bmatrix} \mathbf{C}_{1A}^{40,0} & -\mathbf{C}_{1B}^{40,0} \\ \mathbf{C}_{1A}^{40,1} & -\mathbf{C}_{1B}^{40,1} \end{Bmatrix} & \begin{Bmatrix} \mathbf{C}_{2A}^{40,0} & -\mathbf{C}_{2B}^{40,0} \\ \mathbf{C}_{2A}^{40,1} & -\mathbf{C}_{2B}^{40,1} \end{Bmatrix} & \cdots \end{bmatrix} \begin{bmatrix} \{1\} & & \\ & \{1\} & \\ & & \ddots \end{bmatrix} \begin{bmatrix} f_{S_1} \\ f_{S_2} \\ \vdots \end{bmatrix}, \tag{2.34}$$

where, for example, $f_x^{40,0}$ is the x-axis force component at end 0 of Beam 40. The sub-matrices in the $\mathbf{C}'$ matrix are of the format,

$$\mathbf{C}_{1A}^{40,0} = \begin{bmatrix} c_{1A_x}^{40,0} & 0 & 0 \\ 0 & c_{1A_y}^{40,0} & 0 \\ 0 & 0 & c_{1A_\theta}^{40,0} \end{bmatrix}, \tag{2.35}$$

where $c_{1A_x}^{40,0}$ is the individual force transfer function for the x-axis force component at end 0 of Beam 40 for a unit axial force at end A of the beam where the first secondary actuator is employed. This notation is extended to responses in the y-axis, rotational components; from end B of the actuator beam position; and for end 1 of Beam 40. The signs of the sub-matrices for secondary drive from end B are negative to give the proper representation of a double-

acting actuator. The reason for the diagonal format of the sub-matrices is to ensure that all the net force and net velocity components remain independent and only combined in the final inner product between $\mathbf{f}$ and $\mathbf{v}$; so that the power flow components from the six degrees of freedom are summed and not the force or velocity components. The $\{\mathbf{1}\}$ sub-matrices in $\mathbf{T}$ in (2.34) are vectors which are explicitly,

$$\{\mathbf{1}\} = (1 \quad 1 \quad 1 \quad 1 \quad 1 \quad 1)^{\mathrm{T}}, \tag{2.36}$$

and maps a single value for each secondary actuator value onto the all the six individual transfer functions it relates to. For convenience the force transfer matrix and the transformation matrix are combined to form a transformed force transfer matrix $\mathbf{C}$, as used in (2.28). In a similar way $\mathbf{Y}$, as used in (2.30), is the transformed mobility transfer matrix, where the $\mathbf{Y}'$ matrix (2.33) and its sub-matrices are defined,

$$\mathbf{Y}' = \left[\begin{Bmatrix} \mathbf{Y}_{1\mathrm{A}}^{40,0} & -\mathbf{Y}_{1\mathrm{B}}^{40,0} \\ \mathbf{Y}_{1\mathrm{A}}^{40,1} & -\mathbf{Y}_{1\mathrm{B}}^{40,1} \end{Bmatrix} \quad \begin{Bmatrix} \mathbf{Y}_{2\mathrm{A}}^{40,0} & -\mathbf{Y}_{2\mathrm{B}}^{40,0} \\ \mathbf{Y}_{2\mathrm{A}}^{40,1} & -\mathbf{Y}_{2\mathrm{B}}^{40,1} \end{Bmatrix} \quad \cdot \quad \cdot \right], \tag{2.37a}$$

$$\mathbf{Y}_{1\mathrm{A}}^{40,0} = \begin{bmatrix} y_{1A_x}^{40,0} & 0 & 0 \\ 0 & y_{1A_y}^{40,0} & 0 \\ 0 & 0 & y_{1A_\theta}^{40,0} \end{bmatrix}, \tag{2.37b}$$

where $y_{1A_x}^{40,0}$ is the individual transfer mobility, detailing the x-axis force component at end 0 of Beam 40 for a unit axial force at end A of the beam where the first secondary actuator is employed.

The flexural energy level in the beam arises as a result of the balance between the average energy flowing into the beam at its ends, and the average dissipation of the energy due to its damping. The damping is assumed to be proportional (Tse, Morse and Hinkle, 1978). The power dissipated is equal to the net input power to Beam 40, which for harmonic vibration is defined as half of the real part of the conjugate product of the complex force and velocity vectors, at the joints at the ends of the beam,

$$P = \frac{1}{2}\mathrm{Re}\{\mathbf{f}^{\mathrm{H}}\mathbf{v}\}, \tag{2.38}$$

which can be more conveniently expressed in the linear form,

$$P = \frac{1}{4}\left(\mathbf{f}^{\mathrm{H}}\mathbf{v} + \mathbf{v}^{\mathrm{H}}\mathbf{f}\right). \tag{2.39}$$

Using (2.28) and (2.30) to express this in terms of $\mathbf{f}_s$, the independent variable for the cost function minimisation as,

$$P = \frac{1}{4}\left[\mathbf{f}_s^H\left(\mathbf{C}^H\mathbf{Y} + \mathbf{Y}^H\mathbf{C}\right)\mathbf{f}_s + \mathbf{f}_s^H\left(\mathbf{C}^H\mathbf{v}_p + \mathbf{Y}^H\mathbf{f}_p\right) + \left(\mathbf{f}_p\mathbf{Y} + \mathbf{v}_p\mathbf{C}\right)\mathbf{f}_s + \mathbf{f}_p^H\mathbf{v}_p + \mathbf{v}_p^H\mathbf{f}_p\right]. \tag{2.40}$$

This is written in a general quadratic form,

$$J = \mathbf{x}^H\mathbf{A}\mathbf{x} + \mathbf{x}^H\mathbf{b} + \mathbf{b}^H\mathbf{x} + c, \tag{2.41}$$

where $\mathbf{A}$ is a Hermitian matrix, $\mathbf{b}$ is a complex vector (which is equivalent to the secondary force vector $\mathbf{f}_s$) and c is a real scalar. The positive scalar c represents the value of the cost function due to the primary excitation only (without active control; $\mathbf{x} = \mathbf{0}$). The $\mathbf{x}^H\mathbf{A}\mathbf{x}$ term represents the value of the cost function due to the secondary source excitation only (without primary source of structural excitation), and this is obviously always positive (unless there is an external power input into Beam 40). Based on these physical grounds $\mathbf{A}$ will always be positive definite (see (A.2)). This was verified in practice by confirming that all the eigenvalues of $\mathbf{A}$ are positive. Thus, the derivation of the minimum value of the cost function can be greatly simplified. Also, as the AVC system is *over-determined* (there are more degrees of freedom for sensors than actuators) $\mathbf{A}$ is of full rank (which is also ensured if positive-definite) and thus a minimum will always exist. The minimisation of the quadratic form in (2.41) is detailed in the Appendix A. This yields the optimum secondary control vector,

$$\mathbf{x}_o = -\mathbf{A}^{-1}\mathbf{b}, \tag{2.42}$$

and, therefore, the optimum secondary force vector is,

$$\mathbf{f}_{s_o} = -\left(\mathbf{C}^H\mathbf{Y} + \mathbf{Y}^H\mathbf{C}\right)^{-1}\left(\mathbf{C}^H\mathbf{v}_p + \mathbf{Y}^H\mathbf{f}_p\right). \tag{2.43}$$

From Appendix A the minimised value of the dissipated power is of the form,

$$J_o = c - \mathbf{b}^H\mathbf{A}^{-1}\mathbf{b}. \tag{2.44}$$

Hence the minimum net dissipated power is explicitly,

$$P_o = \frac{1}{4}\left[\left(\mathbf{f}_p^H\mathbf{v}_p + \mathbf{v}_p^H\mathbf{f}_p\right) - \left(\mathbf{f}_p^H\mathbf{Y} + \mathbf{v}_p^H\mathbf{C}\right)\left(\mathbf{C}^H\mathbf{Y} + \mathbf{Y}^H\mathbf{C}\right)^{-1}\left(\mathbf{C}^H\mathbf{v}_p + \mathbf{Y}^H\mathbf{f}_p\right)\right]. \tag{2.45}$$

The average energy level was used as the cost function. This is related by a simple scaling factor, c_d, the beam damping which is independent of frequency. Hence the minimum energy level E_{flex_0}, at frequency ω, of the beam is,

$$E_{flex_0}(\omega) = \frac{P_0(\omega)}{c_d}. \tag{2.46}$$

The average energy level over a frequency band is also used as the parameter to be minimised. The frequency average used is,

$$\left\langle E_{flex_0} \right\rangle = \frac{1}{n}\sum_{k=1}^{n} E_{flex_0}(\omega_L + (k-1)\Delta\omega), \tag{2.47}$$

where n is the number of frequency steps, $\Delta\omega$ the angular frequency spacing and ω_L the lower angular frequency point. $\Delta\omega/2\pi$ is 5Hz for all cases. This is equivalent to the generic cost function average given in Section 2.5. The *total control effort* required to achieve the AVC reductions is taken to be the sum of the squares of the individuals secondary forces. The total control effort, q_s, is then formally,

$$q_s = \sum_{k=1}^{n} \mathbf{f}_s^{\mathrm{H}}(\omega_L + (k-1)\Delta\omega)\mathbf{f}_s(\omega_L + (k-1)\Delta\omega). \tag{2.48}$$

The control is summed over the same frequency range as for the performance studied.

2.4 DEVELOPMENT OF ALTERNATIVE COST FUNCTIONS TO REPRESENT VIBRATION

This section supports the work reported in Chapter 5, in which other Active Vibration Control (AVC) cost functions are considered and compared. The values of different minimised cost functions are derived. It is noted that the force vector **f** used in this section is that used in Section 2.3, and that only global coordinates are used in this section.

2.4.1 THE RIGID BODY KINETIC ENERGY OF A BEAM

The minimisation of the flexural energy in the beam, calculated in Section 2.3, only accounts for the motion of the beam due to its flexure. If the beam does not undergo flexure, its power dissipation and therefore the flexural energy is zero. However the beam may still move as a rigid body and this motion would not be detected by E_{flex}. So, even though E_{flex} may have been reduced to its minimum value, there may exist a significant amount of undetected rigid body

motion, which could dominate the motion of the beam, or any object connected to it. Therefore, a cost function was sought which represents all the beam energy due to its motion; the *flexural energy level* and the *rigid body kinetic energy, E_{rigid}*. The minimisation of this *total vibrational energy* cost function would therefore be superior and achieve the best vibration reduction.

Considering the rigid body kinetic energy of Beam 40 due to movement in the axial direction, globally the y-axis direction, the velocity of the centre of mass of the beam, v_{cm}, is given by the average of the y-axis velocities at the end of the beam. At beam ends 0 and 1 the velocities are,

$$v^0_{cm_y}(t) = \mathrm{Re}\{V^0_y e^{i\omega t}\} \quad , \quad v^1_{cm_y}(t) = \mathrm{Re}\{V^1_y e^{i\omega t}\}, \tag{2.49a,b}$$

where V^0_y and V^1_y are complex amplitudes. The instantaneous rigid body kinetic energy is thus described,

$$KE_y(t) = \frac{1}{2} m v^2_{cm}(t) = \frac{1}{2} m \left(\frac{v^0_{cm_y}(t) + v^1_{cm_y}(t)}{2} \right)^2, \tag{2.50}$$

where m is the total mass of the beam. For harmonic excitation the total time averaged kinetic energy is given by,

$$\overline{KE_y} = \frac{m}{16} \mathrm{Re}\left\{ V^0_y V^{0*}_y + 2 V^0_y V^{1*}_y + V^1_y V^{1*}_y \right\}. \tag{2.51}$$

The rigid body kinetic energy due to the translation of the centre of mass of the beam in its transverse sense, in the x-axis direction, can be expressed in terms of the scaled real part of the product of the x-axis velocities,

$$\overline{KE_{trans_x}} = \frac{m}{16} \mathrm{Re}\left\{ V^0_x V^{0*}_x + 2 V^0_x V^{1*}_x + V^1_x V^{1*}_x \right\}. \tag{2.52}$$

When the beam rotates as a rigid body about its centre of mass the rotational kinetic energy is

$$KE_{rot} = \frac{1}{2} I \dot{\theta}^2, \tag{2.53}$$

where I is the second moment of mass of the beam about its centre and $\dot{\theta}$ is the angular velocity of the beam. For small θ, the instantaneous kinetic energy can be expressed in terms of end velocities, $v^0_{cm_x}$ and $v^1_{cm_x}$

$$KE_{rot_x}(t) = \frac{mL^2}{24} \left(\frac{v^0_{cm_x}(t) - v^1_{cm_x}(t)}{L} \right)^2, \tag{2.54}$$

where L is the beam length. For harmonic excitation the average kinetic energy can be expressed by,

$$\overline{KE_{rot_x}} = \frac{m}{48}\mathrm{Re}\left\{V_x^0 V_x^{0^*} - 2V_x^0 V_x^{1^*} + V_x^1 V_x^{1^*}\right\}. \tag{2.55}$$

The x-axis velocity vectors therefore defines a combined measure of the x-axis translational and rotational rigid body kinetic energies as,

$$\overline{KE_{x,\theta}} = \frac{m}{12}\mathrm{Re}\left\{V_x^0 V_x^{0^*} + V_x^0 V_x^{1^*} + V_x^1 V_x^{1^*}\right\}. \tag{2.56}$$

Hence the total rigid body energy of the beam, E_{rigid}, is obtained from the sum of (2.51) and (2.56);

$$E_{rigid} = \frac{m}{48}\mathrm{Re}\left\{3V_y^0 V_y^{0^*} + 6V_y^0 V_y^{1^*} + 3V_y^1 V_y^{1^*} + 4V_x^0 V_x^{0^*} + 4V_x^0 V_x^{1^*} + 4V_x^1 V_x^{1^*}\right\}. \tag{2.57}$$

This can be expressed succinctly in the matrix equation, where u represents the entire bracketed term in (2.57),

$$E_{rigid} = \frac{m}{48}\mathrm{Re}\{u\} = \frac{m}{48}\mathrm{Re}\left\{\mathbf{u}_1^{\mathrm{H}}\mathbf{u}_2\right\}, \tag{2.58}$$

where $\mathbf{u}_1$ and $\mathbf{u}_2$ are defined as,

$$\mathbf{u}_1 = \begin{pmatrix} 3V_y^0 & 6V_y^0 & 3V_y^1 & 4V_x^0 & 4V_x^0 & 4V_x^1 \end{pmatrix}^{\mathrm{T}}, \tag{2.59a}$$

$$\mathbf{u}_2 = \begin{pmatrix} V_y^0 & V_y^1 & V_y^1 & V_x^0 & V_x^1 & V_x^1 \end{pmatrix}^{\mathrm{T}}. \tag{2.59b}$$

The change of the complex conjugation operation from $\mathbf{u}_1$ to $\mathbf{u}_2$ has no effect since the real part of u is taken. $\mathbf{u}_1$ may then be formed using the velocity vector, $\mathbf{v}$, defined in (2.31),

$$\mathbf{u}_1 = \mathbf{Q}_1\mathbf{v} = \begin{pmatrix} 0 & 3 & 0 & 0 & 0 & 0 \\ 0 & 6 & 0 & 0 & 0 & 0 \\ 0 & 0 & 0 & 0 & 3 & 0 \\ 4 & 0 & 0 & 0 & 0 & 0 \\ 4 & 0 & 0 & 0 & 0 & 0 \\ 0 & 0 & 0 & 4 & 0 & 0 \end{pmatrix} \begin{pmatrix} V_x^0 \\ V_y^0 \\ V_\theta^0 \\ V_x^1 \\ V_y^1 \\ V_\theta^1 \end{pmatrix}. \tag{2.60}$$

Similarly for $\mathbf{u}_2$,

$$\mathbf{u}_2 = \mathbf{Q}_2\mathbf{v} = \begin{pmatrix} 0 & 1 & 0 & 0 & 0 & 0 \\ 0 & 0 & 0 & 0 & 1 & 0 \\ 0 & 0 & 0 & 0 & 1 & 0 \\ 1 & 0 & 0 & 0 & 0 & 0 \\ 0 & 0 & 0 & 1 & 0 & 0 \\ 0 & 0 & 0 & 1 & 0 & 0 \end{pmatrix} \begin{pmatrix} V_x^0 \\ V_y^0 \\ V_\theta^0 \\ V_x^1 \\ V_y^1 \\ V_\theta^1 \end{pmatrix}. \tag{2.61}$$

Expressing the cost function (2.58) in linear form,

$$E_{rigid} = \frac{m}{96}\left(u + u^*\right), \tag{2.62}$$

where $*$ is the conjugate operator. After some manipulation E_{rigid} can be expressed in the simple linear matrix formulation using the velocity component scaling matrix **N**,

$$E_{rigid} = \frac{m}{96}\mathbf{v}^{\mathrm{H}}\mathbf{N}\mathbf{v}. \tag{2.63}$$

where **v** is the velocity vector (2.31), and

$$\mathbf{N} = \begin{pmatrix} 8 & 0 & 0 & 4 & 0 & 0 \\ 0 & 6 & 0 & 0 & 6 & 0 \\ 0 & 0 & 0 & 0 & 0 & 0 \\ 4 & 0 & 0 & 8 & 0 & 0 \\ 0 & 6 & 0 & 0 & 6 & 0 \\ 0 & 0 & 0 & 0 & 0 & 0 \end{pmatrix}. \tag{2.64}$$

Expanding (2.63) using (2.30) the cost function can be expressed in quadratic form,

$$E_{rigid} = \frac{m}{96}\left(\mathbf{f}_s\mathbf{Y}^{\mathrm{H}}\mathbf{N}\mathbf{Y}\mathbf{f}_s + \mathbf{f}_s^{\mathrm{H}}\mathbf{Y}^{\mathrm{H}}\mathbf{N}\mathbf{v}_p + \mathbf{v}_p^{\mathrm{H}}\mathbf{N}\mathbf{Y}\mathbf{f}_s + \mathbf{v}_p^{\mathrm{H}}\mathbf{N}\mathbf{v}_p\right). \tag{2.65}$$

2.4.2 MINIMISING THE TOTAL VIBRATIONAL ENERGY OF THE BEAM

A global cost function is defined which is the *total vibrational energy* of Beam 40 of the structure, E_{total}, combining flexural energy and rigid body kinetic energy,

$$E_{total} = E_{flex} + E_{rigid}. \tag{2.66}$$

This is the sum of two quadratic functions (2.46) and (2.65) resulting in another quadratic form which when expressed in the general quadratic form (2.41) the coefficients are,

$$\mathbf{A} = \frac{1}{4c_d}\left(\mathbf{C}^{\mathrm{H}}\mathbf{Y} + \mathbf{Y}^{\mathrm{H}}\mathbf{C}\right) + \frac{m}{96}\mathbf{Y}^{\mathrm{H}}\mathbf{N}\mathbf{Y}, \tag{2.67a}$$

$$\mathbf{b} = \frac{1}{4c_d}\left(\mathbf{C}^{\mathrm{H}}\mathbf{v}_{\mathrm{p}} + \mathbf{Y}^{\mathrm{H}}\mathbf{f}_{\mathrm{p}}\right) + \frac{m}{96}\mathbf{Y}^{\mathrm{H}}\mathbf{N}\mathbf{v}_{\mathrm{p}}, \tag{2.67b}$$

$$c = \frac{1}{4c_d}\left(\mathbf{f}_{\mathrm{p}}^{\mathrm{H}}\mathbf{v}_{\mathrm{p}} + \mathbf{v}_{\mathrm{p}}^{\mathrm{H}}\mathbf{f}_{\mathrm{p}}\right) + \frac{m}{96}\mathbf{v}_{\mathrm{p}}^{\mathrm{H}}\mathbf{N}\mathbf{v}_{\mathrm{p}}. \tag{2.67c}$$

The optimum secondary force vector, and the minimum cost function value are given in (2.42) and (2.44) with the values of **A**, **b** and c as given in (2.67).

The minimum value of the cost function is obtained if **A** is positive definite. The first term is positive definite for all secondary actuator positions except on Beam 40 (see Section 2.3). The second term is quadratic as **N** is real symmetric and hence semi-positive definite. The sum of a semi-positive definite function and a positive definite function results in positive definite function.

2.4.3 MINIMISATION OF THE SUM OF THE SQUARES OF THE TRANSLATIONAL JOINT VELOCITIES

The first velocity-based cost function studied, J_{trans}, uses the sum of the squares of the translational velocity components at the ends of beam 40. These measurements can be readily obtained using standard accelerometers with the relevant orientations. To be consistent with the cost function derived in the following section, this cost function is scaled so that it is equal to the sum of the rigid body kinetic energies of each half-beam length of beam 40. The time averaged values of kinetic energy at end 0, for example, of Beam 40 in the x-axis and y-axis directions are therefore,

$$\overline{KE_x^0} = \frac{m}{8}\left|V_x^0\right|^2 \quad , \quad \overline{KE_y^0} = \frac{m}{8}\left|V_y^0\right|^2, \tag{2.68a,b}$$

for harmonic excitation. The velocity component adhering to previous notation (2.49). A reduced velocity vector, containing only translational components, may be achieved by pre-multiplying the velocity vector defined in (2.31) with the matrix **P**,

$$\mathbf{P} = \frac{m}{8}\mathrm{diag}\begin{pmatrix}1 & 1 & 0 & 1 & 1 & 0\end{pmatrix}. \tag{2.69}$$

The cost function J_{trans} is then,

$$J_{trans} = \mathbf{v}^{\mathrm{H}}\mathbf{P}\mathbf{v}. \tag{2.70}$$

Expanding with (2.30) results in a quadratic function of the form (2.41) where,

$$\mathbf{A} = \mathbf{Y}^{\mathrm{H}}\mathbf{P}\mathbf{Y}, \tag{2.71a}$$

$$\mathbf{b} = \mathbf{Y}^{\mathrm{H}}\mathbf{P}\mathbf{v}_{\mathrm{p}}, \tag{2.71b}$$

$$c = \mathbf{v}_{\mathrm{p}}^{\mathrm{H}}\mathbf{P}\mathbf{v}_{\mathrm{p}}. \tag{2.71c}$$

The optimum secondary force vector, and the minimum cost function value are given in (2.42) and (2.44) with the values of **A**, **b** and c as given in (2.71).

2.4.4 MINIMISATION OF THE WEIGHTED SUM OF THE SQUARES OF ALL VELOCITY COMPONENTS

In order to provide a more comprehensive velocity-based cost function, the angular velocity at each joint could also be measured. Even though devices to measure angular velocity are not as commonplace as their translational counterparts, low-cost practical devices are readily available. Intuitively, it is a good strategy to reduce all the velocity components at the ends of the beam, to ideally zero. A cost function that pursues this aim is the sum of the squares of all the velocity components. However the arbitrary combination of the squares of the translational and rotary components will produce a cost function in which the relative 'weighting' between these two different quantities will depend on the system of units (*e.g.*, CGS, SI *etc*) in which the cost function is defined. Whilst it is not possible to rigorously define this weighting, for anything other than solely rigid body motion, an attempt is made to produce a sensible weighting. This weighting is achieved by considering the kinetic energy represented by both the linear and rotational velocity components. This cost function is easier to implement in practice than the total energy cost function, since the measurement of flexural energy requires the inter-beam coupling forces, which are not as easily obtained as a velocity measurement, especially more so if the application of active control was an 'add-on' to an existing structure.

To determine a sensible weighting the beam is considered as two half-lengths. The halves are assumed to move as rigid body levers whilst being hinged about the joints at the beam ends. Each translational velocity component is then assumed to represent the kinetic energy of a lumped mass equal to the mass of half of beam 40. Each rotational velocity component is assumed to represent the kinetic energy due to the rotation of the distributed mass of each half-beam length 'lever'. This may appear to disregard the flexural motion of the beam - however in the frequency region considered only the first transverse mode is significant. Considering the beam as two 'rigid body' halves allows the first transverse mode to be approximated, giving some credence to this approximation.

The kinetic energy of each half-length of beam 40 due to the translation in the x-axis and y-axis directions is as given above in the derivation of the cost function J_{trans}, (26). Considering the average rotational kinetic energy of one-half of beam 40 with distributed mass, this is

represented using the rotational velocity component at the beam end. So, at end 0 this is given by,

$$\overline{KE_{\theta}^{0}} = \frac{m}{96}\left|V_{\theta}^{0}\right|^{2}. \tag{2.72}$$

The relative scaling between the translational and rotational components is therefore shown in (2.68) and (2.72). A diagonal pre-multiplying matrix $\mathbf{L}$ which allows the velocity squared cost function J_{all} to be written using the velocity vector defined in (2.31),

$$J_{all} = \mathbf{v}^{\mathrm{H}}\mathbf{L}\mathbf{v}, \tag{2.73}$$

where $\mathbf{L}$ is

$$\mathbf{L} = \frac{m}{8}\mathrm{diag}\left(1 \quad 1 \quad \frac{1}{12} \quad 1 \quad 1 \quad \frac{1}{12}\right). \tag{2.74}$$

Expanding (2.73) with (2.30) results in a quadratic function of the form (2.41) where

$$\mathbf{A} = \mathbf{Y}^{\mathrm{H}}\mathbf{L}\mathbf{Y}, \tag{2.75a}$$

$$\mathbf{b} = \mathbf{Y}^{\mathrm{H}}\mathbf{L}\mathbf{v}_{\mathbf{p}}, \tag{2.75b}$$

$$c = \mathbf{v}_{\mathbf{p}}^{\mathrm{H}}\mathbf{L}\mathbf{v}_{\mathbf{p}}. \tag{2.75c}$$

The optimum secondary force vector, and the minimum cost function value are given in (2.42) and (2.44) with the values of **A**, **b** and c as given in (2.75).

2.5 FREQUENCY-AVERAGED MEASURES OF VIBRATION AND DEFINITION OF PERFORMANCE IMPROVEMENT

In previous sections various parameters representing the vibration of a beam have been derived. It is usually more useful to assess vibration over as an average over a frequency band. This is defined here for a generic parameter or cost function, *CF*, and is the same as the specific case defined (2.47). The frequency average $\langle CF \rangle$ is thus defined,

$$\langle CF \rangle = \frac{1}{n}\sum_{k=1}^{n} CF\left(\omega_{L} + (k-1)\Delta\omega\right), \tag{2.76}$$

where n is the number of frequency steps, $\Delta\omega$ the angular frequency spacing and ω_L the lower angular frequency point. Two frequency bands are used in the work presented here, both have a common frequency spacing such that $\Delta\omega/2\pi$ is 5Hz.

In the study of the reduction of the vibration transmission of the structure, the improvement is measured by the reduction in one of the parameters representing the vibration in Beam 40. Where the reduction is specified using decibels, this is defined as α_{vib},

$$\alpha_{vib} = 10\log\left(\frac{CF_{unopt}}{CF_{opt}}\right), \tag{2.77}$$

where CF_{unopt} is the value of the generic cost function, CF, for the unoptimised structure, and CF_{opt} is the optimised (reduced) value.

2.6 ANALYSIS OF POWER IN STRUCTURE

To understand the mechanisms of the vibration reduction in Beam 40 of the structure, the power reduction is split into constituent parts, whose definitions are now derived. The reductions in the vibrational energy of Beam 40 of the structure achieved by geometric redesign can be attributed to one of two factors; the reduction in the power input to the structure and the redistribution of the power dissipated in the beams such that a smaller proportion in dissipated in Beam 40. The total reduction in the power dissipated in Beam 40 due to optimisation is defined as,

$$\tau_{TOT} = \frac{P_{40}^{unopt}}{P_{40}}, \tag{2.78}$$

where P_{40}^{unopt} and P_{40} are the values of power dissipated in Beam 40 before and after optimisation. The input power to the structure is dissipated in all the beams of the structure. The ratio of the input power, P_{in}, to P_{40} may be expressed as the sum of the power dissipated in all the beams of the structure, which is denoted for each beam N as, P_N. This is defined for both an optimised structure and the unoptimised structure as,

$$\tau = \frac{P_{in}}{P_{40}} = \frac{\sum_{N=1}^{40} P_N}{P_{40}}, \tag{2.79}$$

$$\tau^{unopt} = \frac{P_{in}^{unopt}}{P_{40}^{unopt}} = \frac{\sum_{N=1}^{40} P_N^{unopt}}{P_{40}^{unopt}}, \tag{2.80}$$

where τ^{unopt} and τ represent the power distribution between Beam 40 and the rest of the structure for the unoptimised and optimised structures respectively and an increase in the value indicates the redistribution of power within the structure as to reduce the power in Beam 40. (2.78) can then be expressed as the product of two factors; one describing the reduction of the input power and the other the change in the power dissipation distribution within the structure,

$$\tau_{TOT} = \frac{P_{40}^{unopt}}{P_{40}} = \frac{P_{in}^{unopt}}{P_{in}} \frac{\tau}{\tau^{unopt}}. \tag{2.81}$$

(2.81) may be expressed using decibels,

$$10\log\left(\frac{P_{40}^{unopt}}{P_{40}}\right) = 10\log\left(\frac{P_{in}^{unopt}}{P_{in}}\right) + 10\log\left(\frac{\tau}{\tau^{unopt}}\right). \tag{2.82}$$

Thus the reduction in power dissipation level in Beam 40, α_{TOT}, may be expressed as the sum of the reduction in the input power level to the structure α_{INPUT}, and the change in the *power redistribution* level, α_{REDIST},

$$\alpha_{TOT} = \alpha_{INPUT} + \alpha_{REDIST}, \tag{2.83}$$

where the terms in (2.83) directly correspond to those in (2.82).

When Active Vibration Control techniques are applied to the structure, each actuator can provide a source or a sink of energy. Assuming the actuators are placed on beams *A*, *B* and *C*, the power dissipated (or absorbed) by these beams is represented by P_A, P_B and P_C. Negative values indicate that the actuators are sourcing (or supplying) power to the structure. Separating the actuator power terms, (2.80) becomes,

$$\frac{P_{in}}{P_{40}} = \frac{\sum_{N=1}^{40} P_n + P_A + P_B + P_C}{P_{40}}. \tag{2.84}$$

(2.84) assumes an AVC system with three actuators, but is easily adapted to systems with less actuators. Similarly as for (2.81), (2.78) can be expressed as the product of three factors,

$$\tau_{TOT} = \frac{P_{40}^{unopt}}{P_{40}} = \frac{P_{in}^{unopt}}{P_{in}} \tau_{ACF} \frac{\tau'}{\tau^{unopt}}, \tag{2.85}$$

where τ_{ACF} is the *actuator contribution factor*, and is defined,

$$\tau_{ACF} = 1 + \frac{P_A + P_B + P_C}{\sum_{\substack{N=1 \\ N \neq A,B,C}}^{40} P_N}. \tag{2.86}$$

Its meaning is explained below, with respect to its logarithmic form. τ' is the *passive redistribution factor*, which is similar to τ in (2.79), but it does not include all the beams on the structure, only passive beams (those not containing an actuator), and is given by,

$$\tau' = \frac{1}{P_{40}} \sum_{\substack{N=1 \\ N \neq A,B,C}}^{40} P_N . \tag{2.87}$$

Expressing (2.85) in decibels, in the same way as for (2.82), yields,

$$\alpha_{TOT} = \alpha_{INPUT} + \alpha_{ACF} + \alpha'_{REDIST} , \tag{2.88}$$

where α_{ACF} is the reduction in level due to the actuator contribution, α'_{REDIST} is the attenuation due to the redistribution of the power between Beam 40 and the rest of the passive beams in the structure. α_{ACF} is defined,

$$\alpha_{ACF} : \begin{cases} P_A + P_B + P_C > 0 & +ve \\ P_A + P_B + P_C = 0 & 0 \\ -\left(\sum_{\substack{N=1 \\ N \neq A,B,C}}^{40} P_N \right) < P_A + P_B + P_C < 0 & -ve \\ P_A + P_B + P_C \leq -\left(\sum_{\substack{N=1 \\ N \neq A,B,C}}^{40} P_N \right) & not \quad defined. \end{cases} \tag{2.89}$$

Thus α_{ACF} is positive if the net actuator contribution is to absorb power from the structure, and negative if the net contribution is to supply power to the structure. However, it is not defined is the net power supplied is greater than the power dissipated in all the passive beams. In this case the primary force input to the structure would be absorbing power from the structure.

GLOSSARY OF SYMBOLS FOR CHAPTER 2

The major notation used in this chapter is listed below. Other symbols are defined locally.

$\mathbf{A}$	Hermitian matrix
$\mathbf{b}$	Complex vector
c_d	Common beam damping value
c	Complex scalar
$\mathbf{C}$	Transformed transfer impedance matrix
$\mathbf{C}'$	Transfer impedance matrix
$\mathbf{C}_s$	Structural coupling matrix
$e^{i\omega t}$	Complex time phasor
$\mathbf{E}$	Vector of displacement components from externally applied forces
E_{flex}	Flexural energy of Beam 40
e_N	Energy level of beam N
E_{rigid}	Value of total kinetic energy due to rigid body movement of Beam 40
E_{total}	Total vibrational energy of Beam 40
$\mathbf{f}$	Net force vector for Beam 40
$\mathbf{f}_p$	Force vector for Beam 40 due to primary input
$\mathbf{f}_s$	Vector of secondary forces
$\{\mathbf{f}_N\}^a$	Force vector for beam N at end a, defined in local coordinates
$\mathbf{F}$	Individual beam end force vector for structure
$\mathbf{F}_{XN}^a$	Power vector for beam 40 at end a, defined in global coordinates
$[\mathbf{G}_N]^{ab}$	Green function matrix for beam N with input at a and response at b
I	Second moment of mass of Beam 40 about centre of mass
J	Generalised cost function value
J_{all}	Value of the scaled sum of the squares of all velocity components (kinetic energy due to rigid body motion of Beam 40)

J_{trans}	Value of the scaled sum of the squares of the translational velocity components (rigid body kinetic energy only due to translation of Beam 40)
$\overline{KE}$	Time-averaged kinetic energy component
L	Length of Beam 40
m	Mass of Beam 40
P	Power dissipated in Beam 40
P_{in}	Power input to structure after optimisation
P_{in}^{unopt}	Power input to structure before optimisation
P_N	Power dissipated in Beam N after optimisation
P_N^{unopt}	Power dissipated in Beam N before optimisation
P_o	Minimised dissipated power in Beam 40
$\{\mathbf{P}_N\}^a$	Power vector for beam N at position a, defined in global coordinates
$\{\mathbf{P}_N\}^{damp}$	Power dissipation vector for beam
$\mathbf{q}_s$	AVC total control effort
t	Time variable
$[\mathbf{T}_N]$	Global-local coordinate transformation matrix
$\mathbf{T}$	Transformation matrix
v_b^a	Instantaneous velocity at end a of Beam 40 in global direction b
$\mathbf{v}$	Net velocity vector for Beam 40
$\mathbf{v}_p$	Velocity vector for Beam 40 due to primary input
V_b^a	Complex velocity amplitude at end a of Beam 40 in global direction b
$\{\mathbf{V}_N\}^a$	Velocity vector for beam N at end a, defined in global coordinates
$\mathbf{V}_{XN}^a$	Power vector for beam 40 at end a, defined in global coordinates
$\mathbf{x}$	General complex vector
$\{\mathbf{x}_N\}^a$	Displacement vector for beam N at end a, defined in local coordinates
$\{\mathbf{X}_N\}^a$	Displacement vector for beam N at end a, defined in global coordinates
$\mathbf{Y}$	Transformed transfer mobility matrix

$\mathbf{Y}'$	Transfer mobility matrix
α_{ACF}	Power level reduction in Beam 40 due to operation of AVC
α_{INPUT}	Power level reduction in Beam 40 due to reduction in input power
α_{REDIST}	Power level reduction in Beam 40 due to power redistribution in structure
α'_{REDIST}	Power level reduction in Beam 40 due to power redistribution in structure between passive beams
α_{TOT}	Total power reduction in Beam 40
θ	Rotation of Beam 40
τ	Power redistribution between Beam 40 and the rest of the beams in the structure after optimisation
τ'	Power redistribution between Beam 40 and the rest of the passive beams in the structure after optimisation
τ_{ACF}	Actuator contribution factor
τ_{TOT}	Reduction in power dissipated in Beam 40 due to optimisation
τ^{unopt}	Power redistribution between Beam 40 and the rest of the structure before optimisation
ω	Angular frequency
ω_L	Lower angular frequency
$\Delta\omega$	Angular frequency spacing
$\langle\cdot\rangle$	Frequency-averaged value

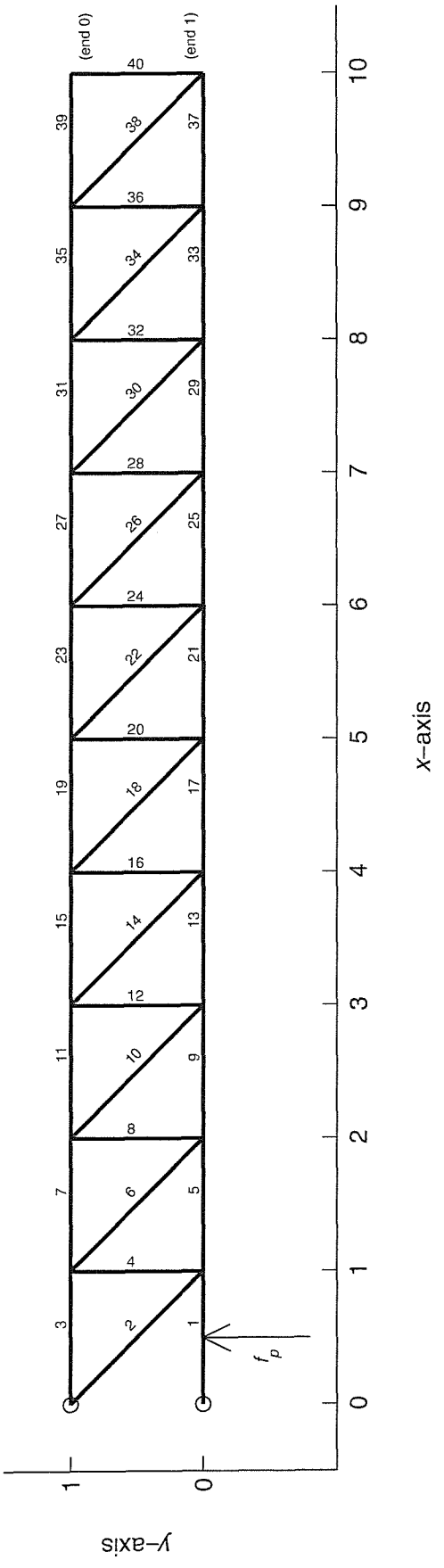

Figure 2.1: Two-dimensional cantilever structure used as the subject of optimising (minimising) the vibration transmission from the base to Beam 40. The global coordinate system and the beam numbering is shown, and also the position of the primary force input, f_p.

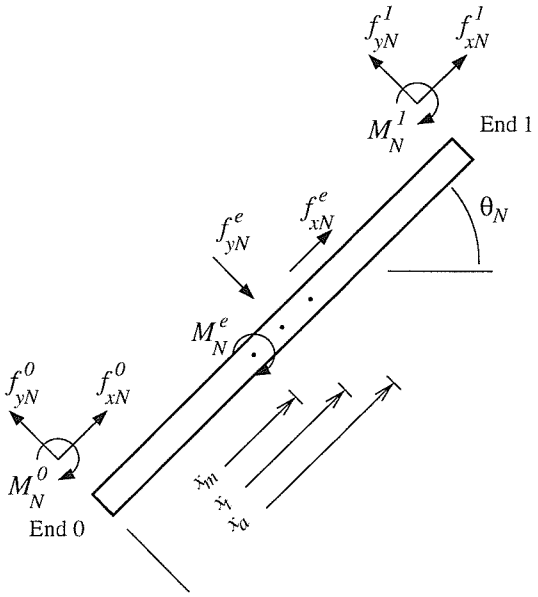

Figure 2.2: General notation of forces and moments at points of external application and at beam ends, with respect to local beam coordinates.

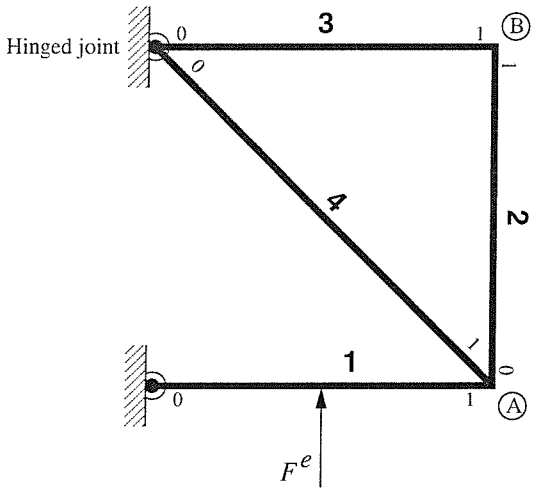

Figure 2.3: Small structure example used to illustrate the receptance model method.

CHAPTER 3

Introduction to Optimisation and Robustness Analysis Methods

3.0 INTRODUCTION

This chapter provides the background to the optimisation algorithms and methods of robustness analysis used in this thesis. Due to the combinatorially large size of some of the optimisation tasks addressed the use of traditional optimisation algorithms is either not possible or will not yield the best results. However, some initial design optimisations are performed using a small sample of traditional techniques for comparison. The traditional techniques used are briefly described, with supporting theory where applicable in an appendix. The genetic algorithm is a more recent optimisation technique which may be used to efficiently find good solutions to combinatorially large or multi-modal search space problems. An introductory qualitative background to genetic algorithms is supported by an appendix giving a more theoretical analysis to describe the expected performance. A more recent optimisation algorithm called Dynamic Hill Climbing, which is a heuristic method which combines elements of stochastic methods and traditional techniques, and is also described.

Whilst optimisation algorithms are generally applied to search for optimal results under nominal conditions, if any one of these solutions is very sensitive to small changes in any of the optimisation variables then the predicted performance may not be practically realisable. This may be either because engineering tolerances are greater than the accuracy of the computer model, or due to changes experienced to any of the optimisation variables in the use of the design. Solutions that are not sensitive to such changes are called *robust*. These solutions are more desirable in practice, even if this is a compromise with the performance of the system under nominal conditions. Robustness analysis is performed on all the optimisation candidates produced in the work detailed in Chapters 4, 5 & 6 using a technique of re-evaluating the design with an ensemble of random perturbations and this method is formally described. In Chapter 7 the use of robustness as an integral part of the performance of the structure in the optimisation process is studied. First it is necessary to achieve a more efficient measure of robustness, and a technique using computer experiments based on orthogonal arrays is assessed, which originates from the field of statistical experimental design and more recently in the field of quality control. The properties of such orthogonal arrays are discussed and a small

array is derived as an example. The second technique, incorporating robustness into the design model is an extension of the standard genetic algorithm in which the interaction between the genetic information and its environment is modelled. In the same way that for individuals to survive they must be both fit and robust in biological systems, the use of additive random perturbations to the phenotype within the genetic algorithm is used to achieve a similar goal: design solutions with optimal and robust performance.

Throughout this chapter reference is made to the Design Exploration System used by the author for the majority of the optimisation work presented in this thesis. This is a software application containing a wide range of optimisation algorithms, and allows integration with user written code. For brevity this will subsequently be referred to in this chapter by its proprietary name: OPTIONS (Dynamics Modelling Ltd., 1996).

3.1 INTRODUCTION TO OPTIMISATION

Optimisation is the problem of finding the minimum value of a scalar quantity, E, which is a function of other variables, called *optimisation variables*. The task is therefore to find the optimum values of these variables. Hence, if U is the value of a function f (the *objective function*), which is multivariate then, expressed mathematically, optimisation is defined,

$$\begin{aligned} &\min U = \min f(\mathbf{x}) = f(\mathbf{x}_o) \\ &\mathbf{x} = \{x_1 \quad x_2 \quad x_3 \quad \ldots\ldots \quad x_n\} \end{aligned} \tag{3.1}$$

where $\mathbf{x}$ is the vector of n optimisation variables. The optimal optimisation variables are denoted by the vector $\mathbf{x}_0$. In some cases, the object of optimisation may be to *maximise* the objective function, this however, may still be expressed and dealt with as a minimisation task, since,

$$\max f(\mathbf{x}) \equiv \min(-f(\mathbf{x})), \tag{3.2}$$

and thus there is no loss of generality in studying the minimisation of an objective function.

The value of the objective function over all possible values of $\mathbf{x}$ forms a multi-dimensional surface, which is often termed the *search space*. Most optimisations have a search space that is bounded by extreme limits on the values of each of the optimisation variables. In addition other constraints may be enforced which are due to limits on the values of parameters (called *constraints*), which are functions of the optimisation variables. These constraints may be either equality constraints or inequality constraints. One final form of constraint is that one or more of the optimisation variables may only assume one of a set of discrete values. This is not

considered here as, even though such a constraint is required in the combined discrete/continuous variable optimisation reported in Chapter 6, it is achieved in a different way. The regions of the search space that do not violate any constraints are called *feasible*, similarly regions where any constraint is violated are called *infeasible*. Thus as well as defining an outer boundary to the search space is it also possible to have isolated infeasible regions within these boundaries.

Thus to complete the mathematical expression of optimisation, (3.1) it must then be additionally subject to the constraints,

$$\psi_i(\mathbf{x}) = 0 \qquad i = 1, p\,, \tag{3.3a}$$

$$\phi_j(\mathbf{x}) \geq 0 \qquad j = 1, q\,. \tag{3.3b}$$

The objective function is thus optimised subject to p equality constraints and q inequality constraints. By convention the inequality constraints are non-negative, positive-bound constraints are achieved by specifying $-\phi_j$ instead.

To keep the search within feasible regions, *penalty* functions can be used to penalise the value of the objective function, so as to make the value of the objective function in such regions extremely undesirable and force the search back to feasibility. In effect this is achieved by distorting the search space in or near regions of infeasibility. Two types of penalty function are available with the OPTIONS software used, and both are briefly described.

The first, and simplest penalty function, requires no significant additional computational overhead. It simply adds a correction to the objective function on the same pass as its evaluation, and only in regions external to feasibility, otherwise it has no effect. For this reason it is referred to here, as in the OPTIONS manual, as the One Pass External penalty function. The penalised objective function, U_p, is

$$U_p = U(\mathbf{x}) + r\sum_{i=1}^{p}|\psi_i| + r\sum_{j=1}^{q}\langle\phi_j\rangle, \tag{3.4a}$$

where the $\langle\ \rangle$ operator defines the operation

$$\langle\alpha\rangle = \begin{cases} \alpha & , \quad \alpha \leq 0 \\ 0 & , \quad \alpha > 0 \end{cases} \tag{3.4b}$$

The value of r used is typically 10^{20}. Whilst being generally successful in its application the penalty it provides is very severe, and it can sometimes stall a search prematurely. This can occur if the minimum in the feasible region lies on, or close to a constraint boundary. If the

search reaches the constraint boundary it will then attempt to crawl along this boundary to find the minimum. If the search direction is coincidentally aligned with the constraint boundary the steep wall imposed by this penalty function can fool the search to prematurely terminate as it would need to pass through regions of increasing value in the search space to find lower regions further along the boundary. The action of the One Pass External penalty function is illustrated in one degree of freedom in Figure 3.1.

Another widely used penalty function is that proposed by Fiacco and McCormick (1968, as cited by Siddall 1982). This penalty function begins to affect the value of the evaluated search space as a boundary constraint is approached from within the feasible region. It does not therefore tend to lead to the possible stalling of searches in these regions as with the One Pass External penalty function. However the evaluation of the penalised objective function normally requires a series of evaluations, with ever increasing severity, and hence it has a higher computational overhead. The form implemented in the OPTIONS package used, defines the penalised objective function, U_p, as

$$U_p = U(\mathbf{x}) + r^2 \sum_{k=1}^{k_s} \frac{1}{\phi_k^s} + \frac{1}{r} \sum_{i=1}^{p} \psi_i^{\,2} + \frac{1}{r} \sum_{j=1}^{q} \langle \phi_j \rangle^2 , \qquad (3.5)$$

where the $\langle\ \rangle$ operator is as described for (3.4). The leftmost penalty term is the summation of the reciprocal of the value of the satisfied constraints raised to the power s, the remaining two terms are only non-zero for unsatisfied constraints. The penalty is therefore comprised of one interior and two exterior terms which operate exclusively for each constraint. The penalised objective function is evaluated a number of times with a decreasing value of r, which initially is equal to one. The advantage of this recursive technique is that the current search point can move along the boundary towards the true constrained minimum instead of being pushed directly towards a point on the constraint boundary by the current search direction, as can occur with the One Pass penalty function. A search using a One Pass penalty function may then not be able to negotiate the 'brick wall' constraint boundary that may be masking a better minimum on or near the boundary.

The value of U_p from the previous pass is used as the starting point for the next pass. This process is repeated until the decrement in U_p falls below a set threshold, which is defined as a given fraction of the previous value of U_p. The effect of the penalty function depends upon whether the point in the current search space is feasible or infeasible. If feasible, as the search point approaches a constraint boundary the exterior term (with the initial value of r as unity) becomes small and the value of U_p increases asymptotically as the search point moves further towards the boundary. However as U_p is re-evaluated with a decreasing value of r this

asymptotic behaviour occurs nearer the actual constraint boundary, and the minimum point on the penalised search space tends towards the boundary and the true constrained minimum. This is shown for one-dimensional case in Figure 3.2, where the effect of decreasing r is shown. If the search point is in the infeasible region, then with r at unity, little effect on the search space is seen. As the value of r is successively decreased then the effect of the distortion caused by the asymptotic behaviour is also decreased. Hence the unconstrained minimum on the search space is distorted so that it is shifted towards the true constrained minimum.

The additional computational overhead is that required to re-evaluate (3.5) for each pass, which typically increases the computational load by a factor of 3. An efficient search strategy (Keane, 1999) is to commence a search using the One Pass External penalty function and then continue from the 'optimum' found using the Fiacco-McCormick penalty function. The use of the latter is to check whether the previous search had become stalled due to the reasons discussed above.

3.2 TRADITIONAL OPTIMISATION TECHNIQUES

Most traditional search algorithms rely on the fact that the search space is monotonically decreasing across all its dimensions. Therefore a path to the minimum points can be gleaned by, at simplest, taking steps in each dimension and determining the 'downhill' direction, or using gradient information for this.

The field of optimisation, even that using traditional techniques, is extremely large and still an area of much research. Indeed achieving a background in the state of the art is a daunting process, not unlike some optimisation tasks themselves. A relatively small number of basic approaches exist, but it is the number of different algorithms spawned from these approaches through the development of each one, and also refinements and combinations of approaches, which make this field so large.

The background of each of the algorithms which are used in Chapter 4 are now briefly explained, however it is outside the scope of this thesis to give more comprehensive details and the reader is referred to the references. Indeed different interpretations of the same algorithms cause even more variants, even though they are commonly described using the same name. As an example the OPTIONS software (used for the optimisations described in this thesis) contains as many as three different variants of some algorithms, commonly named, but available from different suites of software programs.

3.2.1 HOOKE AND JEEVES METHOD

The Hooke and Jeeves search method (Hooke and Jeeves, 1961, as cited by Siddall, 1982) is a direct search method; it does not require or calculate any gradient information about the search space. The optimum is found by taking steps in the directions of each of the axes, and maintaining the steps only if an improvement is made. When no further improvement can be made the step size is reduced. The minimum step size is one of the search parameters and when no further improvement is made at this point the search phase ends. Then the search space vicinity local to the current point is 'peppered' with a number of randomly placed points, for each of which the value of the objective function is additionally evaluated. If any of these points yields a better result, then this is used as the basis for a new search phase. More formally the search algorithm is:

1. Start at initial point in search space.

2. Make the current point the *base point*.

3. Make an *exploratory search* for each coordinate in turn: make an predetermined step in positive sense, if an improvement is seen retain the step, otherwise try for a negative sense, if no improvement is still made then maintain original coordinate.

4. A *pattern move* is then made for which steps are made in all coordinate directions. Each being the difference between the coordinate value for the current and previous base points. If an improvement is seen then maintain pattern move, otherwise cancel pattern move.

5. If the exploratory search has found a better point, then continue from 2, otherwise reduce step size by pre-determined amount and continue from 2.

6. If no improvement is found with the exploratory search and the step size has reached a pre-determined limit, then calculate the objective function at a number of randomly determined points in the vicinity of the current optimum. If any of these yields an improvement, make this point the initial point and repeat the search from 1.

In the implementation of this algorithm (SEEK from the Siddall suite of algorithms in OPTIONS), only two search phases are permitted. The local random based search at the end of the search phase helps to prevent the search stalling if the path is along a boundary constraint where the search may stall due to the coincidental alignment of the coordinate system. This will help to prevent stalling on a constraint boundary even when using the One Pass External constraint.

3.2.2 DAVIDON-FLETCHER-POWELL (DFP) & BROYDEN-FLETCHER-GOLDFARB-SHANNO (BFGS) VARIABLE METRIC METHODS.

Variable metric methods (also called quasi-Newton methods) compute and update stored gradient information about the search space, which is used by the algorithm. Two such methods are Davidon-Fletcher-Powell (DFP) and Broyden-Fletcher-Goldfarb-Shanno (BFGS). In both methods the search space is assumed to be quadratic (so that all partial derivatives of order three and greater are zero). This, of course, is not always true. However using this second order approximation to the search space, applied iteratively, the (local) minimum can be attained. These methods are very similar and the BFGS method is actually a refinement of the DFP method, affecting the update of an estimate of the Hessian matrix. The effect is small, only affecting issues such as the convergence tolerance and round-off error.

Both algorithms are well known and widely used in the field of optimisation. Thus full details are given in Appendix B, and also in (Press *et al*, 1992) for the interested reader.

3.2.3 DYNAMIC HILL CLIMBING

Dynamic Hill Climbing is not a traditional technique, in fact the technique first described by Yuret and de la Maza (1993) in conference proceedings and then in more detail in Yuret's Masters thesis (Yuret, 1994), is approximately 20 years more recent than the introduction of genetic algorithms by Holland (1975). In general the use of this technique has not been well reported, however El-Beltagy and Keane (1998), for example, have applied the technique to a multi-peaked deceptive problem and found that it performs competitively with other popular algorithms (including genetic algorithms in some circumstances). The technique is also one of those included in the suite of optimisers in the OPTIONS package, and hence was readily available to the author.

It is outside the scope of this thesis to fully describe the operation of the algorithm, which is fully described in Yuret (1994). It has, in fact, more operations than a basic genetic algorithm (which is described below). A brief résumé of the algorithm follows:

Whilst genetic algorithms have been used successfully, there are several factors which could be improved upon, according to Yuret. Although genetic algorithms are good for finding regions containing local optima, they are not particularly efficient or good at finding the actual value of each optimal peak, that is, they are not very good hill climbers. Dynamic Hill Climbing therefore has two distinct parts, or *heuristics*. The first is finding the peak of a local region, the local optima. For this Yuret uses two heuristics: one whose step size changes to adapt to the local terrain; the second is one which the directions of each step adapt to the directions of those where recent success has been found. The later has a similar effect to changing the coordinate

system, so that, the most successful direction is represented by a single step and not a combination of others.

Having found a local optimum, the second part of the algorithm is concerned with restarting the search at a point in the search space that is distinct from all previously discovered local optima. In this way diversity in the algorithm is ensured and also the possibility of re-visiting local optima more than once severely reduced. For high dimensional problems a random point in the search space is shown to be very likely to be distant from any other point, whereas for low dimensional search spaces a point randomly placed in the largest interval between previous optima is used.

3.3 GENETIC ALGORITHMS

Genetic algorithms assign new sets of optimisation variables from combinations of a current set of optimisation variables under some strategy in which, on average, those having better values of evaluated objective function are more likely to survive (in rather simplistic terms). Traditional methods of design optimisation often rely on gradient-based methods and where the search space is continuous and uni-modal (and convex) they can perform very efficiently. In designs where the search space is multi-modal and contains many sub-optima these methods can result in a sub-optimal design choices as only the local neighbouring search space is explored. Additionally if the search space is discontinuous then such methods cannot be used.

Evolutionary algorithms have emerged in recent years as being an effective and efficient optimisation technique. They are a stochastic-based class of optimisers, that are not random searches but have random elements in their algorithms that provide diversity to the search enabling all areas of the search space to be available for possible search progression, from any one point within the space. Evolutionary algorithms are best suited to finding optimal solutions to highly combinatorial problems, where an exhaustive search is not practicable or where the surface to be evaluated is multi-modal. In such circumstances the multiple local maxima would deceive conventional gradient searching algorithms.

Evolutionary algorithm is a generic term for a number of guided random search methods, of which the most popular two are genetic algorithms and simulated annealing. In general, genetic algorithms sample the search space more diversely, however simulated annealing has the advantage of requiring less computational effort. The choice, implementation and success of evolutionary algorithms is dependent upon the application. Keane (1995a) shows how different evolutionary algorithms sample a 'difficult' search space. The value of combining algorithms, like genetic algorithms and simulated annealing, is also shown. In the optimisation application

considered in this thesis, genetic algorithms have been used to enable comparison and verification of the work done by Keane (1995b), who had previously found them to be the most preferable optimisation method for the particular problem considered in this thesis.

For the type of problem for which evolutionary algorithms are often applied it can never normally be established whether the true global optimal solution has been found. If repeated application of the algorithm yields near-optimal solutions and in most cases these out perform the existing design, then seeking the true globally optimum design is often not a necessity. In many applications there is little difference in performance between the near-optimal and globally optimal solutions.

3.3.1 GENERAL DESCRIPTION

Genetic algorithms are based on an abstraction of biological evolution. The genetic algorithm was first reported by Holland (1975) but has been publicised mainly through the work of Goldberg (1989). The optimisation process 'evolves' from one generation of design solutions to the next by a process of 'natural selection'. Each generation is formed from a population of a set of *chromosomes* which are themselves strings of numbers (normally binary) representing all of the optimisation variables. The total genetic information contained in a string (each of which represents a design solution) is termed a *genotype*. As in biological systems the organism is formed from the genotype and its interaction with its environment, the result of which is termed a *phenotype*. This is put more into an engineering context by Bäck *et al* (1997a) where they suggest that the phenotype space represents the physical parameters to be optimised, while the genotype space is the representation of these parameters by the algorithm in, for example, binary strings. Thus any quantisation effects occurring in the phenotype representation can readily be seen as 'noise'. The fitness of each phenotype is evaluated by an objective function (or *fitness function*). The value of this function is minimised (or maximised dependant on the specific problem) in order to achieve the optimised design, and thus the smaller the value of each evaluated phenotype the fitter the set of chromosomes (or design solutions) it represents.

The genetic algorithm is initialised with a pool of chromosome strings. Each subsequent generation is then achieved by three key operations: selection, crossover and mutation. A number of the previous generation's chromosomes are selected such that those with greater fitnesses have a higher probability of selection. Some of these chromosomes are then 'mated' in pairs; two mating chromosomes swap information beyond a crossover point which is randomly selected, and two offspring thus result. This is illustrated in Figure 3.3. The new generation is made up of a proportion of newly formed and existing chromosomes from the previous generation. The last operation, mutation, is a random bit change in a chromosome 'bit' with a

small probability, as illustrated in Figure 3.4. The value of the bit is inverted for a binary alphabet. This provides random diversity in the evolution and helps to prevent premature convergence before too little evolutionary experience has been gained.

Only the basic operations necessary to define a genetic algorithm have been described above. There are many additional operations which are applied to improve performance. One such improvement is to prevent 'crowding' (normally termed *niching* or *sharing*) where too many similar individuals exist in the vicinity of a local optimum and dominate a population. This discourages diversity in the search. Further details are available in the general references given at the end of this sub-section.

The average fitness of each generation successively increases and the process is halted after a number of generations by a suitable convergence criterion. Normally the best solution encountered through the entire optimisation is taken as the result. This is achieved using the *elitist* strategy so that the best-so-far solution is guaranteed to survive into the next generation. Goldberg (1989) analysed the underlying nature of the algorithm using *schemata* to represent common patterns within the strings (a subset of the search space). Schemata (singular: schema) are chromosome templates which represent a set of chromosome strings that have common features. He showed that the schemata with higher fitnesses experience on average exponentially increasing trials in subsequent generations. The bias towards particular schema, representing a number of solutions, implies an *implicit parallelism* so that the search space is sampled diversely and efficiently. This is discussed further in the next section. More recently there has been much critical discussion regarding the early work of Goldberg (as for example reported in Mitchell, 1996). In particular many caveats in his schema analysis have been shown, especially when considering that a finite population is used in practice. However this analysis still demonstrates the 'mechanism' by which genetic algorithms achieves better solutions, by (after Mitchell, 1996) *discovering* promising solutions, *emphasising* their significance in each population and *recombining* them to (possibly) produce even better solutions.

A more complete description of genetic algorithms is available from Goldberg (1989), a well referenced book which provides a good introduction to the early use of genetic algorithms, or more recently Mitchell (1996), for example, or more comprehensive texts (Bäck et al, 1997b) on the entire area of evolutionary algorithms.

3.3.2 THEORETICAL ANALYSIS

As discussed in the previous section, although recently both more rigorous and critical analysis of the schema theorem has been performed (Mitchell, 1996), the theorem still estimates the

growth of fitter chromosome strings through evolution, and thus remains of use. The theorem is also used as a basis for the analysis in the next section. However, the shortcomings of the theorem are also briefly discussed below.

The analysis of the operation of genetic algorithms was studied by Goldberg using schemata to represent sets of chromosomes by defining the values of the chromosomes at some positions and allowing others to adopt any possible value. Using these the survival of each schema (and all the chromosomes it represents) may be analysed. The result of this analysis is the well known Schema Theorem or the Fundamental Theorem of Genetic Algorithms (Goldberg, 1989),

$$m(H,t+1) \geq m(H,t)\frac{f(H,t)}{\overline{f(t)}}\left(1-p_c\frac{d(H)}{l-1}-O(H)p_m\right), \tag{3.6}$$

which defines the number of schema H in a current population from the number in the previous generation. $m(H,t)$ is the number of schema H at generation t. $f(H,t)$ is the average fitness of the schema H and $\overline{f(t)}$ the average fitness of the entire population containing chromosomes of length l. $d(H)$ and $O(H)$ are the defining length and order of schema H respectively. These are defined by example in Figure 3.5 and more fully in Appendix B. p_c and p_m are the probability of crossover and mutation respectively. For readers unfamiliar with the Schema Theorem, this is derived in Appendix B. The existence of the inequality in (3.6) stems partly from the probability that during a crossover operation a chromosomes may be spilt within its defining length, but this may have no effect due to similarities between the schema pair. Also, only the disruptive effects of crossover and mutation on schema H are considered (Mitchell, 1996). It is also feasible that these operations on instances of other schemata will generate instances of H.

Mitchell (1996) also discusses other areas where the Schema analysis is misleading or often misinterpreted. The implicit parallelism previously mentioned is the term coined by Holland to indicate that by processing the chromosome strings in a population the algorithm is implicitly processing all the schemata whose instances fall within the population. However this does not imply that the fittest individual of any schema will be found, it will be the schema with the best-observed fitness, and this is based on the actual instances occurring within the population. In general, it is in the realisation of using a finite population where the Schema Theorem starts to fail. For example, at a later stage in the evolution there will be a larger proportion of fitter strings and less unfit strings. With only a relatively small number of the latter the estimate of an unfit schema can be unreliable if the performance is judged on very few individuals. However, the basis by which the basic genetic algorithm achieves the net probabilistic effect of selecting the fitter individuals in each generation is seen, despite the inaccuracies discussed.

This discussion does not extend to other complexities, of which those preventing crowding were briefly mentioned in the previous section and would be the most significant effect in the genetic algorithm used in this work.

3.3.3 ROBUST DESIGN USING A NOISY PHENOTYPE FITNESS FUNCTION

In a biological system, the decoding of the genotype into the phenotype is a function of its environment. During the decoding, perturbations in parameters, such as temperature and nutritional imbalance, may occur. If a genotype is robust to such changes, then the resulting phenotype will be insensitive to these perturbations. However if the decoding of a genotype is sensitive to such perturbations then it is unlikely to survive into subsequent generations. First, if a perturbation causes a fit genotype to be decoded as an unfit phenotype then by virtue of the low fitness it is unlikely to be selected in the next generation. Second, if an unfit genotype is decoded as a fit phenotype, it is likely to survive into the next generation. Even if it survives crossover and mutation, it is unlikely to encounter the same value of perturbation and thus this time may be decoded nearer or lower its true value. Thus those genotypes that are more robust to the perturbations in decoding are more likely to survive. This is essentially the *noisy phenotype* method reported and demonstrated on test problems by Tsutsui and Ghosh (1997). More formally, the fitness function is evaluated with perturbations (or noise) added to the optimisation variable vector **x** (3.1),

$$\begin{aligned} &f(\mathbf{x}+\Delta) \\ &\Delta = \{\delta_1 \quad \delta_2 \quad ..... \quad \delta_n\} \end{aligned} \tag{3.7}$$

where Δ is a perturbation vector, defined from individual, independent perturbations δ_j. The distinction between this approach and those that add a single perturbation to the evaluated objective function, *i.e.*, $f(\mathbf{x})+\delta$ is made. The study of such *noisy fitness functions* has been made (see references cited in Tsutsui & Ghosh, 1997), however these essentially provide a measure of the terrain around the nominal point on the search space of the objective function. This cannot be related to the optimisation variables unless the mapping to the objective function is known. This mapping is often complex and usually highly multivariate. It is far more pertinent to have knowledge of the robustness with relation to the optimisation variables themselves, where the limits can, for example in production, be measured or enforced by tolerances.

Using the schema theorem from the previous section it can be shown that using the noisy phenotype method the same algorithm operation is achieved but using a modified fitness function. This is shown for a one-dimensional case, initially, and extended to more dimensions

later on. From (B.19) in Appendix B, the average fitness of population $\overline{f(t)}$ at evolutionary time step t may be expressed, in terms of the fitness function, $f(x)$ and the probability of each individual occurring within a population, $p(x,t)$, of size n, and is,

$$\overline{f(t)} = \sum_{i=1}^{n} \frac{f(x^i)}{n} \approx \int_x f(x)p(x,t)\mathrm{d}x, \tag{3.8}$$

where i is each population individual. Thus the expected fitness of each schema, H, is given as

$$f(H,t) = \int_x f(x)p(x,H,t)\mathrm{d}x, \tag{3.9}$$

where $p(x,H,t)$ is probability of each individual occurring in schema H at evolutionary time step t. If a value of noise δ^i is added to each population individual, x^i, then the average fitness of the population becomes,

$$f'(t) = \sum_{i=1}^{n} \frac{f(x^i + \delta^i)}{n} = \int_x F(x)p(x,t)\mathrm{d}x. \tag{3.10}$$

$F(x)$ is the expected value of the fitness function evaluating the noisy phenotypes, if the distribution of the additive noise is given by $q(\delta)$,

$$F(x) = \int_{-\infty}^{\infty} f(x+\delta)q(\delta)\mathrm{d}\delta. \tag{3.11}$$

Hence the expected fitness of schema H is then given by,

$$f'(H,t) = \int_x F(x)p(x,H,t)\mathrm{d}x. \tag{3.12}$$

By comparison with (3.9) it is seen that in the same way (3.12) evaluates the expected fitness of the noisy phenotype fitness function, $F(x)$ in place of $f(x)$. Thus a new Schema Function adapted from (3.12) may be written which predicts the expected number of instances in each schema at evolutionary time step t. So,

$$m(H,t+1) \geq m(H,t)\frac{f'(H,t)}{\overline{f'(t)}}\left(1 - p_c\frac{d(H)}{l-1} - O(H)p_m\right), \tag{3.13}$$

Changing the integration variable allows $F(x)$ to be evaluated,

$$F(x) = \int_{-\infty}^{\infty} f(y)q(y-x)\mathrm{d}y. \tag{3.14}$$

Tsutsui & Ghosh (1997) consider the application of adding noise to the genotypes which has a Gaussian distribution. In this thesis a uniform distribution is used to maintain consistency with

the distributions used in assessing the robustness of the optimal design solutions reported in Chapters 4, 5 & 6. This method, whilst providing a general idea of the robustness of the solutions to perturbation, specifically provides a measure for perturbations with a uniform distribution. Thus to minimise the robustness measured in this manner a similar distribution is used. A brief discussion about the relevance of the distribution is discussed in Chapter 4, where robustness analysis is first applied in the work detailed in this thesis.

To quantify the effect of adding noise to a schema representing a genotype a reduction factor is defined. This follows Tsutsui & Ghosh (1997), except that a uniform noise distribution is used. Assume that the objective function consists of a rectangular peak of a one-dimensional function, and is defined to be

$$f(x) = \begin{cases} h & -w \le x \le w \\ 0 & otherwise \end{cases} \tag{3.15}$$

The uniform distribution of the noise, over a range s, is defined such that the area underneath the distribution is unity,

$$q(y) = \begin{cases} 1/s & -s/2 \le y \le s/2 \\ 0 & otherwise \end{cases} \tag{3.16}$$

Then depending on whether the rectangular peak in $f(x)$ is narrower than the noise distribution (*i.e.*, $f(x)$ is considered to be unrobust) or not, a different expected value is obtained for the genotype schema when the point in search space being evaluated is aligned with the centre of the peak in $f(x)$, and defines a reduction factor:

$$F(0) = \begin{cases} h & w \ge s \\ h\dfrac{w}{s} & w \le s \end{cases} \tag{3.17}$$

It is emphasised that because the schemata are being analysed that the expected values of the objective function evaluations are studied and not the fitness of individual, determinate evaluations. Thus, from (3.17) when the peak is too narrow to be considered robust the expected value is reduced by a reduction factor of w/s, whereas if the width of the peak is robust ($w \ge s$) then the full value of the function is expected to be evaluated. In practice a Boolean definition: "robust"/"not robust" is not made, where the function peak is not centrally aligned with the noise distribution, but an overlap still exists, then a diminished expected value is expected. This is illustrated using a function with four rectangular peaks, all of height h, but with different widths, shown in Figure 3.6 this function along with the probability distribution for the noise added to the phenotype. $E[F(x)]$ shows the expected effect of the additive noise on

the evaluation of $f(x)$. The four peaks represent all of the possible cases where $w > s$, $w = s$ and $w < s$. It is seen therefore that the expectation of the evaluated function height is reduced if the peak is narrower than the width of the noise distribution. For all cases the maximum value diminishes at a spatial rate of $h/2s$.

As shown by Wiesmann *et al* (1998), an optimal value of the expected function *E[F(x)]* does not always correspond to an optimal value of the original function. Indeed, where in regions where two narrow peaks exist in close proximity, for example, then the maximum expected value does not occur within the peaks of the function *f(x)*. This is illustrated in Figure 3.7, an example adapted from that shown in Figure 3.6, where the maximum expected value clearly falls in non-optimal regions for the two cases of the scenario shown. Wiesmann *et al* offer no solution to this failing in the noisy phenotype method. As discussed in Chapter 7, however, the search space for the application studied in this thesis is expected to be smoother than the example shown here, and therefore the use of this method is still valid.

To consider the multi-dimensional case (3.11) is firstly expanded to represent a two dimensional case with independent variables, x_1 and x_2, as

$$f'_{x_1,x_2}(H,t) = \int_{-\infty}^{\infty}\int_{x_1} f(x_1+\delta_{x_1})q(\delta_{x_1})p(x_1,H,t)\mathrm{d}x_1\mathrm{d}\delta_{x_1} \cdot \int_{-\infty}^{\infty}\int_{x_2} f(x_2+\delta_{x_2})q(\delta_{x_2})p(x_2,H,t)\mathrm{d}x_2\mathrm{d}\delta_{x_2} \tag{3.18}$$

The resulting fitness of schema H is thus the product of two integrals as there is no interdependence between them. Hence the step to an n-dimensional case may be easily made, where Φ is the multidimensional fitness and $f_i'(H,t)$ the one-dimensional expected fitness, as described in (3.12),

$$\Phi(H,t) = \prod_{i=1}^{n} f_i'(H,t). \tag{3.19}$$

Thus if the example above was extended to a the n-dimensional case the overall reduction factor Φ is the product of all the individual reduction factors,

$$\Phi(0) = \prod_{i=1}^{n} F_i(0). \tag{3.20}$$

where $F_i(0)$ is the individual reduction factor for dimension i, as in (3.17). Hence the reduction factor can increase significantly as the number of dimensions in which the width of the objective function peak is narrower than the rectangular noise distribution window becomes

greater. For example, if for all n dimensions the width of the objective function peak was 90% of the width of the noise distribution window, then the overall reduction factor is 0.9^n. In the structure considered as the subject for optimisation in this thesis there are 36 optimisation variables. For this case the overall reduction factor would be less than 0.02.

Thus the use of the noisy phenotype objective function allows the genetic algorithm to favour more robust solutions, where the solution would be insensitive to perturbation in any of the optimisation variables. The penalty in the evaluated fitness becomes increasingly severe the greater the number of optimisation variables to which the design's performance is sensitive.

3.4 MEASUREMENT OF ROBUSTNESS BY EXPERIMENTS

Robustness is the lack of sensitivity in a system to small, normally unspecified, changes in its design parameters, or in the context of optimisation, in the optimisation variables. The simplest way to test an optimised design for its robustness is to perform experiments in which the optimisation variables undergo realistic changes, or *perturbations*, and measure the effect on the optimised parameters of the design. In the robustness analysis considered in this thesis the expected change in value of the objective function in the face of perturbations represents the robustness. In such a way an expected measure of robustness may be achieved. The statistical accuracy of such an estimate will depend upon the number of perturbations used and how well the statistical distribution reflects those encountered in practice. If the robustness to manufacturing tolerances is studied, then a statistical model for such perturbations might either be available due to some measure of the error in a manufacturing process, or by prediction. In many cases a Gaussian (or normal) distribution may be adopted. However in the robustness analysis presented in this thesis a uniform distribution is used. This is because no information about the perturbation distribution is known, and a uniform distribution is thought to provide the most general case. Thus in this preliminary analysis no assumption is specifically made about the nature of the perturbations, simply the effect of perturbations on robustness is studied. A uniform distribution also simplifies the robustness analysis.

3.4.1 MULTI-VARIATE MONTE-CARLO EXPERIMENTS

One of the simplest methods of measuring the expected robustness of a system is to apply a large number of randomly generated perturbations of pertinent magnitude to the optimisation variables, and measure the change in the system performance by re-evaluating the objective function value. If a sufficiently large number of perturbations are used then the statistical distribution of the change in performance of the system can be estimated.

Thus to investigate the robustness of a design, which has been previously optimised and is characterised by an optimal optimisation vector, $\mathbf{x}_o$, the objective function f is re-evaluated to determine the effect of a set of perturbation vectors Δ_i by forming a set of n perturbed values of the objective function U_i^P to form a vector U^P, so that,

$$U_i^p = f(\mathbf{x}_o + \Delta_i) \quad \text{where} \quad U^p = \{U_1^p \quad U_2^p \quad \ldots \quad U_n^p\}. \tag{3.21}$$

The values of U^P are then sorted in numerical ascending order, by assigning them to values of Y^P,

$$U^p \rightarrow Y^p \quad \text{where} \quad Y^p = \{Y_1^p \quad Y_2^p \quad \ldots \quad Y_n^p\} \text{ such that } Y_j^p \leq Y_{j+1}^p. \tag{3.22}$$

A probability limit is then calculated so that for a percentage, α, of the n experimental results, the performance is better than the value defined by the probability limit. In the robustness analysis considered here this is the case when the value of the objective function is below the value of the probability limit for α percent of experiments. The probability limit is thus defined as,

$$f_\alpha = Y^p_{rnd\left(\frac{\alpha n}{100}\right)}, \tag{3.23}$$

where the function *rnd* rounds the argument to the nearest integer so that it can be used as an index for the data Y^P. The accuracy of this probability limit depends upon the number of perturbed samples, n, used. First, for small n the *rnd* function will cause a 'quantisation' error if α does not lie near an integer value, and effectively a slightly different probability limit is evaluated. Secondly, the smaller the value of n the worse the estimate of the statistical performance, which is actually achieved as n tends to infinity. In all the cases considered in this thesis α is 95%.

3.4.2 PERTURBATION ANALYSIS BY EXPERIMENTAL DESIGN

The statistical design of experiments is a process of planning experiments to collect appropriate data and subsequently analyse using statistical methods to obtain valid and objective conclusions. The science of statistical experimental design first originated with the work of Sir Ronald Fisher (1925) who was motivated by the optimisation of the yield of agricultural crops. Rao (1947) first proposed the use of orthogonal arrays for factorial experimental design, and the development of this field has been continued by, for example, Kempthorne (1952). Taguchi (1987) developed the foundations of Robust Design with the main aim, initially, of improving Quality in manufacture in Japan in the late 1940's. All of this work had been aimed at

statisticians until Phadke (1989) adapted some of these approaches specifically to engineering applications, following Taguchi's work.

Fractional factorial experimental design is an efficient method of evaluating the response of a system to each system parameter, and provides good results if the interactions between these parameters are small. Fractional factorial experiments were initially use for screening experiments, to identify which system parameters are likely to have large effects on the system response. These results would then indicate the factors that should be more thoroughly investigated. In an engineering context the experiments are conducted to investigate the effect of several factors (or parameters) on some phenomenon (or response) of a system. Furthermore, in the application considered in this thesis the experiments conducted are *computer experiments*, and thus there is no experimental error (exactly the same results being yielded for each identical experiment) and experimental replication to address this is not required, allowing the experimental design to be simplified.

Fractional factorial experiments are used here to define the perturbation vectors in (3.21). Each row of the experimental arrays used corresponds to an instance of the perturbation vector Δ_i suitably scaled. Unlike using random uniformly distributed perturbations, where the perturbation value can be any value between defined extremes, using orthogonal arrays only either two or three different levels are used depending on the experimental design array used.

3.4.2.1 ONE-AT-A-TIME AND FULL FACTORIAL EXPERIMENTS

The effect of each factor alone on the change in performance of a system is termed the *main effect*. If all the main effects are independent (*i.e.*, are unaffected by the levels of any of the other factors) then each main effect can be determined by *one-at-a-time* experiments where each factor is altered separately and its effect registered. The values of the other factors are unimportant. Hence, for each factor only one experiment needs to be performed for every factor level.

If the effect produced by each factor is also dependent upon the levels of the other factors, then using one-at-a-time experiments will provide inaccurate and ambiguous results due to *interactions* between the factors. However, the average effect of a factor may be measured by performing experiments over all the combinations of different levels for all the other factors. This approach is known as a *full-factorial* experimental design. One of the advantages of this is that the estimates of the main effects are formed using experiments over all the levels for each factor, and are more representative of the range of conditions encountered in practice. This can avoid misleading conclusions due to the presence of interactions, and additionally, information is available to study specific interactions if these are of interest.

To illustrate the effect of interactions between factors in a system, and how they can lead to misleading conclusions unless the effect of interactions is studied, two very simple systems are considered, with one containing a strong level of interaction (after Montgomery, 1983). Consider two systems X and Y, whose response to two, 2-level factors, A and B, is shown in Table 3.1. Closer examination reveals that in system Y there is strong interaction between the factors A and B. The sign of the effect of either factor depends on the level of the other. This is demonstrated graphically in Figure 3.8. The degree to which the lines are non-parallel indicates the degree of interaction. The average main effects of factor A and factor B (denoted by m_A and m_B) and the interaction between factors A and B (denoted I_{AB}) are defined (after Montgomery, 1983), as

$$m_A = \frac{f(A_2,B_1)+f(A_2,B_2)}{2} - \frac{f(A_1,B_1)+f(A_1,B_2)}{2}, \tag{3.24}$$

$$m_B = \frac{f(A_1,B_2)+f(A_2,B_2)}{2} - \frac{f(A_1,B_1)+f(A_2,B_1)}{2}, \tag{3.25}$$

$$I_{AB} = \frac{f(A_2,B_2)+f(A_1,B_1)}{2} - \frac{f(A_2,B_1)+f(A_1,B_2)}{2}. \tag{3.26}$$

The main effect of a factor is therefore the difference between the average of the response at one level and the average response at the other level. The interaction between factors is the difference between the average of the response with both factors at the high and low level, and the average of the responses with each factor at opposing levels. The numerical values of the main effects of each factor and the interaction between them for both systems are given in Table 3.2. Without investigating for the interaction I_{AB}, it is seen that the main effects m_A and m_B would provide the misleading result that system Y is relatively insensitive to the effect of factors A and B, compared with system X. However I_{AB} reveals that a strong interaction exists for system Y, which would only be evident, in this case, using a full factorial experimental design. If one-at-a-time experiments had been performed, for example, with the main effect of each factor estimated with the other factor at its low value, then the response for the factor combination A_2,B_2 would not have been explicitly measured. In both cases it would have been assumed that A_2,B_2 would yield the largest response, which would be seriously in error for system Y due to the strong interaction. Indeed the conclusion drawn (potentially in error) about the response at factor combinations which are not exclusively tested may depend upon the, probably arbitrary, choice of nominal level of the factors, other than the one being tested.

3.4.2.2 FRACTIONAL FACTORIAL EXPERIMENTS

In the previous sub-section the advantages of full factorial experiments over one-at-a-time experiments were discussed. For a small number of factors and/or with a small number of factor levels this presents no practical problem, but the number of experiments required can grow exponentially with either the number of factors or levels. In Chapter 7 such experiments are performed with 36 factors with both two and three levels. To perform full factorial experiments would require 2^{36} and 3^{36} experiments, respectively. It is not feasible to perform such a large numbers of experiments, especially when these experiments themselves are also used as part of a optimisation algorithm, which itself requires many thousands of evaluations. A *fractional factorial* experimental design is one that only utilises some of the experiments from its full factorial counterpart. In this way the number of experiments required can be greatly reduced. Fractional factorial experiments using orthogonal arrays (which are discussed below) are used as a potentially more efficient way of generating the probability limit defined in (3.23). Fewer experiments are used, but the experiments are *designed* in order to provide certain information, whereas the accuracy using random perturbations simply relies on a large number of different samples and increasing the number of samples increases the accuracy only in a probabilistic sense.

The compromise in using fractional factorial experimental designs is that less information is gained about the system, and it becomes impossible to distinguish between the true main effects of a factor and interactions between factors. It is said that the main effects are *aliased* with certain interactions. However if the value of the interactions is known to be, or can be considered to be small then reasonable estimates of the main effects can be achieved. In the fractional factorial experiments considered in this thesis the full factorial experiment is reduced to those requiring only one experiment more than the number of factors specified in the 'standard' orthogonal arrays used, even though the number of factors is sometimes greater than required for a certain experiment design. This is the minimum experimental design in order to achieve an estimate of the main effects for each factor individually. If the number of experiments was reduced further then 'aliasing' would exist between some of the main effects. This effect is not desired as the sign of each of the interactions is not determinable and thus whether the effect of each aliasing acts constructively or destructively. Thus a composite measure of the main effects with less than the minimum number of experiments described above is not feasible. The fractional factorial experiments are *balanced*, each level of each factor is used equally in the experimental design. Additionally there is an *orthogonal* property of the arrays that allows other types of analysis such as analysis of means and variance to be performed. The orthogonal property is formally defined in the following sub-section. This

property means that the estimates of the statistical properties for each factor individually may be found. Such analyses are not used in this thesis, but are detailed in Montgomery (1983), Taguchi (1987) and Phadke (1989).

The orthogonal arrays used for the fractional factorial experiments in this thesis are detailed in Appendix C (after Taguchi, 1987, as cited by Phadke, 1989). It is too cumbersome to show the derivations of such arrays here. In order to show the procedure of generating such an array, a fractional factorial experiment is derived from a full factorial experiment for five two-level factors. This is not one of the standard arrays catalogued originally by Taguchi. It is chosen as it is not so small that the derivation is trivial (as with the L_4 (2^3) standard array, three two-level factors) whilst not being too cumbersome to include here in full (as would the L_8 (2^7) standard array).

A full factorial experiment for five two level factor requires 32 ($=2^5$) experiments. Denoting the two levels as either positive or negative: '–' and '+', the design is shown in Table 3.3, where the factors are labelled *A* to *E*. All the possible combinations of the factors are thus required. In order to generate a fractional factorial experiment rows are selected on the basis of relationships between factors. These relationships are called *design generators*. The first design generator used is,

$$I=ABD\,, \tag{3.27}$$

where *I* is the identity element, and is equivalent to '+' by definition (Montgomery, 1983). The generator is interpreted by multiplication of the signs of the factors, and thus in (3.27) the generator is satisfied if between the factors *A*, *B* and *D*, either one or three of the factors have the sign '+'. The value of this generator is shown in Table 3.3, following convention it is written *D=AB*, which is one of the aliases of the generator. This is explained below. A positive value in this column indicates the generator identity is satisfied. The second design generator used is,

$$I=ACE\,, \tag{3.28}$$

and its value appears in Table 3.3 under the heading *E=AC*. The fractional factorial experiment is defined by the *defining relation*, which is given by the combination of the two generators,

$$I=ABD=ACE\,, \tag{3.29}$$

which is given in the rightmost column of Table 3.3, under column heading *SEL*. Other design generators may be used in place of the ones employed here. Other definitions of design generators or defining relations, including their *complimentary* or *alternate* halves may also be used. This is outside the scope of this thesis, but is described by Montgomery (1983). It is

noted that with the defining relation used here (as with the standard orthogonal arrays detailed by Taguchi and Phadke) that a row exists with all the factors at the lowest level (in all cases this is the first row). If this corresponds to a perturbation vector which has no effect on the system, then the nominal response is considered within the experiments detailed by the orthogonal arrays, removing the need for a further measurement to achieve this and improving the efficiency of the analysis. The fractional factorial experimental design is summarised in Table 3.4. Only 8 experiments are now required. In this table the factor signs: '–' and '+', have been replaced by: 1 and 2 respectively, to maintain consistency with the orthogonal arrays used, as specified in Appendix C.

By using design generators the main effects are deliberately aliased with interactions between the factors, that is, some main effects and some interactions are indistinguishable. Thus unless interactions are insignificant, then the estimated value of the main effects will contain errors due to these. (3.27) signifies the aliasing of the main effect of D with the interaction between A and B. Noting that the multiplication of any factor by itself results in I, the alias $D=AB$ can be achieved from the generator (3.27),

$$D.I = ABD.B = AB\,. \tag{3.30}$$

Similarly the alias $E=AC$ already used to for the generator (3.28) is given,

$$I.E = ACE.E = AC\,. \tag{3.31}$$

Thus the main effect of E is also aliased with the interaction between A and C. By similar manipulation and combination of the design generators all the aliases are found (although in this particular case no combinations of generators are required). These are summarised in Table 3.5. Thus each entry shows the interactions between each factor. Obviously this table is symmetric, and by convention only one half is shown with the diagonal elements shown bracketed.

In this case, although all the main effects are aliased with interactions, not all possible combinations of second order interactions are aliased with main effects. In all but one of the two-level fractional factorial orthogonal arrays included in Taguchi (1987), and cited in Phadke (1989), the number of columns (*i.e.*, factors) is an integer power of two minus one. In these cases the number of experiments performed is integer power of two (*i.e.*, the number of columns plus one). This is the maximum reduction attainable from a full factorial experiments design while still allowing the individual main effects to be determined from the experimental design. Even if the number of factors required is less than those defined in these arrays all the experiments are still required, if the balancing property is to be retained. Thus in the fractional factorial experiment design in Table 3.4, the number of experiments required is 8, which is the

same as if a fractional factorial design for 7 factors had been derived. The only advantage in the above design over a 7-factor design is that there are fewer interactions between factors. The minimum number of experiments allows sufficient degrees of freedom to calculate the main effects of each of the factors and also their mean, and thus the analysis of means (ANOM) and analysis of variance (ANOVA). ANOM allows the average effect of each factor on the system output and thus allow the optimum value to achieve a desired system response. From this the optimum levels for each factor can be determined. ANOVA allows the average effect of changes in each factor on the system output. This leads to the Taguchi's and Phadke's Signal to Noise (SNR) ratio, which is based on the ratio of the square of the mean response of the experiments, μ^2, to the mean-squared-deviation about the mean, MSD, and is given by,

$$SNR = 10\log_{10}\left(\frac{\mu^2}{MSD}\right). \tag{3.32}$$

For a system for which the target response is a nominal value a function based on (3.32) is the parameter which is minimised. This is not applicable in the use of the fractional factorial arrays as used for the robustness analysis in this thesis where the smaller the system response the better.

The generation of full and fractional factorial orthogonal arrays for experiments using three-level factors is achieved using a similar procedure as described above. It is more complex as modulo 3 (as opposed to modulo 2) arithmetic is required. This is outside the scope of this thesis, but is detailed in Montgomery (1984).

3.4.2.3 THE ORTHOGONAL PROPERTY OF ARRAYS

The fractional factorial experiment design using orthogonal arrays, including that shown in Table 3.4, possess an orthogonal property. This exists between the columns of the experimental design array, and is defined as follows. Assume a column of the design to be L_i, which is comprised of n elements, is

$$L_i = \{w_{i1} \quad w_{i2} \quad . \quad . \quad w_{in}\}. \tag{3.33}$$

The contrast C_i is defined if all the elements add up to zero. This can be assured if the mean of the column is subtracted, and thus is independent of numerical level notation used (although the levels must be a sequential run of integers).

$$C_i = \{w_{i1} \quad w_{i2} \quad . \quad . \quad w_{in}\} - \overline{L_i}. \tag{3.34}$$

Two columns are orthogonal if their inner product is zero. Hence, columns L_i and L_y are orthogonal if

$$C_i.C_y = 0 \qquad i \neq y. \tag{3.35}$$

For an orthogonal experimental design (3.35) must be satisfied between all columns.

3.4.2.4 A COMMENT ON THE FRACTIONAL FACTORIAL ORTHOGONAL ARRAYS USED

The robustness analyses conducted in this thesis use two and three level orthogonal arrays both requiring a minimum of 36 factors. Two standard orthogonal arrays from Phadke (1989), after Taguchi (1987), are used. Maintaining the notation from these references, these are termed L64 (two-level, 63 factor, 64 experiment array) and L81 (three-level, 40 factor, 81 experiment array). These are included in Appendix C, and are included in their entirety even though only the first 36 columns are required. An error in the L64 table (as printed in Taguchi (1987) and repeated by Phadke(1989)) was detected by the author. The values at (experiment, column) positions (32,28) and (32,29) should be 1, otherwise the orthogonal property of the table is lost. This correction has been confirmed by the author (Phadke 1989) and corrected version of the table is given in Appendix C.

3.4.2.5 COMMENTARY ON TAGUCHI'S METHODS

In a later edition of his book, Montgomery (4th edition, 1996) provides a critique of the methods advocated by Taguchi (and thus also Phadke) with respect to experimental design. Whilst Montgomery considers Taguchi's basic philosophy 'sound' and recommended for product design, he criticises Taguchi's statistical methods as often being unnecessarily complicated, inefficient and sometimes ineffective. The main criticisms are directed at the data analysis that follow the use of the experiments using Taguchi's orthogonal arrays, and that a simplified consideration of aliasing can actually be counter-productive in understanding the system performance. Only the orthogonal arrays presented by Taguchi are used here, and thus the contentious area of the data analysis is avoided.

	B_1	B_2
A_1	20	30
A_2	40	52

SYSTEM X

	B_1	B_2
A_1	20	40
A_2	50	12

SYSTEM Y

Table 3.1. Responses of System X and System Y; two 2-level example systems.

	m_A	m_B	I_{AB}
SYSTEM X	21	11	1
SYSTEM Y	1	-9	-58

Table 3.2. The main effects, m_A and m_B, and their interactions, I_{AB}, of System X and System Y.

Expt No.	A	B	C	D	E	D=AB	E=AC	SEL
1	–	–	–	–	–	+	+	+
2	+	–	–	–	–	–	–	–
3	–	+	–	–	–	–	+	–
4	+	+	–	–	–	+	–	–
5	–	–	+	–	–	+	–	–
6	+	–	+	–	–	–	+	–
7	–	+	+	–	–	–	–	–
8	+	+	+	–	–	+	+	+
9	–	–	–	+	–	–	+	–
10	+	–	–	+	–	+	–	–
11	–	+	–	+	–	+	+	+
12	+	+	–	+	–	–	–	–
13	–	–	+	+	–	–	–	–
14	+	–	+	+	–	+	+	+
15	–	+	+	+	–	+	–	–
16	+	+	+	+	–	–	+	–
17	–	–	–	–	+	+	–	–
18	+	–	–	–	+	–	+	–
19	–	+	–	–	+	–	–	–
20	+	+	–	–	+	+	+	+
21	–	–	+	–	+	+	+	+
22	+	–	+	–	+	–	–	–
23	–	+	+	–	+	–	+	–
24	+	+	+	–	+	+	–	–
25	–	–	–	+	+	–	–	–
26	+	–	–	+	+	+	+	+
27	–	+	–	+	+	+	–	–
28	+	+	–	+	+	–	+	–
29	–	–	+	+	+	–	+	–
30	+	–	+	+	+	+	–	–
31	–	+	+	+	+	+	+	+
32	+	+	+	+	+	–	–	–

Table 3.3. Full factorial experimental design for a five-factor, two-level experiment.

Expt No.	*A*	*B*	*C*	*D*	*E*
1	1	1	1	1	1
2	1	1	2	1	2
3	1	2	1	2	1
4	1	2	2	2	2
5	2	1	1	2	2
6	2	1	2	2	1
7	2	2	1	1	2
8	2	2	2	1	1

Table 3.4. Fractional factorial experimental design for five factor, two-level experiment.

	A	*B*	*C*	*D*	*E*
A	*(A)*	*D*	*E*	*B*	*C*
B		*(B)*	–	*A*	–
C			*(C)*	–	*A*
D				*(D)*	–
E					*(E)*

Table 3.5. Two-factor interactions between the factors in the fractional factorial experiment shown in Table 3.4

GLOSSARY OF SYMBOLS FOR CHAPTER 3

The major notation used in this chapter is listed below. Other symbols are defined locally.

A	Experimental array factor
A_n	Level n of factor A
B	Experimental array factor
B_n	Level n of factor B
C	Experimental array factor
C_i	Contrast of array column i
d	Defining length of schema
D	Experimental array factor
E	Experimental array factor
$\overline{f}$	Average fitness of population
f'	As for definition of f, but evaluated using noisy phenotype method
f_α	Value of probability limit α of perturbed objective function
$f(H)$	Average fitness of schema H
f_i	Fitness of chromosome i
$F(x)$	Expected value of fitness function evaluated using noisy phenotype method
H	Schema
I	Identity element
I_{AB}	Interaction between factors A and B
l	Chromosomes length
L_i	Column i of array
$m(H,t)$	Number of schema H occurring in generation t
m_A	Main effect of factor A
n	Number of chromosome strings in population
O	Order of schema
p_c	Probability of crossover

p_m	Probability of mutation
$p(x,H,t)$	Probability of each individual x occurring in schema H in generation t
$p(x,t)$	Probability of each individual x occurring in a population in generation t
q	Noise distribution
r	Penalty value
t	Evolutionary time step
x^i	Population individual
x_n	Individual vector element of $\mathbf{x}$
$\mathbf{x}$	Generalised vector
$\mathbf{x_o}$	Optimised optimisation vector
U	Search space
U_p	Penalised search space
U^p	Vector of values of perturbed objective function
Y^p	Ordered vector, U^p
δ	Perturbation value
δ^i	Value of noise perturbation added to population individual i
ϕ	Inequality constraint
ϕ^s	Satisfied inequality constraint
Δ	Perturbation vector
Φ	Overall reduction factor
ψ	Equality constraint

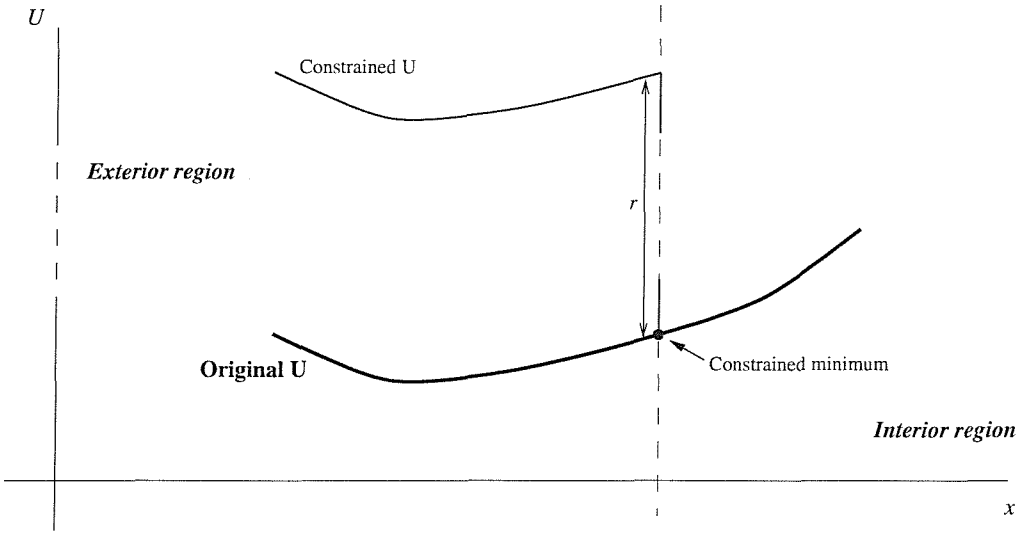

Figure 3.1: The operation of the One Pass External penalty function illustrated for one degree of freedom, using penalty value r.

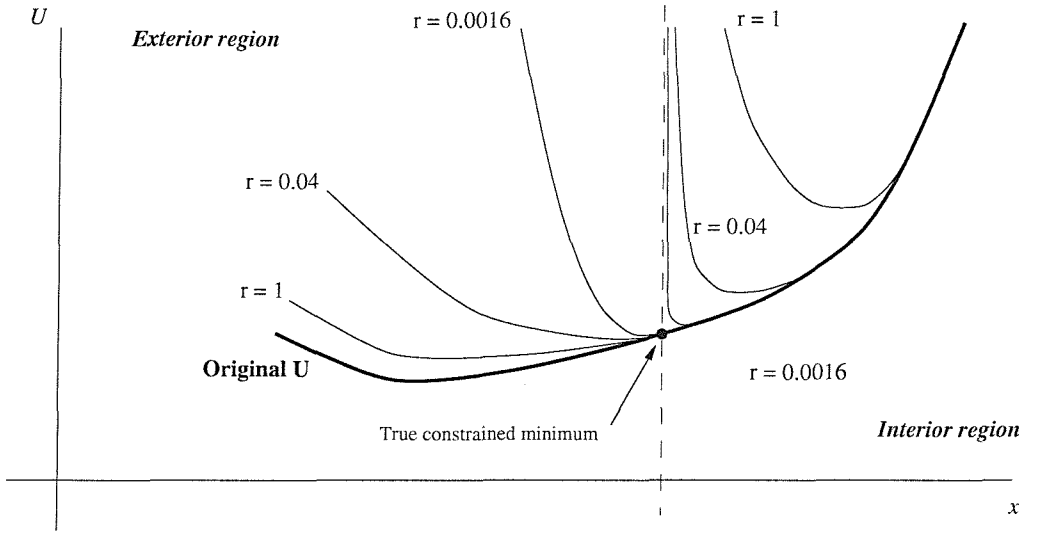

Figure 3.2: The operation of the Fiacco-McCormick penalty function illustrated for one degree of freedom. (After Siddall, 1982)

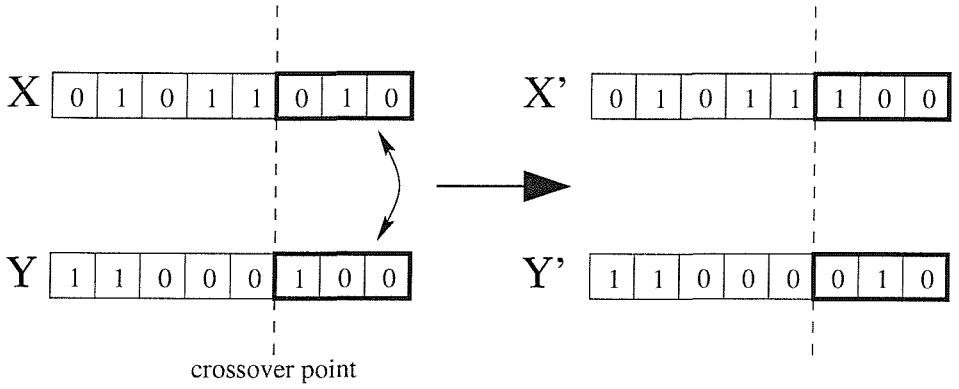

Figure 3.3: The operation of the genetic algorthim operator: Crossover.

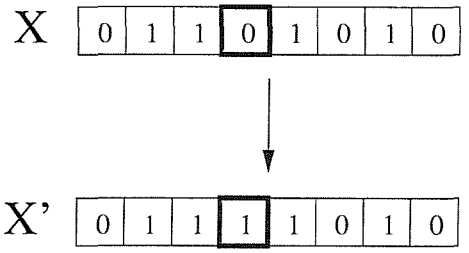

Figure 3.4: The operation of the genetic algorthim operator: Mutation.

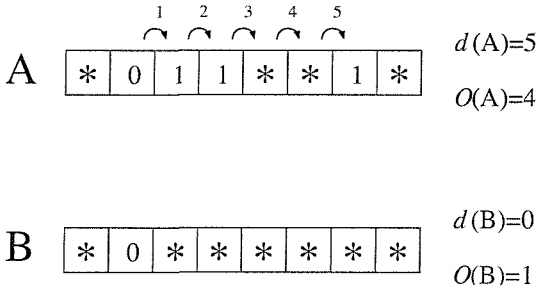

Figure 3.5: Two schema, A and B, with the properties defining length and order denoted for each.

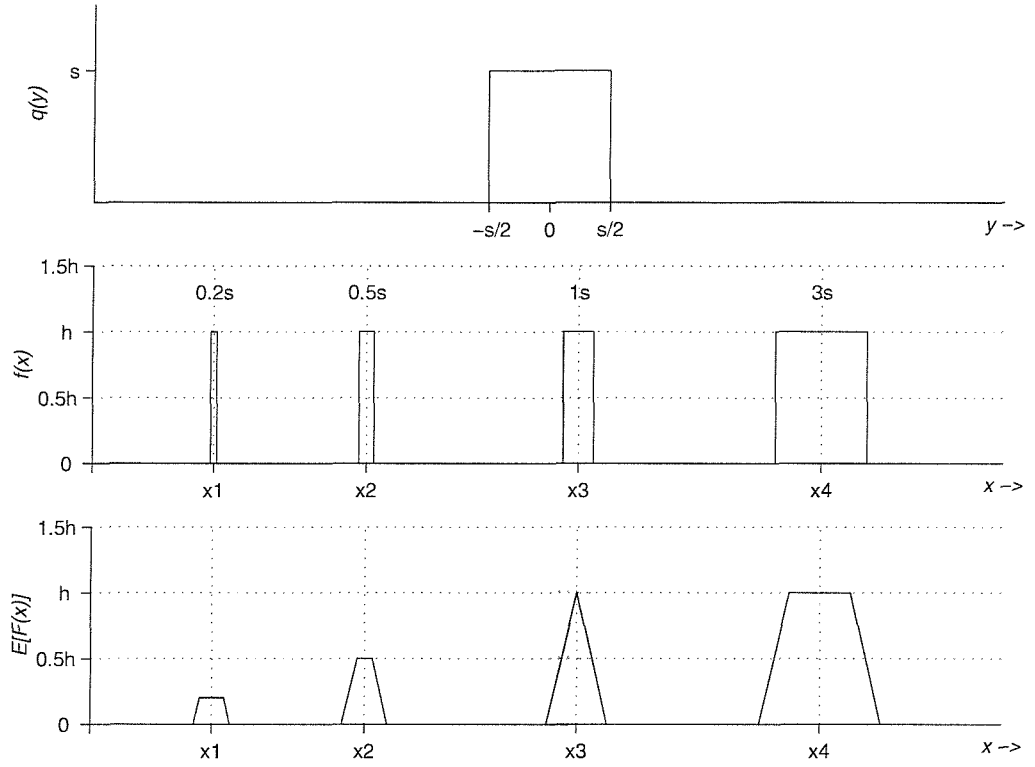

Figure 3.6: An example of the operation of the noisy phenotype genetic algorithm, with noise distribution $q(y)$, on the objective function $f(x)$. The expectation of the evaluated objective function is $E[f(x)]$.

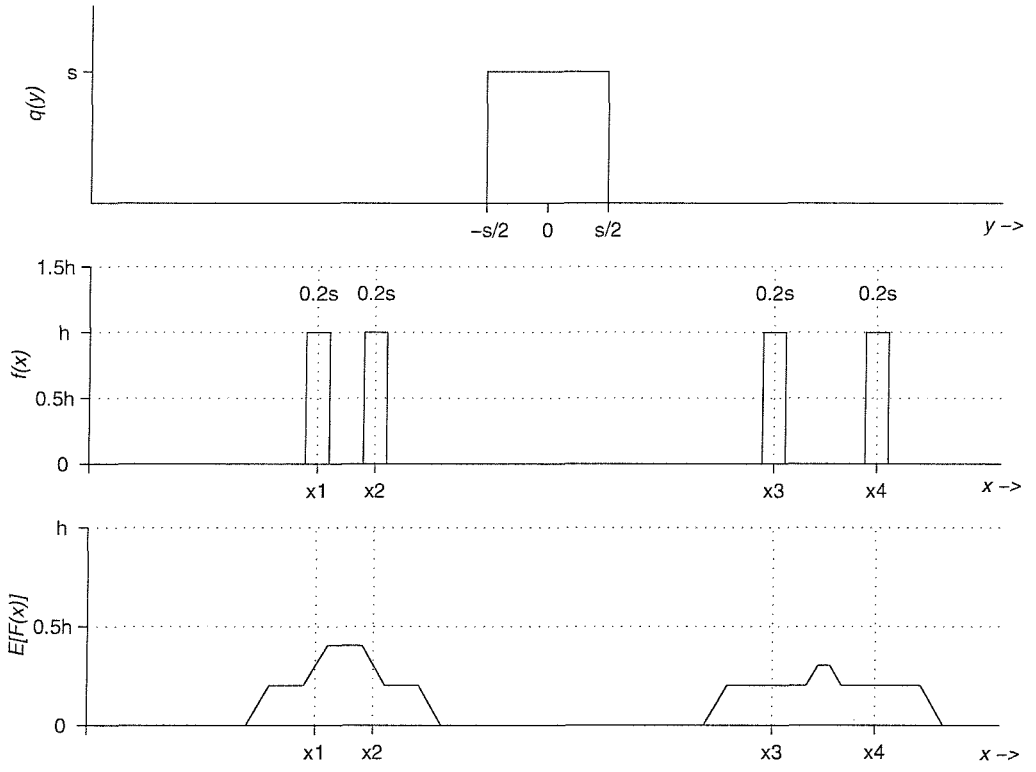

Figure 3.7: Example of features in the objective function $f(x)$ which can result in false optimum, for the noisy phenotype genetic algorithm with noise distribution $q(y)$, as the value of the expectation of the evaluated objective function, $E[f(x)]$, shows.

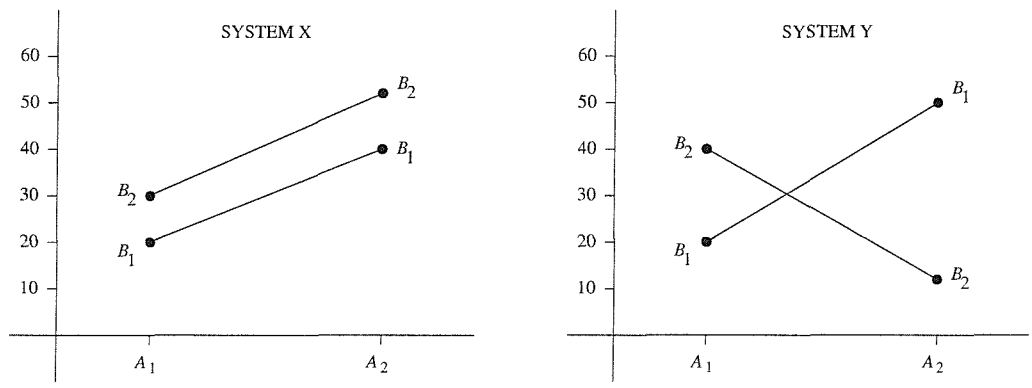

Figure 3.8: The response of systems X and Y to the two-level factors A and B. System Y has a high level of interaction between A and B. (After Montgomery, 1983)

CHAPTER 4

Passive Optimisation Methods and Robustness Analysis

4.0 INTRODUCTION

This chapter describes the optimisation of a regular two-dimensional cantilever structure to reduce the vibration transmission from the base to the end of the structure. The optimisation is achieved by means of redesigning the structure geometry; by allowing the positions of the mid-structural joints to be variable. Unlike the optimisations detailed in Chapters 5 and 6, no external energy source is used in the reduction of the vibration, this optimisation strategy is thus referred to as *passive optimisation.*

The method used here is that of redesigning of the structure geometry, as opposed to maintaining the structure geometry and changing the vibration transmission of the structure by varying the cross-sectional areas of the individual beams, as used by Liu *et al.* (1997 and 1998). In this work the cross-sectional area was allowed to diminish to zero, thus effectively removing the beams and changing the structure topology. The author feels that altering the geometry; constructing a structure using beams of a regular cross-section cut to different lengths, is a more practical solution. It is more complex to machine each beam to a custom cross-section, and if a discrete set of cross-sections were used then this would severely limit the search space considered during optimisation. Also, the union of thick and very thin beams might present practical difficulties, and any additional joint complexities may need to be accommodated in the structure model. Although the static strength of the structures is not considered in the optimisations used by the above authors or the present author, the removal of beams from the structure is likely to result in a weaker static structure, than that by changing the geometry. The effect of the optimisation by geometric redesign on static strength of the structure is briefly considered in Section 4.3.

The optimised designs are achieved using a number of methods: three traditional optimisation methods, using gradient and hill climbing based strategies; a fairly recent heuristic search technique using hill climbing and stochastic-based method of restarting the search; genetic algorithms, a type of evolutionary optimisation technique which is stochastically based. All the optimisation methods were successful to varying degrees.

Although in theory all the optimised designs show better performance than the unoptimised structure, the practical design implementations may not be feasible with exactly the required optimised parameters due to, for example, manufacturing tolerances. Even if this was not the case, the parameters might change during service by, for example, thermal expansion and contraction. If the effect of these changes on the optimised performance is not studied then an optimised design that is predicted to be the best (under *nominal* operating conditions) in service may yield less than optimum performance. Whereas another optimised structure, although having a slightly lower optimised performance under nominal operating conditions, may be less sensitive (more *robust*) to changing operating conditions and be a more practical choice. A geometric perturbation analysis was performed for all the optimised structures produced in this chapter. It was found that the method by which the optimisation seeks the optimal structure designs can have serious consequences on the robustness of the structures produced.

This chapter is structured as follows: Section 4.1 defines the optimisation problem; Section 4.2 describes the application of non-evolutionary methods (three traditional methods and Dynamic Hill Climbing); Section 4.3 details the application of genetic algorithms, and additionally brief analyses of the change in power flow in the structures and the consequential change in static performance of the structure, both due to optimisation, is reported; Section 4.4 reports the robustness analysis applied to all the optimised structures. The conclusions are drawn in Section 4.5.

Throughout this chapter reference is made to the design exploration system used for the majority of the optimisation work presented in this thesis. For brevity this will again be referred to in this chapter by its proprietary name: OPTIONS. See Chapter 3 for further details.

4.1 DEFINITION OF THE OPTIMISATION PROBLEM AND IMPLEMENTATION OF OPTIMISATION

4.1.1 DEFINITION OF THE OPTIMISATION PROBLEM

The optimisation problem considered in this thesis is defined as being: to minimise the vibration transmission of the structure shown in Figure 2.1, such that the effect of vibration forces acting at the base of the structure have the minimum effect on the far most right beam, labelled Beam 40. The excitation is modelled as a force applied to Beam 1 at the base of the structure. This is applied in a transverse sense to the beam at 0.5m from the hinged end, and has an arbitrary value of 1N at all frequencies considered. The vibration of Beam 40 is represented by a measure of the energy dissipated in the beam due to the flexure of the beam. In Chapter 5 an

analysis is reported of the use of different parameters which can be used to represent the vibration in Beam 40. It transpires that the parameter used as the subject of all the optimisations reported here is not, in fact, the most comprehensive. However, for this structure the use of the flexural energy dissipated in Beam 40 is shown to still be a very good representation of the overall vibrational energy, in the frequency range considered. It was also the parameter used by Keane in his optimisation scenario (Keane, 1995b).

In the optimisation studied in this chapter, the optimisation variables are the non-extreme joint positions; the relative positions between the fixed joints at coordinates (0,0) and (0,1) and the end joints at coordinates (10,0) and (10,1) are to remain unchanged. Thus there are 18 joint positions to be determined by the optimisation, each defined by its x and y coordinates, making 36 optimisation variables in total. So that the number of bays in the structure is maintained, and to prevent joints touching or overlapping, limits are imposed on the freedom of each joint coordinate. The limits are ±0.25m about each nominal joint coordinate. This gives the joints the maximum freedom without and parts of the structure being allowed to overlap. The structure parameters were detailed in Chapter 2, as the optimisation details above are those used by Keane (1995b), thus the optimisation scenario is identical.

4.1.2 IMPLEMENTATION OF THE STRUCTURE IN OPTIONS

All the optimisations reported in this chapter were achieved using the OPTIONS package. This is linked to the computational model for the structure, based on the receptance analysis method, detailed in Chapter 2. This is the same way in which optimised structures were previously produced by Keane (1995b), and experimental verification by Keane and Bright (1995) also showed that the optimisation had produced a structure which had a greatly reduced vibration transmission in practice. A successful comparison of the receptance model with a finite element analysis model was also shown by Shankar and Keane (1995), albeit with a larger value of beam damping.

Each optimisation variable is coded into a 16 bit representation scaled linearly between the limits. This gives a precision of about 10 μm, which while practically unrealistic was retained for consistency with aforementioned previous work of Keane. This precision is thought to unjustifiably strict, and 12 bits may provide a more realistic precision (of 0.12mm) for such a structure, however the number of bits does not affect the operation or the speed of the algorithm.

In order to gain an appreciation for the complexity of the optimisation, Figure 4.1 shows the contour plot showing the average energy level in Beam 40, over the frequency range 150Hz to 250Hz, with both the x and y coordinate variations allowed under optimisation limits for joint 8

at coordinates (4,1). Here the true multi-modal nature of the problem is evident. This graph is obtained, however, with the remaining optimisation variables at their nominal position whilst in the optimisation process the surface shown here would also vary as other variables are adjusted.

The size of the optimisation problem can be appreciated from the fact that there are 36 variables, each represented by a 16-bit number, giving 65536^{36} (in the order of 10^{173}) possible combinations. Even if 12-bit representation had been used, as discussed above, this still would yield a search space in the order of 10^{130} possible combinations. If the objective function took a mere 1ms to evaluate (in practice each objective function evaluation at each frequency took about four seconds at each frequency value, on the hardware platform detailed later) then of the order of 10^{119} years would be needed to exhaustively explore the search space. Bäck (1996) uses for comparison quantities relating to the universe, stating 10^{80} as being the number of stable elementary particles in the universe.

In the optimisations that follow in this chapter, the energy level of Beam 40 of the structure (shown in Figure 2.1) is minimised over three frequency bandwidths. The objective functions used represented the energy in Beam 40, i) at a single frequency (185Hz), ii) as an average over a 20Hz bandwidth (175Hz to 195Hz comprising five linearly spaced frequency points), and iii) as an average over a 100Hz bandwidth (150Hz to 250Hz, using 21 linearly spaced frequency points). These optimisations are subsequently referred to as single frequency, narrow band and broad band optimisations.

4.2 OPTIMISATION USING NON-EVOLUTIONARY METHODS

The structure was optimised using traditional optimisation techniques, and a relatively new technique called Dynamic Hill Climbing. The traditional techniques used are (referred to by the names of their originators): Hook and Jeeves, Davidon-Fletcher-Powell (DFP) and Broyden-Fletcher-Goldfarb-Shanno (BFGS). These techniques were described in Chapter 3. These four optimisation techniques are taken as a representative sample of non-evolutionary algorithms currently used. It is not intended to present an in-depth study comparing different optimisation techniques, but a brief study to support the use of genetic algorithms for this type of optimisation problem is included here. The use of other Evolutionary Algorithms was not investigated, although Keane has already performed a comparison against Simulated Annealing for a similar optimisation problem (see Keane, 1994).

Two penalty functions are available to the author by using OPTIONS: One Pass External and Fiacco-McCormick. The first is a simple way of imposing constraints which has no significant

further computational expense, the latter is a more sophisticated technique requiring successive re-evaluations of the objective function, but can perform better than the One Pass External method in some cases. These issues were discussed in detail in Chapter 3, as was the composite optimisation strategy adopted here; using a two-phase search for all non-evolutionary algorithms except Dynamic Hill Climbing (where the One Pass External is used). The optimisation strategy is to initially perform a search using the One Pass External penalty function, then restart the current point using the Fiacco-McCormick penalty function. This is an efficient strategy as the first, and probably most significant, part of the search is performed with no significant additional computational overhead. Then the Fiacco-McCormick penalty function is used to enable the search to localise on the minimum. As discussed in Chapter 3, a typical problem with the One Pass External penalty function is that it is possible it may prematurely terminate its search when the minimum lies on or near a boundary on the search space. The use of the Fiacco-McCormick penalty function, although computationally more costly, is more adept in these situations. However it is feasible that simply restarting the search, which entails resetting search parameters (e.g. the step size, and in the case of DFP and BFGS, the Hessian matrix to the identity matrix), may enable further successful exploration.

The parameters defining the non-evolutionary search techniques used here are given in Tables D.1 to D.5 in Appendix D. Both the fixed parameters and those capable of being assigned in OPTIONS are given. As it was not intended to perform an in-depth analysis of optimisation methods, then a sapient choice of parameters was made. With the Hook and Jeeves algorithm and DFP, slight adjustment of the initial choices of the parameters OPT_TOL and G, respectively, were made in order to encourage convergence.

The implementation of Dynamic Hill Climbing available in OPTIONS, always started the search from the same initial point (*i.e.*, the regular structure shown in Figure 2.1). Thus the first local search would always be the same, and thus would be redundant if more than one optimisation was performed, even using different random number seeds for the search algorithms. For a high dimensional problem, such as the one considered here, the next search start point is simply a random jump in the search space, as discussed in Chapter 3. Four random structures were generated within the optimisation limits which, in addition to the regular structure, provides a different start point for each search. In addition a different random number seed was also used for each optimisation resulting in structures labelled with suffices DHC_A to DHC_E. The regular structure is the start point corresponding to suffix DHC_A, the other initial structure topologies are shown in Figure 4.2.

4.2.1 SINGLE FREQUENCY OPTIMISATION USING NON-EVOLUTIONARY METHODS

The results of applying the three traditional search techniques (DFP, BFGS and Hook & Jeeves) are shown in Figures 4.3, 4.4 and 4.5. Each of these shows the final optimised structure and resulting frequency response of the energy in Beam 40 after both phases of the search. The frequency response for the unoptimised structure is shown with a dashed line and for the optimised structure dotted. The actual frequency used for the objective function on the latter is denoted by a cross. The frequency response over a wider frequency band, 50Hz to 350Hz, is shown and is subsequently referred to as the wide band response. The wide band average energy level is also shown. The optimisation history is shown separately for the first search phase, where the One Pass External penalty function is applied, and also for the second phase, in which the Fiacco-McCormick penalty function is used. The optimisation histories show the result of each evaluation of the objective function used in the algorithms. However for the Hook and Jeeves method, each single optimisation step requires more than one evaluation. Each single step involves an exploratory search for each individual coordinate in is made, each requiring the objective function to be evaluated, and then a pattern move. The results are also included in Table 4.1, which summarises the optimisation results for this chapter.

In optimising the performance of the structure at a single frequency of 185Hz, the Hook and Jeeves search is seen to achieve the best result at the end of both search phases, ultimately giving an attenuation of over 73dB. However it takes the largest number of evaluations, due to the apparent slow convergence of the second phase. The DFP and BFGS algorithms produce similar results, which is not too surprising since they are closely related. The 'spikes' in the optimisation history for the BFGS are thought to be due to points in the search where the Hessian matrix becomes either singular or non positive-definite. Although the algorithms are closely related, the implementation in OPTIONS uses different software suites. The most apparent distortion in the optimised structures is seen as a result of applying the DFP algorithm even though this is the least successful. The distortion in the bay second bay from the base is pronounced (Figure 4.3).

Five optimised structures were achieved using the Dynamic Hill Climbing algorithm. Each structure was obtained starting with one of the five different initial structures, and a different random number seed at the beginning of the optimisation. The optimised structure with the best performance is shown in Figure 4.6. This is also included in Table 4.1, along with the average performance for the five structures. The best structure achieves a better attenuation than for all the traditional methods. The average performance, however is not as good as that for the Hook and Jeeves search. Another point in the favour of Dynamic Hill Climbing is that the resulting

structures have been achieved using about one-third of the number of evaluations required by the Hook and Jeeves algorithm in this case. The structure shown, SF_DHC_D, does not result from using the regular structure as the start point of the optimisation and also shows the most apparent distortion of all the optimised structures presented for this optimisation case.

4.2.2 NARROW BAND OPTIMISATION USING NON-EVOLUTIONARY METHODS

The optimised structures resulting from applying the three traditional optimisation methods to minimise the average vibration transmission over the narrow frequency band are shown in Figures 4.7, 4.8 and 4.9, whose format is described above, the range of frequencies used for the objective function are denoted by a solid line with crosses showing the component frequencies. The results are also summarised in Table 4.1. As for the single frequency case, the Hook and Jeeves search is seen to provide the best attenuation out of the three methods, after both search phases, ultimately achieving an attenuation of 47dB. However, again this method shows slow convergence in the second phase. The next best value of attenuation was achieved by the DFP algorithm. In general the second phase is seen to provide little improvement in the performances of the algorithms. The amount of apparent distortion in the optimised structures does not provide any indication the attenuation achieved. The most apparent distortion is seen in the optimised structure resulting from the DFP algorithm, while the least distorted appears to be that resulting form the Hook and Jeeves search, which is the most successful.

Application of the Dynamic Hill Climbing algorithm resulted in five optimised structures, the most successful of which, N_DHC_A, is shown in Figure 4.10. This optimised structure achieves almost an attenuation of 70dB, and the average performance of all the five structures is almost 66dB, which is still better that the attenuation achieved by any of the three traditional methods. The best optimised structure results from using the regular structure as a start point, but the resulting performance is not achieved from the minimum local to this point. It is also seen that the average performance of the Dynamic Hill Climbing algorithm provides the best performance for the least number of evaluations.

4.2.3 BROAD BAND OPTIMISATION USING NON-EVOLUTIONARY METHODS

The result of applying the three traditional optimisation methods to the structure to minimise the average performance over a frequency band of 150Hz to 250Hz is shown in Figures 4.11, 4.12 and 4.13. The format of these figures is as described above and the results are again summarised in Table 4.1. As with the results reported for optimisation of the performance over the previously reported frequency band and single frequency, the Hook and Jeeves search

provides the best performance at the end of each search phase as well, achieving almost 25dB attenuation in this case. Although, it is again, the computationally most expensive. The second phase provides no improvement for the DFP algorithm and little improvement for the other two methods. Again, slow convergence is seen for the Hook and Jeeves search. This method whilst providing the best value of attenuation also results in the optimised structure which is the apparently least distorted of the three.

The structure with the best optimised performance resulting from using the Dynamic Hill Climbing algorithm, B_DHC_D, is shown in Figure 4.14. Its performance is given in Table 4.1 along with the average performance of the five optimised structures produced using this algorithm. Structure B_DHC_D achieves over 10dB greater attenuation over the best achieved with the three traditional methods, and the average performance of the structures is also better. The average number of evaluations required using Dynamic Hill Climbing is in the middle of the range for the three traditional methods. However, as the second phase of the optimisations using traditional methods did not achieve much improvement in values of attenuation, their values of optimised performance could be judged to have been achieved after the first phase. Dynamic Hill Climbing is thus seen to be more successful but requires a greater computational effort. Finally, it is noted that comparing the optimised structure B_DHC_D, with the initial structure used for this optimisation (in Figure 4.2), that the optimisation has made the originally very distorted structure, become apparently less distorted.

4.2.4 DISCUSSION OF OPTIMISATION RESULTS USING NON-EVOLUTIONARY METHODS

The Hook and Jeeves search achieved the best performance out of all three traditional optimisation methods employed, for optimisation of the performance at a single frequency and also the average performance over two frequency bands. In all cases the second phase of the search achieved very little improvement in the performance but was very computationally expensive. However, the results achieved after the first phase are still better than for the other two methods after the second phase. The next best method was the DFP algorithm, which was except for the single frequency case was also the second best after the first search phase.

Dynamic Hill Climbing achieved better performance attenuation than the three traditional methods. It is the only algorithm so far considered that allows a search that commences from an initial point that is not the regular structure. (Unless, for example, with the Hook and Jeeves search the initial step was so large that it resulted in a jump to a point in a different 'valley' with a lower value). Even where the best attenuation was found from an optimisation which commences with the regular structure, it was not the first minimum evaluated in the

optimisation run that provided the best minimum. This indicates that any of the minima local to the regular structure does not provide the best performance, however well any of the algorithms locate the true minima. (It cannot be guaranteed that all algorithms start at the same initial point commence searching in the same direction, and therefore descend into the same local minimum.)

Further investigation was not conducted to improve on the success of any of these algorithms, or the speed at which convergence has been achieved. It will be seen that even though performance improvements may well be achievable, when the robustness of the structures is considered (in Section 4.4) attempts to improve the success of the optimisations using the three traditional methods and Dynamic Hill Climbing may be academic.

The effect of the optimisations performed on the wide band response is also given in Table 4.2. It is seen that for the DFP algorithm a trend is suggested in which the narrower the frequency band over which the objective function is averaged the greater the wide band attenuation. This result is surprising as the optimisation only considers the performance over the frequency band used to evaluate the objective function, the response outside this band is an uncontrolled consequence of optimisation. With the other two traditional methods, there is little difference in the wide band response attenuation between the single frequency and narrow band optimisation, however in the case of the broad band optimisation the reduction is smaller. The mean wide band attenuation for the five optimisations using the Dynamic Hill Climbing algorithm are very similar to those for the single frequency and broad band cases. A smaller attenuation in seen for the narrow band case, although the range between the maximum to minimum values of attenuation is very similar for all frequency bands.

4.3 GENETIC ALGORITHM OPTIMISATION

The use of genetic algorithm optimisation was applied to the structure optimisation problem, previously described. As with the optimisations using non-evolutionary techniques, the energy in Beam 40 of the structure was minimised at a single frequency, and the average energy was also minimised over two frequency bands.

4.3.1 APPLICATION OF GENETIC ALGORITHM TO STRUCTURE

The binary strings representing the coordinates for the 18 variable joints of the structure are concatenated to form one long 'chromosome' which is the unit of population for the genetic algorithm optimisation. Details of the optimisation parameters used, which define the genetic algorithm process in full, are contained in Table D.6 in Appendix D. The parameter names

used in OPTIONS and commonly used notation are also included. As with most optimisation algorithms, the values of such parameters can affect the performance and therefore the success of the optimisation. The values used here were, again, taken from the previous work by Keane (1995b). Genetic algorithms were used an optimisation tool, and a study of the success of genetic algorithms against various parameter values was not investigated. The parameters were taken on the basis of the success reported by Keane.

4.3.2 GENERATION OF OPTIMAL DESIGNS

For the single frequency and narrow band optimisations the genetic algorithm was assigned to calculate optimised candidate structures by evaluating 1000 structure designs (which were realised as 5 generations, each of population size 200), and for the broad band optimisation 4500 structure designs (15 generations each of 300). The broad band optimisation was that studied by Keane (1995b), the other optimisations are included to study the effect of averaging the performance over a number of frequencies on, ultimately, the robustness of the performance of the structures.

It is unlikely that the global optimum structure design will result for the optimisation (and even if it did it would not be possible to verify this), but genetic algorithm optimisation was applied to produce ten different candidate structures. These were uniquely achieved by discarding a different number of random number samples, from the random number generator used by the algorithm, before commencing the optimisation process. This is specified by the parameter value GA_RANDM (see Table D.6). The values used were: 0 and then the first nine prime numbers, and the resulting structures are labelled with label suffices "_A" to "_J". As for the non-evolutionary optimisation results discussed above, for each optimised candidate the energy response for a wider bandwidth, 50Hz to 350Hz in 5Hz steps, was calculated and is subsequently referred to as the wide band response. This enables the effect of optimisation in the regions outside of frequency band considered by the optimisation to be seen.

4.3.2.1 SINGLE FREQUENCY OPTIMISATION

The optimisation was first performed using an objective function equal to the energy level of Beam 40 at a single frequency, 185Hz. The single frequency optimisation, evaluated on hardware platform A described in Appendix E, took approximately 1 hour to produce each optimised candidate. A summary of the results for each case is included in Table 4.1 to enable comparison with other optimisation techniques.

Figure 4.15 shows the best candidate geometry, SF_E, achieved from the ten optimisation processes performed. Figure 4.16 shows the third best candidate geometry, SF_A, which as

discussed below in Section 4.4, is a more practical structure to implement. The optimised structure topology is shown in the top-left hand corner, the frequency response in the top right-hand corner and the history of the objective function against generation in the bottom left-hand corner, which shows the value of the best objective function value achieved after each generation. The final linear value of the objective function is also stated. The frequency response for the unoptimised structure is shown with a dashed line and for the optimised structure as dotted. The frequency value used as the objective function is denoted by a cross. The numerical results for all ten candidates are summarised in Table 4.3, and the reductions in the objective function and wide band average energy level achieved are shown in decibels relative to the unoptimised structure

As the frequency at which the performance is evaluated is in a dominant resonant peak in the nominal response, it is not surprising that substantial reductions can be achieved in minimising the objective function. Since the peaks in the frequency response are likely to occur due to the cumulative effect of individual system resonances, and such resonances are often sensitive to parametric changes. To diminish the resonance response is therefore relatively easily achievable, but to reduce the response further requires that the conditions occurring at this frequency have an overall destructive effect. Here the reductions achieved in the objective function range from 53.0dB (structure SF_I) to 69.2dB (structure SF_E). The reduction of the wide band response is more consistent, ranging from 4.7dB (structure SF_J) to 11dB (structure SF_D).

4.3.2.2 NARROW BAND OPTIMISATION

This optimisation was performed with an objective function which was the average of the energy level of Beam 40 at five frequencies, 175Hz to 195Hz in 5Hz steps. The candidate geometry which gave the best performance produced by ten narrow band optimisations is shown in Figure 4.17. The frequency range used by the objective function is shown as a solid section on the dotted response, with crosses additionally denoting the actual frequency points used. For this analysis each optimisation, evaluated on hardware platform A described in Appendix E, took approximately 5 hours to produce each optimised candidate. The numerical results for all ten candidates are summarised in Table 4.4.

All of the optimised structures achieved reductions in the objective function with a range of 38.1dB to 47.5dB. The average wide band response is also reduced from between 5.2dB to 12.5dB. Even though only a small part of the frequency range was considered during the optimisation it is not surprising that this still achieves global reductions in the wide band response, since the optimisation window covers a dominant resonance peak in the response of

the structure. In the non-optimised case this peak is significant in the wide band frequency average energy level. The structure achieving the best objective function reduction is structure N_B, followed closely by structure N_G. The best wide band frequency average reductions are found in structures N_J and N_I respectively.

4.3.2.3 BROAD BAND OPTIMISATION

This type of optimisation was finally performed with an objective function which was the average of the energy level of Beam 40 at 21 frequencies, 150Hz to 250Hz in 5Hz steps. The best of the ten optimised candidates produced is shown in Figure 4.18. Even though the structural and optimisation algorithm parameters used were also those used by Keane (1995b), the starting conditions used in his work could not be assured and therefore it is unlikely that any of candidates produced here would be identical to any of those reported by Keane, which is the case. However, the performance improvements achieved are of a similar magnitude. For this analysis each optimisation, evaluated on hardware platform A described in Appendix E, took approximately 105 hours to produce each optimised candidate. The numerical results for all ten candidates are summarised in Table 4.5.

The best reduction achieved in the objective function is 34.5dB, structure B_E, which is shown in Figure 4.18, followed closely by 34.1dB (structure B_F). However these structures do not appear high in the ranking when ordered in terms of wide band response reduction. In this respect the best two structures are structures B_D and B_A. The frequency range of the objective function covers a more significant part of the wide band response than for the narrow band optimisation, but the results show that this does not imply consistency in the ranking of the best structures in both objective function and wide band response.

4.3.2.4 ANALYSIS OF POWER FLOW IN STRUCTURES OPTIMISED BY GENETIC ALGORITHMS

The aim of the optimisation is to reduce the power dissipation in Beam 40 (which is synonymous with reducing the energy level). With no external source of energy this is achieved by two mechanisms; the reduction of the input power to the structure and the redistribution of the power dissipated in the structure, so that a smaller proportion is dissipated in Beam 40. As detailed in Chapter 2, these two effects may be represented by the level reductions α_{INPUT} and α_{REDIST}. Both these have been calculated and are presented for the broad band case in Table 4.6, in which the actual values of power are also given. The reduction in input power to the structure shows little variation for the ten optimised structures and has an average value of 10.7dB. The redistribution of the power distribution shows a slightly greater variation, and has an average value of 22.3dB. Thus these two effects are both important in the reductions

achieved, although the power redistribution in the structure provides twice the reduction in level than that for the input power. The three power components in the structure (the input power, the power in Beam 40 and the power in the remainder of the structure) are depicted graphically in Figure 4.19 for all ten optimised structures. The reduction in input power is apparent, however due to the relatively small values of the power in Beam 40 for the optimised structures, the height of these bars cannot been seen. This emphasises the relative values between the components and is included here for comparison with results presented in subsequent chapters. The details of the power distributions in all the beams of the structure for the unoptimised structure and the optimised structure B_E are shown in Figure 4.20. The optimisation has caused large decreases in the power dissipated in the beams near the base of the structure, and the power transmitted through the structure is dramatically reduced.

For the single frequency and narrow band optimised structures only the values of α_{INPUT} are shown in Tables 4.3 and 4.4. The values of α_{REDIST} may be deduced from (2.83). It is seen that similar reductions in the input power are found when an average is taken over each set of ten candidates, but in general greater reductions are found as optimisation frequency band decreases. For the narrow band case there is a wide variation in values for each structure, a range of almost 10dB. As greater reductions are found in the attenuation of the power level of Beam 40 with decreasing bandwidth, and since the average input reductions are similar, this implies that the greater reductions are achieved with a greater redistribution of power within the structure.

4.3.2.5 MODAL FREQUENCY ANALYSIS OF STRUCTURES OPTIMISED BY GENETIC ALGORITHMS

A further investigation was performed in order to gain an insight into the mechanisms by which the reductions in vibration transmission of the optimised structures have been achieved. Using the finite element analysis (FEA) model package *IDEAS-5* (Structural Dynamics Research Corporation, 1997) a modal frequency analysis of the unoptimised and some optimised structures were performed.

The geometry of the structures were imported to the FEA model, the beams where modelled using 10 linear beam elements per beam, each with the following parameters: Young's Modulus of Elasticity 6.03×10^{-10} N/m^2, Material density 2370 kg/m^3, beam cross-sectional dimensions 47.02mm (x-y plane) by 24.59mm. These values were used so as to give the same values of EA and EI as specified for the beam in Section 2.1. Using FEA, beam inter-coupling forces are not easily attainable, thus the modal analysis was conducted using one of the velocity components at one end of Beam 40.

A comparison for the velocity component, V_x^1 (the x-axis velocity component at end 1 of Beam 40), was conducted using the receptance analysis method and the FEA method for the unoptimised structure, and the results are shown in Figure 4.21. Also, this comparison was performed for the three best optimised structures resulting from the genetic algorithm optimisation for the single frequency, narrow band and broad band cases, and the results are given: structure SF_E (Figure 4.22), structure N_B (Figure 4.24) and structure B_E (Figure 4.26). In general it can be seen that, although there are discrepancies between the responses produced by the models, reasonably good agreement is seen, and that the peaks and troughs in the responses from both models occur at similar frequencies, although the amplitudes are not always the same. The worse deviation is seen for the two responses for structure B_E between 250Hz and 300Hz. A similar comparison was performed by Shankar and Keane (1995) who achieved better apparent agreement between the velocity responses obtained from the same two methods. However, there are two main differences between theirs and the author's model. First, a regular structure with only four-bays was used, and any compounded modelling errors in each bay are thus greater in a structure with ten repeated bays. Second, Shankar and Keane used a generous value of $100s^{-1}$ for the value of beam damping. This is a factor of five greater and means that the individual modes will have a half-power bandwidth of approximately 100Hz. Thus the resulting frequency response is much smoother, and much less sensitive to errors in individual modal frequencies. The sensitivity of the structural model, and thus the difficulties in obtaining an accurate match between two methods of modelling, can be demonstrated by the small effects of rounding the beam dimensions used. If the actual beam dimensions (47.02mm by 24.59mm) were to be approximated as 50mm by 25mm, then the change in the first two natural bending frequencies of a 1m length beam changes from 244Hz and 672Hz, to 260Hz and 714Hz, as predicted by an Euler-Bernoulli beam model. Thus errors caused by the sensitivity of the model frequencies might explain the discrepancies in the amplitude mismatch of peaks in the velocity responses. As a peak in the responses is likely to occur from the cumulative effect of a number of modal responses, then any small changes in each individual modal frequency will affect the peak maximum, although the change in frequency may not, in fact, be at all large.

The change in the modal frequency distribution of the optimised structures compared to that for the unoptimised structure is shown in Figures 4.23, 4.25 and 4.27 for structures SF_E, N_B and B_E respectively. First, it can be seen that for the unoptimised structure two modal clusters occur, in the frequency range of interest, at 185Hz and 240Hz. With reference to the value of energy level in Beam 40 against frequency (see, for example Figure 4.3) and velocity response, in Figure 4.21, that there are peaks in both of these responses at these frequencies. It is

assumed that these peaks occur due to the modal clusters. The effect of the optimisation process for all cases appears to be to 'smooth out' the modal frequency distribution, and thus remove the effect of the modal clustering. On each figure the frequency range over which the performance is evaluated is shown, and it is seen that the dispersing of the modal clusters occurs even for clusters outside this frequency range. Indeed, two further modal clusters can be seen at frequencies 95Hz and 310Hz, which although they are well outside the frequency band used for all the optimisation cases, have also been dispersed as a result of optimisation.

To investigate whether the 'modal dispersion' is due to the optimisation process, or simply the irregularity of the optimised structures, two intermediate structure designs were randomly taken from within the first generation of the genetic algorithm optimisation which resulted in structure B_E. One intermediate design has worse performance than the unoptimised structure, and the other one has better performance. The modal distributions of each were evaluated, and are shown in Figures 4.28 and 4.29. It is seen in both cases that a 'smoothing' of the modal frequency distribution has occurred, and thus it is concluded that the modal smoothing is mainly due to the irregularity of the structure geometry. However, comparing these modal distributions with those for the three optimised structures presented above it is seen that the modal distributions for the optimised structures are 'smoother'. Thus the optimisation does provide an additional effect, and thus seeks an irregular structure that has an optimal performance. Simply providing an irregularity to the structure geometry, even though this may 'smooth' the modal distribution, does not necessarily imply a reduction in the vibration transmission of the structure.

4.3.2.6 CONSEQUENCE OF OPTIMISATION ON STATIC STRENGTH OF STRUCTURE

The static tip stiffness of the ten optimised structures obtained by genetic algorithm optimisation using a broad band objective function was briefly investigated. The geometry of the candidates was imported into a Finite Element Analysis package for this purpose. Each beam of the structure was represented as 50 beam section models each having the same physical properties as those used for the receptance theory model, as reported in Section 4.2.3.5. A force, of arbitrary value 100N, was applied at joint 20 at position (10,1) in the y-axis direction and the vertical deflection measured. The magnitude of the force has no significance as a analysis used was a linear one and non-linear effects, such as buckling, are not considered. From this the "static tip stiffness" of each structure was measured, and is included in Table 4.5.

Firstly, it is seen that the unoptimised structure has the highest tip stiffness. That is not surprising since the unoptimised traditional design, historically, is based, no doubt, on static strength. Structure B_I is the 'weakest' structure in this respect (and also is incidentally the worst in terms of dynamic optimised behaviour). However, in general there in no observed relationship between the ranking of the optimised structures and their static strength. The static strength of the best optimised candidate shows a reduction to 67% of that of the unoptimised structure. The optimised structure with the best static strength is B_J, ranked 6th by dynamic performance, which only shows a reduction to 89% of the static strength.

4.3.2.7 DISCUSSION OF GENETIC ALGORITHM OPTIMISATION RESULTS

All optimisation trials using objective functions based on either an average of the energy levels over a band of frequencies, or that using the energy level at a single frequency, have produced substantial reductions in the objective function. It is not known whether the global optimum is contained within each of the ten candidates. The mean and the maximum-to-minimum (max-to-min) ratio of the range of objective function values and the wide band response values across the ten candidates produced from each of the optimisation cases are shown in Table 4.2. The wider the bandwidth of the objective function the smaller the mean reductions achieved across the ten candidates, it can also be seen that the variation (max-to-min ratio) across the candidates in each optimisation case decreases with optimisation bandwidth.

Each optimisation seeks to achieve a reduction in the objective function, and the resulting wide band response indicates that this is achieved at the expense of the response outside the optimisation 'window'. This is shown by increases in the structural vibration transmission at some frequencies outside the objective function frequency range. Considering the reductions in the wide band response for the optimised candidates for all three optimisation cases there are only small differences in the mean reductions and variations (max-to-min) in the wide band reductions across each set of ten candidates. This indicates that in a global (*i.e.*, wide band) sense the overall vibrational energy transmission achieved is similar, which is supported by modal analysis of the optimised structures. This shows that a modal redistribution, while dispersing modal clusters does not alter the general modal density.

The fact that simply applying random changes to the structure does not necessarily produce a better design is evident from Figure 4.30. This shows the value of the objective function for all the structure designs evaluated in the entire genetic algorithm which resulted in the best structure for the broad band case, B_E, which is shown in Figure 4.18. The value of the objective function for the unoptimised structure is 0.33 $x10^{-6}$ J as marked on the y-axis. Each generation contain consists of 300 design evaluations, which are plotted in a sequential fashion.

It is seen that there many structures in the initial generation which have worse performance than the regular structure although most are better. The first generation is made up of the original, unoptimised structure design and the remaining initial population is randomly composed. As the genetic algorithm proceeds, generation by generation, it is seen that the average values of the each generation improves. However, even in the ninth generation a structure design exists which has worse performance than the nominal design (at approximately evaluation 2700). This may have resulted from either a crossover or a mutation operation, but does not succeed to the following generation.

4.3.3 OVERALL SUMMARY OF THE SUCCESS OF THE ALL OPTIMISATION METHODS

The results from all the optimisations detailed above are summarised in Table 4.1. In optimising the performance of the structure the most successful traditional optimisation technique, out of three used, was the Hook and Jeeves search. Even though this exhibited very slow convergence in the second search phase (using the Fiacco-McCormick penalty function), its performance after the first phase (using the One Pass penalty function) was also found to be better than the other two methods after both phases. From the five optimised candidates resulting from using the Dynamic Hill Climbing algorithm, the best candidate was better than any other candidates, including those using genetic algorithms. The mean energy attenuation over the five candidates was better than for the mean for the ten candidates using genetic algorithms, except for the broad band optimisation case. Thus it is seen that the two algorithms that allow exploration of the search space away from the region local to the initial point which represents the regular structure have produced structures with better optimised performance. The way in which is this is achieved is different for these two algorithms. The candidates produced using genetic algorithms are not necessarily at located at any local minima, as there is no local 'hill climbing' (or descending) element to this algorithm. It has been suggested that a good strategy is to use genetic algorithm optimisation followed by a gradient search (Ibaraki, 1997). In this way, the minima local to the solutions produced by the genetic algorithm are guaranteed to be found. This strategy was not adopted here and the justification is demonstrated by studying the robustness of each of the optimised candidates produced above, which is reported in the following section.

The mechanisms by which the reductions in vibration transmission were achieved by the optimise studies were also studied. Firstly a power analysis of the structures showed that the reductions in the vibration were achieved by a decrease of power into the structure from the primary force, but most significantly by a redistribution of power in the structure so less power is dissipated in Beam 40. A modal analysis showed that peaks in the response of the regular

structure were due to modes with similar modal frequencies. It was seen that irregular structures did not contain this 'clustering' of modal frequencies whether their overall response was better or worse than the unoptimised structure. The optimised structures had a greater smoothing effect on the modal distribution, although as seen this is not the only explanation for the reduced vibration transmission. Thus, the success of the optimised design candidates seems, in part, therefore to come from the non-repetitive nature of the geometry. Although the non-repetitive nature alone does not imply better performance, it is a common feature of all the optimised candidates. Part of the success of all the optimisation methods can probably therefore be attributed to the fact that the traditional periodic design is a particularly bad design in respect to the transmission of vibrational energy. The periodicity of the structure, whilst being favourable on aesthetic grounds allows similar frequency components, that would propagate relatively unimpeded through one bay section, through all the bay sections. Also, the static strength of some optimisation structures was evaluated. It was found that the static strength was reduced in the range of 50% to 90% of that of the unoptimised structure, and thus there was no significant compromise between static and dynamic performance, in this case.

4.4 ROBUSTNESS ANALYSIS

The robustness of the performance to geometric perturbations was analysed for each of the optimised structures obtained using each optimisation method for the single frequency case, for the narrow band and broad band objective functions, reported above. 300 sets of joint perturbations were generated and applied to the joint positions of each structure and the objective function re-evaluated and recorded. Each set contained 18 pairs of random numbers distributed uniformly between -1 and 1. Each pair relating to the x and y coordinates for each joint. The same 300 sets of joint perturbations were used for each analysis. Each of the joint perturbations were added to the joint coordinates for each structure in turn, suitably scaled. The change in the resulting objective function represents the sensitivity of the performance of the structure to small changes in the joint positions. For all cases studied in this and subsequent chapters 300 sets of joint perturbation were found to be sufficient to estimate the reported probability distribution and probability limits derived. This was validated by comparing some of the results with those produced using 1000 sets of joint distributions. Any changes in the 'shape' of the histograms or the probability limits were insignificant.

4.4.1 ROBUSTNESS OF UNOPTIMISED STRUCTURE

A brief study of the performance of the unoptimised structures due to geometric perturbations was conducted. The perturbed performance is presented for a perturbation scaling factor of

0.01 for the random perturbations. This causes the maximum perturbation to each joint coordinate to be ±10mm in both x and y axes. (The effect of this scaling factor is studied below for the narrow band genetic algorithm optimisation case). The results are shown in Figure 4.31 by displaying the value of perturbed structure performance obtained using a histogram. For this and following histograms the range is divided equally into ten bars between the minimum and maximum values (when scaled logarithmically). The nominal (unperturbed) value is indicated by a thin solid line superimposed upon each histogram plot and the nominal value is not part of the data represented by the histogram. The average energy level over the frequency bandwidth used for the optimisation is higher for the single frequency case as there is a strong resonant peak in the frequency response at this frequency, similarly the narrow bandwidth has a higher average than the broad band optimisation bandwidth. The robustness is determined by the spread of the results, the narrower this is, the more robust the structure. It is seen that for all the optimisation bandwidths considered the robustness is similar. The bold solid line is the 95% performance probability limit probability, which determines the performance value for which 95% of the applied perturbations result in better performance. This is a measure of both the nominal value and robustness and is used as an indicator in selecting the best, but practically achievable structure. This is discussed in more detail in the following section.

4.4.2 ROBUSTNESS OF STRUCTURES OPTIMISED BY NON-EVOLUTIONARY TECHNIQUES

The robustness of the optimised structures produced using the non-evolutionary methods was studied, using a perturbation scaling factor of 0.01 (corresponding to ±10mm joint coordinate freedom). The results are shown in Figures 4.32, 4.34 and 4.36, when optimised at a single frequency, and when optimised as the average performance over the narrow and broad frequency bands, respectively. The robustness of each the performance of each structure is indicated by the width of each histogram, the nominal performance is depicted by a thin solid line. The thick bold line show the 95% probability limits. The 95% probability limits are also summarised in Table 4.2.

The optimised candidate produced using the DFP and BFGS algorithms appear to have resulted in relatively robust structures in for the single frequency, narrow band and broad band optimisation cases. Additionally, the structure B_DHC_D, produced by the Dynamic Hill Climbing algorithm is also seen to be robust. Thus if robustness alone was the foremost performance criterion then these structures would be selected. However, if the absolute performance is also important then the 95% probability limit enables candidate structures to be selected on a basis combining both absolute performance and robustness. The best structures are then seen to be SF_DHC_A, N_DHC_B and B_DHC_D for the single frequency, narrow

and broad band cases respectively. It is noted that only the latter candidate would have been chosen on grounds of nominal performance. All the optimised structural designs produced by the non-evolutionary methods are less robust than the unoptimised structure, with the exception of N_BFGS, B_DFP and B_BFGS. The single frequency optimised structures are very unrobust, some of the histograms spreading over a range of four orders of magnitude, in general the narrow band optimised structures are seen to be slightly more robust. The robustness of the worse broad band optimised structures is a little over one order of magnitude.

It is apparent that for many of the optimised structures, the nominal performance is unlikely to be realised in practice, as the performance deteriorates for all geometric perturbations applied. This indicates the importance of robustness analysis in selecting a practical candidate, and the inadequacy of using the nominal performance alone. Indeed, for most of the candidates produced here there the nominal performance appears to give little indication of each structure's performance unless it is realised exactly in practice (with the precision specified by the optimised design). It is also seen that, with the exception of B_DHC_D, there is a trade-off between robust performance and nominal value. Thus only structures whose nominal performance is likely to be realised, are in general, those structures whose nominal performance is one of the lower ranked. The relative impracticality of the optimised designs produced using non-evolutionary optimisation methods is apparent by comparison with the optimised candidates produced in the following section.

An indication of the lack of robustness of the optimised structures achieved by the Hook and Jeeves and Dynamic Hill Climbing methods can be gleaned from studying the optimisation histories, as shown in Figures 4.5, 4.9 and 4.13, and Figures 4.6, 4.10 and 4.14, respectively. In these techniques the hill climbing is composed of intermediate exploratory searches in each joint coordinates in turn and pattern moves. The results of each objective function evaluation for these is shown in the optimisation histories. The presence of large spikes in a history indicates the 'unrobustness' of the present position in the search space, as the small changes can be considered akin to a perturbation. Also, the 'shotgun' search at the end of the first phase for the Hook and Jeeves search is similar to a perturbation analysis, giving an idea of the robustness of the solution at this point in the optimisation.

4.4.3 ROBUSTNESS OF GENETIC ALGORITHM OPTIMISED STRUCTURES

A robustness analysis was performed for all ten optimised candidates resulting from the genetic algorithm optimisation. For the narrow band optimised structures, the effect of the size of the range of the perturbations used in the robustness analysis is also investigated. For all the results

presented, a summary is included in Table 4.2 to enable comparison between the perturbed performance with optimised structures resulting from other optimisation methods.

4.4.3.1 ROBUSTNESS OF SINGLE FREQUENCY OPTIMISED STRUCTURES

The robustness of the optimised structures obtained using genetic algorithm optimisation at a single frequency was briefly studied for a perturbation scaling factor of 0.01. This causes the maximum perturbation to each joint coordinate to be ±10mm, as previously discussed. The perturbed values of the objective function are displayed using a histogram to indicate the statistical spread about the nominal value, Figure 4.33. As before, the nominal value is indicated by a thin solid line superimposed upon each histogram plot, the 95% probability limit by a bold solid line and the results are ranked in order of decreasing nominal performance. The results are listed in Table 4.3. It can be seen that, for example, S_E and S_D are less robust than structures S_A and S_G to small perturbations in structure geometry. If solely the robustness of the structures were the paramount design goal then structure S_A is shown to have the best performance in this respect. However even though this structure is more robust its nominal (unperturbed) performance is not as good as structure S_E.

It can be seen that the entire distribution of the performance for structure SF_D is worse than for the nominal structure for all perturbation cases (the nominal structure performance is not included in the distribution population). The size of the joint perturbations used here represents a generous manufacturing tolerance of 10mm. However it is unlikely that the nominal performance of this structure would be still be practically realisable. As shown below, where the effect of the size of the perturbations is studied, the perturbations used here are still representative of the robustness seen for smaller perturbations. Comparing the perturbed performance of the single frequency optimised structure with that of the perturbed performance of the unoptimised structure in Figure 4.31, it is seen that in general the structures have a lower robustness after optimisation. Only structures S_A and S_G have maintained a similar level robustness through optimisation.

Considering the absolute perturbed structure performance the 95% probability limits indicate that the best structure is seen to be structure S_A, followed closely by structure S_G and then structures S_E, S_J and S_F. Structure S_A is shown in Figure 4.16. It was ranked third in terms of nominal performance but is a more practical structure than S_E. This revelation is not indicated by any characteristic of the topology of either structure.

4.4.3.2 ROBUSTNESS OF NARROW BAND OPTIMISED STRUCTURES

The robustness of the narrow frequency band optimised structures was first investigated using a scaling factor of 0.01 for the random joint coordinate perturbations up to ±10mm. The nominal and perturbed performance of each structure is shown in Figure 4.35 with the 95% probability limits, shown following the convention of Figure 4.33. The results are also listed in Table 4.4. On grounds of robustness alone structure N_I is the most robust structure, however its absolute performance is generally worse than most of the other candidates. This optimised structure is the only one whose robustness is comparable to the unoptimised structure, shown in Figure 4.31. Using the 95% probability limit the best structure is seen to be structure N_B, which for this optimisation case also happened to have the best nominal performance.

The choice of the maximum size of perturbations used above (determined by the perturbation scaling factor) was arbitrary to some extent, though it was chosen in order to represent a typical maximum manufacturing tolerance. In order to verify that the above results are not dependent on this scaling factor, and that there is some degree of 'linearity' in the results against small changes in the scaling factor, two additional scaling factors were investigated. The results for scaling factors of 0.005 and 0.02 (perturbations of up to ±5mm and ±20mm) are shown in Figures 4.38 and 4.39 respectively for the narrow band optimised structures. In both cases the absolute values defining the distribution are changed due to the different size of the applied perturbations. The ranking of the 95% probability limits for a scaling factor of 0.005 across the structures are almost identical to those for 0.01, although the differences between structures N_C and N_H becoming smaller. The performance limits for a scaling of 0.02 shows more radical changes in ordering than for those with 0.01 scaling. In particular the original 'best choice' performance of structure N_B has deteriorated. These results suggest that a scaling factor of 0.02 is too large to be considered a 'small' perturbation for these structures, producing results strongly dependent upon the range of perturbation amplitudes.

4.4.3.3 ROBUSTNESS OF BROAD BAND OPTIMISED STRUCTURES

The robustness of the broad band optimised structures was also investigated using a perturbation scaling factor of 0.01. The nominal and perturbed performance of each structure is shown in Figure 4.37 with the 95% probability limits following the convention of Figure 4.33. The results are also listed in Table 4.5. The most robust structure is structure B_D followed closely by structure B_J, and these are seen to be more robust than the unoptimised structure, whose perturbation performance is shown in Figure 4.31. In general it is seen that the perturbations have less effect on the broad band optimised structures than the other two cases, although the performance of some structures are clearly more sensitive to

perturbations than others. This is shown by the reduced (vertical) baseline of the histograms. For the least robust structure B_B this covers only one order of magnitude. Using the 95% probability limit the best structures are seen to be structures B_E and B_H.

4.4.4 DISCUSSION OF ROBUSTNESS ANALYSIS RESULTS

The results of all the robustness analyses for all the optimised structures presented in this chapter are summarised in Table 4.2. The promising performance of the non-evolutionary methods, which appeared to be very good on the grounds of nominal performance, is not found to be realisable as shown by the robustness analysis of the structures. Even though some of these structures showed better nominal performance than the optimised structures produced by genetic algorithm optimisation they are, in general, seen to be very unrobust. Their nominal performance is unlikely ever to be realised in practice as any applied geometric perturbation deteriorates their performance. The 'optimality' of such structures is thus seen to be false in a practical sense. The differences between the nominal performance and the performance for the 95% probability limit for structures produced by non-evolutionary methods and genetic algorithms is seen by comparing these values shown in Table 4.2. This is also readily apparent by comparing Figures 4.36 and 4.37 for the broad band case, for example. The reason the structures resulting from the use of non-evolutionary techniques are thought to be so unrobust is the nature in which the optimisations produce optimal solutions. Gradient search methods seek local minima, features in the search space that are often due to the destructive effects between many individual responses of the structure. These minima are special positions in the search space where these effects are simultaneously at a minimum, but as many rely on so many contributory elements there are also often sensitive to changes in any one of them. These may be visualised as very sharp dips or valleys in the search space, and the performance indicated in such features are only attainable at this exact point in the search space, and therefore sensitive to any changes in the optimisation parameters. The performance of the optimised candidates produced by the genetic algorithm optimisation is seen not to be as sensitive as those produced by the non-evolutionary methods, even though there is variation between the robustness of individual optimised structures. In the selection of a practical optimised candidate the analysis of the robustness of the structures is therefore still prudent. The use of the optimised candidates produced by the non-evolutionary methods was not studied further.

The optimised structures obtained using genetic algorithm optimisation for the single frequency, and both narrow and broad band objective functions demonstrate different levels of robustness. By comparing the spread of the distributions for the candidates for each case an

indication of the typical robustness inherently achieved with each type of objective function can be seen. A perturbation scaling of 0.01 (corresponding to perturbations up to ±10mm) is common for each optimisation case in Figures 4.33, 4.35 and 4.37. It is seen that for the same perturbations the wider the frequency band considered by the objective function the smaller the spread. For the single frequency case the spread of each candidate's distribution varies from three orders of magnitude to one order of magnitude, for the narrow band case the spread varies from one to two orders of magnitude, for the broad band case all the candidates variations fall approximately within one order of magnitude. Hence it is seen that the wider the bandwidth of the objective function the more inherently robust the candidates produced by the optimisation. However, only some of the candidates of the broad band optimisation are shown to be more robust than the unoptimised structure.

Table 4.2 shows the mean and the maximum-to-minimum (max-to-min) ratio of the range of the 95% probability limits across the ten candidates produced from each of the optimisation cases. The mean of the 95% probability limits is seen to decrease with increasing objective function bandwidth, whereas the max-to-min ratio is seen to decrease. This trend is similar to that for the corresponding objective function value results. This is explained by the fact that the 95% probability limit is a combined measure of the nominal performance and the robustness for each candidate. However, for the single frequency case, the max-to-min ratio is noticeably greater due to the relative lack of robustness of the candidates produced from single frequency optimisation.

The geometric perturbations used in the robustness analysis, and the results obtained from them, are a measure of statistical performance due to an ensemble of uniformly distributed perturbations. If the distribution of the perturbations was to differ greatly from being uniform, then other optimised structures may be preferable. In the absence of any information about the perturbation distribution then the assumption of uniform distribution is thought to be prudent. If the distribution of the perturbations was known then this could be applied in the analysis to produce more specifically relevant results.

4.5 CONCLUSIONS

Optimisation of an existing traditional design of a lightweight cantilever structure, to reduce the vibrational energy transmission from the base to the end beam, was performed. The optimisation criterion was based on three types of objective function, one using the energy level at a single frequency (185Hz), one using an energy level average over a narrow band of frequencies (175-195Hz), and one using an energy level average over a broad band of

frequencies (150-250Hz). Optimised structures were achieved using three traditional methods (consisting of two gradient based and one hill climbing technique), Dynamic Hill Climbing (a hill climber with stochastic search restart) and genetic algorithms. The latter two methods have random elements to their operation so five and ten candidates, respectively, were produced for each.

The optimisation process achieves significant reductions in the energy transmission in the frequency band over which the objective function was evaluated although, in general the energy level over a wider frequency band remained fairly constant. A modal analysis for structures produced using genetic algorithms showed that the very nature of irregular geometries 'smoothes out' modal frequency clusters which are often responsible for peaks in the frequency response, but only on a local basis. However, the virtue of an irregular structure does not imply better performance and the optimisation process is still required to find the modal conditions which result in the large reductions in vibration transmission seen. The amount of apparent distortion in the optimised structures was not found to be a good indicator of the minimised performance, the most distorted structures not necessarily being the best optimised structures. The consequence of the optimisation of the structures (concerned with the dynamic performance) on the static strength of the candidates obtained for the broad band genetic algorithm optimisation was briefly studied. All these optimised candidates were found to have an inferior static tip stiffness compared to the original, and there was no relationship found between the static strength and the ranking of the optimised candidates. The static tip stiffness was reduced by about 50% to 90% across all ten candidates, compared to the unoptimised structure.

The robustness (lack of sensitivity) of the optimised performance to small changes in the structure geometry of all optimised structures resulting from all optimisation methods was analysed by applying small perturbations to the positions of the non-extreme joint positions. By applying an common ensemble of random joint perturbations to each candidate the statistical distribution of the resulting performance change could be studied. It was found that some structures are more robust to such perturbations than others. In particular it was found that the optimised structures produced by the optimisation methods that produce optimised structure be seeking, exact, local minima are very unrobust. In many cases, to such an extent that it is unlikely that the structures would be practically realisable. In general the optimised structures resulting from genetic algorithm optimisation are much more robust, although to varying degrees. The amount of apparent distortion of the optimised structures, or any form of the geometry does not indicate the degree of robustness of a structure. In general it is found that the wider the response bandwidth considered by the objective function in the optimisation process,

the less the spread in nominal performance across the ten candidates produced in each case, and also the more robust the design candidates obtained. This is thought to be because the wider bandwidth will result in an objective function which is dependent upon the combined effect of many modes and is therefore less sensitive to changes in any one particular mode.

A smaller and a larger size of random joint perturbations were additionally applied to the narrow band genetic algorithm optimised candidates uniformly distributed between ±5mm and ±20mm. It was found that a similar ranking of results was obtained for perturbation up to ±5mm and the original perturbation size (±10mm). The ranking was not preserved perturbations up to ±20mm because, it is thought, they were no longer small compared to the size of the structure.

The choice of the best optimised candidate depends upon both the absolute value of the nominal (unperturbed) performance, and the robustness of the structures performance to perturbations. A criterion is suggested which defines the best candidate to be that whose performance is the best for 95% of all perturbations applied. This is used to indicate the statistical expectation of the structure performance. This criterion is applied to the candidates enabling the best candidate, in terms of both robustness and absolute performance, to be identified.

Optimisation Bandwidth	Optimisation method		Penalty Function			
			One Pass		Fiacco-McCormick / Final	
			Objective function attenuation (dB)	Number of evaluations	Objective function attenuation (dB)	Total Number of evaluations
Single Frequency (185Hz)	DFP		39.6	2667	49.6	6180
	BFGS		41.6	2038	48.4	4375
	HOOK & J		70.9	2576	73.4	9530
	DHC	mean	-	-	68.1	3031
		max	-	-	82.3	2773 [1]
	GA	mean	-	-	59.0	1000
		max	-	-	69.2	1000
Narrow Band (175 - 195Hz)	DFP		40.6	4646	41.0	5459
	BFGS		29.2	2876	30.4	4939
	HOOK & J		46.2	2400	47.2	8123
	DHC	mean	-	-	65.9	4161
		max	-	-	69.8	6229 [1]
	GA	mean	-	-	42.9	1000
		max	-	-	47.5	1000
Broad Band (150 - 250Hz)	DFP		22.6	1808	22.6	2018
	BFGS		17.8	2037	19.9	4297
	HOOK & J		24.1	2473	24.9	8075
	DHC	mean	-	-	28.4	4188
		max	-	-	36.8	4091 [1]
	GA	mean	-	-	32.6	4500
		max	-	-	34.5	4500

[1] number of iterations corresponding to the DHC optimisation achieving the maximum attenuation.

TABLE 4.1. Summary of optimisation performance for all optimisation methods. Attenuation refers to reduction achieved in optimisation bandwidth.

Optimisation Bandwidth	Optimisation method		Objective function (dB)	Wide band response (dB)	95% probability limit for objective function (dB)
Single Frequency (185Hz)	DFP		49.6	14.1	39.1
	BFGS		48.4	9.95	34.7
	HOOK & J		73.4	7.72	37.0
	DHC	mean	68.1	7.03	33.4
		max-to-min	20.5	10.1	21.8
	GA	mean	59.0	7.39	44.0
		max-to-min	16.2	6.03	21.1
Narrow Band (175 - 195Hz)	DFP		41.0	8.28	34.4
	BFGS		30.4	10.8	28.8
	HOOK & J		47.2	8.61	26.0
	DHC	mean	65.9	3.50	40.9
		max-to-min	6.04	12.0	10.4
	GA	mean	42.9	8.13	37.7
		max-to-min	9.31	7.32	10.6
Broad Band (150 - 250Hz)	DFP		22.6	4.93	19.6
	BFGS		19.9	6.12	17.5
	HOOK & J		24.9	3.81	11.4
	DHC	mean	28.4	8.3	20.0
		max-to-min	12.4	10.5	16.0
	GA	mean	32.6	9.07	29.7
		max-to-min	3.50	8.89	4.96

TABLE 4.2. Summary of optimisation performance, wide band responses and 95% probability limits for all optimisation methods. Attenuation refers to reduction achieved in optimisation bandwidth.

Rank	Structure	reduction in objective function (185Hz) (dB)	reduction in wide band average energy (50-350Hz) (dB)	95% probability limit for objective function (dB)	Power input reduction (185Hz) (dB)
-	unopt.	0	0	-	0
1	SF_E	69.2	10.7	56.5	13.6
2	SF_D	67.3	11.0	39.6	10.5
3	SF_A	63.9	9.8	60.2	13.4
4	SF_G	62.4	6.4	58.2	13.9
5	SF_J	60.9	4.9	55.6	15.0
6	SF_F	60.4	7.6	55.3	13.4
7	SF_C	60.3	6.5	39.1	14.4
8	SF_H	58.8	5.8	50.7	14.0
9	SF_B	56.5	8.0	39.1	13.9
10	SF_I	53.0	7.4	46.3	11.3
average		59.0	7.4	44.0	13.5

TABLE 4.3. Results summary for the Single Frequency objective function optimised using genetic algorithms. Input power reduction is also shown.

Rank	Structure	reduction in objective function (175-195Hz) (dB)	reduction in wide band average energy (50-350Hz) (dB)	95% probability limit for objective function (dB)	Power input reduction (175-195Hz) (dB)
-	unopt.	0	0	-	0
1	N_B	47.5	8.6	42.5	9.29
2	N_G	47.1	9.8	36.6	12.7
3	N_F	45.5	7.8	42.2	14.3
4	N_J	44.9	12.5	41.7	13.4
5	N_A	44.4	6.7	41.3	5.83
6	N_C	43.8	8.5	39.7	13.2
7	N_H	43.2	6.6	40.2	13.0
8	N_D	41.8	5.2	36.3	8.31
9	N_I	41.5	10.7	39.0	8.87
10	N_E	38.1	9.6	31.9	11.1
average		42.9	8.1	37.7	11.7

TABLE 4.4. Results summary for the Narrow band objective function optimised using genetic algorithms. Input power reduction is also shown.

Rank	Structure	reduction in objective function (150-250Hz) (dB)	reduction in wide band average energy (50-350Hz) (dB)	95% probability limit for objective function (dB)	Static tip stiffness (KN/m)
-	unopt.	0	0	-	98.6
1	B_E	34.5	9.5	31.9	65.6
2	B_F	34.1	7.2	31.1	69.0
3	B_H	33.9	9.0	31.7	75.8
4	B_B	33.3	12.3	27.8	69.2
5	B_C	32.8	5.3	29.2	66.0
6	B_J	32.3	11.6	30.9	87.6
7	B_A	32.3	12.7	29.8	83.3
8	B_G	32.0	8.4	30.0	71.7
9	B_D	31.6	14.2	30.2	54.3
10	B_I	31.0	8.3	26.9	46.8
average		32.6	9.1	29.7	-

TABLE 4.5. Results summary for the Broad band objective function optimised using genetic algorithms. Input power reduction and static tip strength is also shown.

Structure	Primary force input power		Power dissipated		Power redistribution
	($x10^{-5}$ W)	Reduction (dB) α_{INPUT}	in structure ($x10^{-5}$ W)	in Beam 40 ($x10^{-9}$ W)	(dB) α_{REDIST}
unoptimised	36.4	0	35.7	$6.69x10^{-6}$ W	0
B_E	2.89	11.0	2.89	2.40	23.4
B_F	2.82	11.1	2.82	2.58	23.0
B_H	2.89	11.0	2.89	2.70	22.9
B_B	3.13	10.7	3.13	3.10	22.7
B_C	4.59	9.0	4.59	3.55	23.8
B_J	3.75	9.9	3.75	3.93	22.4
B_A	2.53	11.6	2.53	3.93	20.7
B_G	2.52	11.6	2.52	4.19	20.4
B_D	3.64	10.0	3.64	4.59	21.6
B_I	3.55	10.1	3.55	5.37	20.8
average	3.23	10.7	3.23	3.63	22.3

TABLE 4.6. Power levels within the optimised structures, over a bandwidth of 150Hz to 250Hz.

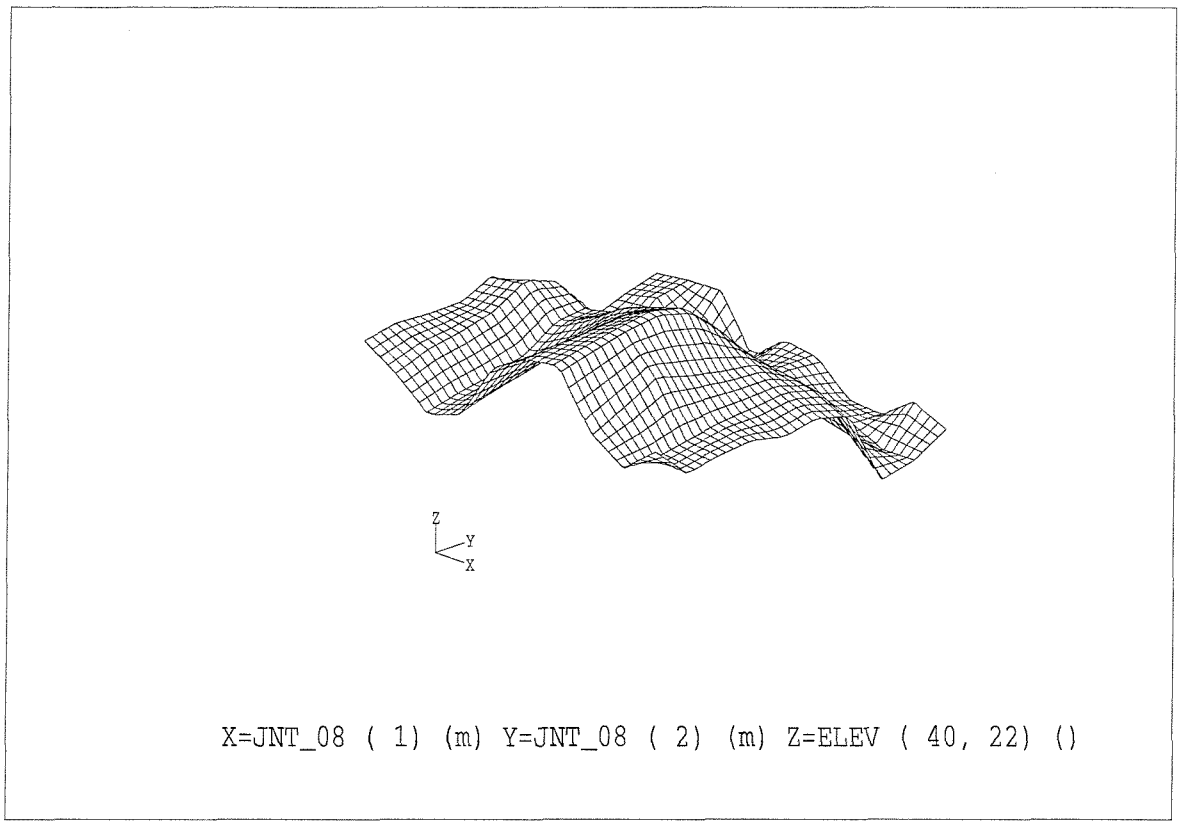

Figure 4.1: Contour plot of the linearly-scaled broad band objective function against x and y coordinates for joint 8 within the optimisation limits.

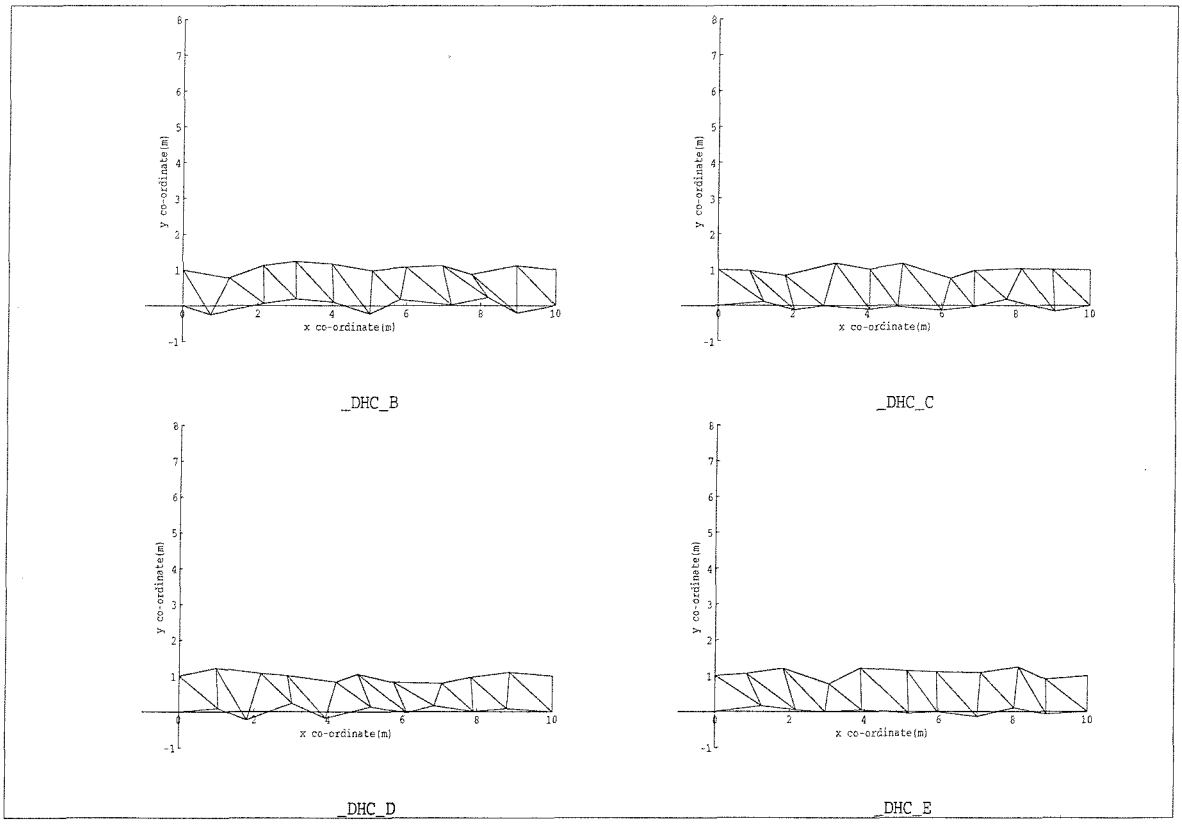

Figure 4.2: Four randomly generated structures used as start points for the Dynamic Hill Climbing optimisations.

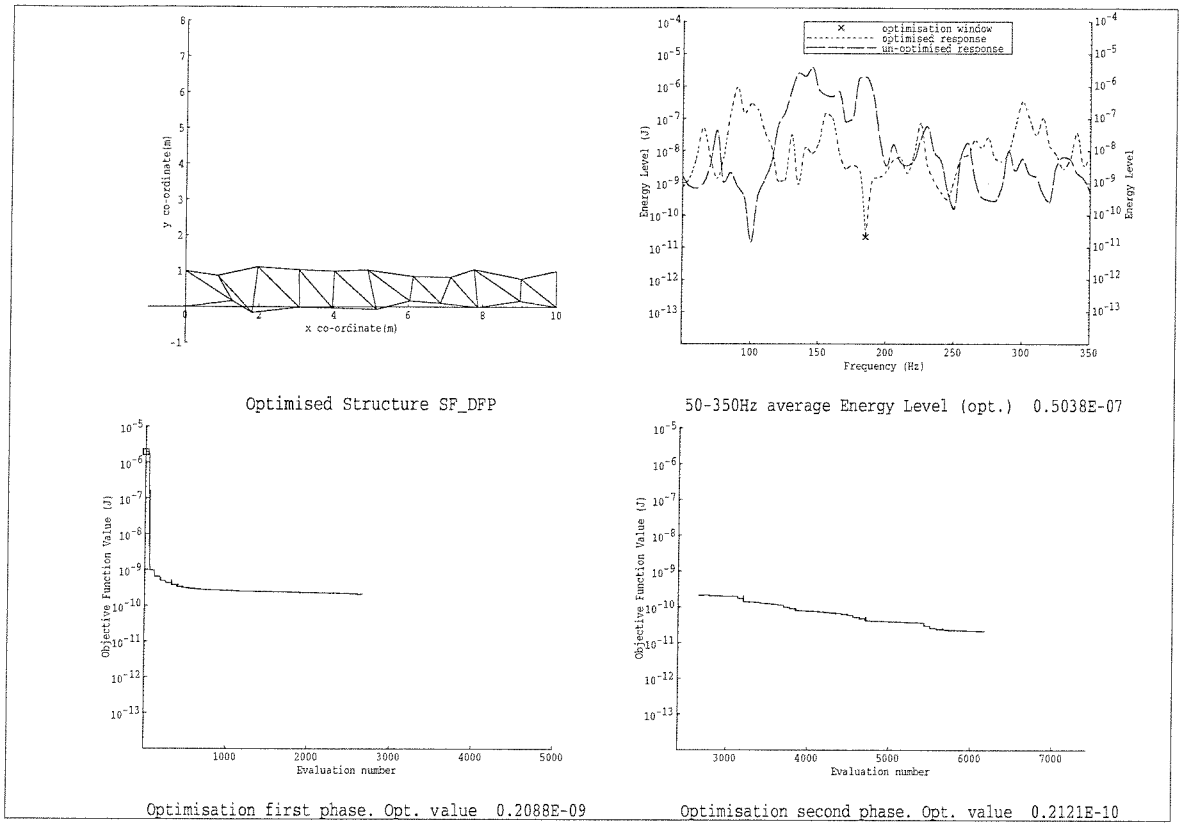

Figure 4.3: Structure optimised for performance at 185Hz achieved using the Davidon-Fletcher-Powell method.

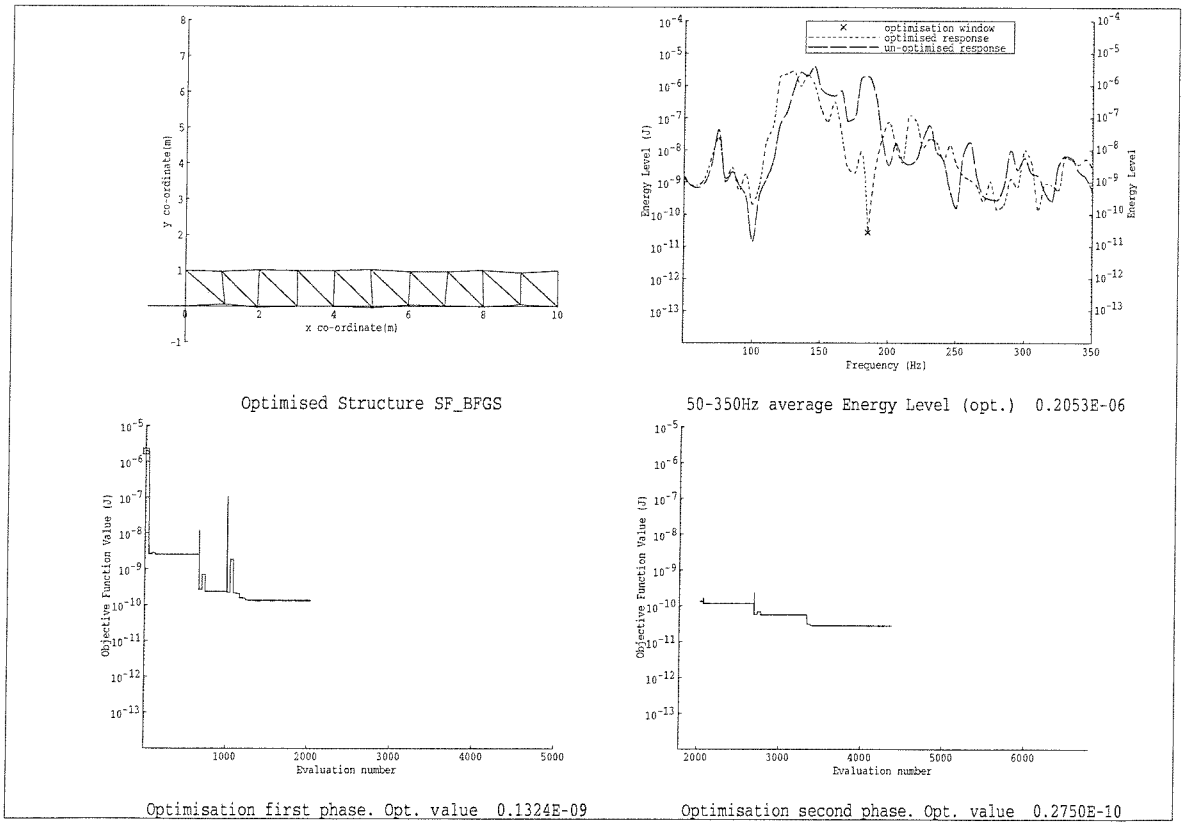

Figure 4.4: Structure optimised for performance at 185Hz achieved using the Broyden-Fletcher-Goldfarb-Shanno method.

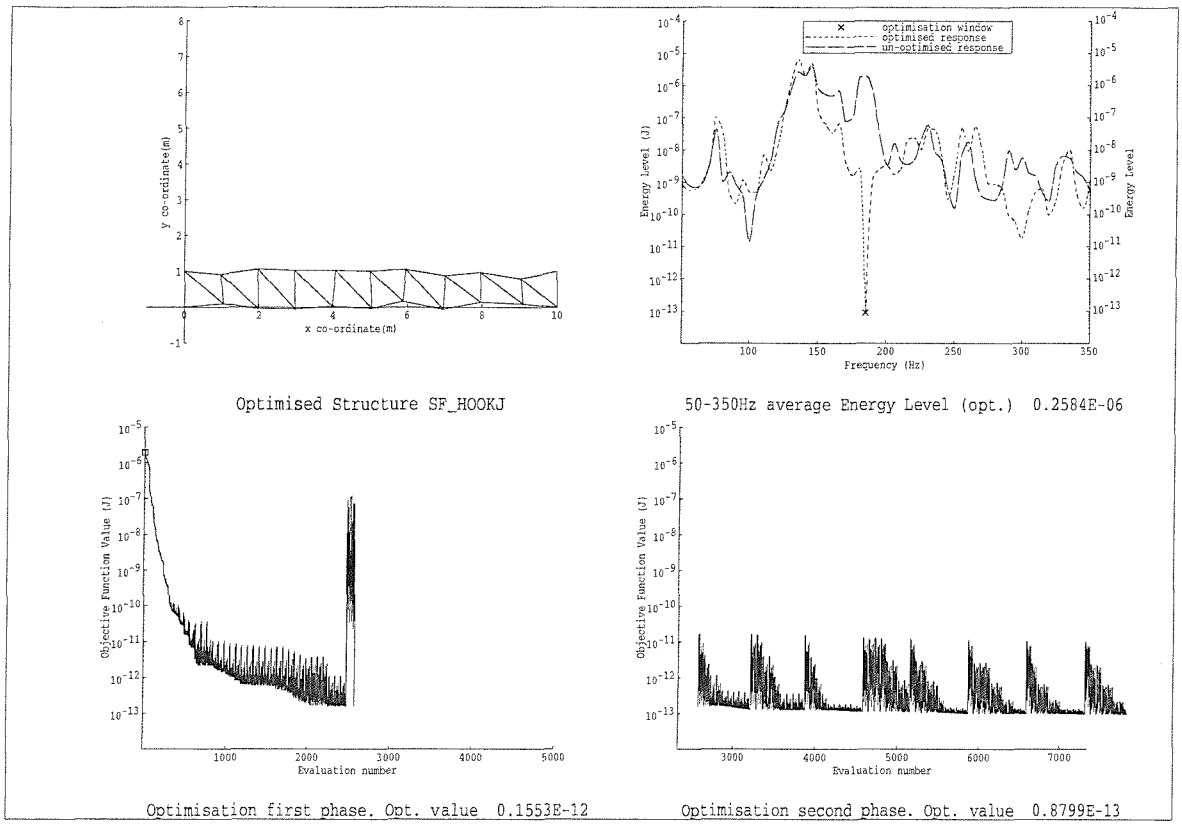

Figure 4.5: Structure optimised for performance at 185Hz achieved using the Hook and Jeeves method.

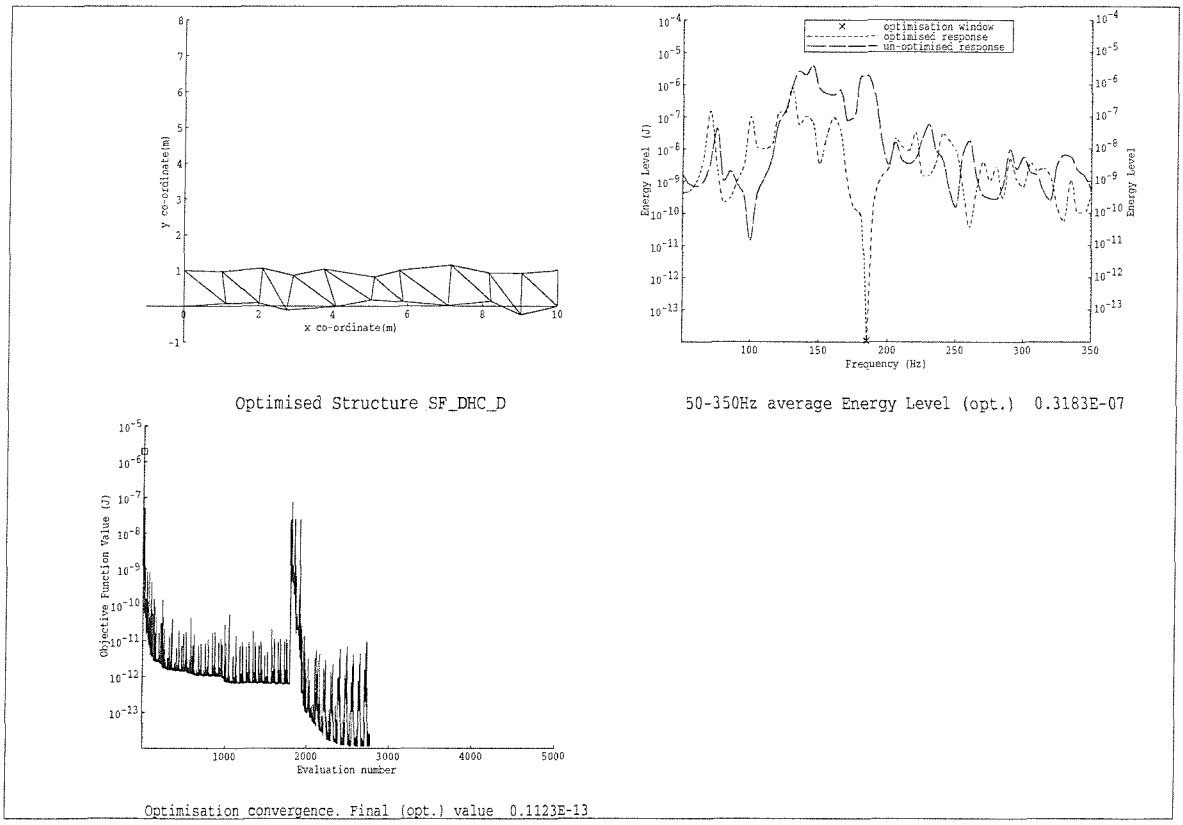

Figure 4.6: Structure with best optimised performance at 185Hz achieved using Dynamic Hill Climbing.

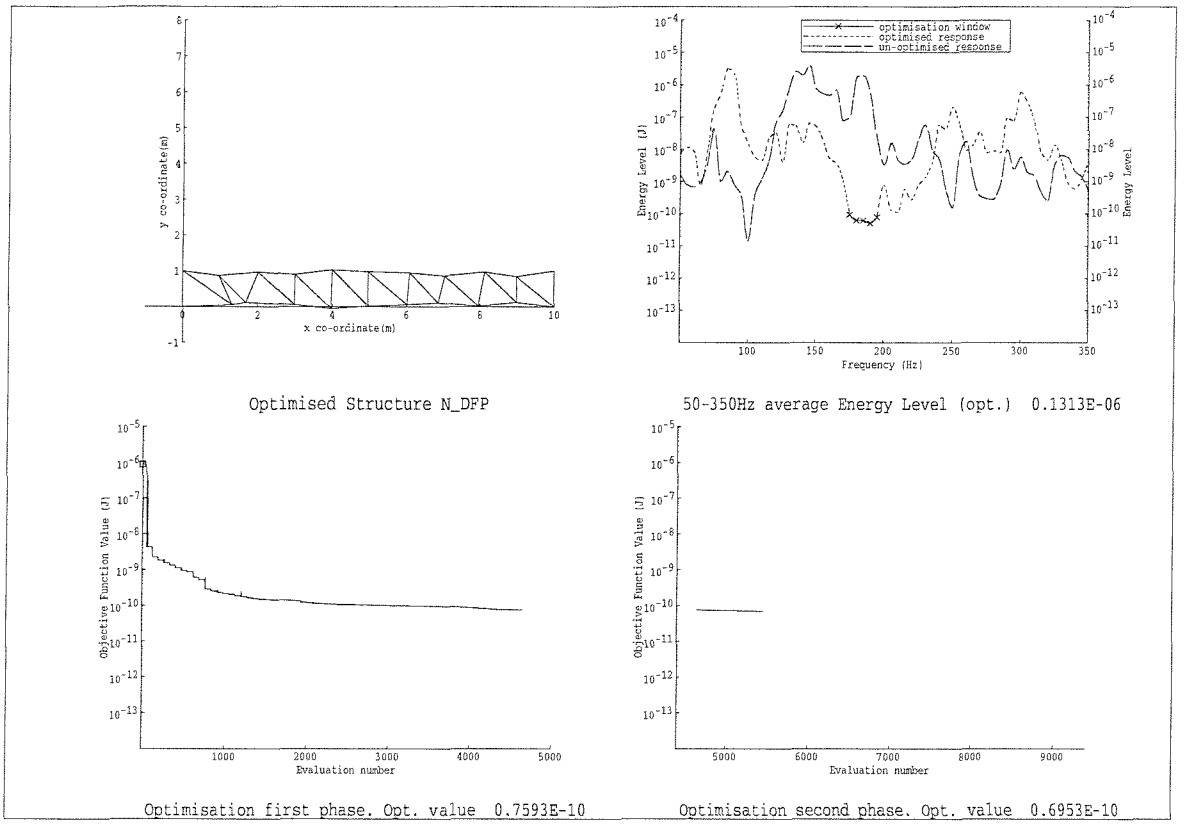

Figure 4.7: Structure optimised for average performance over frequency band 175Hz to 195Hz, achieved using the Davidon-Fletcher-Powell method.

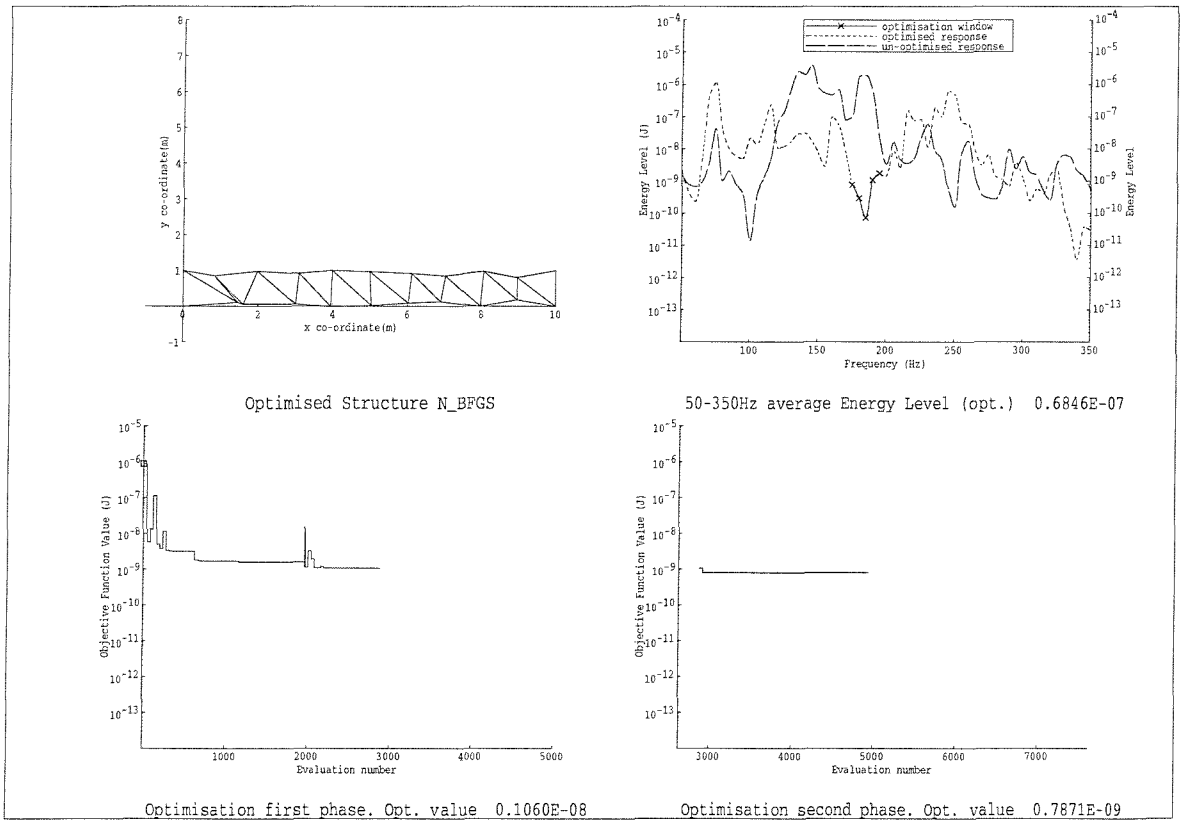

Figure 4.8: Structure optimised for average performance over frequency band 175Hz to 195Hz, achieved using the Broyden-Fletcher-Goldfarb-Shanno method.

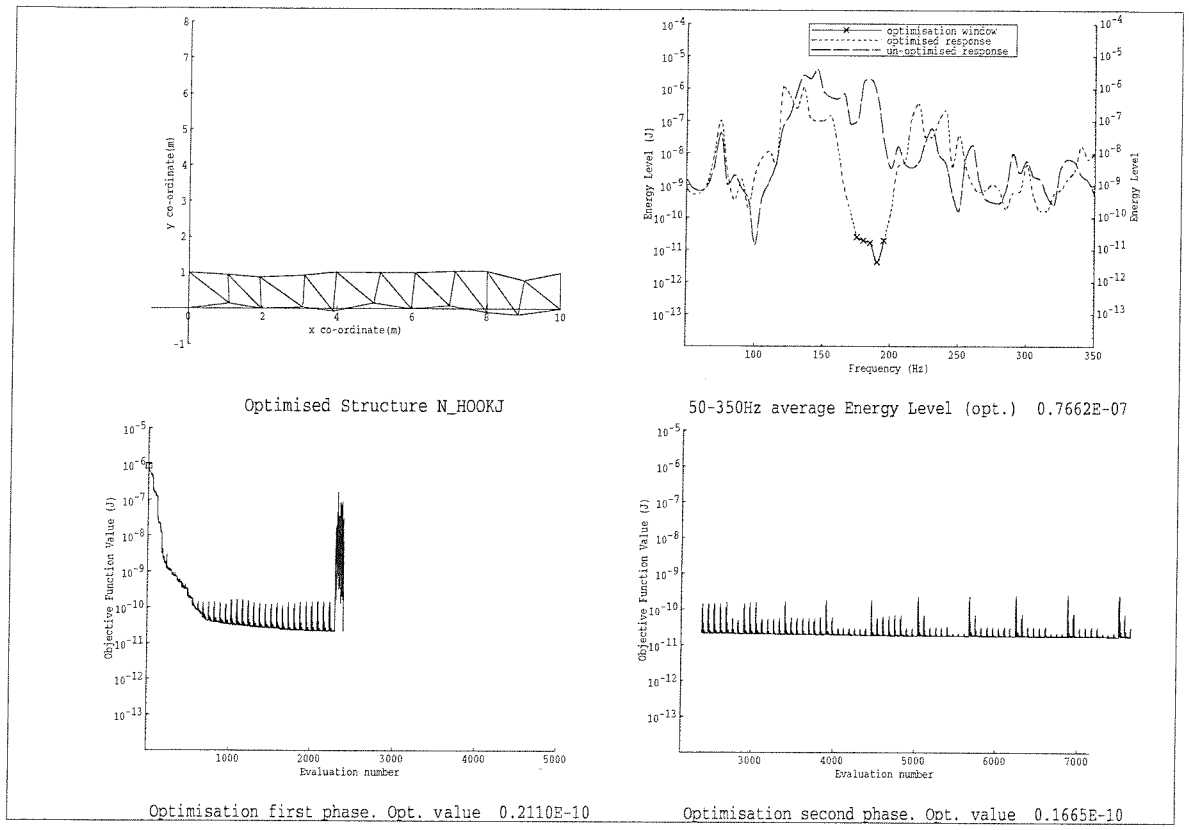

Figure 4.9: Structure optimised for average performance over frequency band 175Hz to 195Hz, achieved using the Hook and Jeeves method.

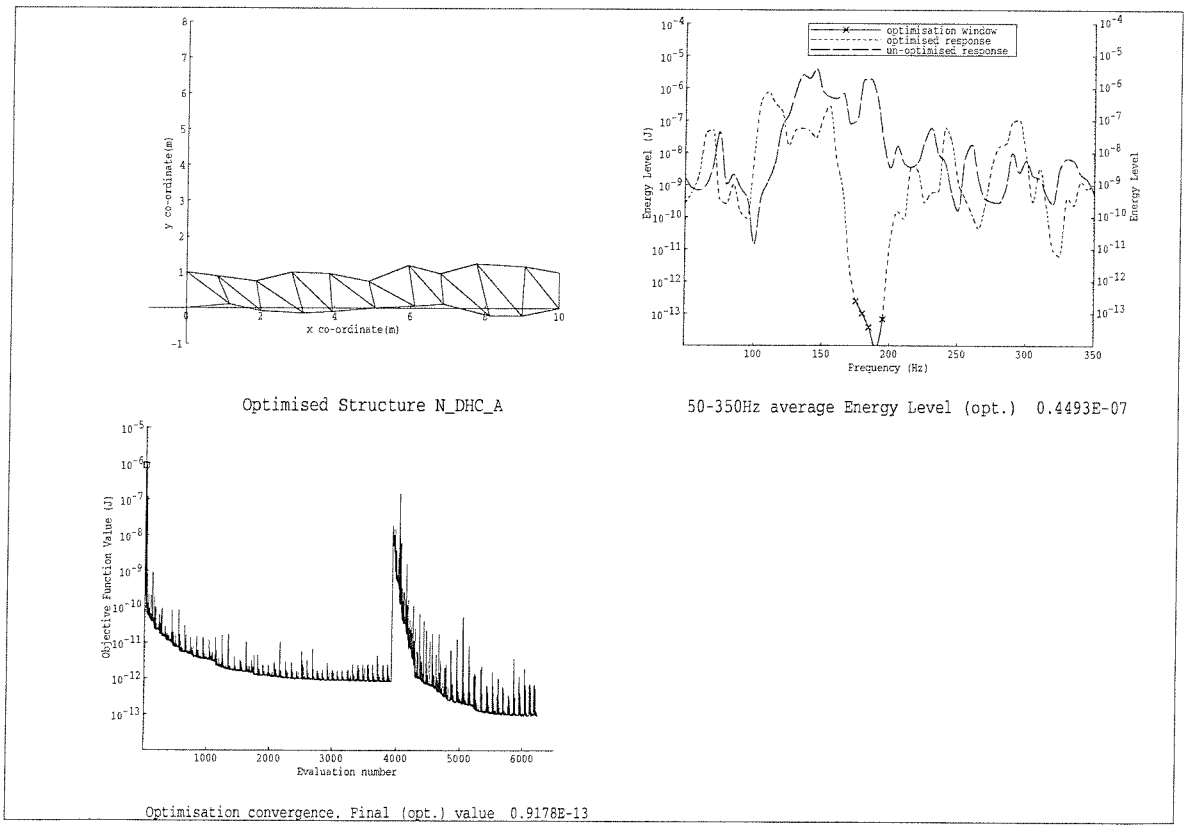

Figure 4.10: Structure with best optimised average performance over frequency band 175Hz to 195Hz, achieved using Dynamic Hill Climbing.

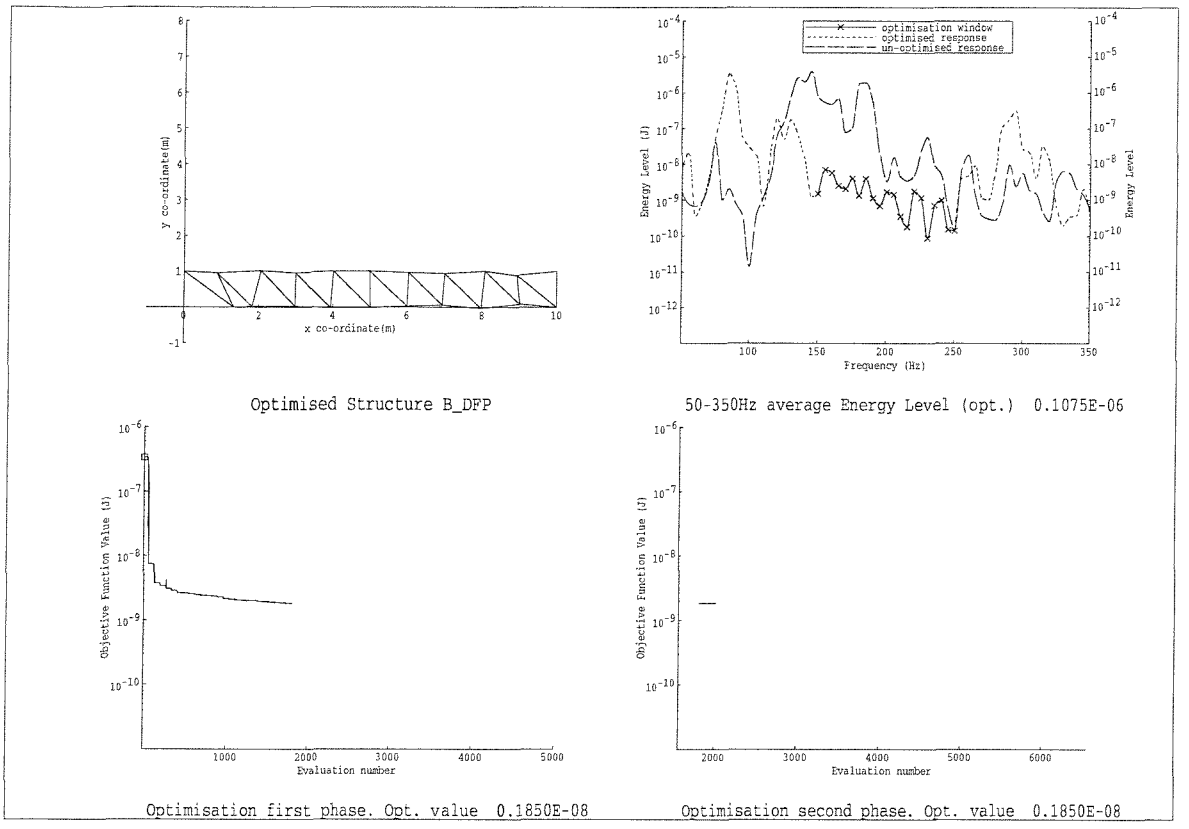

Figure 4.11: Structure optimised for average performance over frequency band 150Hz to 250Hz, achieved using the Davidon-Fletcher-Powell method.

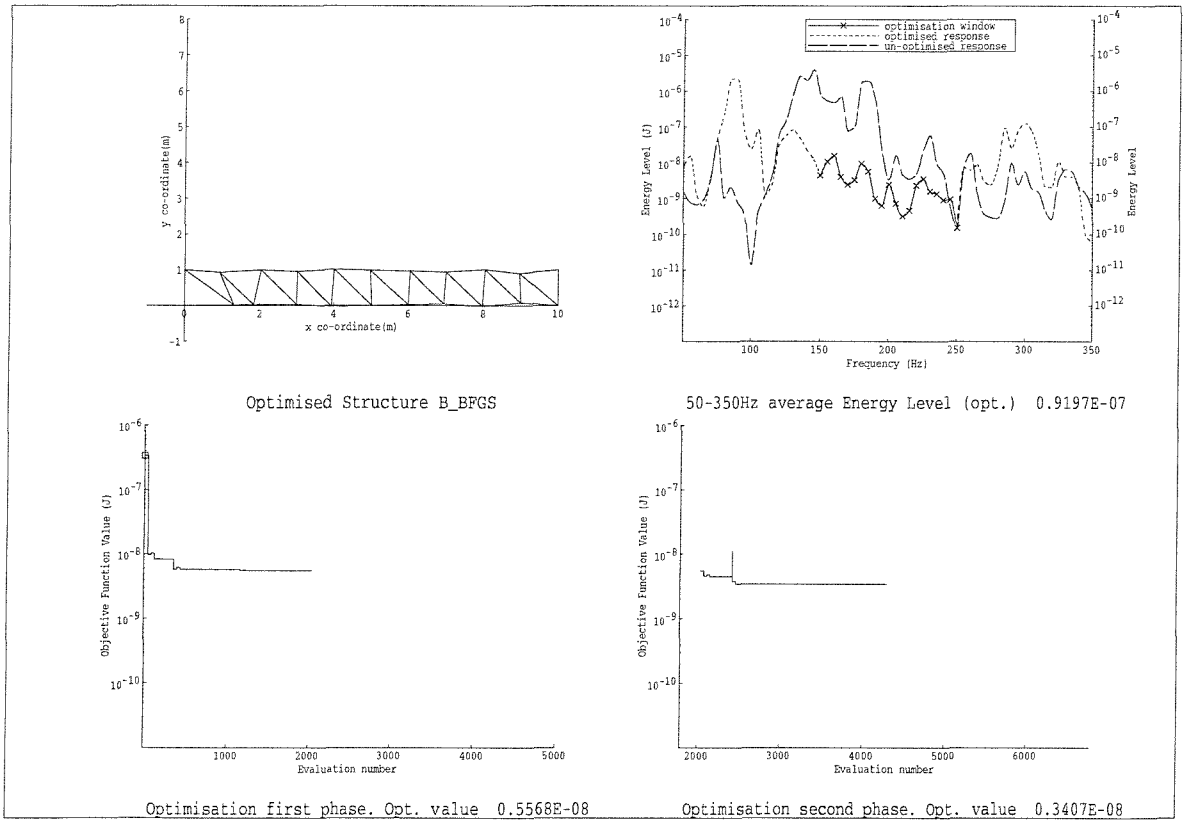

Figure 4.12: Structure optimised for average performance over frequency band 150Hz to 250Hz, achieved using the Broyden-Fletcher-Goldfarb-Shanno method.

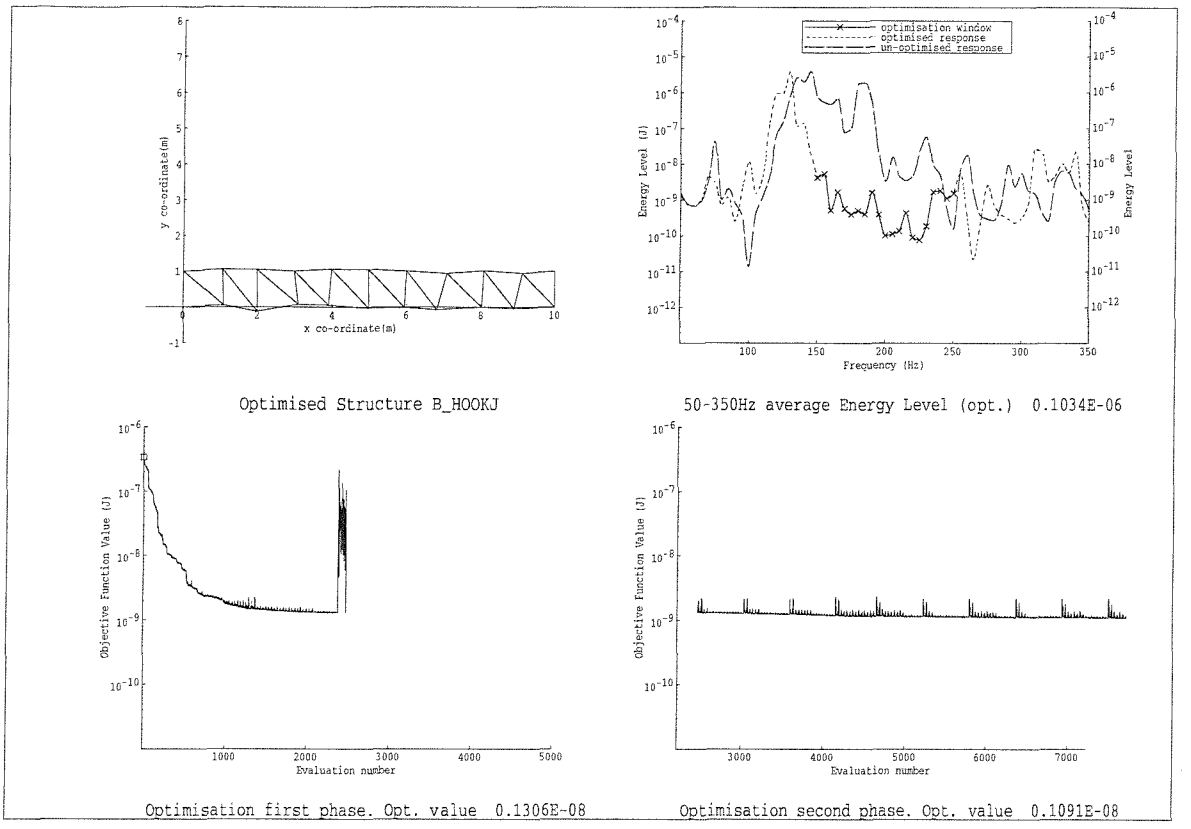

Figure 4.13: Structure optimised for average performance over frequency band 150Hz to 250Hz, achieved using Hook and Jeeves method.

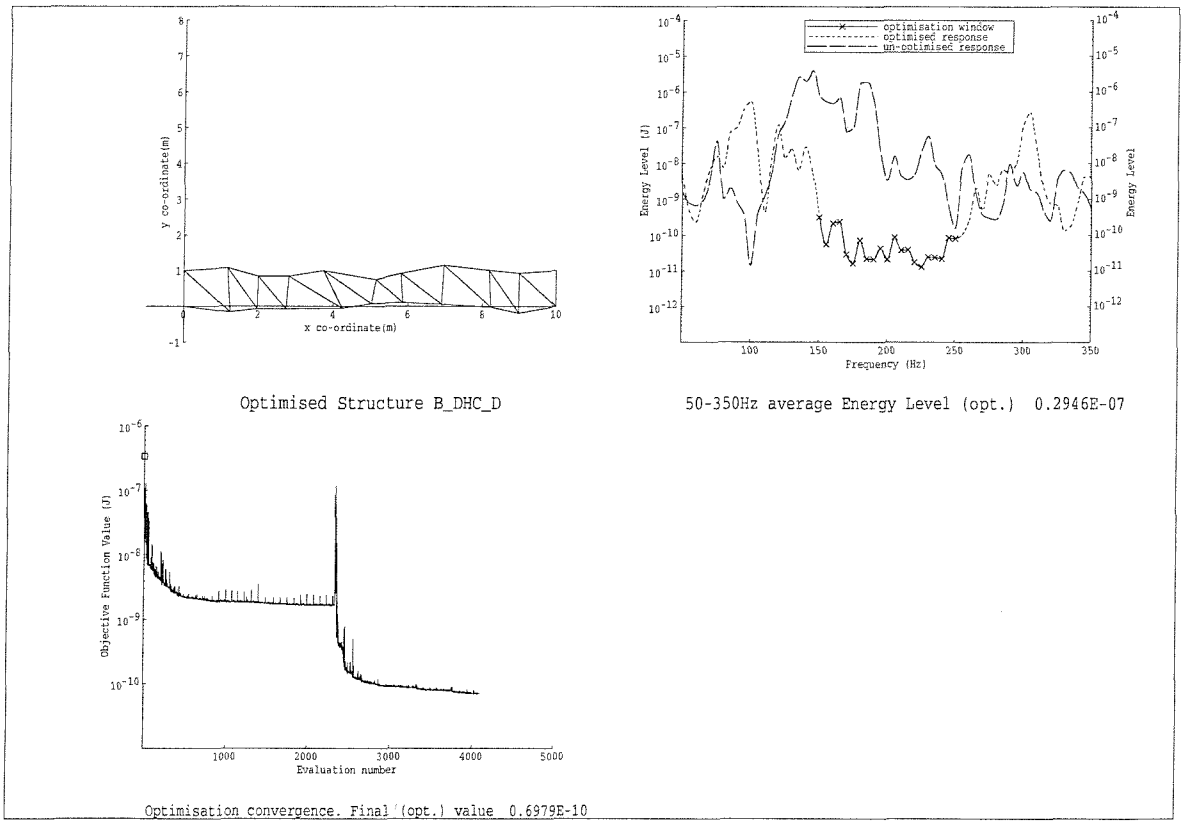

Figure 4.14: Structure with best optimised average performance over frequency band 150Hz to 250Hz, achieved using the Dynamic Hill Climbing.

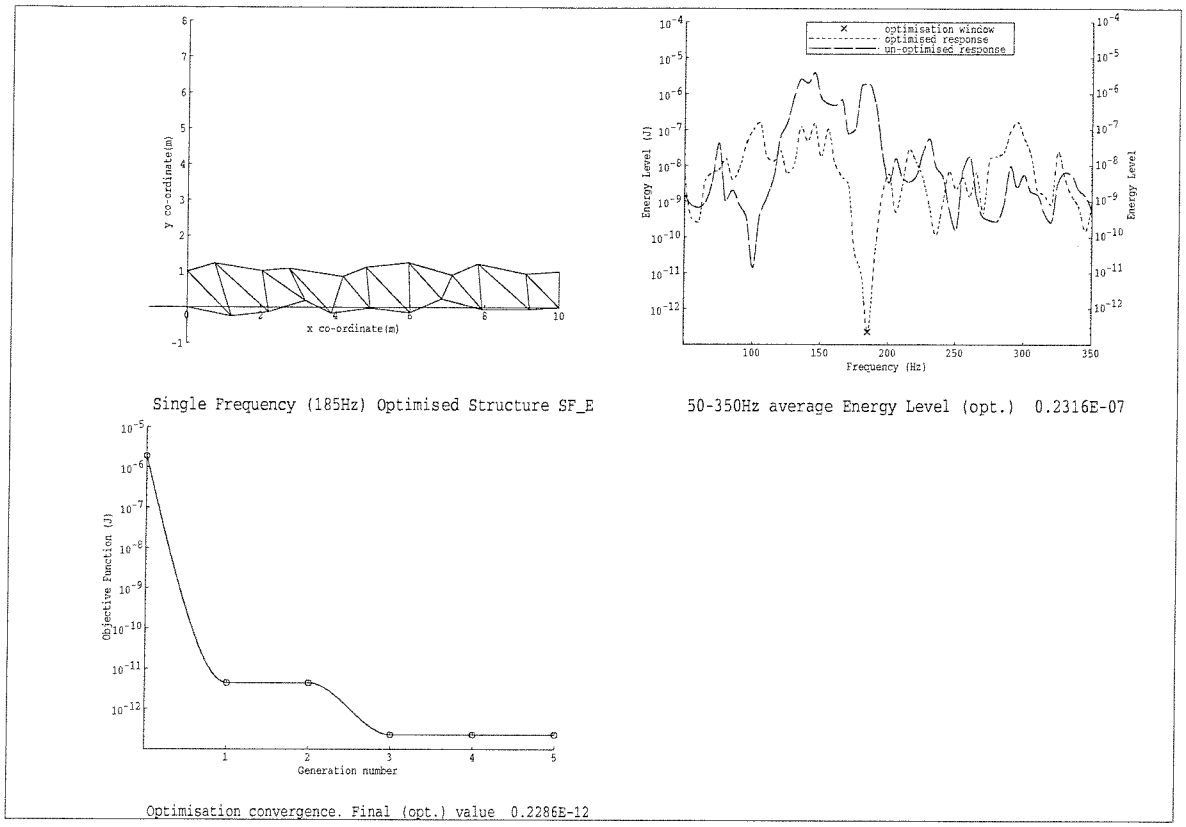

Figure 4.15: Structure with best performance at 185Hz achieved using genetic algorithm optimisation, SF_E.

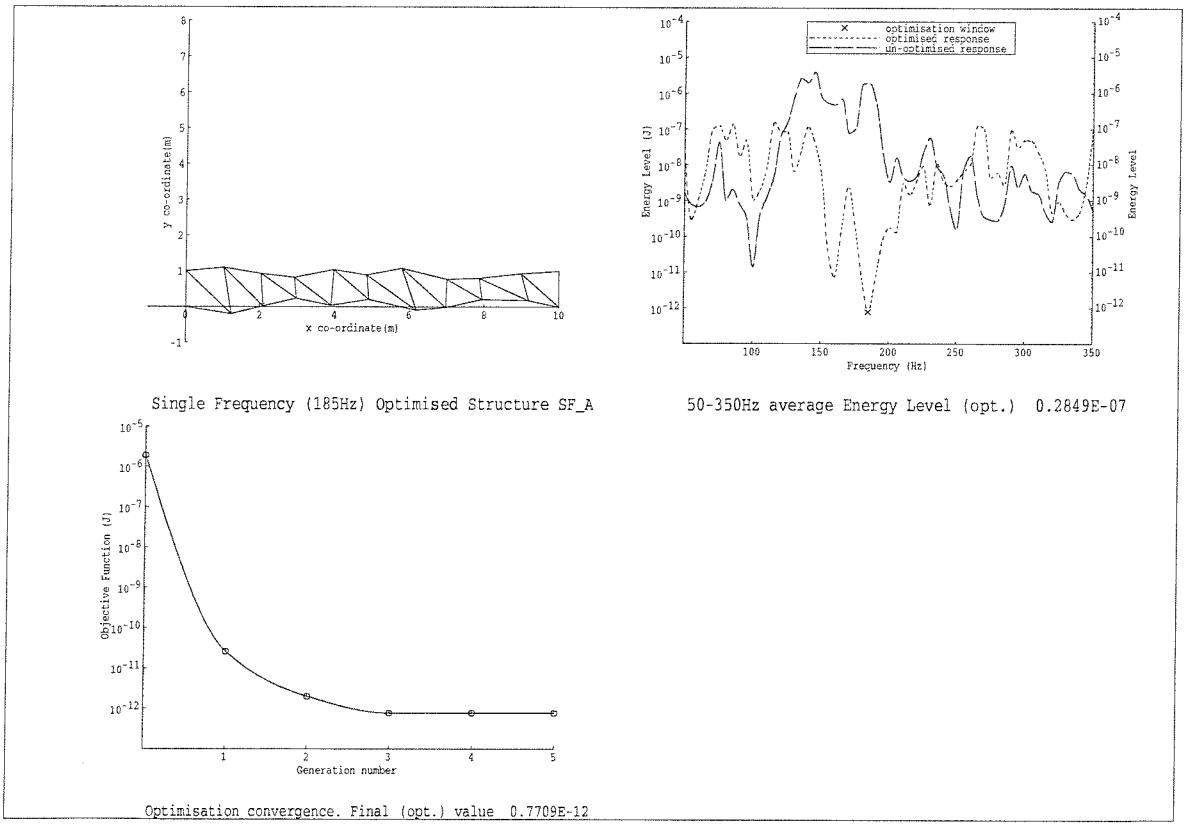

Figure 4.16: Structure ranked third for performance at 185Hz, achieved using genetic algorithm optimisation, SF_A.

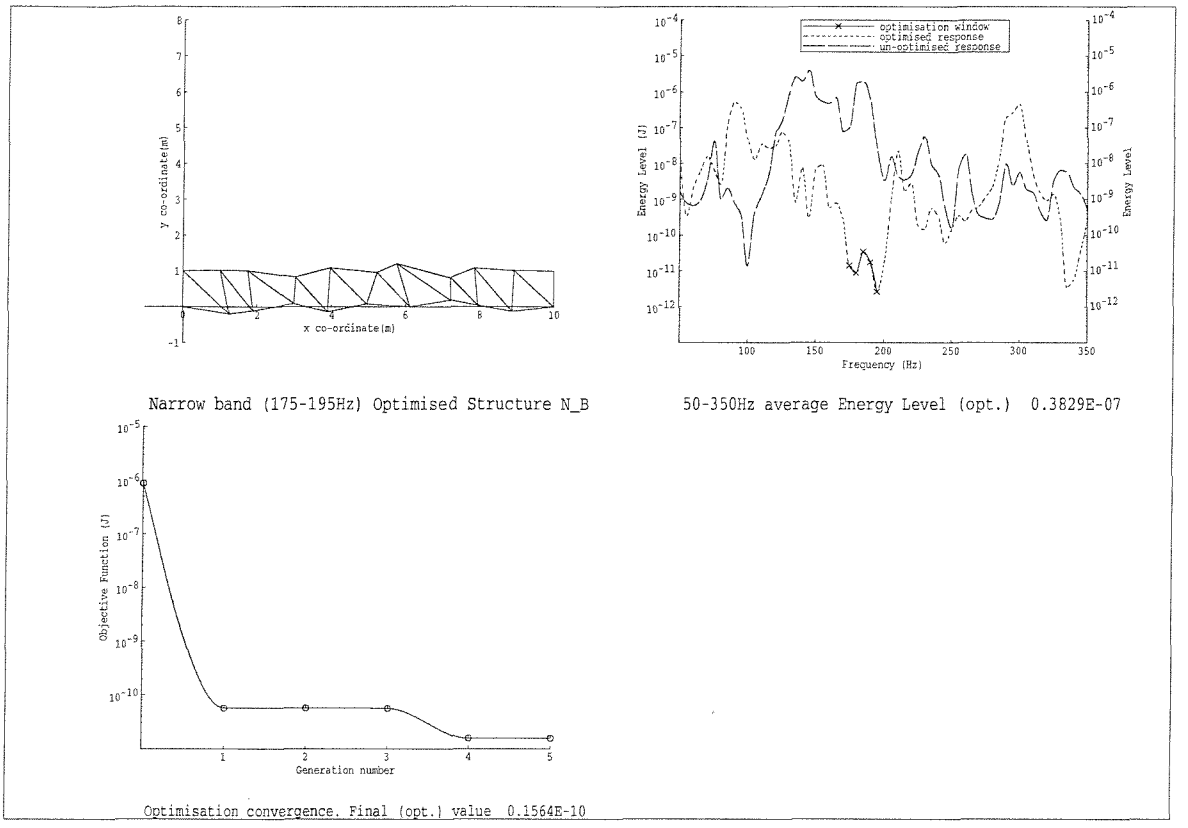

Figure 4.17: Structure with best optimised average performance over frequency band 175Hz to 195Hz, achieved using genetic algorithm optimisation, N_B.

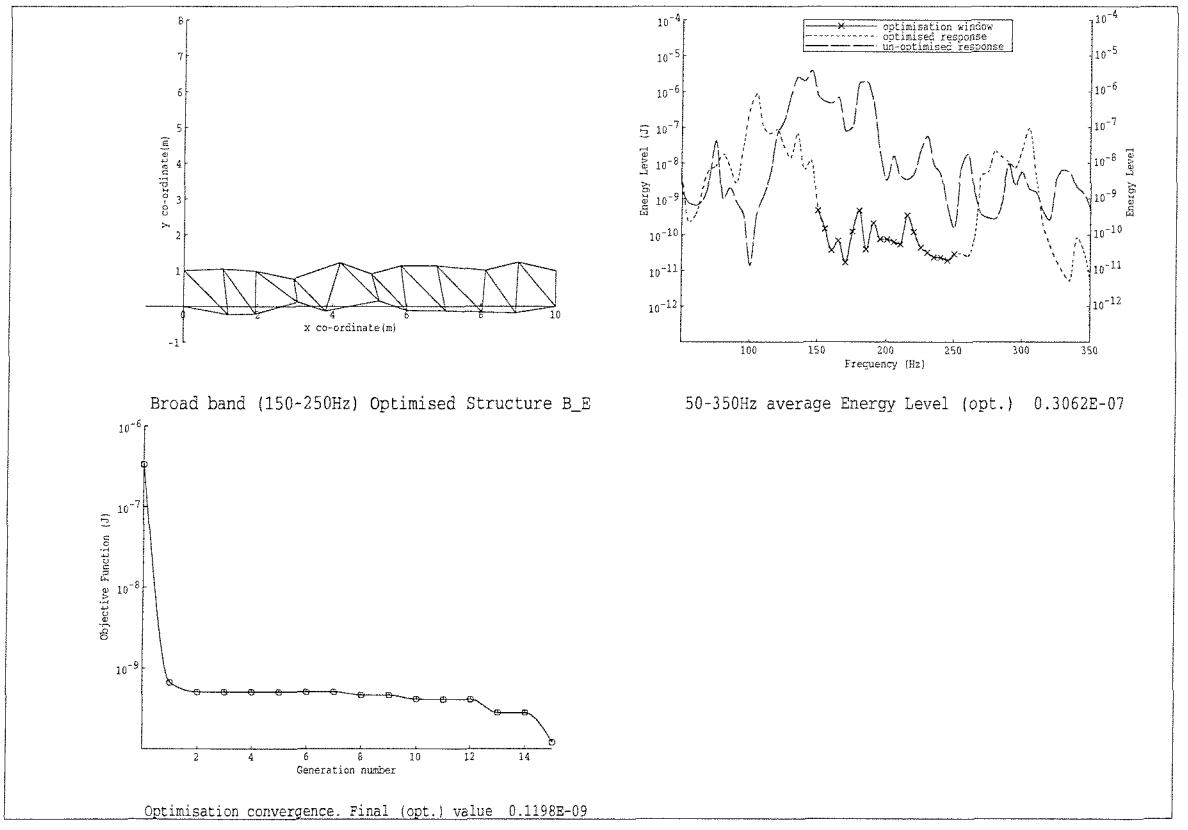

Figure 4.18: Structure with best optimised average performance over frequency band 150Hz to 250Hz, achieved using genetic algorithm optimisation, B_E.

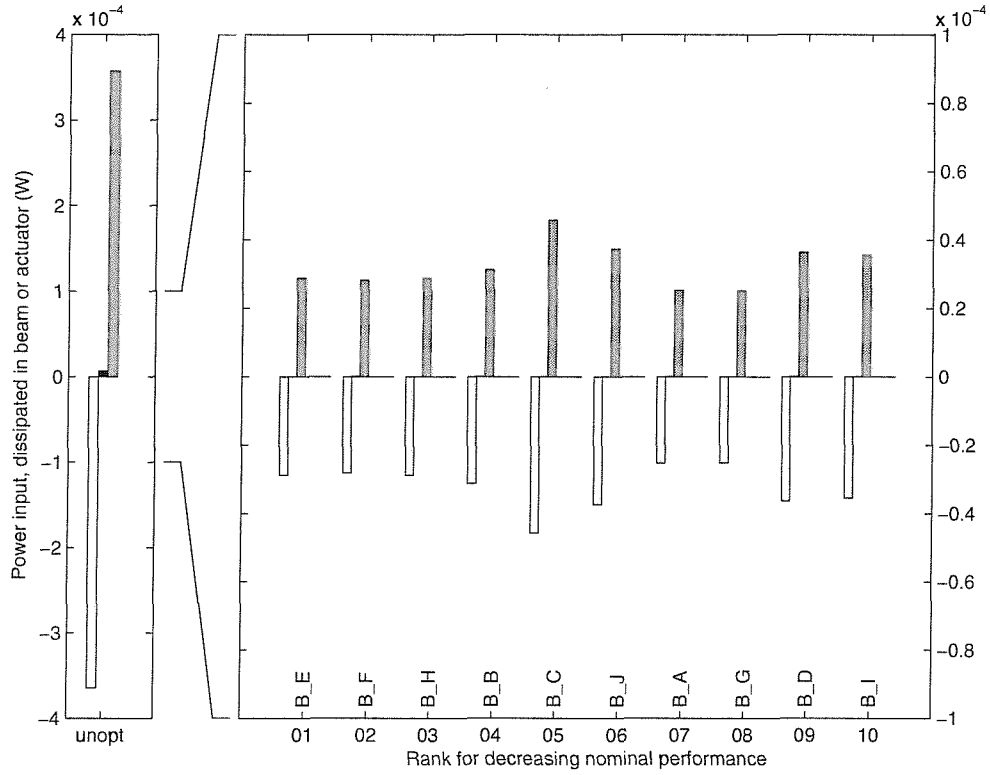

Figure 4.19: Power components in the broad band optimised structures. Light grey: Power input to structure, Dark grey: Power dissipated in Beams 1 to 39, Black: Power dissipated in Beam 40 (N.B. Power dissipated in Beam 40 is only distinguishable for unoptimised structure. For optimised structures range is 2.40×10^{-9} to 5.37×10^{-9} W.)

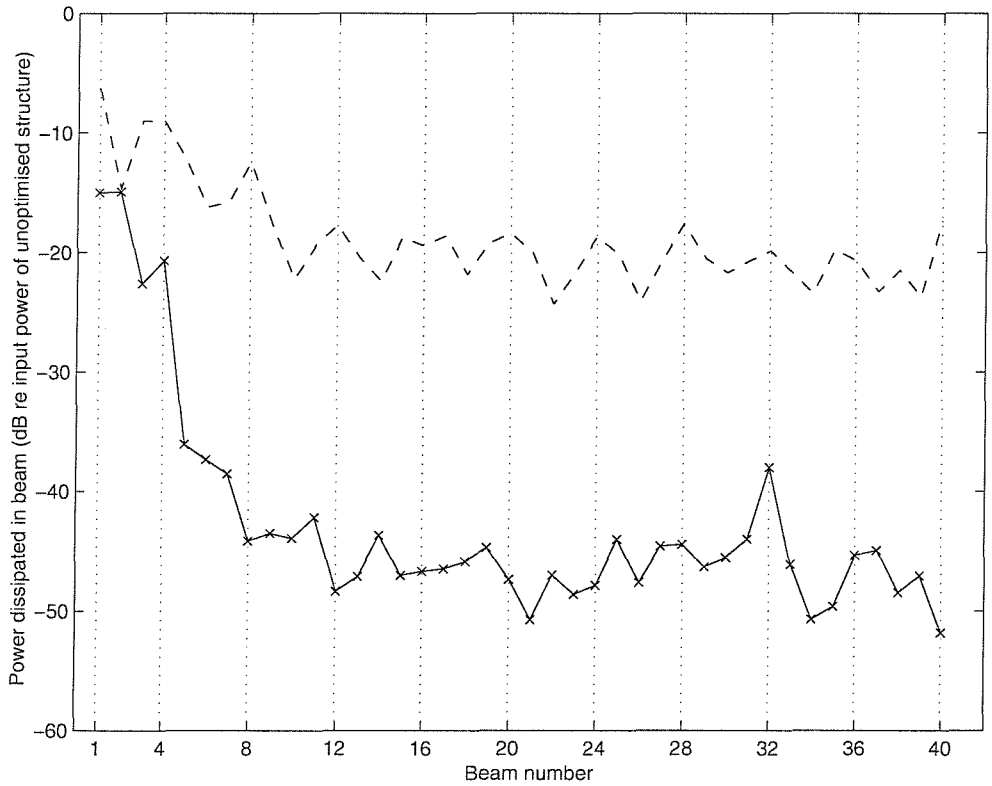

Figure 4.20: Power dissipation in each structure beam for the unoptimised structure (dashed) and optimised structure B_E. Each vertical gridline denotes the vertical beam separating adjacent bays.

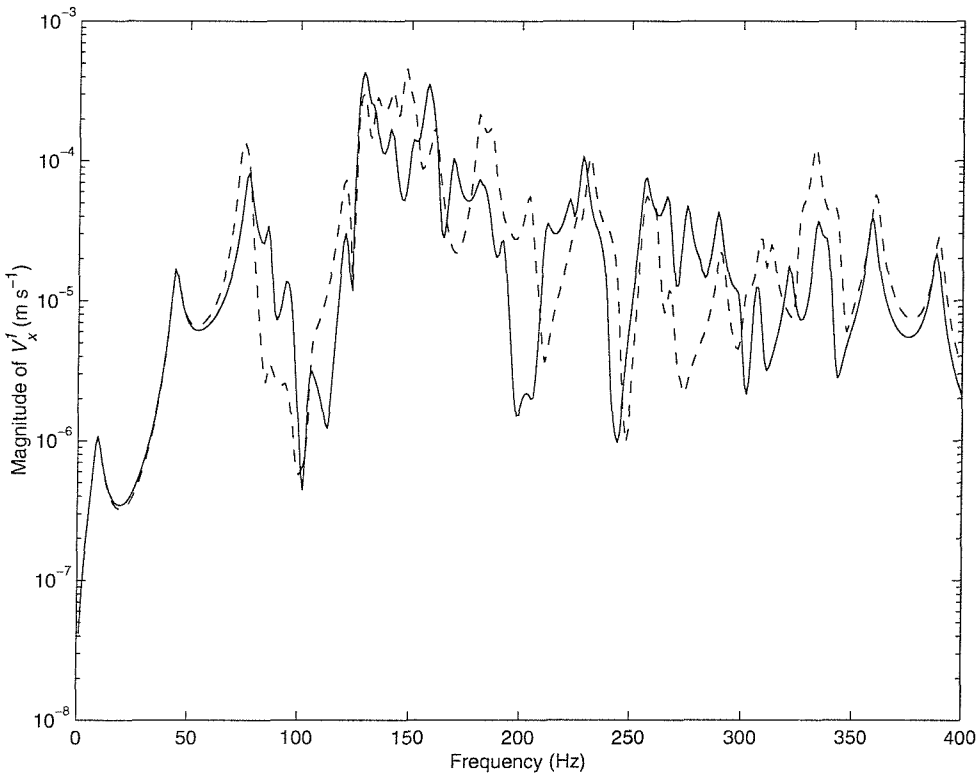

Figure 4.21: Comparison of velocity response V_x^1 of Beam 40 obtained by receptance analysis model (- - -) and FEA model (——) for the unoptimised structure.

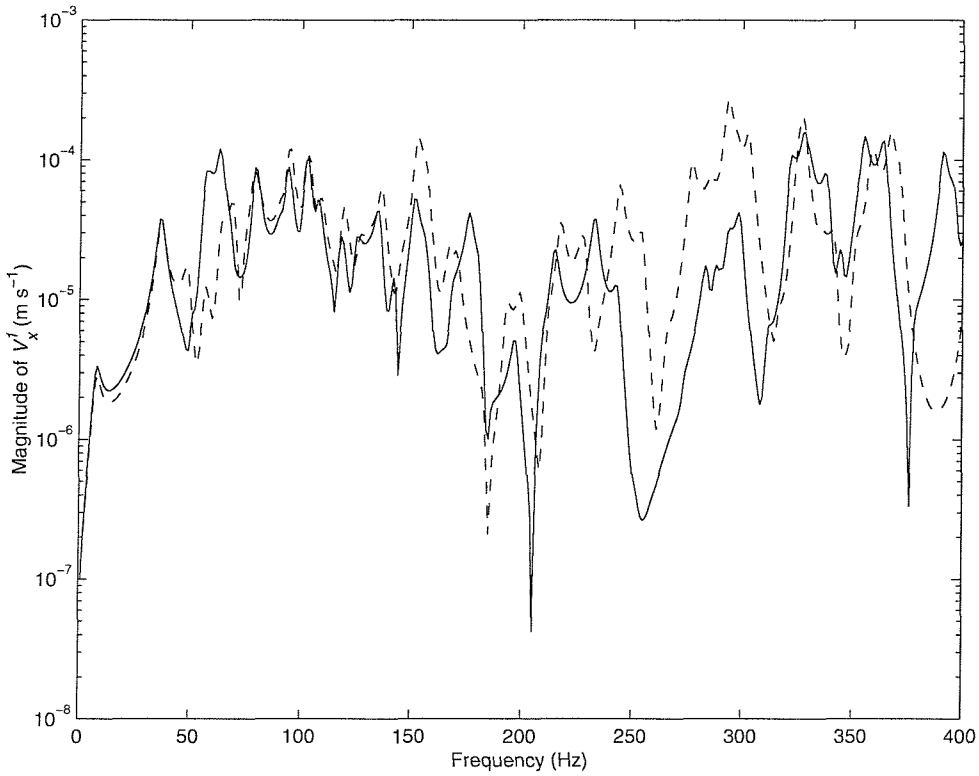

Figure 4.22: Comparison of velocity response V_x^1 of Beam 40 obtained by receptance analysis model (- - -) and FEA model (——) for the optimised structure SF_E.

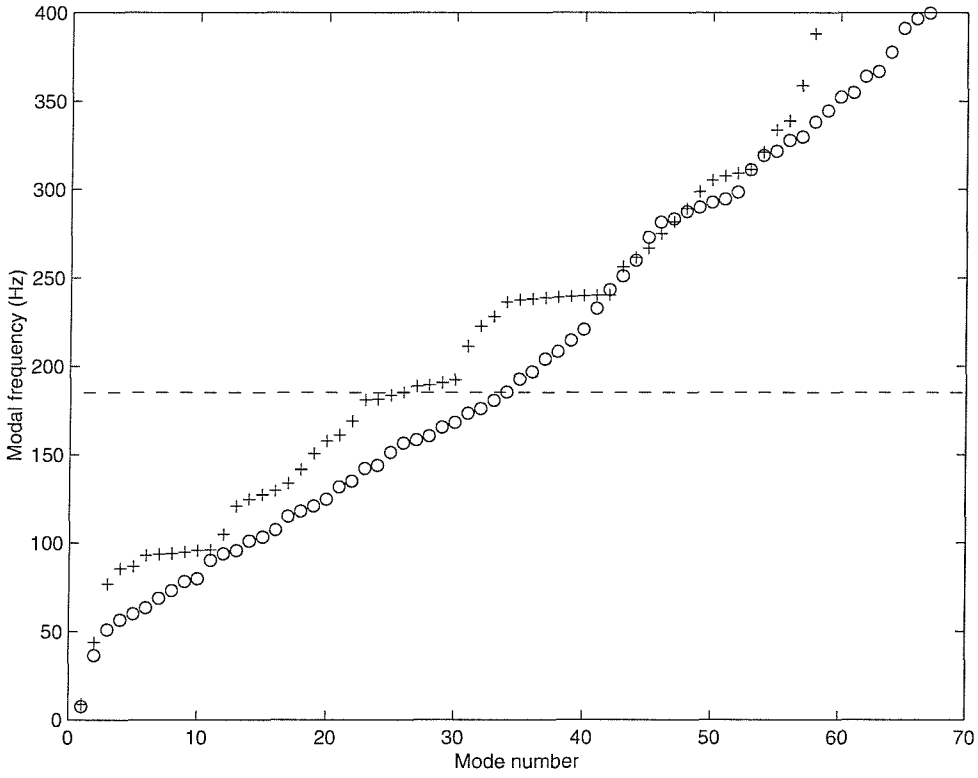

Figure 4.23: Effect of optimisation on modal frequency distribution for optimised structure SF_E. Frequency at which performance is optimised is shown by dotted line. (+ unoptimised structure, ◯ SF_E)

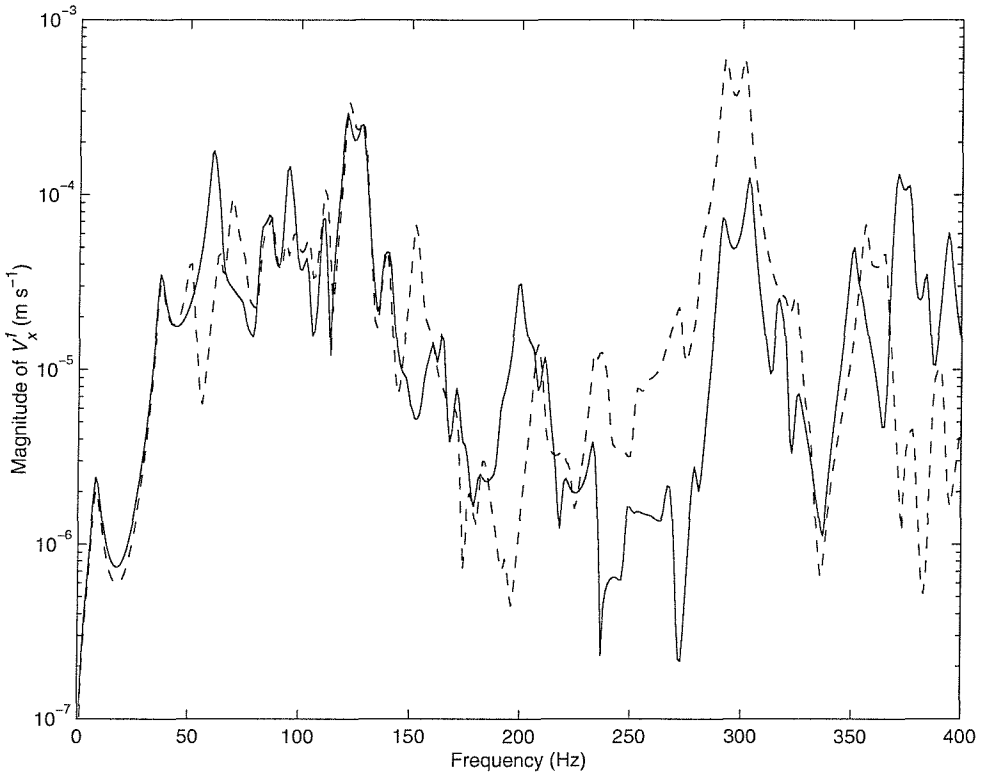

Figure 4.24: Comparison of velocity response V_x^1 of Beam 40 obtained by receptance analysis model (- - -) and FEA model (——) for the optimised structure N_B.

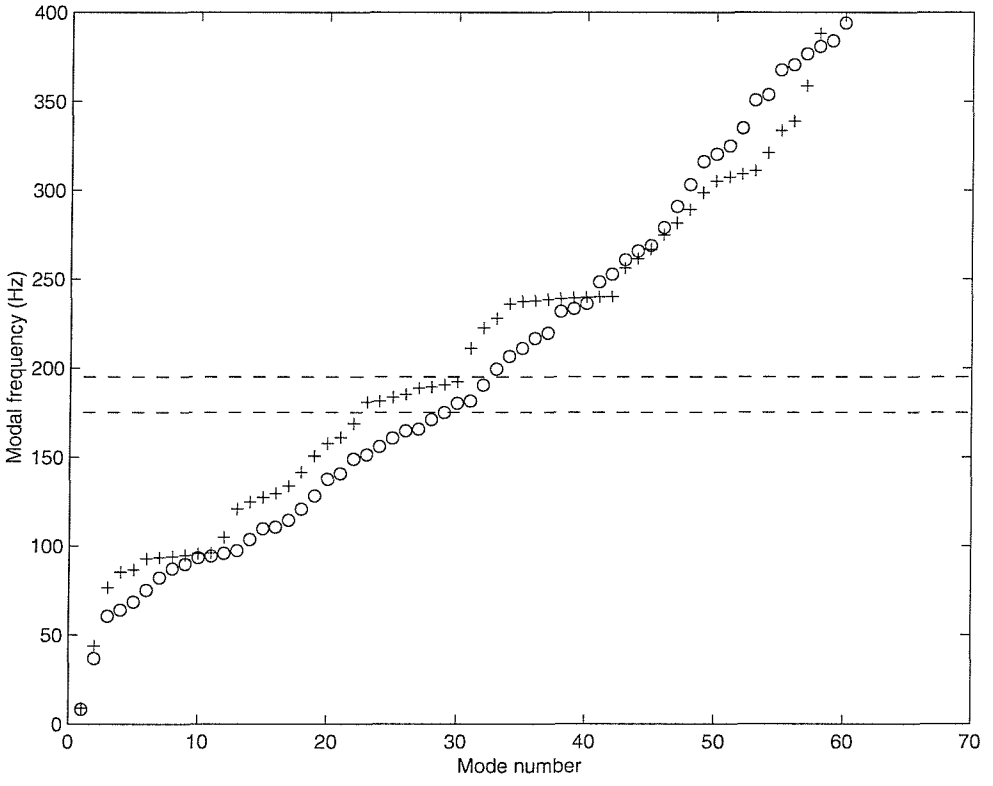

Figure 4.25: Effect of optimisation on modal frequency distribution for optimised structure N_B. Frequency band over which average performance is optimised is shown by dotted lines. (+ unoptimised structure, ◯ N_B)

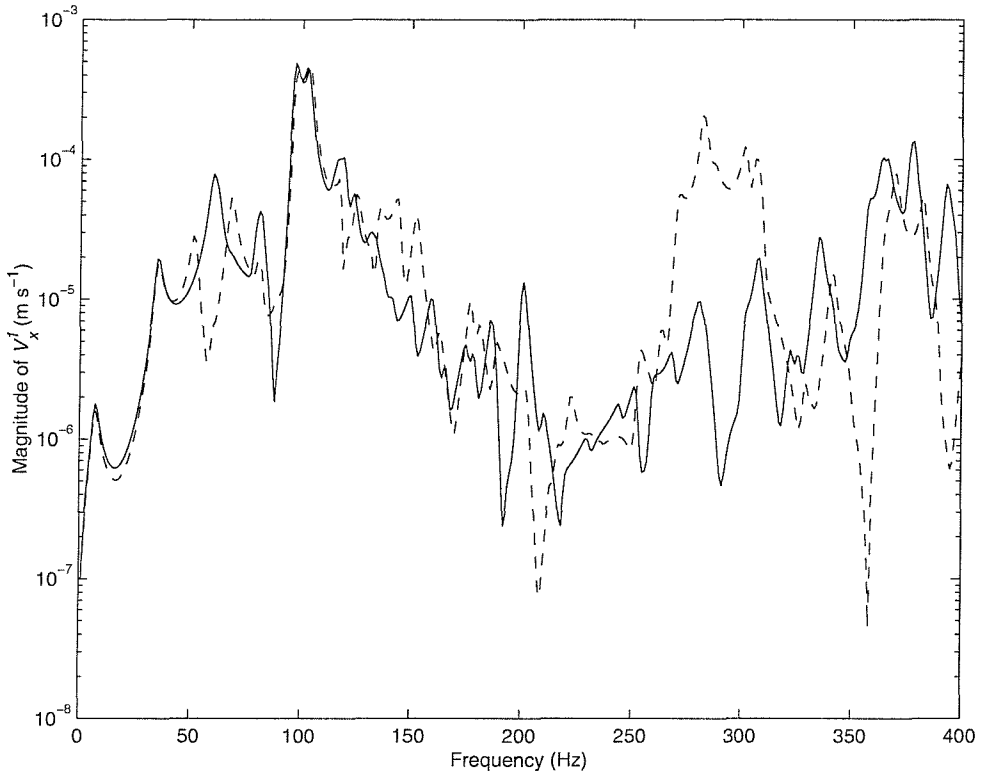

Figure 4.26: Comparison of velocity response V_x^1 of Beam 40 obtained by receptance analysis model (- - -) and FEA model (——) for the optimised structure B_E.

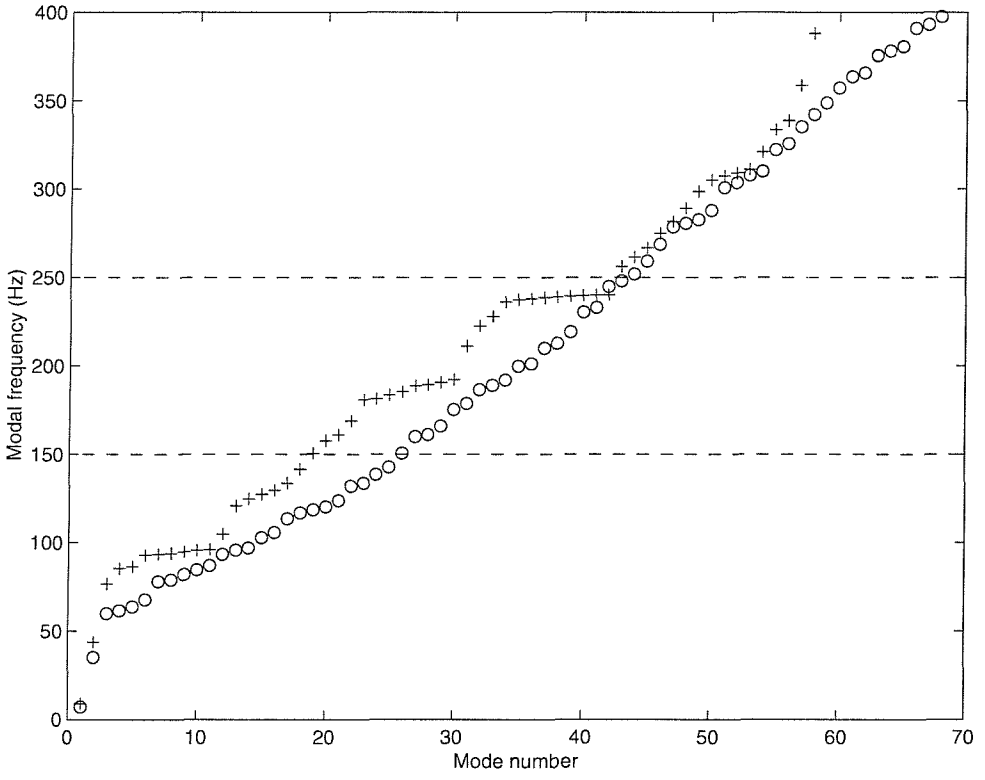

Figure 4.27: Effect of optimisation on modal frequency distribution for optimised structure B_E. Frequency band over which average performance is optimised is shown by dotted lines. (+ unoptimised structure, ◯ B_E)

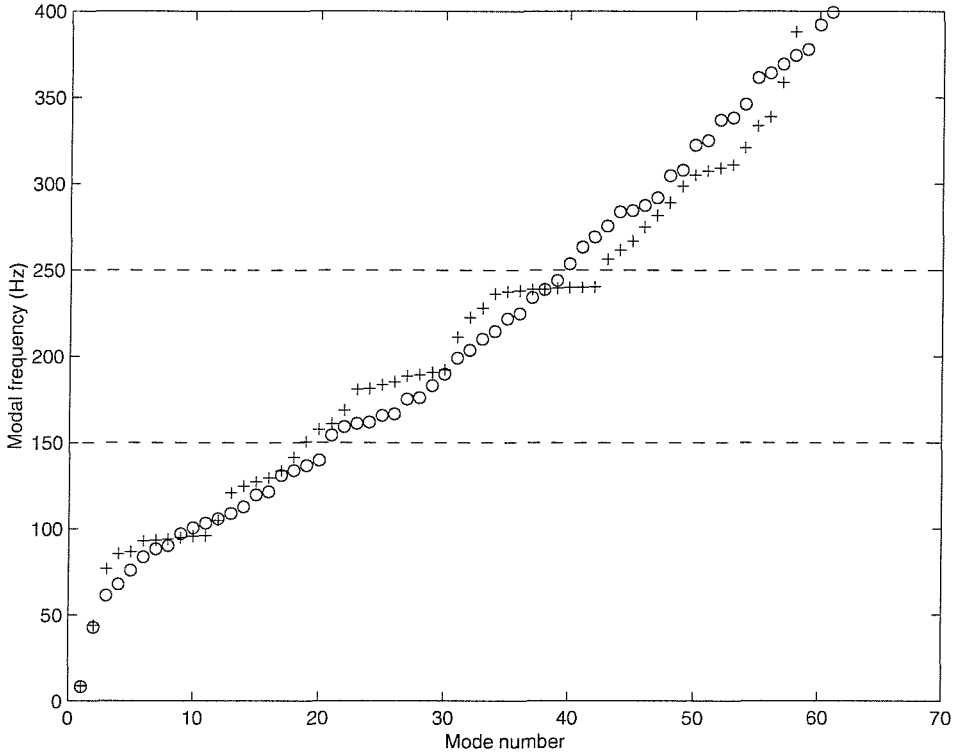

Figure 4.28: Effect of optimisation on modal frequency distribution for the 103rd structure design in the first generation of the GA optimisation resulting in structure B_E. The value of the objective function is 0.55×10^{-7} J, which is less than for the unoptimised structure. (+ unoptimised structure, ◯ 103rd structure)

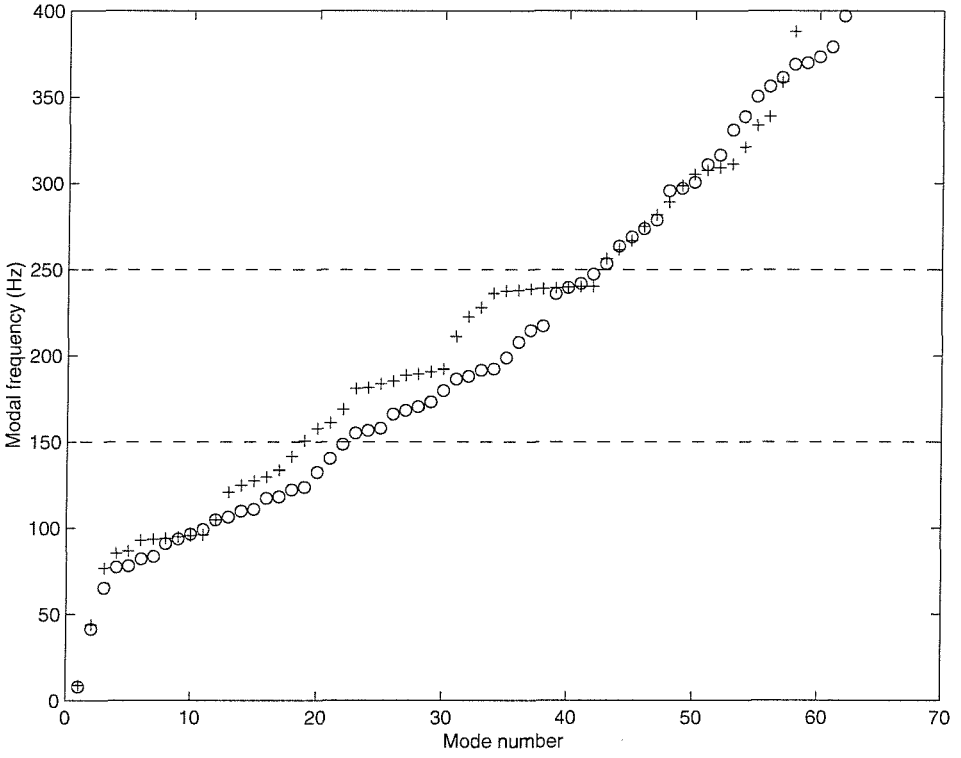

Figure 4.29: Effect of optimisation on modal frequency distribution for the 51st structure design in the first generation of the GA optimisation resulting in structure B_E. The value of the objective function is 0.43×10^{-6} J, which is greater than for the unoptimised structure. (+ unoptimised structure, ◯ 51st structure)

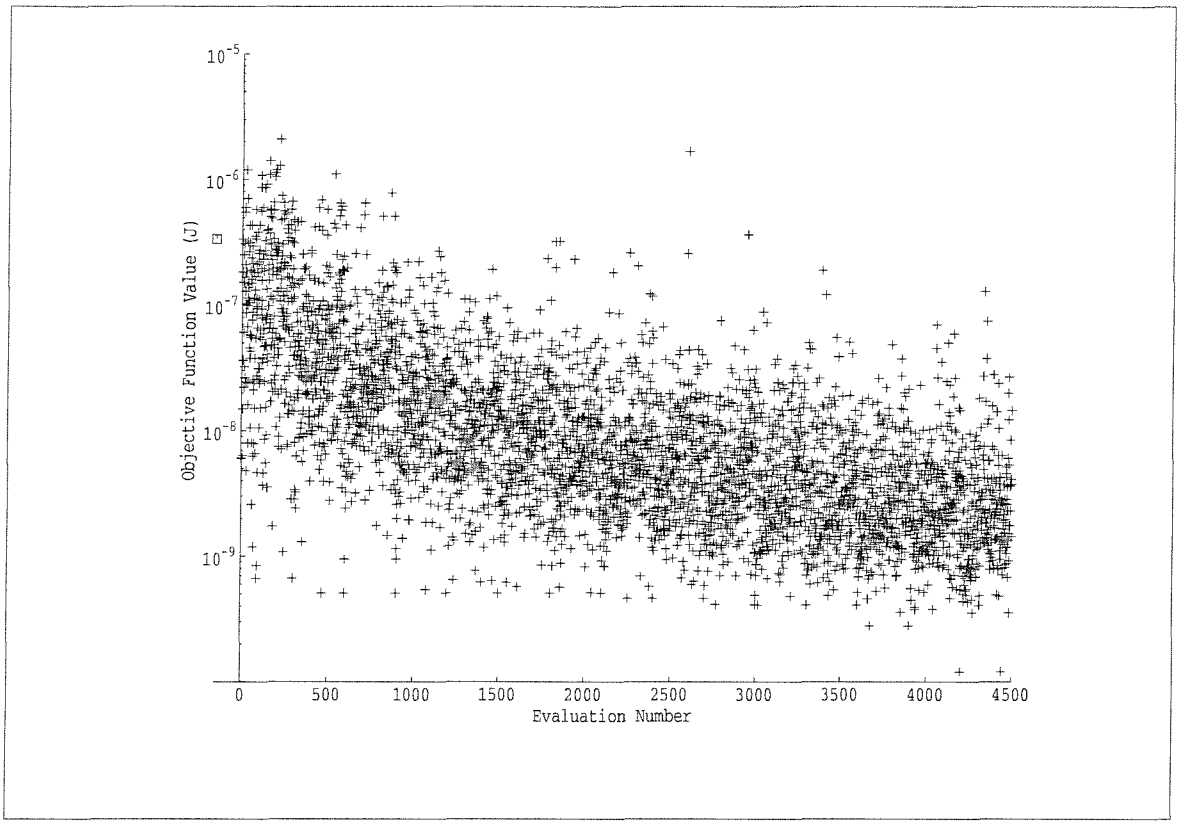

Figure 4.30: Results of all objective function evaluations used by the genetic algorithm resulting in structure shown in Figure 4.18. Unoptimised value of objective function is equal to 0.33×10^{-6}J as marked on y-axis.

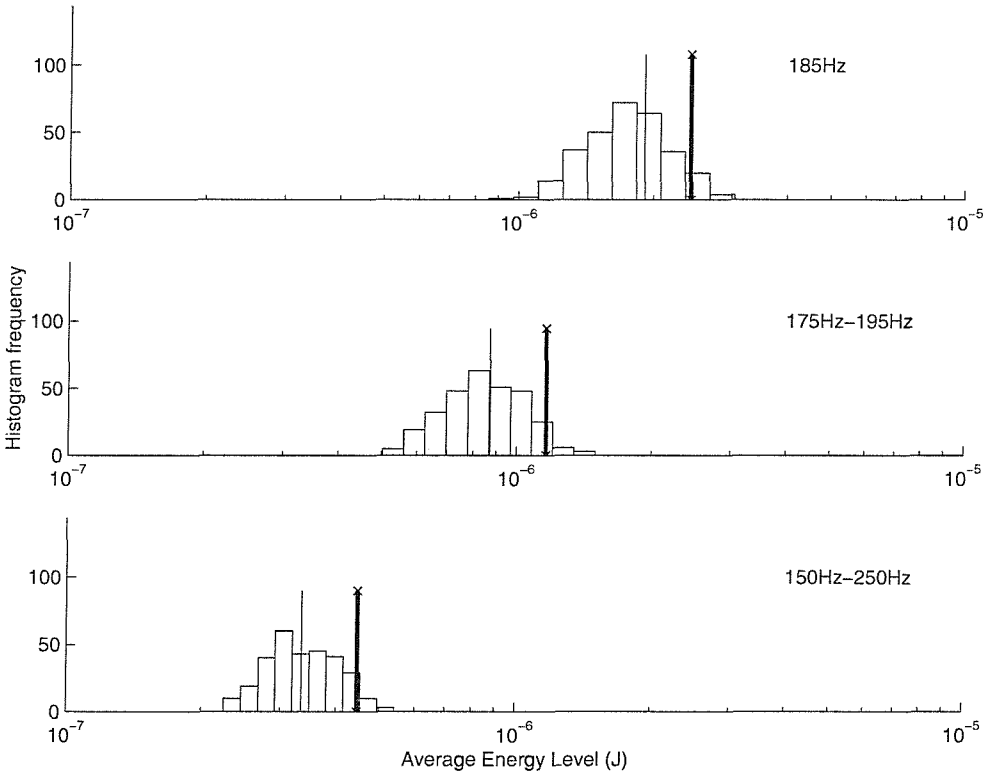

Figure 4.31: Statistical distribution and 95% probability limits (bold line) for the unoptimised structure for all optimisation bandwidths, and for a perturbation scaling of 0.01. The nominal value is denoted by the thin line.

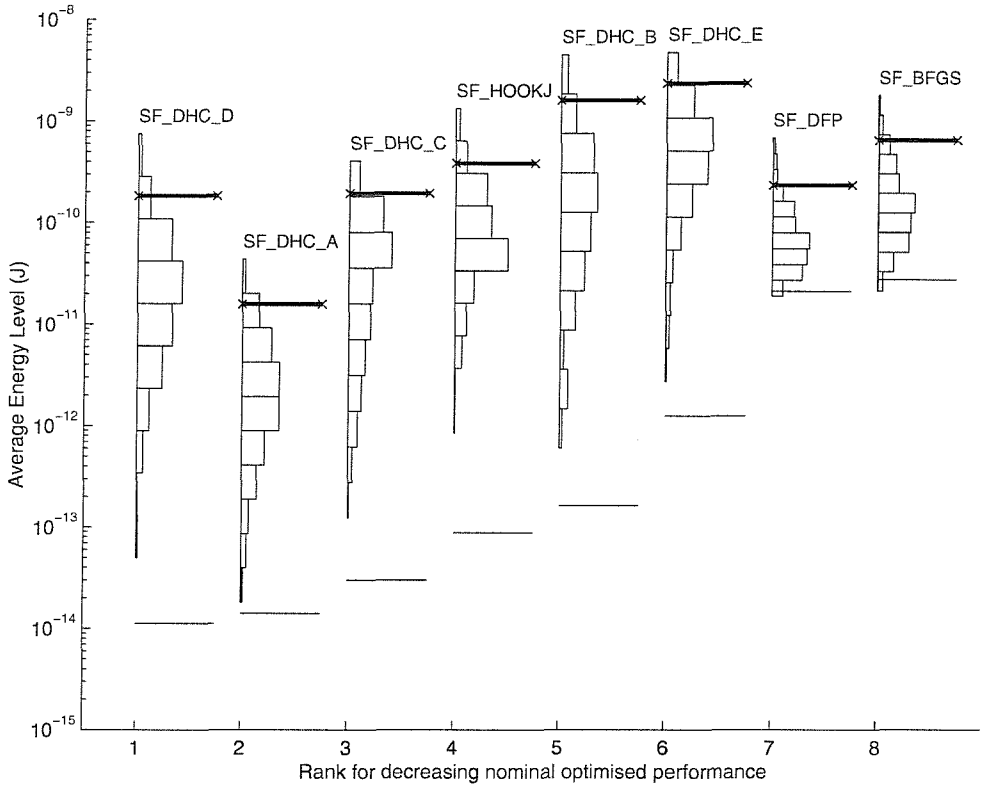

Figure 4.32: Statistical distribution and 95% probability limits for the Single Frequency optimised structures achieved using non-evolutionary methods, for a perturbation scaling of 0.01.

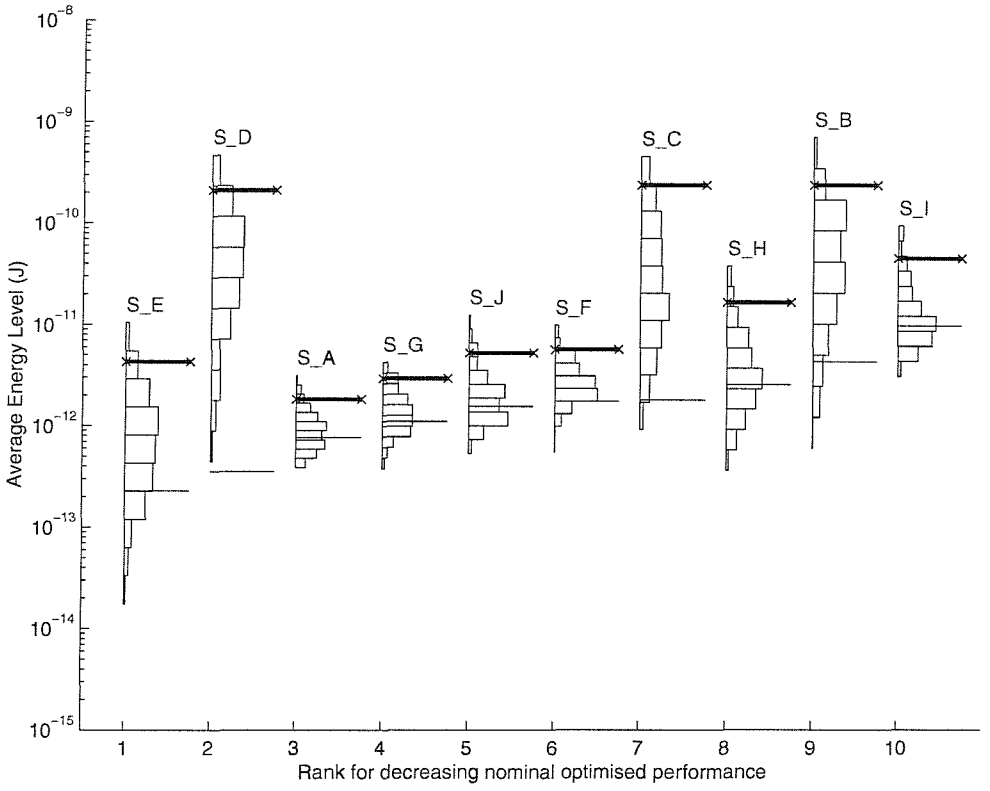

Figure 4.33: Statistical distribution and 95% probability limits for the Single Frequency optimised structures achieved using genetic algorithm optimisation, for a perturbation scaling of 0.01.

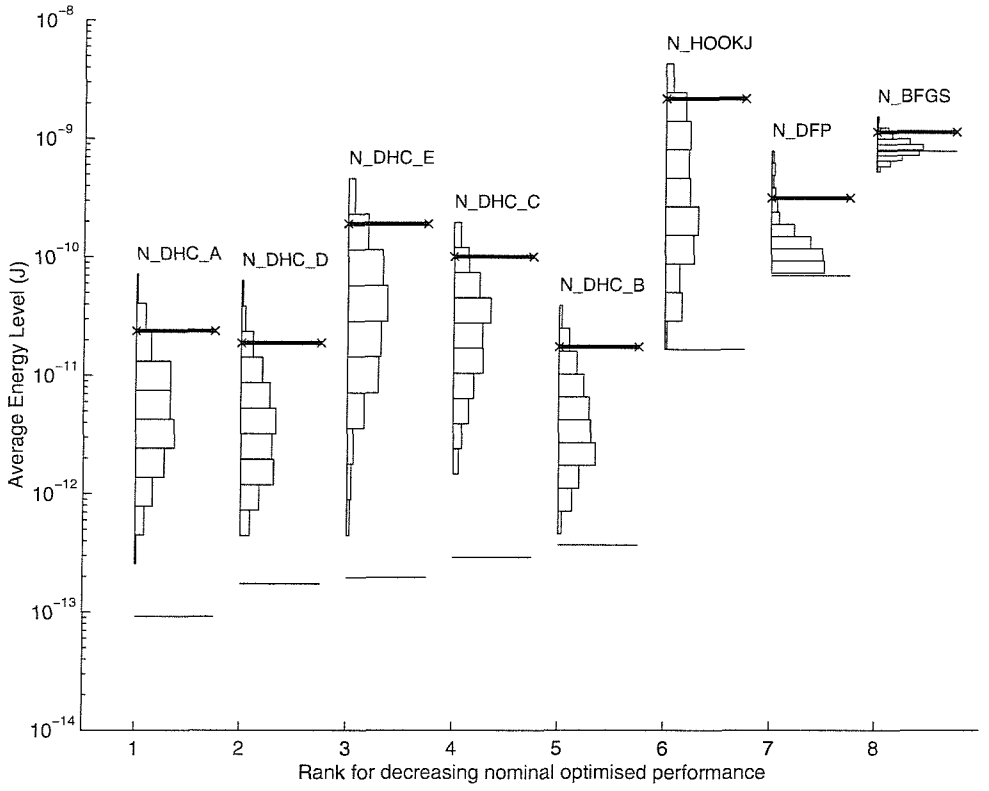

Figure 4.34: Statistical distribution and 95% probability limits for the Narrow Band optimised structures achieved using non-evolutionary methods, for a perturbation scaling of 0.01.

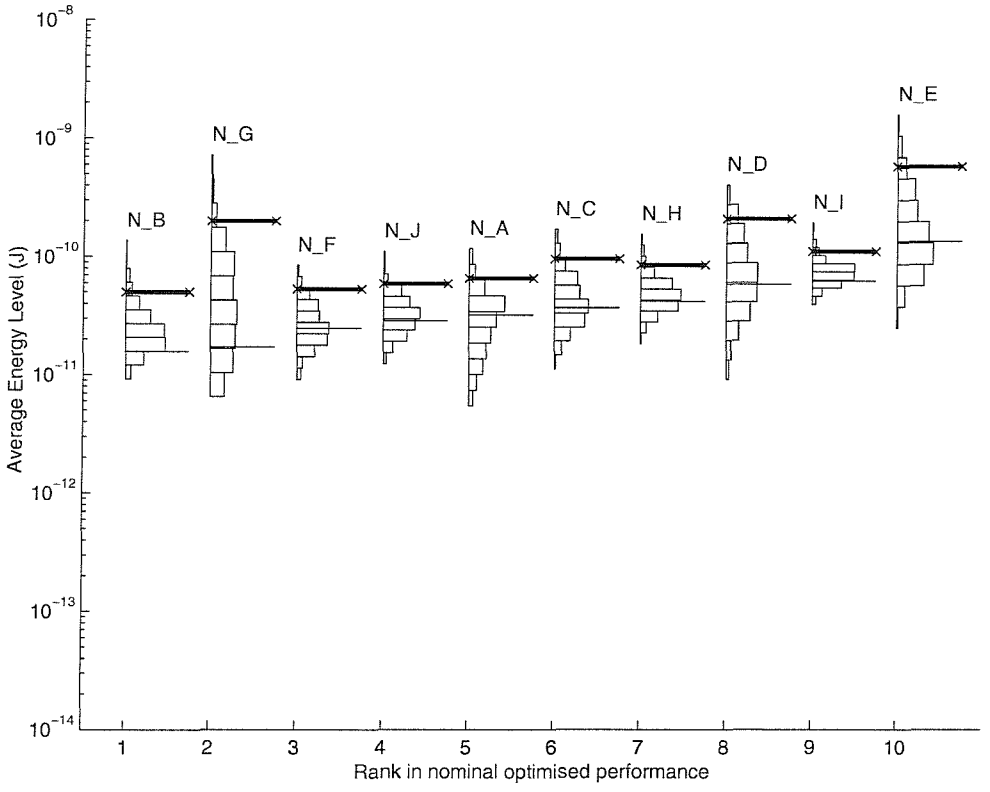

Figure 4.35: Statistical distribution and 95% probability limits for the Narrow Band optimised structures achieved using genetic algorithm optimisation, for a perturbation scaling of 0.01.

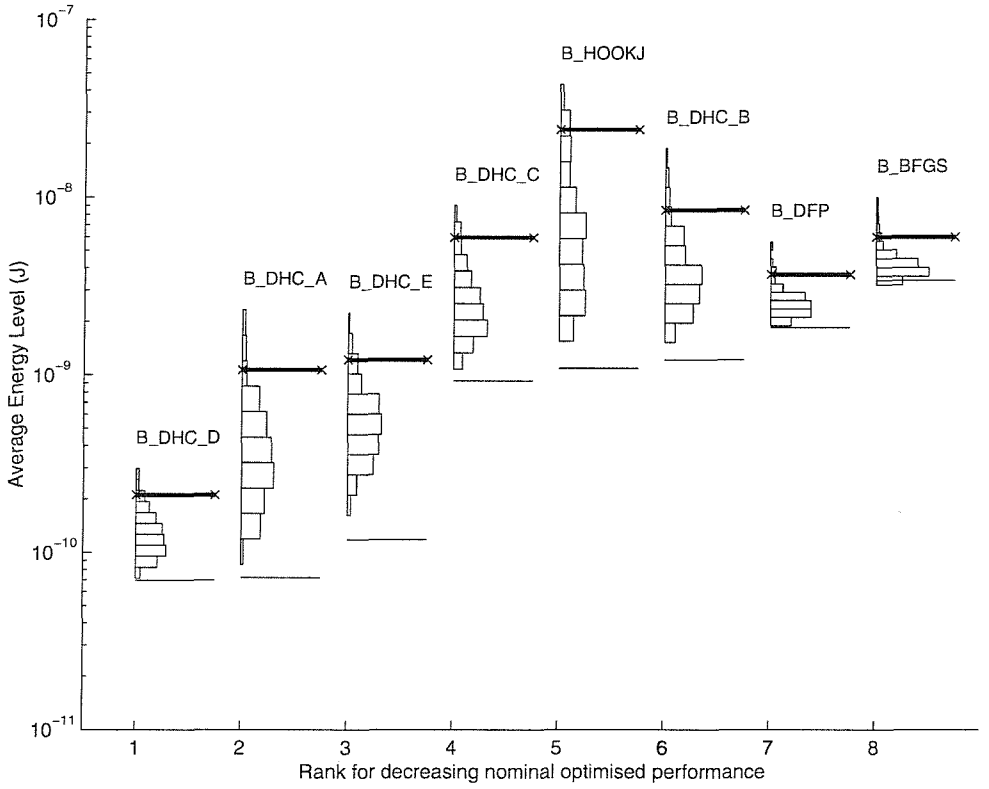

Figure 4.36: Statistical distribution and 95% probability limits for the Broad Band optimised structures achieved using non-evolutionary methods, for a perturbation scaling of 0.01.

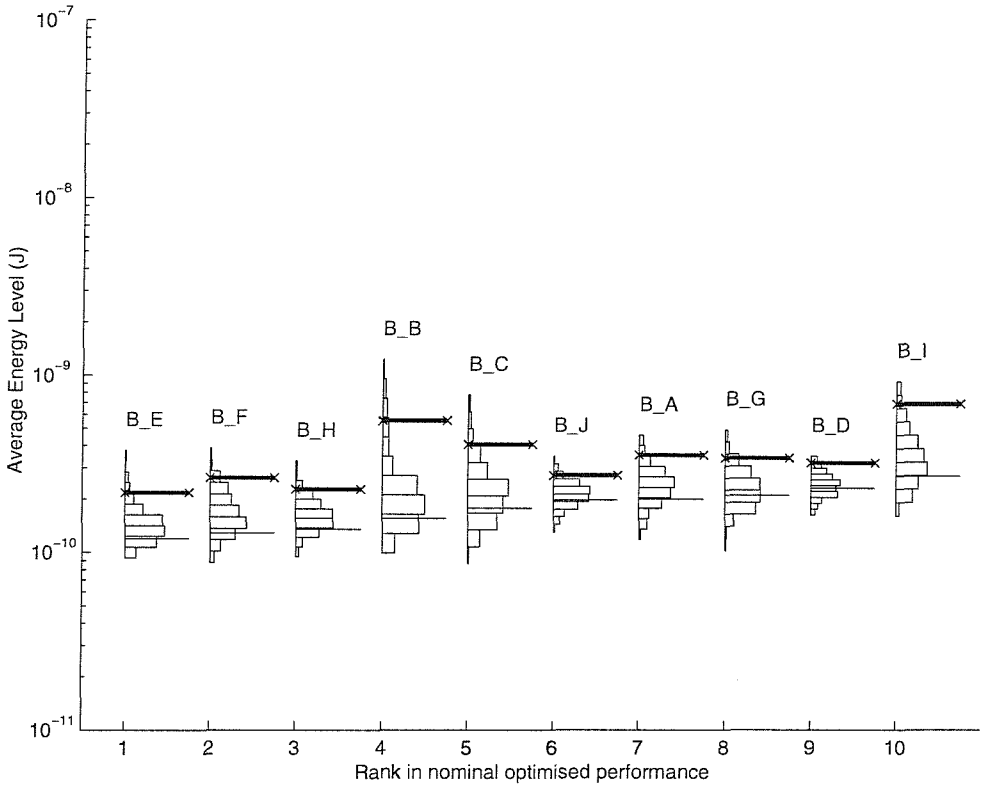

Figure 4.37: Statistical distribution and 95% probability limits for the Broad Band optimised structures achieved using genetic algorithm optimisation, for a perturbation scaling of 0.01.

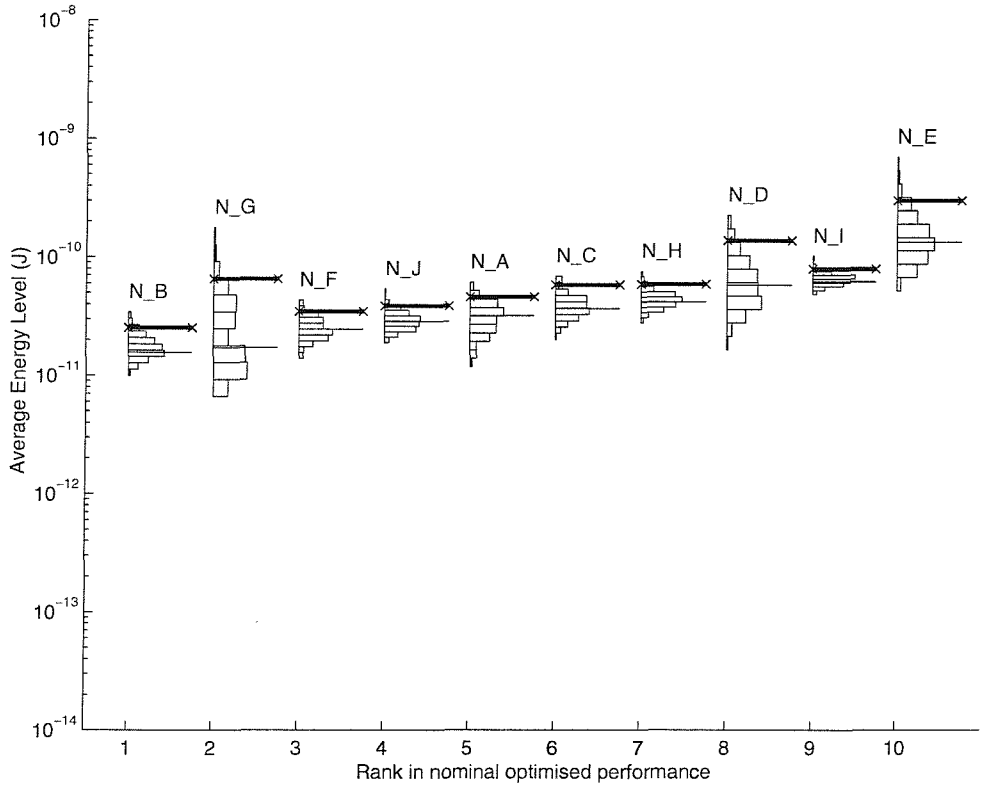

Figure 4.38: Statistical distribution and 95% probability limits for the Narrow Band optimised structures achieved using genetic algorithm optimisation, for a perturbation scaling of 0.005.

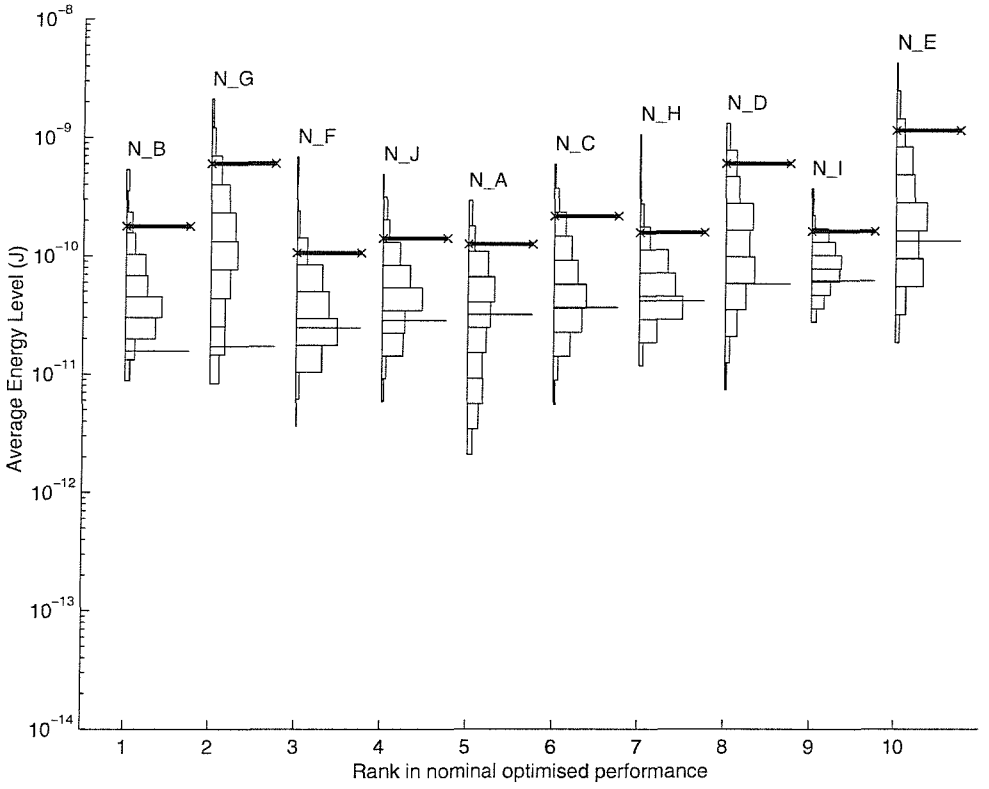

Figure 4.39: Statistical distribution and 95% probability limits for the Narrow Band optimised structures achieved using genetic algorithm optimisation, for a perturbation scaling of 0.02.

CHAPTER 5

Active Optimisation Methods and Robustness Analysis

5.0 INTRODUCTION

The chapter describes the optimisation of the regular two-dimensional lightweight structure to reduce the vibration transmission from the base to the end of the structure, the same optimisation aim as defined in Chapter 4. However, the optimisation strategy used here is to maintain the regular geometry of the structure and use feedforward Active Vibration Control (AVC) methods. These methods were described in Chapter 2, and use secondary source vibration actuators to 'counter' the primary vibration emanating from the structure base. As an external source of energy is required to drive the actuators, this optimisation strategy is thus referred to as *active* (or *active-only*) *optimisation*. The optimisation task is to find optimal actuator positions which allow the best value of attenuation to be achieved.

In selecting the best optimal actuator positions the control effort required to drive the actuators in the AVC system also needs to be considered, with the aim of finding positions which give good values of attenuation with realisable levels of control effort. The robustness of the performance of AVC systems to geometric perturbations is then studied, in the same way as for the passively optimised candidates, presented in Chapter 4 to determine the most practical systems. The robustness of the level of control effort required also needs to be considered, to ensure that the energy demand of the system remains feasible in the face of small changes in the geometry.

The level of success achieved by an AVC system is determined here by the reductions achievable in the *cost function* (the parameter whose value is minimised as the optimisation aim). The physical success in reducing the vibration is thus depends upon how well the cost function represents the physical vibration. Parameters representing vibrational energy are generally the best cost functions, but sometimes difficult to measure in practice. The effect of using different cost functions as the focus of the optimisation is also studied. This allows the parameter used to be critically accessed, especially in the light that it evolves that it is not, in general, the most comprehensive measure of all of the vibrational energy.

In a feedforward AVC system for the control of broadband disturbances there exists causality constraints due to delays introduced in the signal processing. Due to the dispersive nature of

flexural waves this constraint becomes more stringent as the control frequency increases, as discussed for example by Elliott and Billet (1993). The primary input force used represents a vibration disturbance entering the structure by its base but is considered to be modelling the effect of a source which is not itself immediately located on the base. Thus, it is assumed here that if broadband disturbances are being controlled that there is sufficient advance between the reference signal (which is taken directly from the source) and the vibration entering the structure base, so that no such causality problem occurs.

This chapter is structured as follows: Section 5.1 defines the process of selecting the optimal actuator positions on the regular structure, based on nominal performance, for differing numbers of actuators. Section 5.2 studies the contributions of the AVC actuators to the vibrational power in the structure, which is distinct from the control effort, to investigate their mechanism of control. Section 5.3 investigates the use of three other AVC cost functions in the optimisation process. Section 5.4 studies the robustness of the performance and control effort requirements of AVC systems with optimal actuator positions. Conclusions from the chapter are summarised in Section 5.5.

5.1 SELECTION OF OPTIMAL ACTUATOR POSITIONS

The success of AVC depends strongly on the actuator positions used. The physical reasons for this were discussed in Chapter 2, in terms of the dynamic mechanical 'coupling' between the primary forces and the secondary actuators and the end beam. The average energy level in Beam 40 over the frequency band 150Hz to 250Hz was used as the parameter to be minimised. This corresponds to maximising the average attenuation of this parameter. The frequency band was comprised of 21 equally spaced frequency points, 5Hz apart, from 150Hz to 250Hz. This is the same as used for broad band optimisation for the passive structure which was studied in Chapter 4. It is assumed that the vibrational disturbance can be accurately represented by 21 tones at the stated frequencies and that a reference signal of sufficient quality exist so that the optimum secondary force, and hence the attenuation, can be achieved independently at each frequency. The total control effort was also calculated for each case. The control effort, which has the units of N^2, is evaluated for the 1N transverse primary force used. If the primary force was increased the control effort required would increase in proportion to the square of the primary force.

Using the receptance analysis model, described in Chapter 2, transfer force and mobility measurements between the primary force input location and both ends of all the possible actuator locations, and both ends of Beam 40 were evaluated, for all frequencies considered.

This then allows the matrices **C** and **Y** to be constructed for each actuator combination evaluated during the optimisation. The resulting values of AVC attenuation are calculated using equations (2.45), (2.46), (2.76) and (2.77), and total control effort is calculated using (2.43) and (2.48). These equations were implemented using MATLAB script (MathWorks, Inc., 1997).

The optimum actuator positions were sought for the application of AVC using one, two and three actuators. This was achieved by exhaustively evaluating the attenuation resulting for each of the possible combinations of actuators positions, with each number of actuators. Beam 40 was not considered as a candidate position (as explained in section 2.3). Hence for one, two and three actuators there are 39, 741 and 9139 possible combinations respectively. Using hardware platform A (detailed in Appendix E) it took approximately 20 and 100 minutes to find the best actuator positions for the two and three actuator cases respectively. Because combinations and not permutations are sought it is important that the algorithm generating the candidate actuator positions does not produce and then discard repeated combinations. This would be very wasteful and would effect the run-time of such algorithms by a factor of 36! for the three actuator case, for example. Even if the cost function was not evaluated for the repeated combinations the formulation of all the permutations is still very expensive, and can dominate the optimisation evaluation time.

The presence of an actuator on a beam was not considered to change its mechanical properties so as not to unnecessarily complicate the study, although as discussed by Zimmerman (1993) this can be an important consideration in a practical system. Zimmerman showed that the inclusion of the actuator mass could change the optimum actuator positions for a specific application. The purpose of the optimisations performed in this thesis is to investigate optimisation methods and not to design a specific structure.

Figure 5.1 shows the ten best positions to minimise the average energy level in Beam 40 using AVC with one actuator, the results are summarised in Table 5.1. The positions are ranked in decreasing energy attenuation, which is also shown. The attenuation range is 10.8dB to 8.5dB. The actuator positions do not appear to follow any particular rule, positions at the extreme ends of the structure are included in the best ten. A general rule of thumb in active control is to treat the unwanted vibration nearest its place of origin (Fuller *et al*, 1996). This does not seem to be borne out in the best ranked ten candidates. One of the actuators is, however, on the same beam as the external vibration is introduced. The secondary actuator produces axial force whilst the external primary force is, however, in the transverse direction, and a large value of control effort is required in this case.

The total control effort required to achieve each level of attenuation (for the primary force used) is also shown alongside each actuator position. There is a large range of control effort values ranging from 1,390 to 17,200 N^2. This illustrates the fact that the choice of candidate must be made on the basis of both achievable attenuation and total control effort required. The second best ranked candidate is likely to be the position chosen in practice since it has good control performance and a low control effort. It is emphasised that the total control effort does not represent the vibrational power applied by the actuators, this is studied in the following section.

Figures 5.2 and 5.3 shows the ten best sets of actuator positions for two and three actuators respectively and the results are summarised in Tables 5.3 and 5.5. For two actuators the achievable values of attenuation range from 31.1dB to 26.9dB, with total control effort range from 11,000 to 53,900 N^2. Here the 3rd ranking set of actuator locations appears to be a good practical choice since it has good control performance and a low control effort. For three actuators the range of achievable values of attenuation is 50.8dB to 44.0dB, and the total control effort range is 24,400 to 234,000 N^2. This range is large due to one 'rogue' set of actuator locations with a particularly high value of control effort. With two actuators, there again appears to be no particular rule in the placement of the actuators for the best ten AVC set of actuator positions. However the actuator positions chosen are all found to be only on the first 7 leftmost structure bays. This trend in seen to continue for the three actuator case, the actuators now only appearing in the 5 leftmost structure bays; the left half of the structure. The values of attenuation achieved using two actuators are similar to those achieved by the optimised structures resulting from the passive optimisation, detailed in the previous chapter. Figure 5.4 shows the best ten actuator positions for four actuators. This case is not considered any further since the values of attenuation shown (up to 119dB) would not be achievable in practice using a control system with a realistic noise floor. However, the inclusion of these results does demonstrate the trend noted above; that the larger the number of actuators the more the actuator position found are closer to the primary excitation at the base of the structure. Here the actuators are restricted to the 4 leftmost bays. Furthermore it was found that the best 5 sets of actuator positions only use actuator positions in the 3 leftmost structure bays.

The effective total control effort of the primary force is $21N^2$, since the primary force at each frequency is 1N. The control effort required by the AVC system is much larger is all cases. The smallest control effort of all the optimal positions presented is for the single actuator position SG_B, and is greater by a factor of over 60.

It is possible to augment the cost function used here in the ranking of each AVC actuator position, with a term to penalise positions with higher control efforts and produce a bias

towards lower control effort solutions. This has been previously implemented (Baek and Elliott, 1995), but was not considered here, since it would unnecessarily complicate the study.

The frequency band average attenuation is shown in Figures 5.1 to 5.4. Within the frequency band different levels of attenuation are achieved at individual frequencies. Figure 5.5 shows that the attenuation response at the 21 individual frequencies considered, for the application of AVC with actuator positions DB_A (shown in Figure 5.2). Since a feedforward control strategy is used, the AVC system has no effect to the performance of the vibrational energy to Beam 40 outside the band of frequencies controlled. Comparing the vibrational energy reduction achieved by both the passive optimisation (detailed in Chapter 4) and active optimisation, it is found that the application of AVC with two actuators produces similar magnitudes of reductions as with the passive case.

5.2 POWER ANALYSIS OF STRUCTURE WITH OPTIMISED ACTUATOR POSITIONS

The total control effort is used as an indication of the electrical power required by an AVC system, and is an important practical consideration when selecting optimal actuator positions. This measure is distinct from the net power supplied to, or absorbed from, the structure by the actuators. For example, if the force and velocity components at both ends of an actuator are in "phase-quadrature" then there is no net power into or out of the actuator, however a net supply of energy would still be required for the actuators. This is because even if a reciprocal transducer were used the typical efficiency would be too small to be useful. The vibrational power in the structure and the net power contribution of the actuators in achieving the reduction in the vibrational energy in Beam 40 were investigated to gain a physical insight into the role of the AVC system.

As discussed in Chapter 4 for a structure optimised solely on geometric redesign, the two mechanisms that achieve the reductions in Beam 40 are the reduction of the input power and the redistribution of power within the structure. The use of AVC introduces another power contribution, that from the actuators, which can either provide a net source of power to the structure, or additional dissipation by absorbing power. The addition of this effect allows the reduction in the dissipated power in Beam 40 to be represented as in Chapter 4, but using an additional third term, called the *actuator contribution*, which describes the net effect of the actuators to the power within the structure, as detailed in Section 2.6. It is important to note that the application of AVC achieves more than simply absorbing power from the structure, it affects the force and velocity components at the ends of Beam 40 to reduce the power

dissipation there. To achieve this it may provide a net input or absorption of power. The actuator contribution only describes the net power contribution, it does not detail the interaction between actuators, which themselves might have larger contributions than the net contribution. However, the individual actuator contributions are presented graphically to enable some understanding of the mode of operation of AVC in each case. It should also be noted that the power redistribution term used in this case is the passive redistribution attenuation, α'_{REDIST}, (see (2.88)), which only considers power in beams without actuators, as opposed to structural power redistribution.

Tables 5.2, 5.4 and 5.6 show the three component power reductions of the reduction in power dissipation in Beam 40, for all of the structures with optimal actuators positions using one, two and three actuators. The results are also shown in Figures 5.6 to 5.8, where the individual actuator power contributions are shown. In all cases the input power is reduced very little by AVC and in some cases the input power is actually increased. On average, this increase is from 0.6dB to 1.0dB when using one to three actuators. The net actuator contributions are also relatively small, and mainly supply energy, though they also absorb energy for a few cases especially for actuator positions using three actuators. Thus the majority of the total reductions are achieved from the redistribution of the power in the structure in favour of Beam 40. In Figures 5.6 to 5.8 the individual power contributions for AVC using the optimal actuator are shown, and the interactions between the individual power contribution for the two and three actuator cases are revealed. For the one actuator case the actuator is acting as an energy source in all except the best actuator position. In most cases the magnitude of the power contribution is much smaller than the other power components, although for actuator position SG_D it is a major source of the power in the structure. For the two and three actuator cases the arrangement between the two actuators is not fixed, being a mixture of energy sources and energy absorbers. With reference to optimal actuator position TR_D it is clear that a small net power contribution (of 0.3dB in this case) does not imply small individual contributions. This provides one reason for the difference between net actuator contribution and control effort, although in this case the total control effort is relatively small, as for TR_D. The phase relation between the force and velocity components additionally needs to be considered to explain such differences.

The power dissipation distribution for the structure using the 'best' optimal actuator positions for one, two and three actuators is shown in Figures 5.9 to 5.11. For the one actuator case SG_A, the actuator affects the distribution such as to reduce the power dissipation in Beam 40, but also slightly increase the dissipation in the beams at the base of the structure. However a variation in the dissipation can still be seen in beams towards the end of the structure,

particularly Beam 40, indicating a significant level of power transmission beyond the actuator. From Table 5.2 it is seen that the power input is also slightly increased. For the two actuator case DB_A, in Figure 5.10, the dissipation in the beams at the base of the structure is somewhat reduced, and a reduction in power is seen from the second structure bay onwards, where the actuators are situated. In the last few bays little dissipation is seen indicating that there is only a small level of power transmission. In the three actuator case TR_A, Figure 5.11, an increase in the power dissipation in Beam 1 is seen, however from Table 5.6 it is seen that there is a reduction in input power to the structure. This emphasises that the input power to the structure (input to Beam 1) is distinct from the power dissipated by Beam 1. In this case there is little power transmission beyond the rightmost actuator and in general the power dissipation decreases further towards Beam 40.

Thus using only one actuator it appears, from the cases presented, that the main control mechanism is simply to redistribute the vibration to reduce the power in Beam 40, and it is suggested that the power dissipation distribution in the remainder of the structure is a consequence of this action. The reflected vibration from the structure end is likely to be a contributory effect. With two and three actuators, however, the AVC system has more degrees of control freedom and seems to adopt a 'strategy' of blocking the power flow along the structure, and additionally reducing the input power by a small amount as well.

5.3 EFFECTIVENESS OF DIFFERENT COST FUNCTION PARAMETERS FOR ACTIVE VIBRATION CONTROL

The success of an Active Control of Vibration system is dependent upon both the cost function being minimised and the positions of the controlling actuators. The cost function used affects the best actuator positions since their performance is judged on the attenuation of this parameter. However, the physical success will be dependent on how well the cost function represents the actual physical vibration. Sometimes the most meaningful cost function can be calculated in a theoretical model but is difficult to measure in practice, and a compromise to a more practical one is often made. Four cost functions are considered in this study with the aim of reducing the vibration transmitted from the base to the end of the structure studied in this thesis, and their performances in reducing the *total vibrational energy* of the end beam, which is generated as the parameter E_{total}.

In addition to the flexural energy level in Beam 40, E_{flex}, which has been used as the parameter minimised in all the optimisation results presented in Chapter 4 and above in this chapter, another energy-based cost function is also used which represents the total vibrational energy,

E_{total}. The two other cost functions studied are based on velocity measurements: the sum of the squares of velocity components, J_{trans}, using solely translational velocity measurements, and one additionally using rotational velocity measurements, J_{all}. All the cost functions were formally defined in Chapter 2. E_{flex} does not give a proper representation of all the vibrational energy of the beam as it does not represent any rigid body motion. Thus to investigate the potential consequences of using E_{flex} as the cost function instead of E_{total} a comparison was conducted, and this was also extended to the two velocity-based cost functions.

Then, for each cost function a ranking of the best actuator positions on the structure achieving the best reductions in the cost function is determined. For each of these actuator positions the consequential attenuation in the total vibrational energy is evaluated whilst minimising these other cost functions. Thus the effectiveness of these cost functions in reducing the total vibrational energy can be evaluated.

5.3.1 INITIAL STUDY INTO RIGID BODY KINETIC ENERGY OF A BEAM

To demonstrate that the choice of cost function can have important consequences on the success of an active control system, two single frequency scenarios are presented ahead of the full analysis. The first case, Case 1, is that using an actuator on Beam 3 of the structure at a frequency of 170Hz. Figure 5.12 shows the effect on the total vibrational energy (E_{total}) when using E_{flex} and E_{total} as the cost functions. Both the constituent rigid and flexural energy components are also shown. It is seen that in minimising E_{flex} an increase in the value of E_{rigid} is seen, which then becomes the dominant component of E_{total}, and further reductions in E_{flex} will not reduce the total vibrational energy further. However, when E_{total} is used as the cost function the minimum value of E_{total} is thus achieved, even though a small increase in E_{rigid} occurs.

The results of this comparison are summarised in Table 5.7, which also details the reductions in all of the other parameters considered when each is used as the cost function being minimised. The table also includes the results for a second case (Case 2); of using two actuators on Beams 5 and 9 at a frequency of 160Hz it is again seen here that the use of E_{total} as the cost function is superior to E_{flex}. In this particular case the use of E_{flex} increases the rigid body kinetic energy, whilst the use of E_{total} reduces it by about 6dB with less than 1.5dB being sacrificed in the reduction in the value of E_{flex}. Also, for Case 2, using either J_{trans} or J_{all} as the cost function yields good reductions in E_{total}, which are better than those obtained using E_{flex} as the cost function. Here J_{trans} is seen to achieve substantial reductions in the rigid body kinetic energy, but it is the smaller reduction in E_{flex} in this case which makes the reduction achieved in E_{total} second to that for J_{all}. The result of using J_{trans} and J_{all} as cost functions in Case 1, however, is not seen to be as successful. This can be explained by the fact that the actual

reductions in the cost functions themselves are only 0.05dB and 1.3dB for J_{trans} and J_{all} respectively (compared to 41.0dB and 9.2dB for Case 2). From this brief analysis it can be seen that the success in using each parameter as the cost function appears to be very much dependent upon the frequency at which the performance is considered. To provide a more practical comparison the average performance over a frequency band is used in the next section.

A brief comment is first made on the physical significance of the rigid body kinetic energy. For the application of active control with E_{flex} for Case 1, the kinetic energy in the transverse sense (x-axis direction) is 6μJ/N^2 (per Newton primary input force squared). The use of the E_{flex} cost function increases the peak displacement from about 30nm/N (per Newton primary input force) to about 0.42μm/N for the 1m beam length mass of 2.74kg. Using E_{total} as the cost function this increase is not as large and the peak displacement after control and is about 0.18μm/N. The value of the axial, transverse and rotational rigid body kinetic energy components can be directly related to the corresponding motions of the beam (which are the same at all positions on the beam, by definition). It is not generally feasible to relate E_{flex} directly to motion at any particular point on the beam. This relationship depends upon the frequency of the vibration and the particular point on the beam. Generally, therefore, the precise 'significance' of the flexural and rigid body energies of the beam cannot be determined.

In Chapter 2 E_{flex} was derived from the net power transmitted into (and therefore dissipated in) Beam 40. This is the algebraic sum of the power components at both ends of the beam, for all the three degrees of freedom of movement allowed. Physical insight is gained into the mechanism by which the minimisation of the cost function can achieve reductions in the flexural vibration of the beam by studying the individual power components. Figure 5.13 shows the effect of applying active control on the individual power components at the ends of the beam, using both E_{flex} and E_{total} as the minimised cost function. The same shading scheme is used as that used previously, the dark and light shaded bars represent the value of individual component values without active control and with active control respectively. The sum of the values indicated by the dark shaded bars, when normalised with respect to the beam damping represents the flexural energy level of the beam at this frequency (see (2.27)). The coordinate notation corresponds to the global coordinates system shown in Figure 2.1, where the numbering for the ends of Beam 40 is also denoted. A positive value indicates power transmitted in the direction of the positive sense of the corresponding axis. So, for example in Figure 5.13, without active control the y-direction component at beam end 1, Py1, is positive and indicates power transmitted into the beam, along its axis, at the other beam end, Py0, is negative and also indicates power transmitted in the beam.

In Figure 5.12 the reduction in the value of E_{flex} for Beam 40, when E_{flex} is used as the cost function, is evident. For most cases it is normally expected that this is achieved by reducing the individual power components for each beam end. In Figure 5.13, however, for Case 1 the application of active control *increases* the components whilst decreasing the cost function. Using E_{flex} as the cost function the reduction in this parameter is seen to be achieved by an increase in the values of the individual power components, whilst using E_{total} as the cost function results in even larger increases. Applying the conservation of energy this apparent contradiction can be resolved if there exists a net flow of energy through the beam. In other words, Beam 40, albeit the furthest beam from the input of vibrational energy in a damped structure, is not the end chain in the flow of energy in the structure, but can also act as an energy 'source' to adjoining beams.

The differing levels of success in using each of the four different cost functions is due to the fact that each cost function is a different representation of the same physical vibration. This fact is illustrated in Figure 5.14, which shows the value of the four parameters without active control over the frequency range 50Hz to 350Hz. All of the parameters show similar responses indicating higher and lower levels of beam vibration, although J_{trans} is seen to be the least consistent.

5.3.2 EFFECT ON E_{TOTAL} WHEN MINIMISING OTHER COST FUNCTIONS

The results above show that the success of using each cost function to reduce the value of E_{total} is frequency dependent and this is reinforced for each cost function over a frequency range. Each cost function parameter was minimised (*i.e.*, used as the cost function) when using actuators on Beams 5 and 19, as in Case 2 above. The minimum value of the cost function for each frequency in the range 50Hz to 350Hz (at 5Hz intervals) is plotted against the same parameter value without active control in Figure 5.15. The average performance of the cost function over the band of frequencies of interest will provide a measure of the average success of using each cost function. The frequency averaged cost function is defined, for a generalised cost function, in (2.76) where each cost function replaces the general parameter, *CF*. Figure 5.15 shows the results for each of the four cost functions considered. Reductions, even though slight in some cases, are achieved at all frequencies within this range for all the parameters. The success of using the other cost functions was evaluated by determining the level of E_{total} in the beam at each frequency as a consequence of minimising each cost function. The results are shown in Figure 5.16, which confirms the variation with frequency suggested in the previous sub-section. It is seen that the best reductions in E_{total} are achieved using the two

energy-based cost functions. Using J_{trans} as the cost function actually increases the value of E_{total} (by almost two orders of magnitude) at some frequencies.

5.3.2.1 EFFECT OF COST FUNCTION ON OPTIMUM APPLICATION OF ACTIVE CONTROL

As discussed in Section 5.1, it is possible for the structure studied here to perform an exhaustive search over all possible actuator configurations, for a small number of actuators, to determine the best configurations. This has already been achieved for $\langle E_{flex} \rangle$ and was achieved for the remaining three cost functions and the best ranked actuator positions were selected for one, two and three actuators. Beam 40 was not used as a candidate position for an actuator. Hence for each number of actuators there are 39, 741, 9139 possible actuator positions.

For the best sets of actuator positions, determined using each cost function parameter, the consequential attenuation of E_{total} was then evaluated. E_{total} has been shown above to be as the best representation of the overall vibrational energy and hence is used as the reference by which the success of using other cost functions is evaluated. If a particular cost function is a good representation of the total vibrational energy of the beam (E_{total}), then the high and low values of attenuation in the cost function parameter will correspond to high and low values of E_{total}. The cost function can then be said to be a *predictable* measure of E_{total}. This will lead to the ranking of actuator positions on the basis of the cost function parameter such that the higher ranked ones will provide the best reduction in E_{total} for the cost function. Also, similar values of attenuation should be achieved when using each cost function as when using E_{total}.

SINGLE ACTUATOR ACTIVE CONTROL

The success of using each of the four frequency-averaged cost functions in an active control system using a single actuator was studied. The results are presented in Figure 5.17. Each graph shows the consequential attenuation achieved in $\langle E_{total} \rangle$ for each actuator position, which has been ranked in performance of the cost function parameter attenuation. The attenuation for each cost function is shown by the plain line, and is thus monotonically decreasing due to the ranking. It is stressed that each rank number does not necessarily correspond to the same actuator position for each cost function. The best of the cost functions, apart from the reference is $\langle E_{flex} \rangle$ which appears to yield similar reductions to $\langle E_{total} \rangle$. $\langle E_{flex} \rangle$ thus appears to be a predictable measure of $\langle E_{total} \rangle$, so that the actuator positions which give high values of attenuation in $\langle E_{flex} \rangle$ also give high values of attenuation in $\langle E_{total} \rangle$. Next, the use of $\langle J_{all} \rangle$ also provides good attenuation in $\langle E_{total} \rangle$, however this parameter is not such a predictable measure of $\langle E_{total} \rangle$ as $\langle E_{flex} \rangle$. Some of the better values of attenuation achieved in $\langle E_{total} \rangle$ are found at lower ranked positions and thus would not normally be selected on the basis of the cost

function performance. Despite this, the use of this cost function is not as disastrous as would be the case with the use of $\langle J_{trans} \rangle$. In this case the ranking obtained on the basis of the cost function is no use in predicting good values of attenuation in $\langle E_{total} \rangle$. Here all the attenuation values in $\langle E_{total} \rangle$ are below 5dB and in a few cases (including the second ranked position) the use of this cost function actually increases $\langle E_{total} \rangle$. Thus, $\langle J_{trans} \rangle$ is neither a good nor a predictable measure of $\langle E_{total} \rangle$.

To aid comparison between the absolute values of consequential attenuation achieved in $\langle E_{total} \rangle$ for each cost function, all of the values of attenuation in $\langle E_{total} \rangle$ achieved with a single actuator against the individual rankings for each cost function are presented on common axes in Figure 5.18. It is emphasised that each rank may represent different actuator position combinations for each cost function. To gain a physical insight into why the performance of some cost functions are better than others, the values of consequential attenuation in $\langle E_{total} \rangle$ achieved for each cost function are split into the two constituent parts $\langle E_{flex} \rangle$ and $\langle E_{rigid} \rangle$, as studied in Section 5.3.1. These are also presented in Figure 5.18. From the reference values used for the dB scale shown on the axes for each of these components (the energy level without AVC) it is seen that the significant energy component is $\langle E_{flex} \rangle$. Thus to achieve good values of attenuation in $\langle E_{total} \rangle$ each cost function needs to produce good values of attenuation in $\langle E_{flex} \rangle$. This is achieved, to differing degrees of success, for all of the cost functions, except $\langle J_{trans} \rangle$, and its poor performance in representing $\langle E_{total} \rangle$ is thus explained. It is interesting to note, however, that the use of $\langle J_{trans} \rangle$ does provide a good and a predictable measure of the rigid body kinetic energy of the beam. The actuator positions which give good reductions in $\langle J_{trans} \rangle$ also provide relatively good reductions in $\langle E_{rigid} \rangle$ (at best 10dB greater than for other cost functions) which almost monotonically decrease with the ranking for this cost function.

MULTI-ACTUATOR ACTIVE CONTROL

The investigation was extended to an active control system utilising two and three actuators. The results are presented in Figures 5.19 and 5.20, directly in the combined format of Figure 5.18. The ranking of the x-axis refers, again, to the individual ranking for each of the cost functions, and does not imply common actuator positions at each rank value. It is not feasible to show all the ranked positions and in these cases only the top 100 are shown. The order of success between the cost function parameters in minimising $\langle E_{total} \rangle$ is similar to that when using a single actuator. $\langle E_{flex} \rangle$ is found to yield very predictable reductions in $\langle E_{total} \rangle$, which are also of similar magnitudes for both cases. The second best cost function, again, is $\langle J_{all} \rangle$. In general it achieves in between 5dB and 10dB less reduction in $\langle E_{total} \rangle$ than either energy-based cost function. Again, $\langle J_{trans} \rangle$ is the worst in this respect. It is seen that this is due

to the use of this cost function not providing good reductions in $\langle E_{flex} \rangle$, although it still continues to provide large reductions in $\langle E_{rigid} \rangle$, generally 15dB and 30dB greater than for other cost functions, for two and three actuators respectively. The best ranked positions for $\langle J_{trans} \rangle$ yields reductions of over 80dB in $\langle E_{rigid} \rangle$ for the three actuator case.

5.3.3 DISCUSSION OF RESULTS

It is seen for the optimal application of active control over a band of frequencies, which relies on determining the best actuator positions for single and multiple actuators, that there is little difference in using $\langle E_{total} \rangle$ or $\langle E_{flex} \rangle$ as the cost function parameter. E_{total} is in general a more comprehensive representation of all types of vibration of the beam. It does not require any additional parameter measurements than those required for E_{flex}. Although the application of active control at single frequencies in Section 5.3.1 was shown to suggest that E_{total} is the best cost function, especially where the lack of reduction or increase of E_{rigid} has consequences on the reduction of E_{total}. The frequency-averaged $\langle E_{rigid} \rangle$ is seen to be less significant than $\langle E_{flex} \rangle$, and so generally $\langle E_{flex} \rangle$ is found to perform well as a cost function. It is suggested that this is due to the nature of the beams used in the structure considered here. The beams used are 'thin' beams and therefore relatively flexible, also the natural frequencies for transverse vibration are much lower than for axial vibration. The first transverse mode occurs at about 240Hz which is in the frequency band studied, whereas the first axial mode occurs at about 2.5kHz. Therefore the detection of rigid body motion is thought to be more important for a structure using beams with a greater cross-section (normally termed 'rods' or 'bars') which only support axial vibration. The development and use of the E_{total} cost function has, however, allowed this to be verified.

Two velocity-based cost functions were also investigated to find their effectiveness at reducing E_{total}. Using only a velocity measurement in the near field of a source has been shown to have worse performance than outside the near field of a source by Pan and Hansen (1993). This is equally applicable to a structural discontinuity, where all the velocity measurements are taken in this case. So, the velocity-based cost functions can only be expected to be approximations of E_{total}. It is seen that the incorporation of the rotational velocity components at the ends of each beam is very important to achieve good, predictable reductions in E_{total} , and J_{all} shows a much better performance over simply using the J_{trans} cost function. When using three well-positioned actuators, the J_{all} cost function is seen to have average reductions, over the frequency bandwidth considered, of 5dB to 10dB less than the E_{total} cost function. For the J_{trans} cost function the attenuation is over 25dB less. J_{trans}, however, does provide a very good representation of the value of E_{rigid} of the beam, and consistently achieves predictable and much

greater reductions than for the other cost functions. Therefore for a structure comprised of rigid beams (or rods) the use of E_{rigid}, which is well approximated by the slightly simpler J_{trans}, parameter may be sufficient. Thus, the rotational velocity component would not be required.

Whilst E_{total} is seen to be a better measure of the vibrational energy of the beam it is seen that there is no serious disadvantage in using E_{flex} as a cost function, for the frequency averaged measure of vibration used for the particular structure considered here. Thus, the use of E_{flex} was maintained in the optimisation work that follows to maintain consistency with the optimisation results reported in Chapter 4.

A final note is included on the weighting between the translational and rotational velocity components used in the formulation of J_{all}. The addition of the kinetic energy components due to the rotation of Beam 40 was modelled by considering the beam to be composed of two rigid levers, whose lengths were half that of the beam, and each half-beam hinged about one end. However, this is an approximation, and as only the first flexural modeshape is significant in the frequency range considered, the shape of this modeshape could be easily determined exactly. As the velocity is a function of distance along each half-beam, the net kinetic energy due to flexure of each beam half can therefore be accurately calculated. The approximation used here over-estimates the actual kinetic energy of the first mode by a factor of about 3. With a smaller significance of the rigid body kinetic energy component in J_{all}, a better estimate of E_{total} may be produced.

5.4 STUDY OF ROBUSTNESS OF ACTUATOR POSITIONS

A study of the robustness of the performance of the various actuator positions to geometric perturbations was performed in order to determine the candidates that are more practical to implement. The same set of 300 perturbations were applied to the structure as used for the robustness analysis of the passively optimised structures in Chapter 4. The perturbations are uniformly distributed between ±10mm about each nominal joint coordinate and are applied to both the x and y coordinates of each of the middle 18 joints of the structure.

As discussed in Chapter 4 regarding the robustness of the passively optimised structures the effect of the geometric perturbations is to change the mechanical impedance between the primary force input and the ends of Beam 40. With the application of AVC to the structure this is also extended to the ends of actuators. In practice, this changes the transfer impedance and mobility matrices $\mathbf{C}$ and $\mathbf{Y}$, which are detailed in Section 2.3. For each set of geometric perturbations these matrices are re-evaluated and then the maximum theoretical attenuation calculated from the closed form equation (2.46) and auxiliary equations described in

Section 2.3. In the same way the control effort is re-evaluated. Thus the optimum secondary force vectors are recalculated to achieve the best attenuation attainable for each perturbed plant. Evaluating the perturbed performance for an AVC system in this way corresponds to applying the AVC system to a real structure where manufacturing tolerances are the perturbations from the nominal design. It is also assumed that the controller has an accurate model of the time plant response (Nelson and Elliott, 1992: Chapter 5). If the plant were to change over periods comparable or less than the update period of the plant model, the AVC system would be operating with an inaccurate model of the plant. This is could to be due to geometric changes to the structure caused by significant changes in the static load, or maybe through thermal expansion and contraction. The perturbation analysis performed here is not intended to cover robustness under these conditions. These perturbations are likely to be structured, and the perturbations to each joint position could no longer be treated independently, as in this analysis. The robustness of the control performance and effort for the one-, two- and three-actuator systems has been evaluated.

5.4.1 PERTURBATION ANALYSIS OF AVC SYSTEM PERFORMANCE

Figures 5.21, 5,23 and 5.25 show the results of the perturbation analysis for the best 10 ranked one-, two- and three-actuator actuator positions, detailed earlier in this chapter. These figures consist of histograms showing the statistical distribution of the minimised average energy level in Beam 40 and the results for each structure are displayed in order of ranking under nominal conditions, the value of which is represented by the thin solid line on each histogram. The 95% probability limit is shown by a solid bold line. This indicates that the value of minimised energy level which, for the 300 experiments performed, is less than or equal to this limit for 95% of the perturbations applied. The results are also summarised in Tables 5.1, 5.3 and 5.5. As with the perturbation analysis performed in Chapter 4, 300 perturbations were found to be sufficient to find the 'shape' of the distribution, and hence the calculated limit will be a reasonable estimate of the actual 95% limit. The graphs show the reduced vibration energy level with logarithmic axes as in Figure 4.32 for the perturbation analysis for the passively optimised structures to facilitate comparison the optimisation results presented in Chapter 4. In the field of AVC it is more common to deal with value of attenuation expressed in decibels, a second y-axis on the right is included for this purpose.

Considering first the single actuator AVC actuator positions in Figure 5.21 it is seen that there is little difference between the robustness of the performance when using the ten best optimised actuator positions, all candidates showing a performance spread of just under 10dB. Using two actuators (Figure 5.23) it is seen that DB_D is the most robust candidate, for which the entire

spread of the statistical distribution is about 3dB, while most of the other actuator positions appear to have a statistical spread of about 10dB. Using three actuators (Figure 5.25) it is seen that the majority of the distributions have a range of one order of magnitude with a few, notably actuator positions TR_G and TR_J, whose distribution spread approaches 20dB. In general the three actuator positions achieve reductions of 15dB to 20dB better than with two actuators. If robustness alone was the primary consideration then DB_D is the best two-actuator position. There is no obvious 'best choice' for either the single or the three-actuator positions in terms of robustness.

Using the 95% probability limits, a selection of the most practical actuator positions may be made in terms of both robustness and absolute performance. For each number of actuators the best actuator positions selected on nominal performance also have the best 95% probability limit. In most applications the minimum reduction is the important factor. For the single actuator positions there is little difference in the selection of the candidates using either the nominal performance or the 95% probability limit. For the two-actuator positions the choice of nominally well ranked positions DB_B and DB_C become less favourable. It is also seen that there is little difference in performance between positions DB_A and DB_D in terms of this criterion, but the latter is more robust. Even the worst perturbed performance is better than the majority of the perturbed performance values for DB_A. This set of actuator positions is also seen to have a small probability of having much poorer performance than the 95% limit. Considering the 95% probability limit for the three-actuator positions more diversity in the 95% probability limits is seen that using the single actuator positions. It is also noted that the average difference between the nominal performance and the 95% probability limits for each number of actuators is only about 3dB or 4dB, whilst the average nominal attenuation ranges from about 10dB to 45dB.

5.4.2 PERTURBATION ANALYSIS OF AVC SYSTEM CONTROL EFFORT

Another consideration exists when applying AVC apart from the achieved performance; the control effort required to achieve this. There will be a limit on the control effort with a practical system, either to individual actuator effort or total system effort. In general AVC actuator positions with smaller required control effort is preferable. Robustness analysis should also consider the control effort. As the structure is perturbed the control effort required is likely to change, and even if the performance is insensitive to such changes, if the control effort increases significantly above its nominal value than a practical system may not be able to maintain the predicted vibration reduction. This is avoidable if the increase is predicted and the demand remains feasible.

Figures 5.22, 5.24 and 5.26 show the effect of the robustness analysis on the total control effort for the best ten single, two- and three-actuator positions, with same format as Figure 5.21. It is re-iterated that the scale used on the graph is logarithmic, and that a factor of over 5 exists between the nominal control effort for TR_B and TR_C, for example, which emphasises the importance of the consideration of control effort. It is seen that for both two and three actuator systems the range of total control effort, both nominal and perturbed, are similar even though the three-actuator case produces larger reductions of the vibration. In general, there is less diversity in the robustness of the control effort than with the performance, again in the single actuator case little diversity is seen in the robustness. However, the cost of increased control effort is often realised in linear terms, and the absolute value of the control effort is important. Actuator arrangement DB_D, which is favoured in terms of its performance, is seen to require, for 95% of the perturbation cases, about four times more total control effort than DB_C. The compromise of performance and control effort will vary depending on the application. Considering the three actuator positions results it is seen that TR_C, whilst well ranked in terms of performance, is particularly costly in terms of control effort. Initially TR_F may seem to be a 'bad choice' due to the large spread of the distribution. However, it is apparent that the 'rogue' high value of control effort arises from the results of only one perturbation, and if this particular perturbation value had not appeared in the set of 300 perturbations then this set of actuator positions would appear more robust. This justifies the use of a 95% probability limit, and not simply the worst case. Indeed, using the 95% probability limit, TR_F is ranked third in terms of minimum expected control effort.

5.4.3 DISCUSSION OF PERTURBATION ANALYSIS RESULTS

It has been shown that for an AVC system it is necessary to consider the robustness of both the performance and control effort in selecting practical systems. Each set of actuator positions can be robust in terms of performance, total control effort, or both. When ranked in terms of either nominal performance the more *performance robust* a set of actuator positions is, the more likely its ranking will remain high in terms of the 95% probability limit. However, *control effort robustness* is also important if the application is to be realised practically. Thus it may be advisable not to use a set of actuator positions that, even though is robust in terms of performance, does not indicate good control effort robustness. It was found, in general, that all the AVC systems studied here had a similar performance robustness to geometric perturbations, which is in contrast to the passively optimised structures studied in Chapter 4 where large variation in robustness of the structures was observed.

5.5 CONCLUSIONS

The optimisation of the average vibration transmission of a two-dimensional lightweight cantilever structure was performed, over a frequency band of 150Hz to 250Hz. Unlike for the passive optimisation detailed in the previous chapter, in this case the regular geometry of the structure remained fixed, and the use of Active Vibration Control (AVC) was applied using optimal actuator positions to achieve vibration reductions. For simplicity the actuators were assumed to be mass-less and consideration of control effort was not made part of the optimisation objective. The optimisation task was thus, to find the optimal actuator positions on the grounds of vibration transmission. This was achieved for AVC systems using one to four actuators. For this, the optimisation task was not that combinatorially large, and it was feasible to perform an exhaustive search of all possible actuator combinations. The number of possible actuator positions increases rapidly as the number of actuators used increases, however the use of four actuators yielded values of attenuation which would not be realisable in practice, and all subsequent study was limited to systems using one to three actuators only. Using two actuators, similar reductions were obtained as for the passive optimisation reported in Chapter 4.

Even though the performance of the AVC system was optimised, the control effort, which is the practical power requirement of a system, needs to be considered in selecting a system. This was calculated for all optimal actuator positions. The choice of best optimal positions is made upon consideration of both the performance and the control effort. It is seen that between AVC systems with similar values of attenuation the control effort can vary significantly. Normally a system with a lower control effort is preferable.

An analysis was performed of the power dissipation within the structure (which is distinct from the control effort) for the optimal AVC systems studied. Studying the power contribution of the actuators enables an insight into the vibrational role of the AVC system to be achieved through the three power components; input power, structural power dissipation and net actuator power contribution. In general, it is seen that the reductions in power dissipation in Beam 40 are due to the redistribution of power within the structure, due to the AVC system. Using one actuator it is seen that the AVC system acts to reduce vibration in Beam 40. With two or three actuators it adopts the additional 'strategy' of blocking the power transmission along the structure. Thus the system would be less sensitive to changes in the end impedance of the structure, which may vary if additional masses were attached here.

The effectiveness of an AVC system, in part depends upon how well the parameter (cost function) minimised actually represents the physical vibration of the beam. A comparison of

using alternative AVC cost function parameters was performed. The parameter used here was adopted from earlier work. An investigation was performed to compare the physical success of using this parameter, the Flexural Energy Level (E_{flex}) with three others. An additional energy-based cost function was studied: the Total Vibrational Energy (E_{total}), and two velocity-based cost functions: the Sum of the Squares of the Translational Velocity components (J_{trans}) and the Weighted Sum of the Squares of all Velocity components (J_{all}). The latter used the rotational velocity component in addition to the translational components at each beam end.

A brief single frequency analysis showed that the use of E_{flex} as the cost function can result in significant increases in E_{rigid} and so limit of the reduction attainable in E_{total}. E_{total} is confirmed as being the most comprehensive measure of beam vibration and was used as a reference to compare the success of using the other three cost functions. An insight into the changes of energy flow by the application of active control at the ends of Beam 40 showed that it is the balance between the energy flow between each beam end, and not the absolute magnitude of the individual components (which can be increased by the AVC), which is important. For single actuators combinations it was found that whilst the frequency-averaged version of E_{total} , $\langle E_{total} \rangle$, is the most comprehensive cost function, it is found that there is little disadvantage in using $\langle E_{flex} \rangle$. This is thought to be because the structure is comprised of thin 'flexible' beams and so bending motion is dominant in the frequency band of interest. Even though single frequency cases studied showed the shortcomings of not controlling E_{rigid}, this was not borne out when using cost functions averaged over a frequency band. Generally, reducing $\langle E_{rigid} \rangle$ is thought to be more important if less-flexible beams, or rods, were used as the structural elements.

Using $\langle J_{all} \rangle$ as a cost function was found to be the better velocity-based cost function in reducing $\langle E_{total} \rangle$. For three-actuators AVC systems the reductions in $\langle E_{total} \rangle$ were generally 10dB less than those achieved by minimising either $\langle E_{flex} \rangle$ or $\langle E_{total} \rangle$. The use of $\langle J_{trans} \rangle$ as a cost function was not found to yield good reductions in $\langle E_{total} \rangle$ at all. However it was found to provide a very good prediction of the E_{rigid} component alone, which may prove useful in structures comprised of more rigid beams.

The robustness of the ten best-ranked AVC actuator positions on the structure for one to three actuators was then studied, in order to find the positions which are more practical in the sense of having more resilient performance in the face of small changes in the structure geometry. As with the passively optimised structures in Chapter 4, this was achieved by applying a set of random perturbations enabling the statistical distribution of a performance to be obtained. Whilst the average nominal attenuation varied from about 10dB to 45dB using one to three

actuators, the variation of the average 95% probability limit in each case was similar. Another consideration in the application of AVC, is the control effort. This may be important when choosing the best solution under nominal conditions and could be incorporated into the optimisation search, but was not considered during the optimisation here. However under structural perturbations the control effort is seen for some AVC actuator arrangements to increase by factors over ten times. If the control effort is not considered and under structural perturbations it is seen to rise beyond the capabilities of a practical system then the predicted performance will not be realised. Hence for AVC systems there are two types of robustness: *performance robustness* and *control effort robustness*. A 95% probability limit was applied to performance and control effort statistical distributions obtained from the perturbations applied. This is basis for determining the worse value (for performance or control effort) that will only be breached for an estimated 5% of perturbation instances (assuming the same perturbation distribution), and thus enables the most practical AVC systems to be identified.

Rank	Structure	Actuator position (Beam number)	Overall nominal attenuation (dB)	95% probability limit attenuation (dB)	Control effort (N^2)	95% probability limit control effort (N^2)
1	SG_A	20	10.8	8.3	17200	27200
2	SG_B	30	10.2	6.3	1390	2080
3	SG_C	7	9.9	6.4	7730	11900
4	SG_D	1	9.1	5.3	11100	17900
5	SG_E	12	8.9	5.1	13000	18400
6	SG_F	28	8.9	5.5	2520	3710
7	SG_G	10	8.8	5.5	2860	5000
8	SG_H	38	8.7	4.8	1770	2700
9	SG_I	31	8.5	4.9	1650	3110
10	SG_J	11	8.5	6.2	14700	23800
average		-	9.2	5.7	7392	11580

TABLE 5.1. Results summary for AVC using best performance ranked single-actuator positions over bandwidth 150Hz to 250Hz.

Structure	Primary force input power reduction, α_{INPUT} (dB)	Redistribution of power within passive beams of structure, α'_{REDIST} (dB)	Net actuator contribution α_{ACF} (dB)	Net power dissipated in actuators ($x10^{-7}$ W)
SG_A	-0.6	11.1	0.3	0.244
SG_B	0.7	10.3	-0.8	-6.14
SG_C	1.0	9.6	-0.7	-4.86
SG_D	0.8	11.0	-2.7	-26.9
SG_E	0.5	9.3	-0.8	-6.55
SG_F	0.6	8.7	-0.4	-3.17
SG_G	1.5	8.4	-1.1	-7.47
SG_H	0.3	9.1	-0.7	-6.37
SG_I	0.1	9.0	-0.6	-5.17
SG_J	0.8	8.9	-1.3	-10.3
average	0.6	9.6	-	-

TABLE 5.2. Power levels in structure using single-actuator optimal positions, over a bandwidth of 150Hz to 250Hz.

Rank	Structure	Actuator positions (Beam number)	Overall nominal attenuation (dB)	95% probability limit attenuation (dB)	Control effort (N^2)	95% probability limit control effort (N^2)
1	DB_A	2, 4	31.1	28.1	43500	70600
2	DB_B	2, 16	28.0	25.2	22800	37300
3	DB_C	16, 28	27.8	25.7	13600	23400
4	DB_D	8, 25	27.5	26.8	53900	66200
5	DB_E	14, 16	27.4	24.4	38300	54200
6	DB_F	4, 16	27.4	25.4	49700	68200
7	DB_G	25, 28	27.4	25.2	13400	26500
8	DB_H	10, 16	27.2	24.6	20100	34800
9	DB_I	12, 17	27.1	23.6	33200	46600
10	DB_J	14, 28	26.9	22.9	11000	24800
average		-	27.7	25.0	29950	45260

TABLE 5.3. Results summary for AVC using best performance ranked two-actuator positions over bandwidth 150Hz to 250Hz.

Structure	Primary force input power reduction, α_{INPUT} (dB)	Redistribution of power within passive beams of structure, α'_{REDIST} (dB)	Net actuator contribution α_{ACF} (dB)	Net power dissipated in actuators ($x10^{-7}$ W)
DB_A	3.6	27.4	0.2	0.690
DB_B	0.4	29.5	-1.9	-18.4
DB_C	0.02	28.3	-0.5	-4.21
DB_D	1.9	26.5	-0.9	-5.67
DB_E	0.004	28.5	-1.1	-10.2
DB_F	-0.4	28.5	-0.7	-6.74
DB_G	1.5	27.1	-1.3	-9.01
DB_H	0.2	28.7	-1.6	-15.7
DB_I	0.4	26.8	-0.04	-0.312
DB_J	-0.4	27.8	-0.5	-4.89
average	0.9	28.0	-	-

TABLE 5.4. Power levels in structure using two-actuator optimal positions, over a bandwidth of 150Hz to 250Hz.

Rank	Structure	Actuator positions (Beam number)	Overall nominal attenuation (dB)	95% probability limit attenuation (dB)	Control effort (N^2)	95% probability limit control effort (N^2)
1	TR_A	2, 4, 13	50.8	47.6	46100	63300
2	TR_B	1, 8, 10	49.1	43.9	45300	70500
3	TR_C	7, 8, 9	47.3	43.9	234000	443000
4	TR_D	3, 8, 9	46.4	42.9	55600	98200
5	TR_E	2, 4, 9	46.1	44.7	54900	61900
6	TR_F	2, 3, 4	46.0	44.9	40400	49200
7	TR_G	12, 16, 19	44.8	37.5	24400	33900
8	TR_H	2, 7. 8	44.6	40.9	52700	83600
9	TR_I	1, 4, 8	44.4	41.3	33200	53000
10	TR_J	10, 16, 19	44.0	37.4	29100	45400
average		-	45.9	41.3	60570	100200

TABLE 5.5. Results summary for AVC using best performance ranked three-actuator positions over bandwidth 150Hz to 250Hz.

Structure	Primary force input power reduction, α_{INPUT} (dB)	Redistribution of power within passive beams of structure, α'_{REDIST} (dB)	Net actuator contribution α_{ACF} (dB)	Net power dissipated in actuators ($x10^{-7}$ W)
TR_A	1.8	45.3	3.6	13.5
TR_B	1.1	50.5	-2.5	-21.9
TR_C	-1.3	49.9	-1.4	-17.9
TR_D	-0.1	46.2	0.3	2.55
TR_E	1.8	40.5	3.8	14.0
TR_F	2.8	39.1	4.1	11.7
TR_G	0.1	44.7	0.01	0.00706
TR_H	0.9	45.4	-1.8	-14.9
TR_I	1.8	44.9	-2.3	-17.4
TR_J	-0.4	45.1	-0.6	-6.34
average	1.0	46.4	-	-

TABLE 5.6. Power levels in structure using three-actuator optimal positions, over a bandwidth of 150Hz to 250Hz.

Case	Actuator positions	Frequency (Hz)	AVC cost function	Attenuation achieved in each parameter by minimising cost function shown (dB)				
				E_{total}	E_{flex}	E_{rigid}	J_{trans}	J_{all}
1	3	170	E_{total}	3.20	5.45	-6.16	-6.01	-3.30
			E_{flex}	2.18	7.05	-9.21	-9.01	-5.01
			J_{trans}	0.26	0.27	0.067	0.050	-0.14
			J_{all}	-2.07	-1.92	-4.24	-4.01	1.29
2	5, 19	160	E_{total}	6.37	6.35	6.46	6.63	8.37
			E_{flex}	4.55	7.71	-0.72	-0.50	-0.53
			J_{trans}	5.12	4.25	45.9	41.0	3.52
			J_{all}	6.20	5.89	7.99	8.25	9.15

Table 5.7. Summary of results showing the effect on the values of the four cost function parameters and E_{rigid}, when each parameter is minimised as an AVC cost function for two sets of actuator positions at two different frequencies.

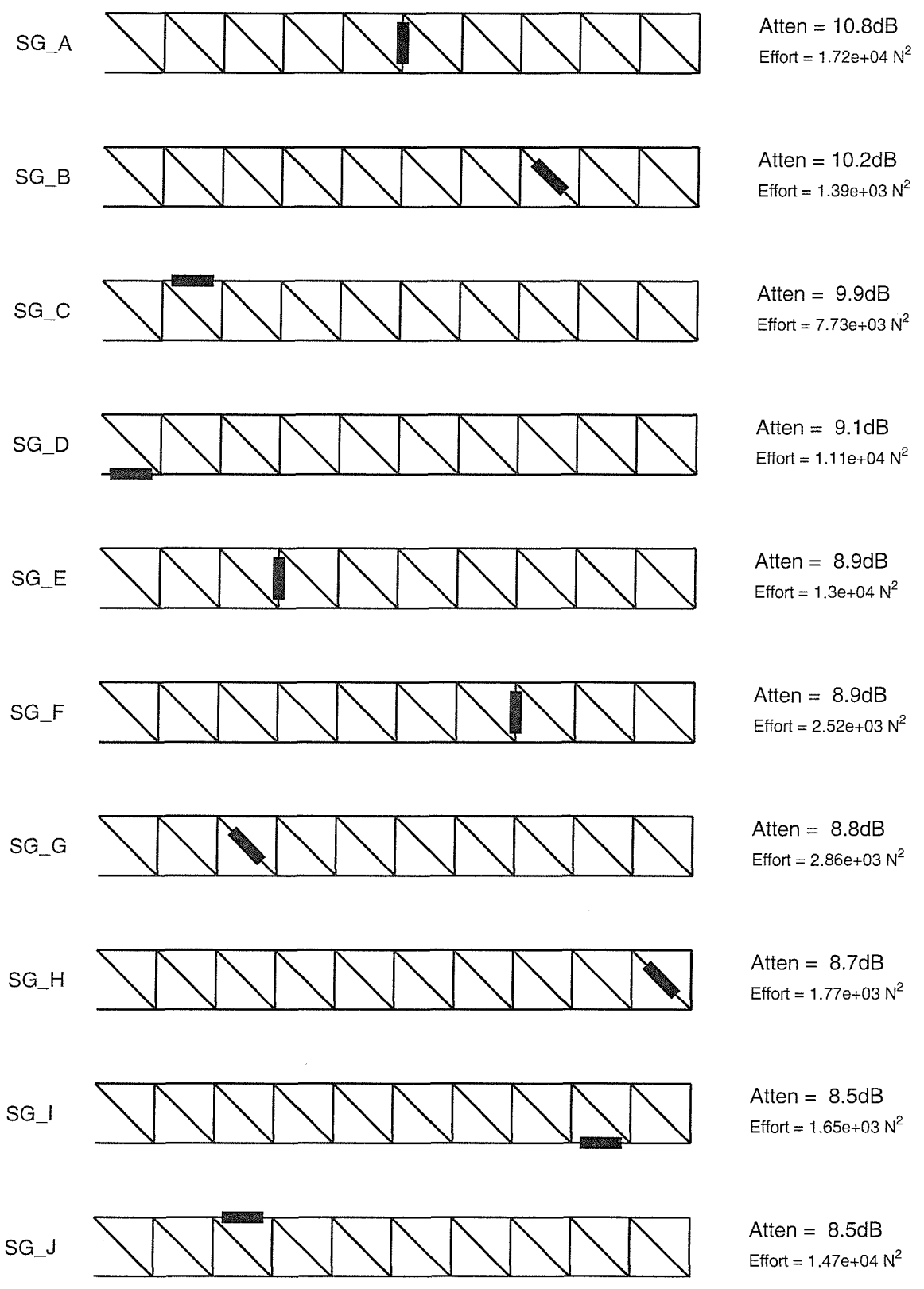

Figure 5.1: The ten best performance ranked single–actuator positions for the frequency band 150Hz to 250Hz.

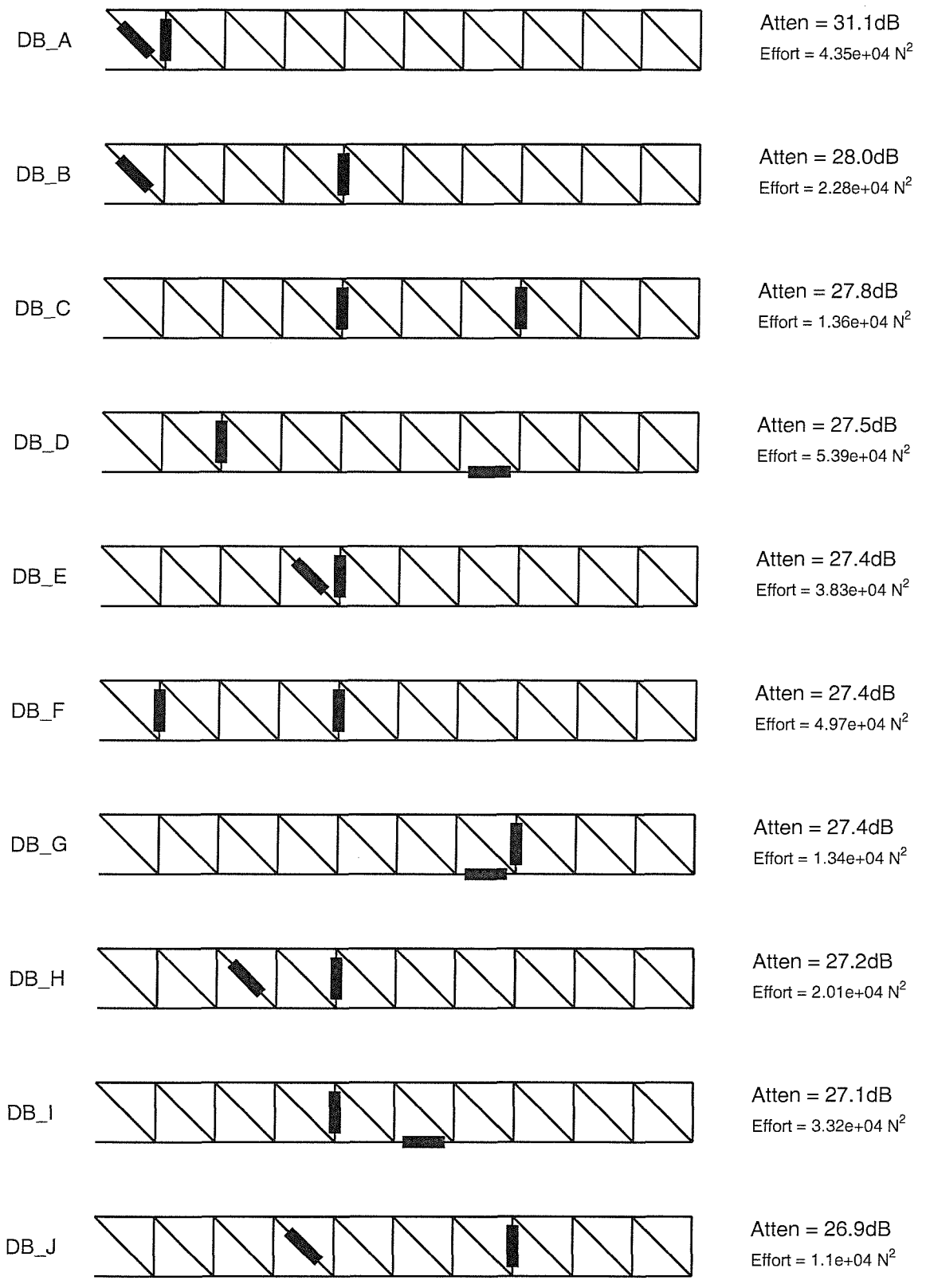

Figure 5.2: The ten best performance ranked two–actuator positions for the frequency band 150Hz to 250Hz.

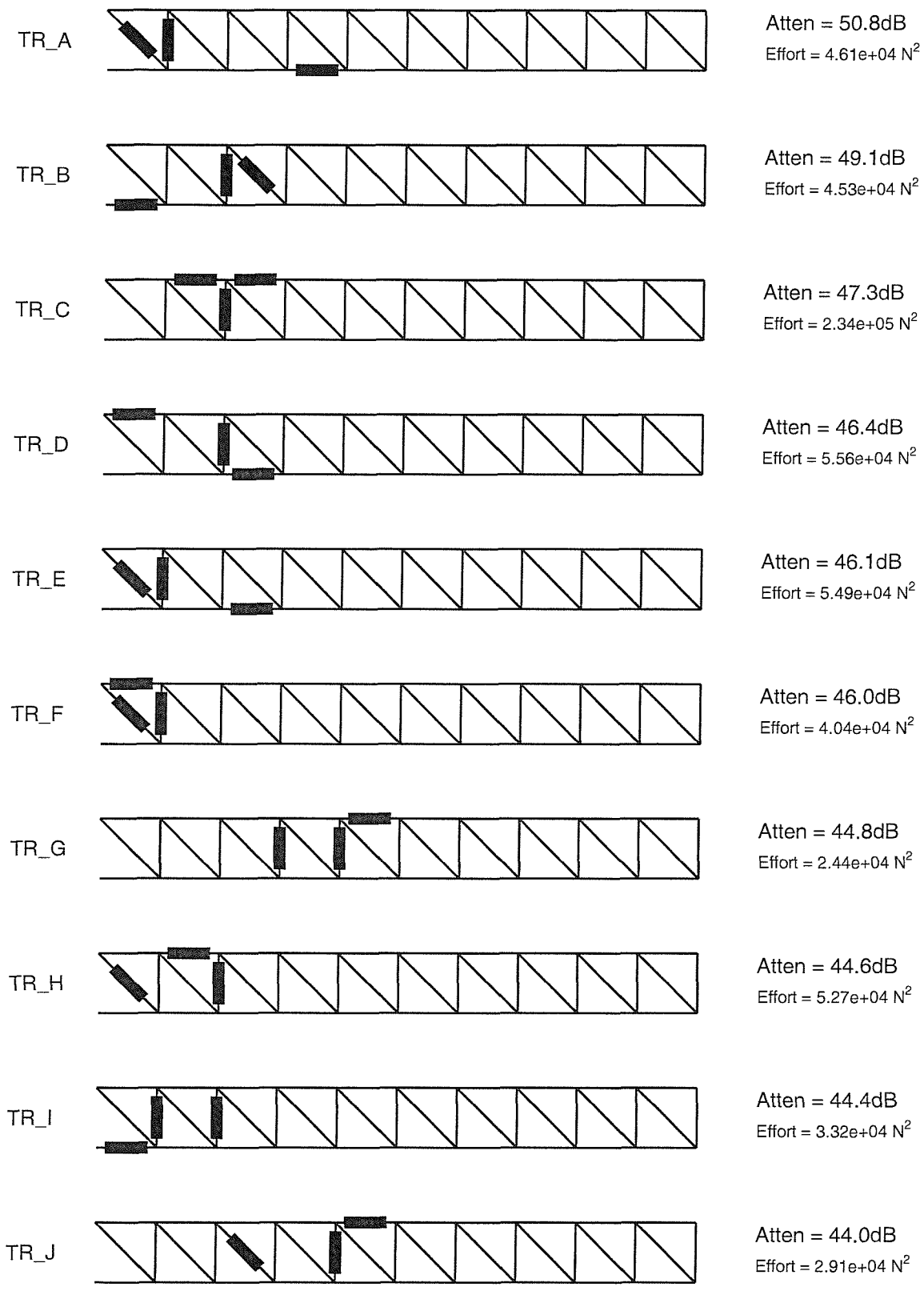

Figure 5.3: The ten best performance ranked three–actuator positions for the frequency band 150Hz to 250Hz.

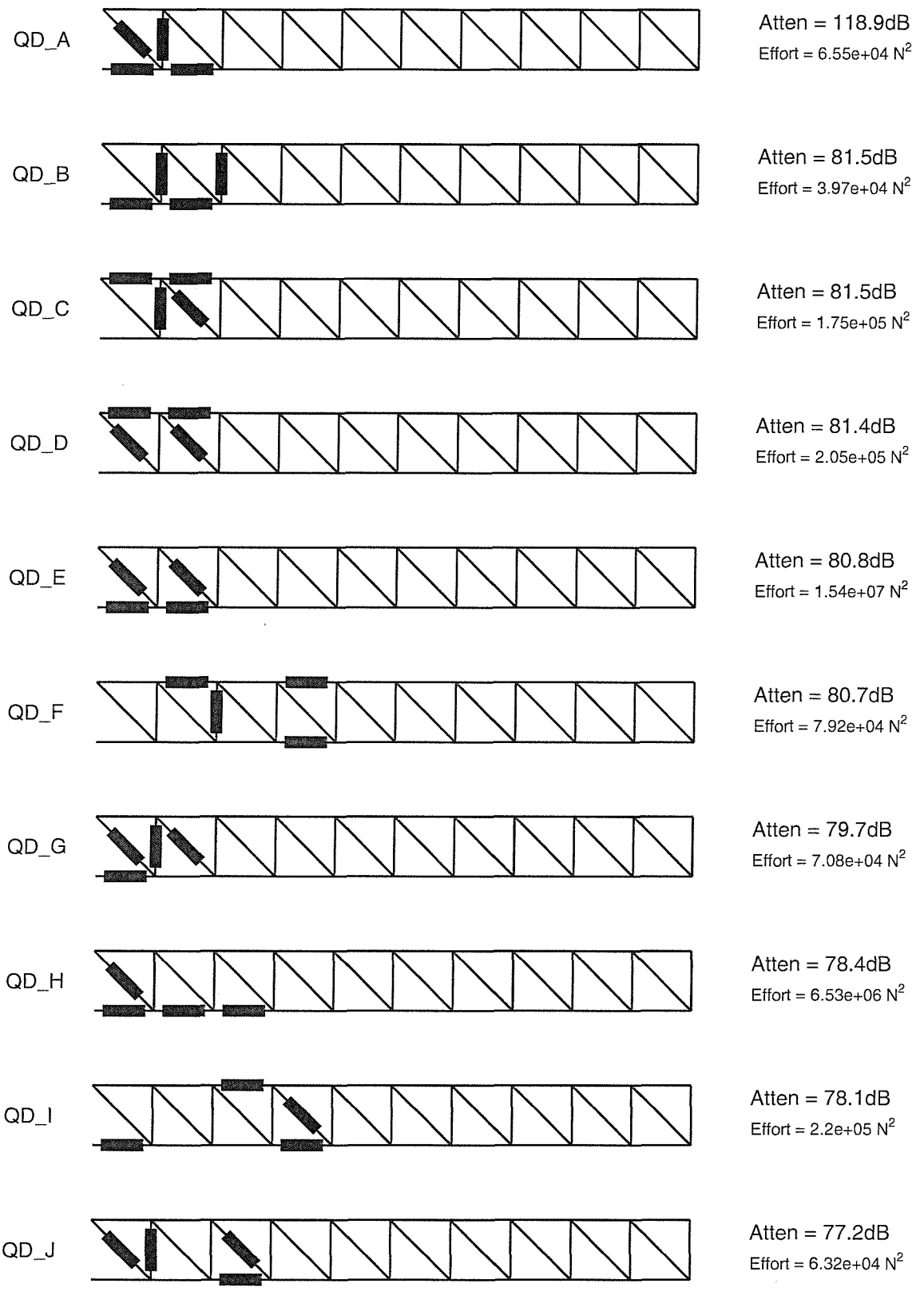

Figure 5.4: The ten best performance ranked four–actuator positions for the frequency band 150Hz to 250Hz.

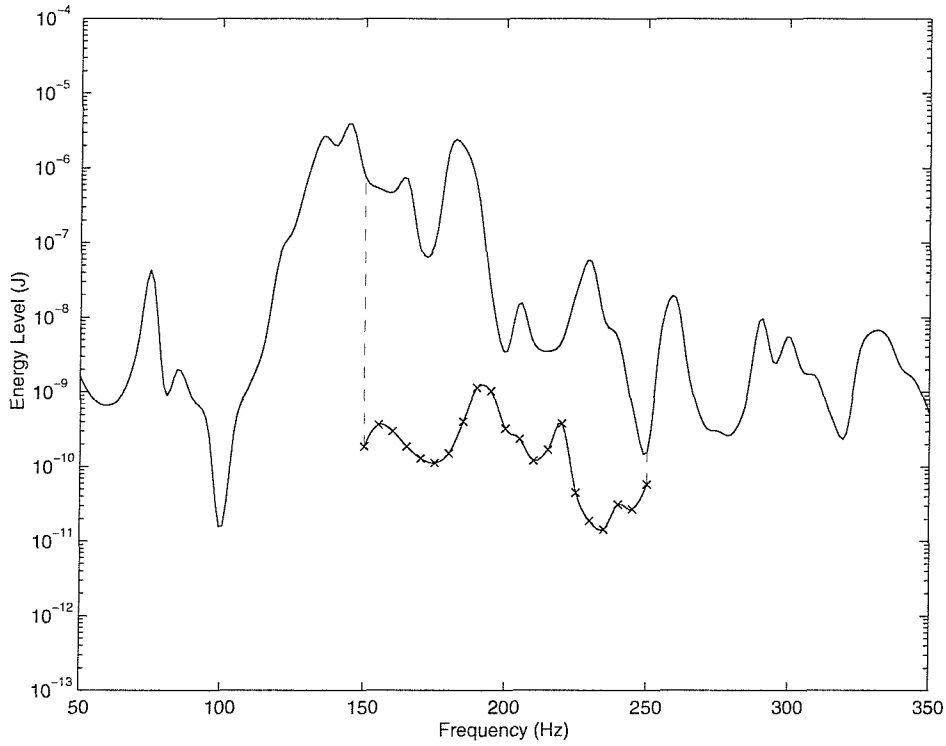

Figure 5.5: Frequency response of the structure without AVC, and the reduced response obtained with AVC, within the frequency band applied, for the actuator positions DB_A in Figure 5.2.

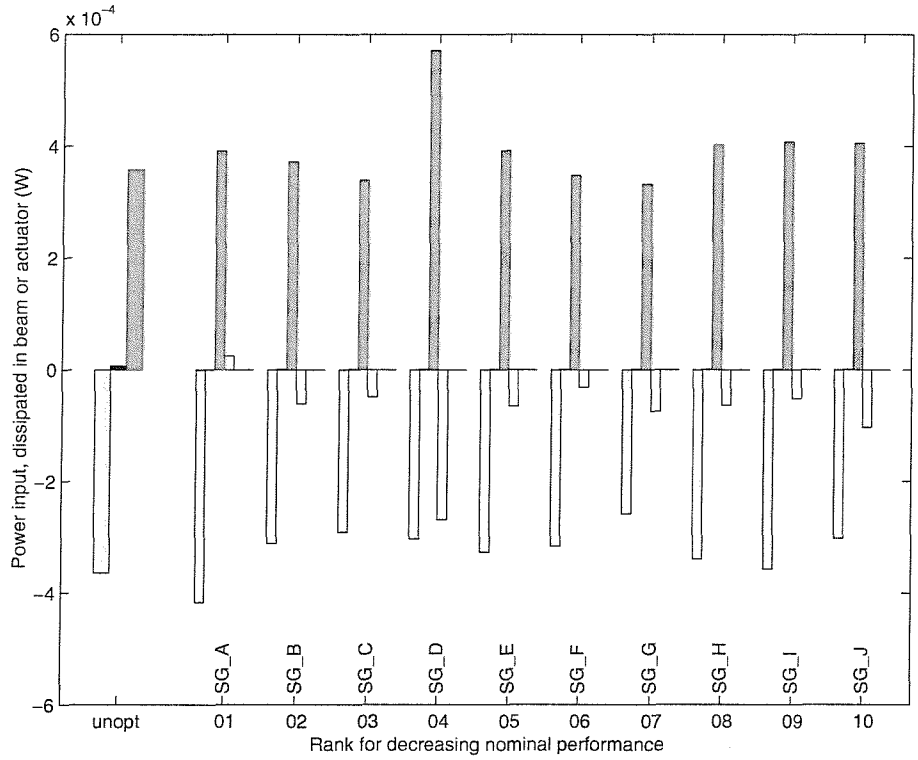

Figure 5.6: Power components in each structure using AVC with optimised single-actuator positions. Negative values of dissipation indicate power supplied to the structure. Light grey: Power input to structure, Dark grey: Power dissipated in Beams 1 to 39 without actuators, Black: Power dissipated in Beam 40, White: Power contributions from actuator. (N.B. Power dissipated in Beam 40 is only distinguishable for structure without AVC. With AVC range is 5.53×10^{-7} to 9.54×10^{-7} W.)

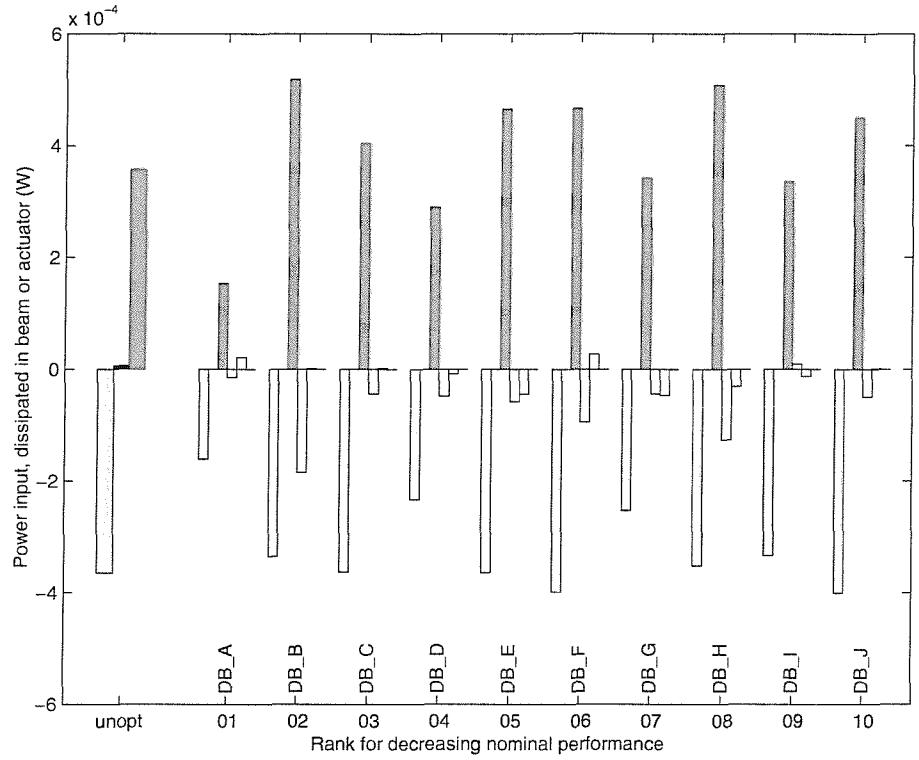

Figure 5.7: Power components in each structure using two–actuator optimised AVC positions. Key as for Figure 5.6. The values of power for each actuator are shown from left to right for increasing beam number position. (N.B. Power dissipated in Beam 40 is only distinguishable for regular structure without AVC. With AVC range is 5.18×10^{-9} to 1.36×10^{-8} W.)

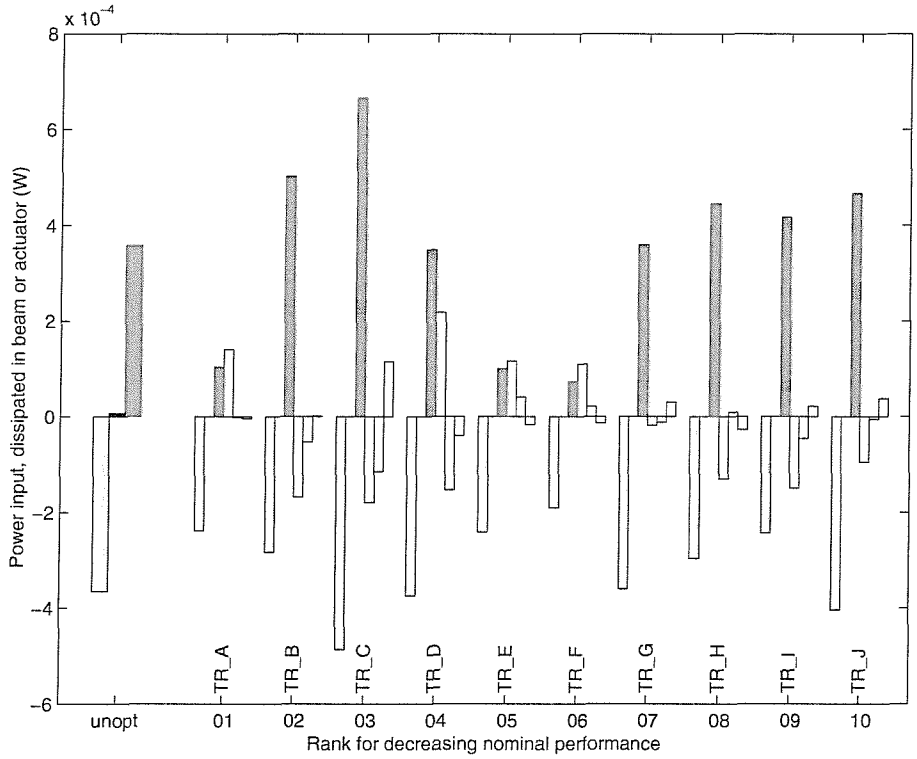

Figure 5.8: Power components in each structure using three–actuator optimised AVC positions. Key as for Figure 5.6. The values of power for each actuator are shown from left to right for increasing beam number position. (N.B. Power dissipated in Beam 40 is only distinguishable for regular structure without AVC. With AVC range is 5.62×10^{-11} to 2.68×10^{-7} W.)

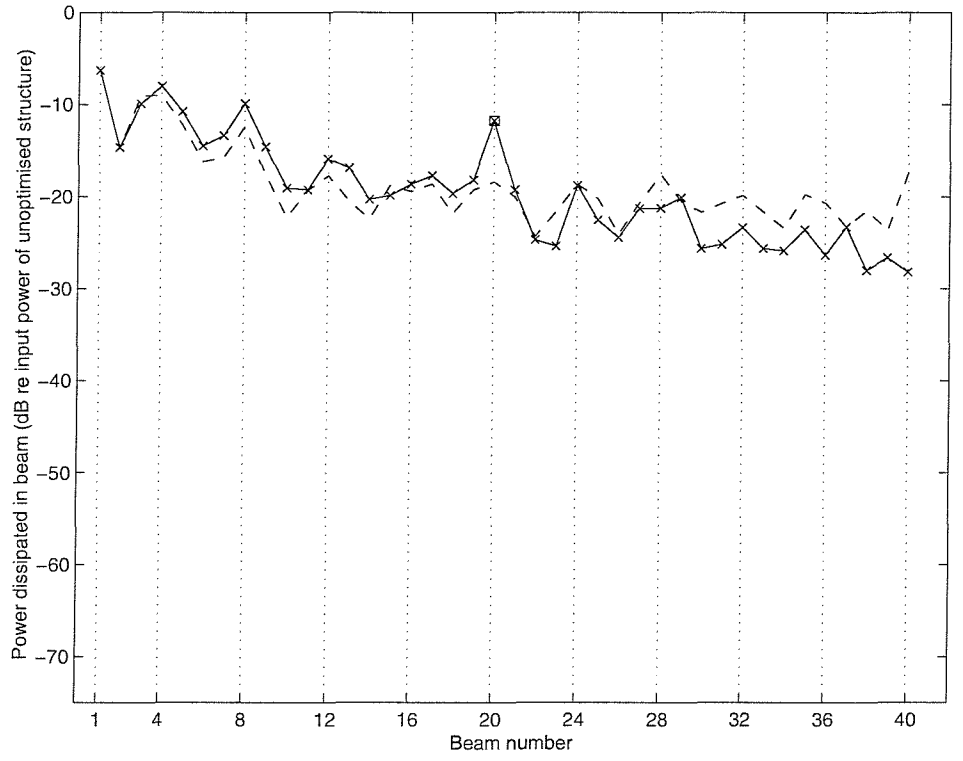

Figure 5.9: Power dissipated in each beam of the structure for optimal single–actuator position SG_A. Vertical gridline represents vertical beam at end of each bay. - - - no AVC, —— with AVC. Actuator position is denoted □.

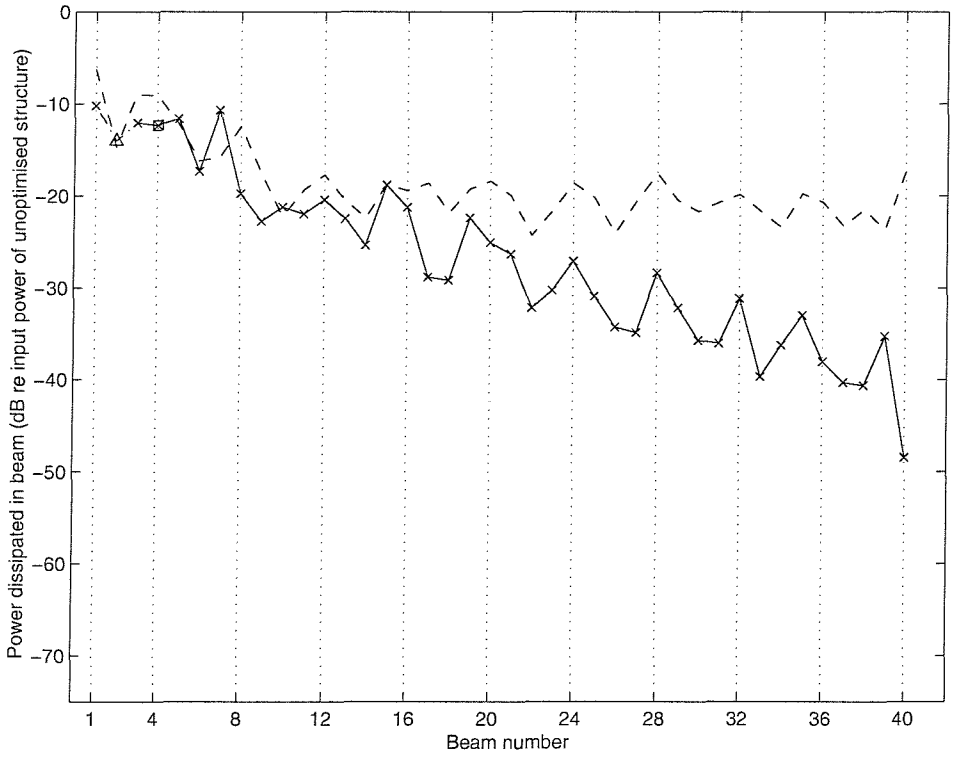

Figure 5.10: Power dissipated in each beam of the structure for optimal two–actuator position DB_A. Vertical gridline represents vertical beam at end of each bay. - - - no AVC, —— with AVC. □ denotes position of actuator dissipating power, △ denotes position of actuator sourcing power (with magnitude shown in the same sense as for dissipation).

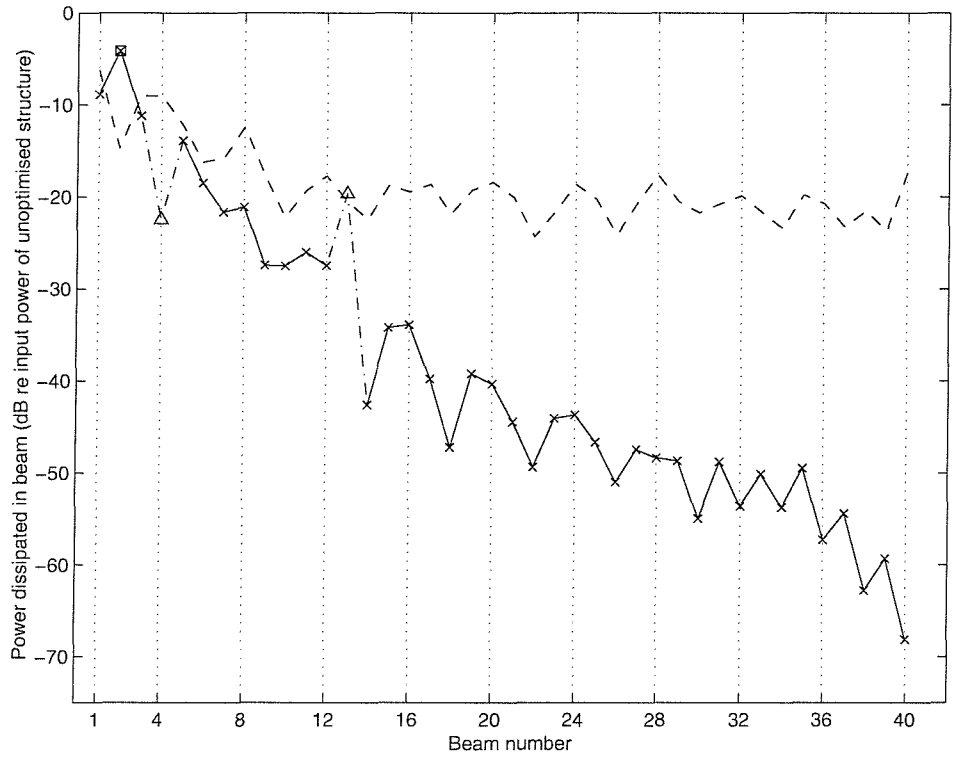

Figure 5.11: Power dissipated in each beam of the structure for optimal three–actuator position TR_A. Vertical gridline represents vertical beam at end of each bay. - - - no AVC, —— with AVC. □ denotes position of actuator dissipating power, △ denotes position of actuator sourcing power (with magnitude shown in the same sense as for dissipation).

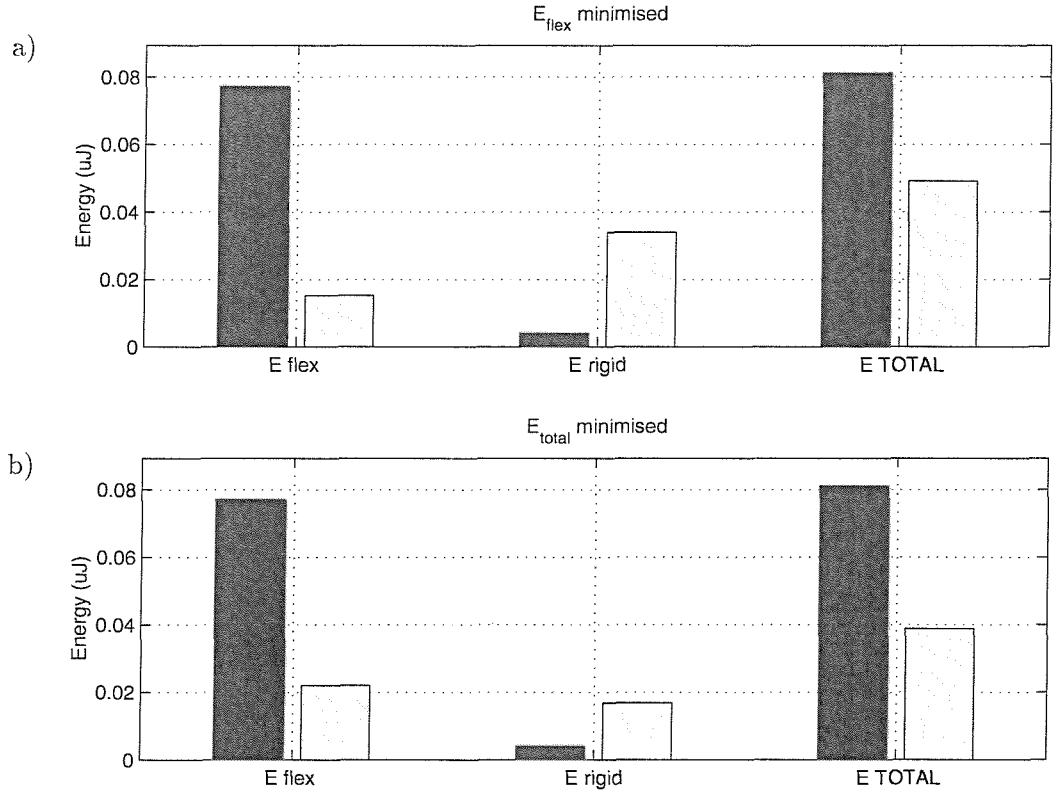

Figure 5.12: Effect of applying active control on E_{flex}, E_{rigid} and E_{total} of Beam 40 for Case 1 with a) E_{flex} and b) E_{total} used as the cost function. (Shading scheme: Dark: no active control, Light: active control applied).

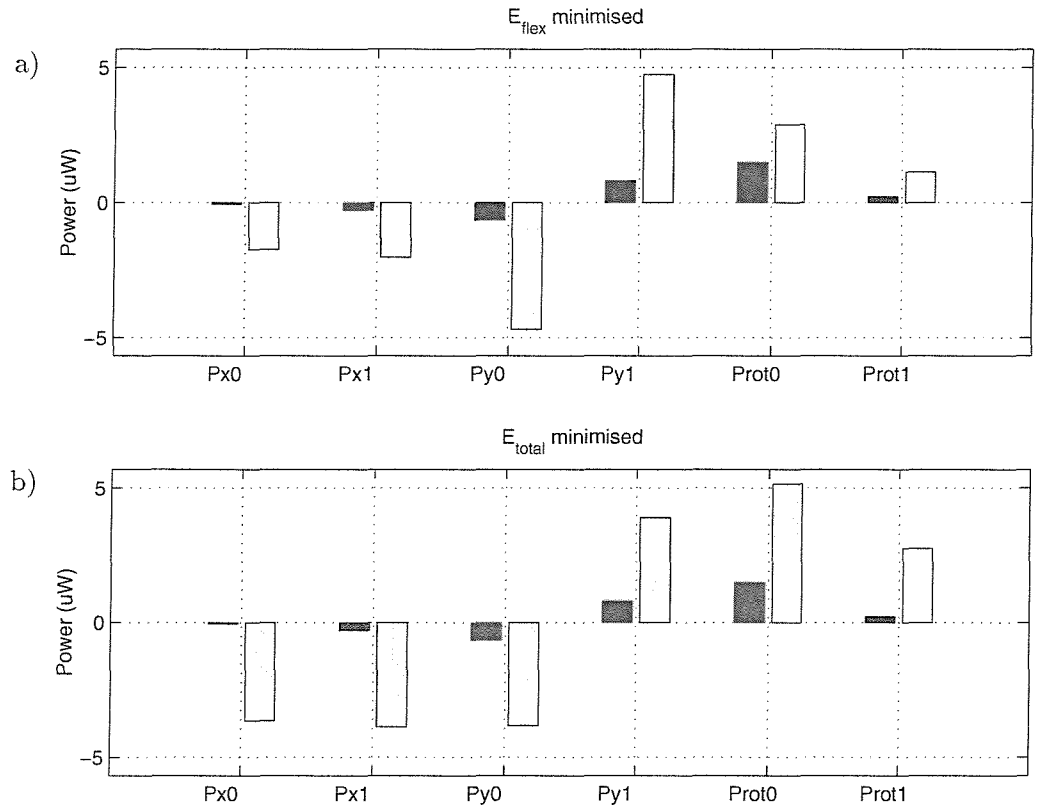

Figure 5.13: Effect of applying active control on power components at the ends of Beam 40, for x, y and θ (rotational) components for Case 1 with a) E_{flex} and b) E_{total} used as the cost function. *e.g.*, Px0 is power flow in x-direction at end 0. (Shading scheme: Dark: no active control, Light: active control applied).

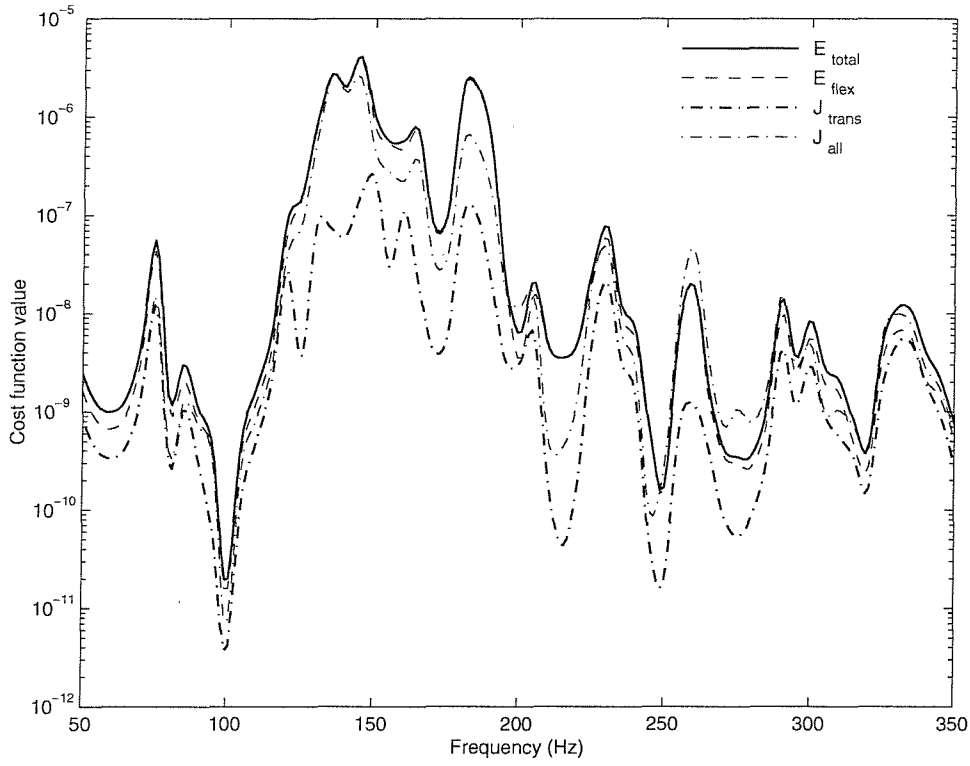

Figure 5.14: The variation of the values of the four different parameters used to quantify the vibration of Beam 40 with excitation frequency when uncontrolled. Each cost function is scaled to represent energy (J).

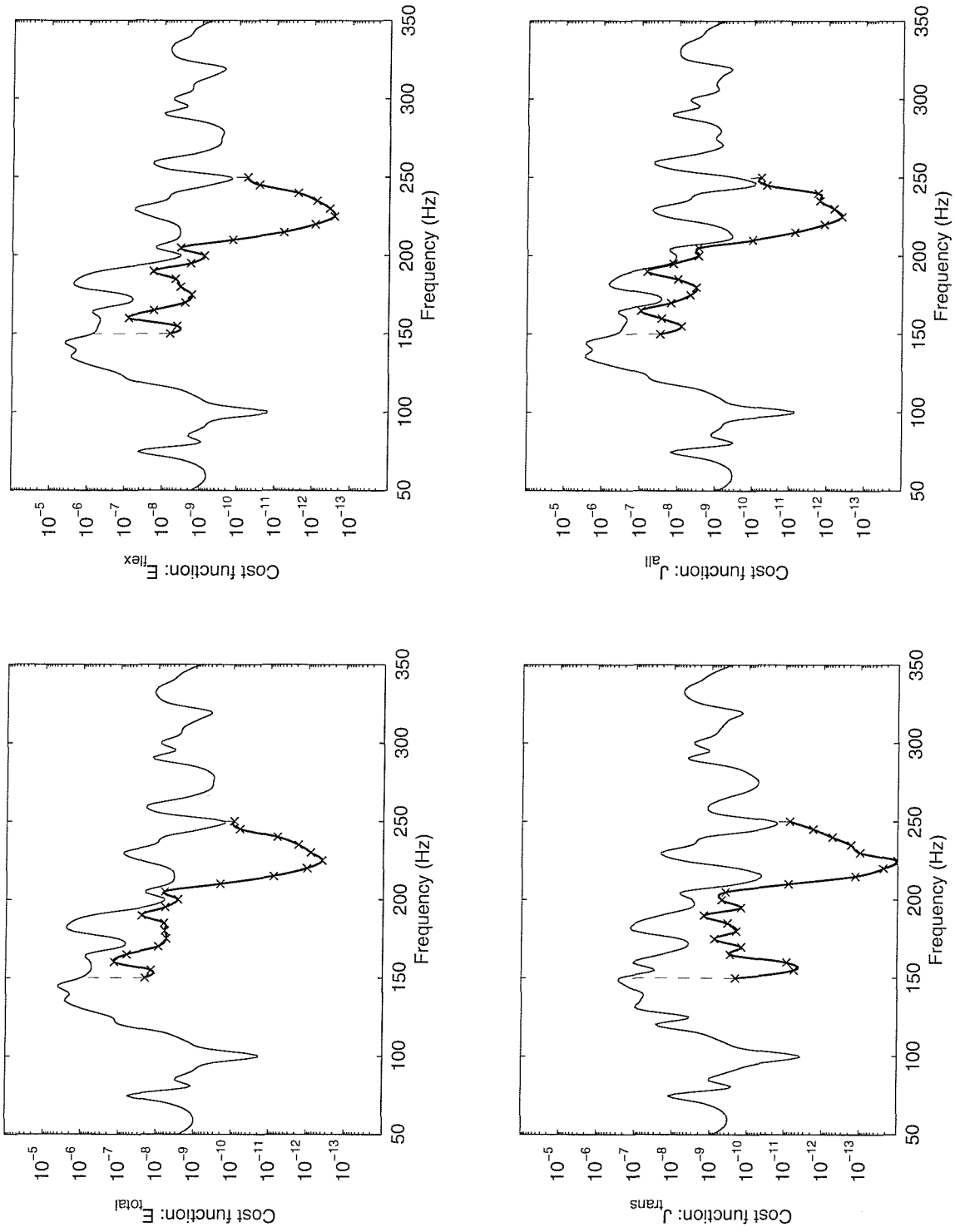

Figure 5.15: Variation of the values of the four parameters, E_{total}, E_{flex}, J_{trans} and J_{all}, with frequency, and their corresponding minimised values when used as a cost function over the frequency band for which active control is applied with two actuators on Beams 5 and 19 (Case 2). Each cost function is scaled to represent energy (J).

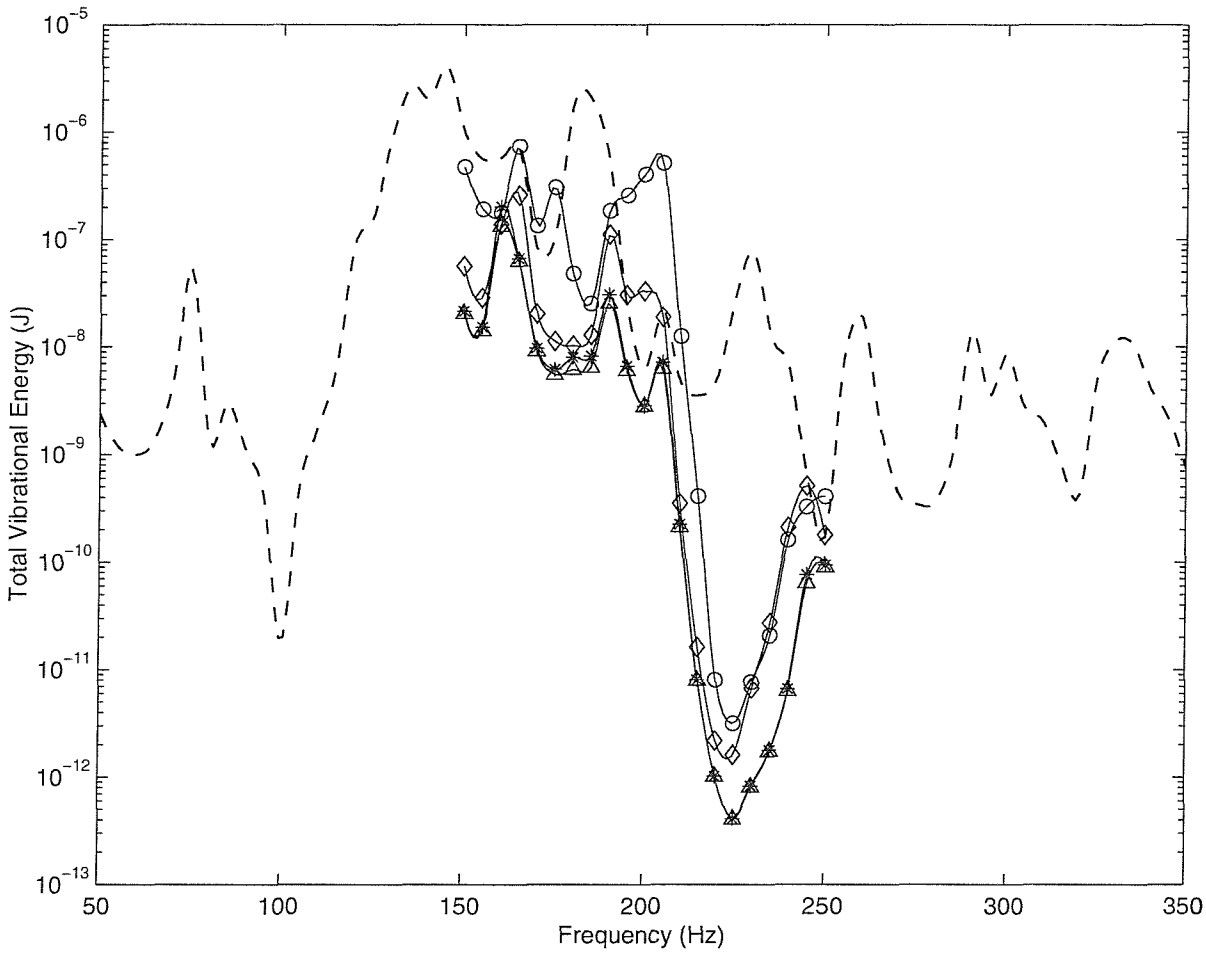

Figure 5.16: The values of total vibrational energy (E_{total}) produced as a consequence of applying active control with each parameter as the cost function, with minimised cost function values as shown in Figure 5.8. E_{total}: $\triangle$, E_{flex}: $*$, J_{trans}: $\circ$, J_{all}: $\diamond$, uncontrolled: - - - .

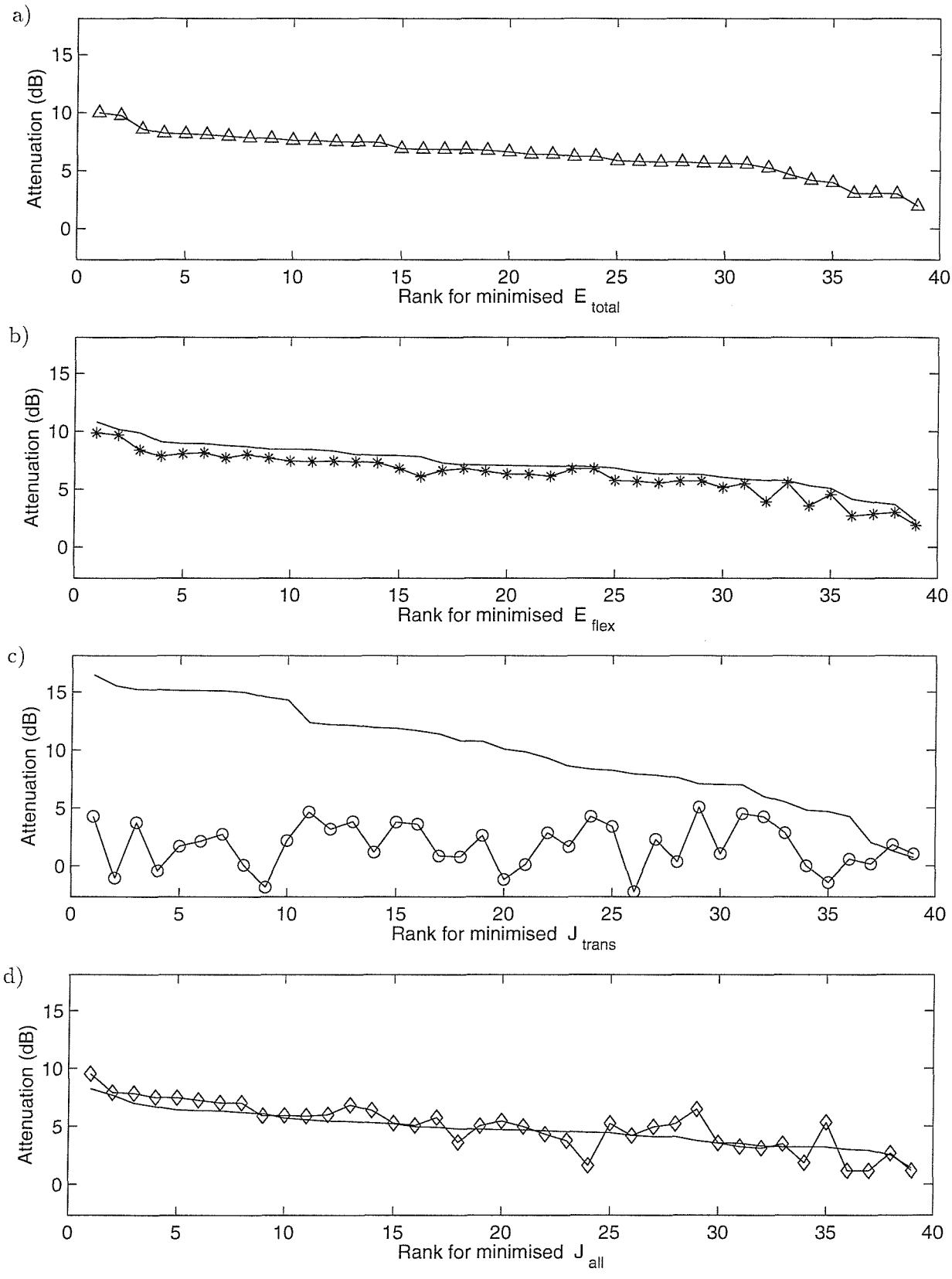

Figure 5.17: Attenuation achieved in each cost function and E_{total} for all single–actuator positions using each cost function. The actuator positions are ranked in order of decreasing attenuation achieved for each cost function parameter (shown as plain line). The attenuation in E_{total} for each instance is shown when using as the cost function: a) E_{total}: $\triangle$, b) E_{flex}: $*$, c) J_{trans}: $\circ$ and d) J_{all}: $\diamond$.

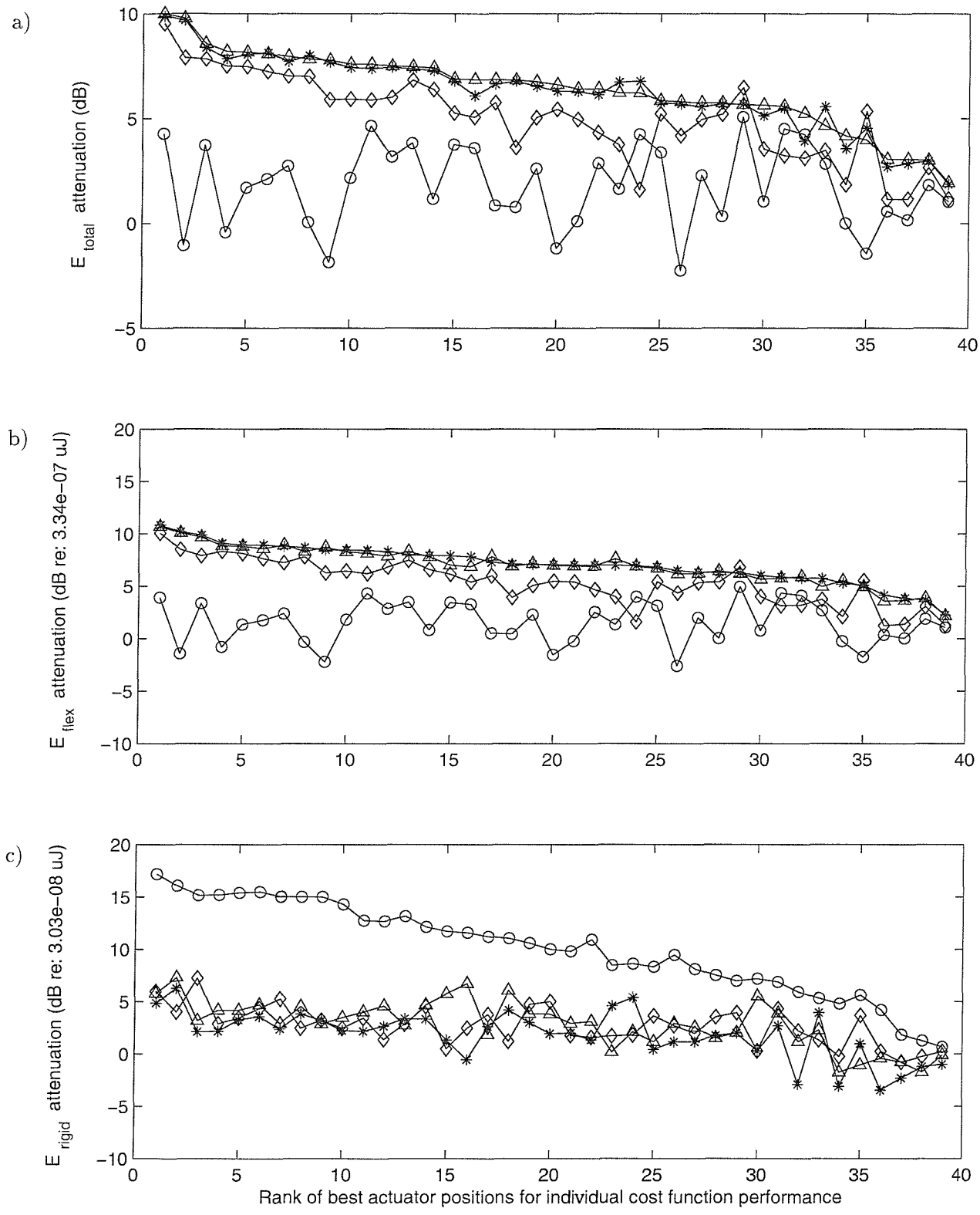

Figure 5.18: a) Summary of results in Figure 5.17: performance achieved in E_{total} by minimising each cost function parameter with results plotted on common axes, and each cost function denoted by the same symbols as in Figure 5.17. Values of attenuation in b) E_{flex} and c) E_{rigid} are also shown for corresponding actuator position combinations as in a). (Cost function E_{total}: $\triangle$, E_{flex}: $*$, J_{trans}: $\circ$, J_{all}: $\diamond$).

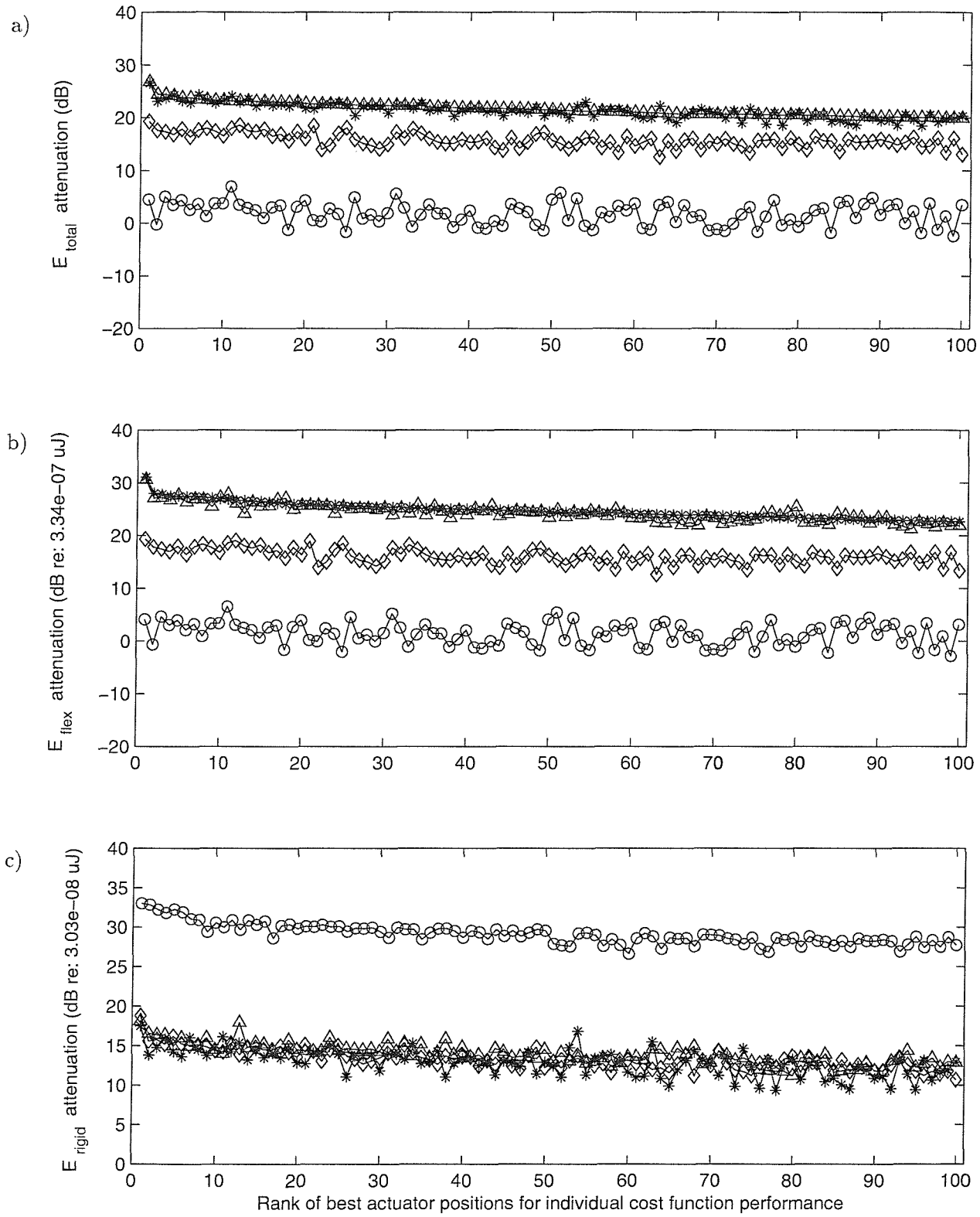

Figure 5.19: Attenuation achieved in a) E_{total}, b) E_{flex} and c) E_{rigid} for all two-actuator positions using each cost function. The actuator positions are ranked in order of decreasing attenuation for for each cost function: E_{total}: $\triangle$, E_{flex}: $*$, J_{trans}: $\circ$, J_{all}: $\diamond$.

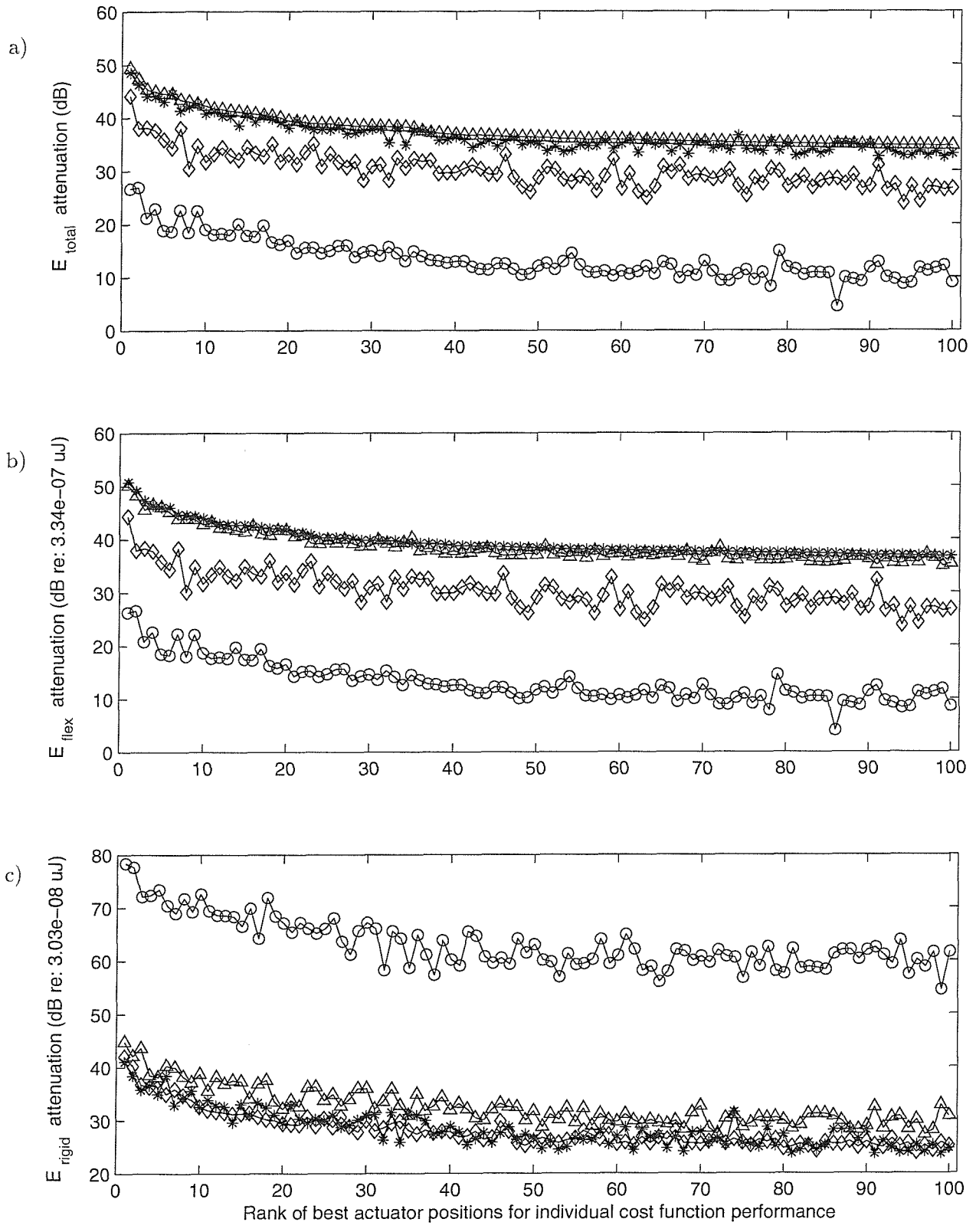

Figure 5.20: Attenuation achieved in a) E_{total}, b) E_{flex} and c) E_{rigid} for all three–actuator positions using each cost function. The actuator positions are ranked in order of decreasing attenuation for for each cost function: E_{total}: $\triangle$, E_{flex}: $*$, J_{trans}: $\circ$, J_{all}: $\diamond$.

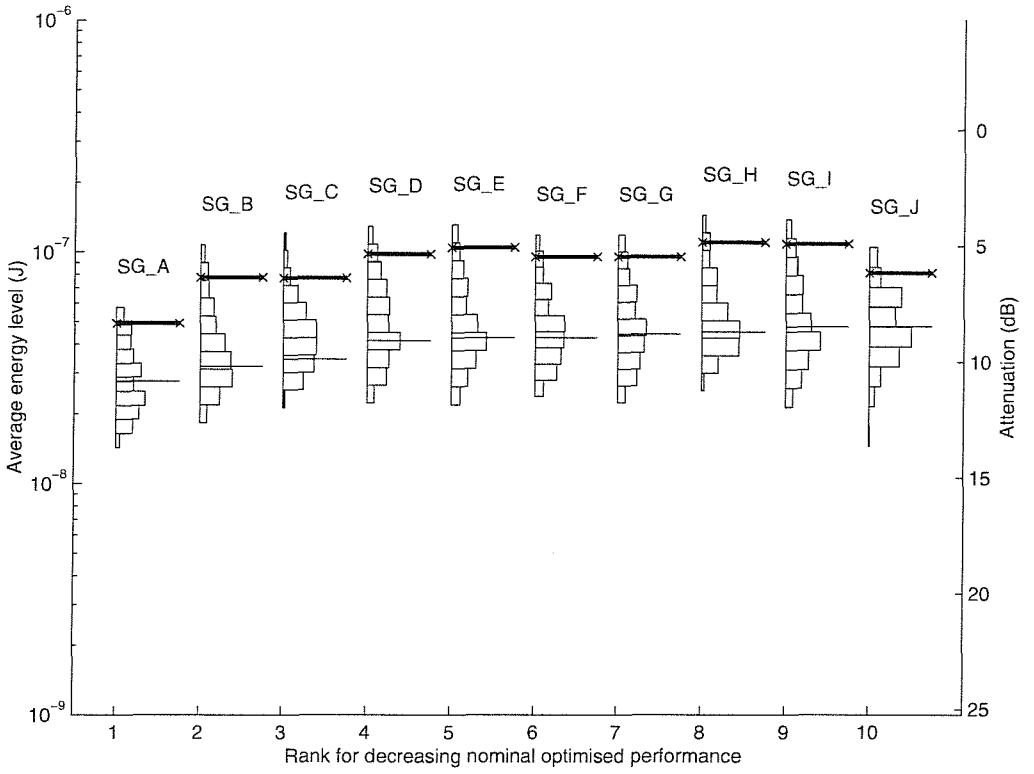

Figure 5.21: Statistical distribution and 95% probability limits (bold lines) for AVC performance, for frequency band 150Hz to 250Hz, of the ten best ranked single–actuator positions. Values of nominal performance are shown by thin lines.

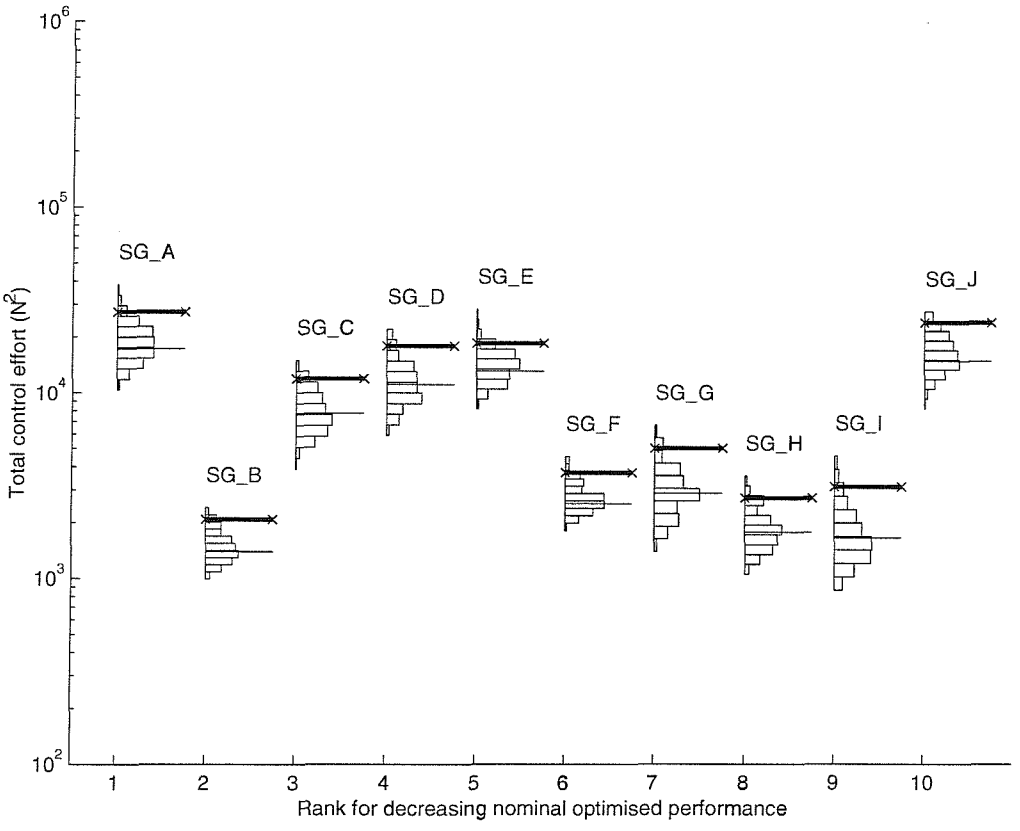

Figure 5.22: Statistical distribution and 95% probability limits (bold lines) for AVC total control effort, for frequency band 150Hz to 250Hz, of the ten best ranked single–actuator positions. Values of nominal control effort are shown by thin lines.

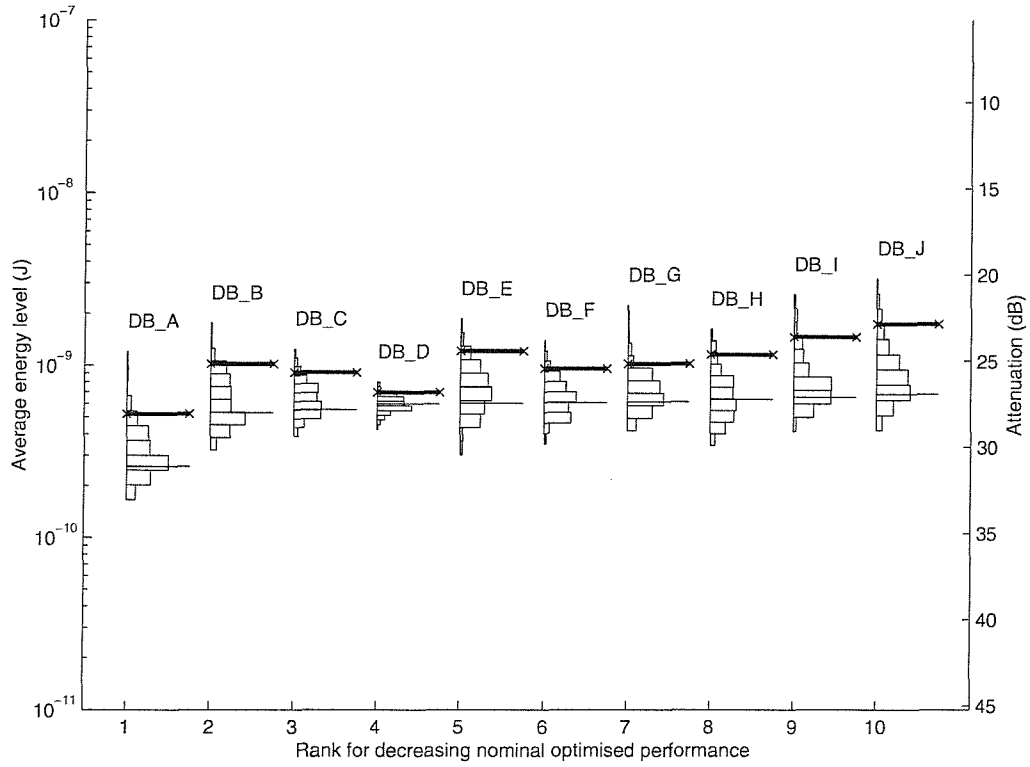

Figure 5.23: Statistical distribution and 95% probability limits (bold lines) for AVC performance, for frequency band 150Hz to 250Hz, of the ten best ranked two-actuator positions. Values of nominal performance are shown by thin lines.

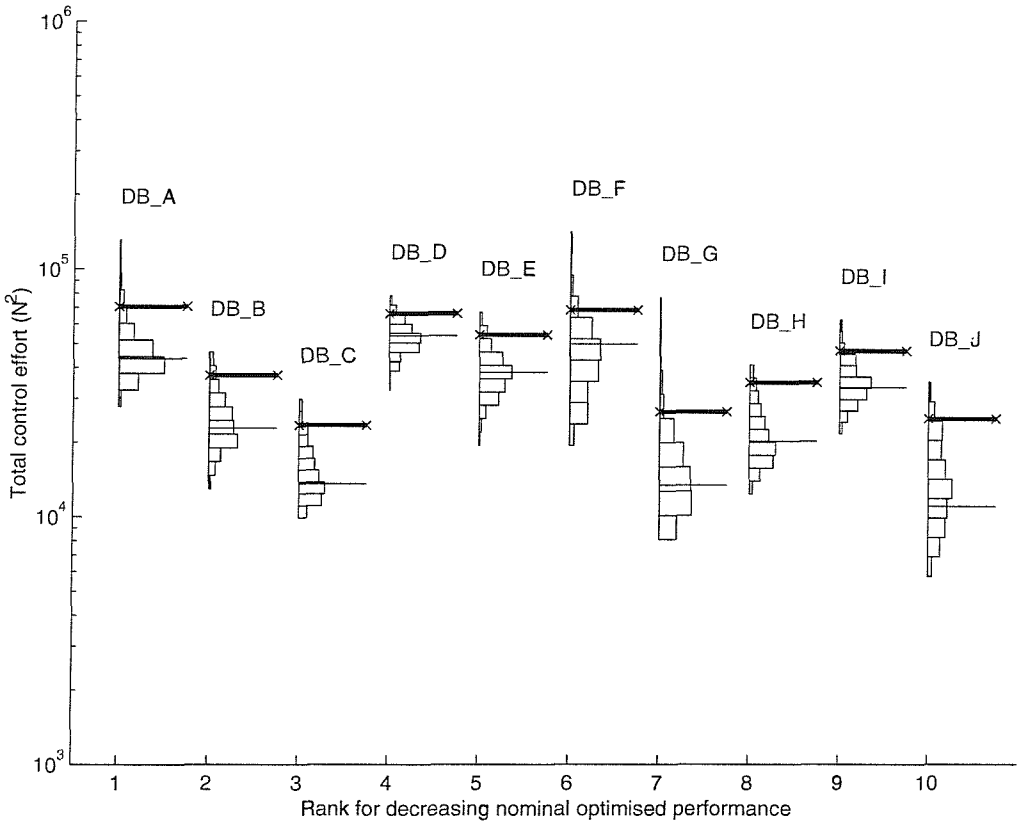

Figure 5.24: Statistical distribution and 95% probability limits (bold lines) for AVC total control effort, for frequency band 150Hz to 250Hz, of the ten best ranked two-actuator positions. Values of nominal control effort are shown by thin lines.

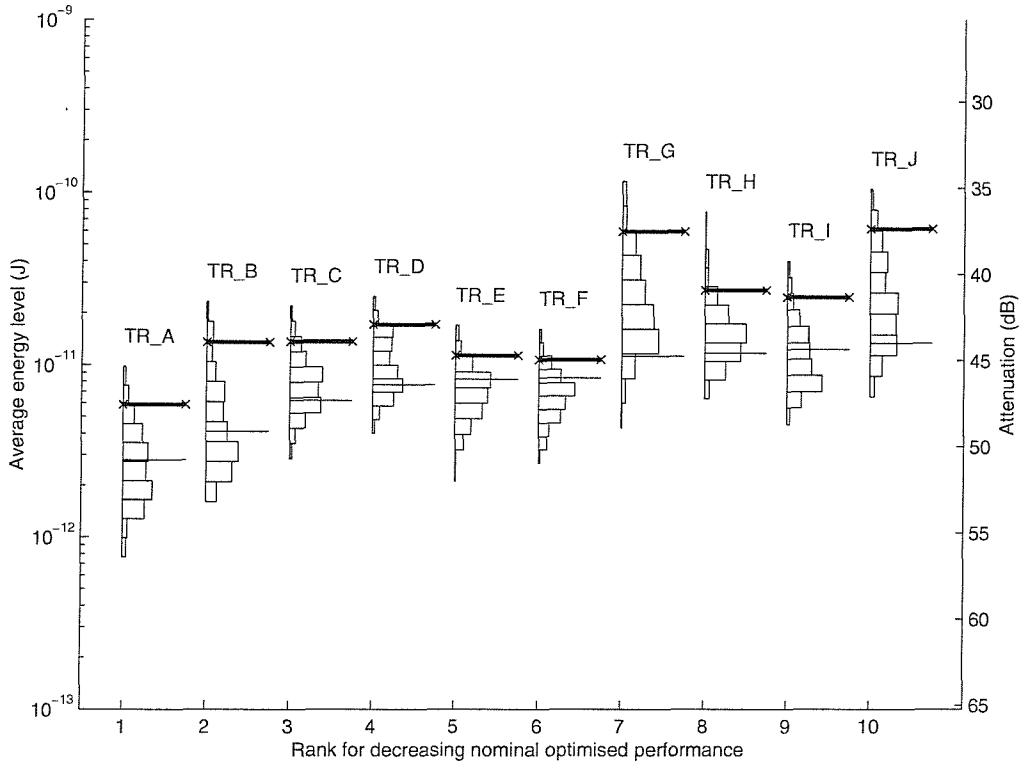

Figure 5.25: Statistical distribution and 95% probability limits (bold lines) for AVC performance, for frequency band 150Hz to 250Hz, of the ten best ranked three–actuator positions. Values of nominal performance are shown by thin lines.

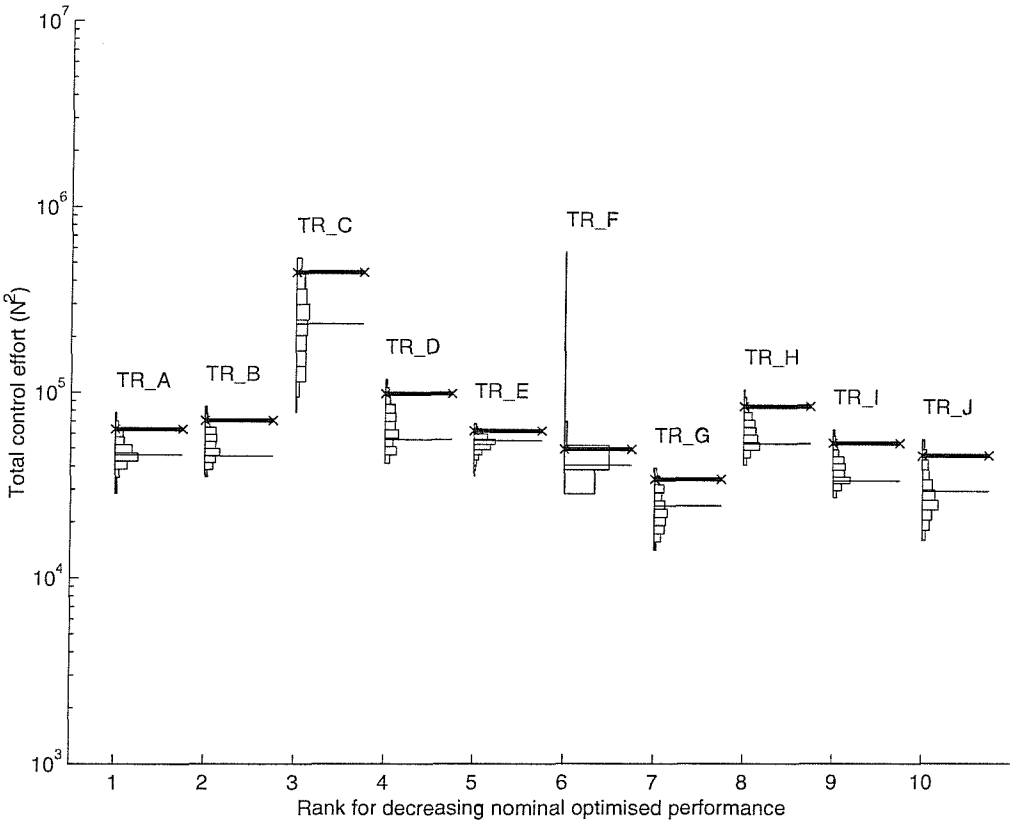

Figure 5.26: Statistical distribution and 95% probability limits (bold lines) for AVC total control effort, for frequency band 150Hz to 250Hz, of the ten best ranked three–actuator positions. Values of nominal control effort are shown by thin lines.

CHAPTER 6

Combined Passive and Active Optimisation Methods and a Comparison of Optimisation Strategies

6.0 INTRODUCTION

The previous two chapters have dealt with the reduction of the vibration transmission of the two-dimensional structure which is the subject of the study in this thesis, using passive and active optimisation methods; by optimising the geometry of the structure and also by finding the optimal actuator positions for AVC on the regular unoptimised structure. Both methods have been successful to varying degrees. A sensible progression is then to combine both these methods, to generate structures which have optimised geometries and use Active Vibration Control (AVC) with optimal actuator positions. The first method used is to find optimal actuator position on the structures whose geometries have been previously optimised using passive optimisation (in Chapter 4), the second to optimise both the geometry and actuator positions simultaneously. The first method, termed the *passive-then-active* method is identical to the active-only optimisation performed in Chapter 5, except geometrically optimised structures are used in place of the regular structure. The second method, termed *combined optimisation*, is similar to the passive optimisation, being a highly combinatorial problem and is solved using genetic algorithms. More than one variation of this strategy is presented. As before, the robustness of the optimised structures is studied, so that the best candidate in terms of practical application can also be made.

Having presented optimisation results using four different strategies, both here and in the previous two chapters, a comparison between all of these methods is performed, and the success and consequences of using each method are assessed. This in done for both nominal and perturbed performance.

Throughout this chapter reference is made to the design exploration system used for the majority of the optimisation work presented in this thesis. For brevity this will again be referred to in this chapter by its proprietary name: OPTIONS. See Chapter 3 for further details.

This chapter is structured as follows: Section 6.1 presents the optimised structures resulting from using the passive-then-active optimisation strategy and Section 6.2 presents those

achieved using the combined optimisation methods. Section 6.3 presents a power analysis, to gain an insight into the mechanisms by which the structures achieve better performance, including the role that the AVC system plays. Robustness analyses of all the optimised structures are presented in Section 6.4. Comparisons of the success of, and consequences of using, each optimisation strategy used in this and the preceding two chapters are made in Section 6.5. Conclusions are presented in Section 6.6.

6.1 PASSIVE-THEN-ACTIVE OPTIMISATION

Ten passively optimised structure geometries were found on the basis of their average performance over the frequency band 150Hz to 250Hz, as described in Chapter 4. AVC actuators were then added to these structures to achieve further reductions in vibration transmission. The remaining task is, therefore, to find the optimum actuator positions for each of the ten geometrically optimised structures to realise the maximum vibration reduction.

6.1.1 GENERATION OF OPTIMAL ACTUATOR POSITIONS

The actuator positions were found using an exhaustive search in exactly the same way as the optimal actuator positions on the traditional structure design, as detailed in Chapter 5. The only difference here is that irregular structure geometries are used. To calculate the effect of AVC the structure plant model matrices **C** and **Y** (see Section 2.3) were calculated for each structure geometry-actuator combination considered in the optimisation process. Optimal actuator positions were found for the application of active control using one, two and three actuators. As before, the number of potential actuator positions is not a prohibitively large number, and an exhaustive search is employed. Therefore the optimal actuator positions are guaranteed to be found in each case. The active-then-passive counterpart is not investigated, as this has less practical application - to optimise a structure around fixed actuator positions.

6.1.2 OPTIMISATION RESULTS

The optimum actuator positions on the structures which have previously been geometrically optimised are shown in Figures 6.1, 6.2 and 6.3 using one, two and three actuators respectively for each of the structures. The structures are shown ranked in order of net overall performance, with structure label suffices _A to _J which correspond to the optimised structure geometries presented in Chapter 4 as B_A to B_J. With one actuator it is seen that the actuator positions are all within the first six leftmost structure bays, with two actuators nine optimal actuator-pairs occur in the first four leftmost bays (the other in the fifth bay), and with three actuators six sets of optimal actuator positions occur in the first three leftmost bays (with the

remainder in the fourth bay). Thus the larger the number of actuators used, the more the optimal actuators positions occur in the structure bays near the base of the structure. This is a similar finding the that of the optimal actuator positions on the regular structure in Chapter 5. The optimal actuator positions for each structure are also given in Table 6.12. Further comparison with other optimisation strategies is left until later on in the chapter.

The best performance using one actuator yields a value of attenuation of 46.0dB, for two actuators this value is 67.8dB and for three actuators 96.1dB. Here the attenuation achieved by each structure is split into its two component parts; the attenuation due to the structure geometry alone and the additional attenuation due to the AVC system. The values of attenuation achieved for using three actuators were in the region of the practical limit achievable a realistic noise floor (55dB to 60dB) and would not be realised in practice. Therefore only the one and two-actuator systems, shown in Figures 6.1 and 6.2, are considered further and the performance and total control effort are summarised in Tables 6.1 and 6.3. The contributions of the geometric optimisation to the vibration attenuation are common for structures with the same label suffix, which is in the range 34.5dB to 31.0dB. The range of AVC attenuation contributions is 12.7dB to 5.9dB for one actuator and 34.1dB to 31.0dB for two actuators. These are similar to the range of values of AVC attenuation achieved with the unoptimised structure, discussed in Chapter 5. The major component of the attenuation is that due to the structure for one actuator, whilst the contributions of the geometric optimisation and the AVC system are of similar significance for two actuators.

The effective total control effort of the primary force is $21N^2$ as discussed in Chapter 4. The total control effort required for each of the structures is also given in Tables 6.1 and 6.3. For one actuator the smallest total control effort is about 13 times smaller than that for the primary force, the largest requirement is over 30 times larger. For two actuators the smallest total control effort is of a similar magnitude to that for the primary force, the largest is over 50 times larger.

6.2 COMBINED OPTIMISATION OF STRUCTURE GEOMETRY AND ACTUATOR POSITIONS

The second form of combined optimisation studied was that of combining the structure geometry and the actuator position at the same time. The ability to perform this type of optimisation problem is one which sets genetic algorithms (or in general, evolutionary algorithms) apart from classical methods. The highly combinatorial nature of this problem has already been discussed Chapter 4, however the addition of optimising the actuator positions

make the optimisation problem a discrete one. The overall optimisation procedure is referred to simply as *combined optimisation*.

To evaluate the average energy level of Beam 40 in practice, using the receptance analysis model for the structure, the net forces and velocities at the ends of Beam 40 were calculated separately due to the primary force and the forces at each end of the actuators. The individual force and velocity contributions from all the force inputs were then summed for each degree of freedom of Beam 40 (as the system is linear). Then using the net values of the force and velocity for each degree of freedom the net power dissipation in Beam 40 can be evaluated.

6.2.1. CHROMOSOME REPRESENTATION FOR COMBINED OPTIMISATION

The use of the chromosome and its representation for the structure geometry has been discussed in Chapter 4. For the 18 joints allowed to move under optimisation, the joint position is represented as 36, 16-bit numbers, concatenated to form a 576-bit chromosome. The addition of the actuator positions to the optimisation therefore entails augmenting the chromosome to allow the representation of actuator positions. In OPTIONS it is possible to represent a discrete optimisation variable by detailing all the discrete values permitted. This is then represented in the chromosome by a binary string, whose length is sufficient to represent the total number of discrete levels. Thus for optimisations using one actuator, the 39 possible actuator positions could be represented as a 6-bit binary string. The total chromosome length would then be 582 bits, of which only 6 represent the actuator positions (equivalent to about 1% significance). It was not felt that this strategy was the best one to use because of the small significance of the actuators position representation in the chromosome, and that there would be a relatively small probability of the actuator position being affected by the crossover and mutation operators of the genetic algorithm. This would result in relatively little evolution of the actuator positions compared to the structure geometry. Therefore another representation was used, allowing the actuator position to have greater significance in the chromosomes. A 16-bit optimisation variable between zero and unity was used to represent the actuator positions. For one actuator this represented the 39 candidate actuator positions using a linear scaling, such that if the variable were assigned by a uniform random distribution, then each actuator position would have an equal probability of selection. For two and three actuator positions the optimisation variable was scaled similarly to form an index representing all possible actuator combinations (*i.e.*, 1 to 741 for two actuators and 1 to 9139 for three actuators). This number was used to code an actuator combination in a repeatable and deterministic fashion. Again, each combination has exactly the same probability of selection if the optimisation variable were assigned by a uniformly distributed random variable. In this way the proportion of the

chromosome representing the actuator positions is one-thirty seventh of the total length (36 joint coordinate position parts and one actuator part). Whilst this is greater than using discretely defined actuator positions as described above, the actuator position still has a relatively small significance compared with that of the geometry (of about 2.7% of the chromosomes length).

An additional chromosome construction was also used, so that any effect of the significance of the length representing the actuator position could be seen. For this chromosome, instead of using one optimisation variable, eight such variables were used and then combined to form a single index. This *extended* chromosome has a representation of the actuator positions which is about 18% of the chromosomes length. Each of the eight optimisation variables are between the limits zero and unity. They are combined by summing the variables and converting to a zero to one range using a modulo one operator. Thus, where each of the optimisation variables is represented by o_i, the final actuator combination index j is given,

$$j = \left(\sum_{i=1}^{8} o_i \right) (\mathrm{mod}\, 1). \tag{6.1}$$

Using this combination method j will be within the range 0 to 1 (non-inclusive) and will still be uniformly distributed if all the individual variables are so distributed.

In earlier work the author used a combination method that was a simple arithmetic average of the individual variables o_i was used,

$$j_{biased} = \frac{1}{8} \sum_{i=1}^{8} o_i \,. \tag{6.2}$$

If these are uniformly distributed then this leads to a distribution of the combination of variables which approaches a Gaussian or Normal distribution as the number of variables combined increases (by the Central Limit Theorem, Hoel 1984). Obviously this gives a biased representation for actuator positions occurring in the middle of the range of the index. For the one actuator case this biases towards actuator positions in the middle of the structure. The resulting structures are still presented below as they allow an observation to be made on the effect that this has on the optimisation.

6.2.2 OPTIMISATION RESULTS

The parameters used for the optimisation are the same as those used for the broad band optimisation detailed in Chapter 4. The genetic algorithm was comprised of 4500 objective function evaluations, arranged as 15 generations of population size 300. Other parameters

detailing the optimisation are given in Table D.6 in Appendix D. The only additional difference being the use of a longer chromosome to represent the joint positions of the structure and the actuator positions, as detailed above.

6.2.2.1 COMBINED OPTIMISATION USING STANDARD CHROMOSOME

The resulting structure geometries and optimal actuator positions for the best ranked of the ten candidate designs produced with one and two actuators and using the standard length chromosome are shown in Figures 6.4. and 6.5. Each candidate took about 160 and 220 hours to produce, for one and two actuators respectively, on hardware platform B detailed in Appendix E. The unoptimised value of performance is shown on the y-axis with a square, but the immediate improvement is due to the operation of AVC with the initial actuator position (which corresponds to j=0 in (6.1)). The performance and total control effort for all the candidates produced for each case are summarised in Tables 6.5 and 6.7 respectively. The contribution of the structure geometry is also given with no AVC operating. For the one-actuator case the contribution of the geometry to the attenuation ranges from 28.4dB to 17.5dB whilst the AVC attenuation range is 29.9dB to 20.6dB, so both components are of similar significance. For the two actuator case the geometric contribution range is 22.8 dB to 15.5 dB and the AVC attenuation range is 64.9dB to 52.3dB and the AVC attenuation is then the dominant component in the values of total attenuation achieved. Optimisation using a larger number of actuators was not considered as the values of attenuation achieved using two actuators are in the region of the limit of being realisable in practical AVC systems with a realistic noise floor. The positions of the actuators for all the candidates are given in Table 6.12. For one actuator, all the actuator positions occur in the three leftmost structure bays and Beam 4 is an actuator location for two of the candidates. For the two-actuator case, again, all the actuators positions occur in the three left most bays, however in this case there are two-actuator position pairs Beams 1,4 and Beams 1,5 which occur in three and four times respectively in the ten candidates. Thus a similar trend is seen as with the passive-then-active optimisation, that the higher the number of actuators the more they occur towards the structure base.

The total control effort required to achieve the stated performance for each structure is given in Tables 6.5 and 6.7. For one actuator, the smallest total control effort is smaller than the effective primary force total control effort ($21N^2$), and the structure with the largest value is CO1_I, the structure with the best performance, and this is over 10 times larger than the effective primary control effort. For two actuators, the range is from about three to over 80 times.

The significance of the representation of the actuator position in the geometry was a concern in the definition of the chromosome, as discussed above. To show the distribution of the actuator positions considered throughout the optimisation, various parameters representing the actuator positions at each evaluation of the genetic algorithm and the best position in each generation are shown in Figure 6.6 for structures CO1_I and CO2_G, the best ranked one and two actuator structures. The parameter SRC_IND is the source (actuator) position index which is used to determine the actuator positions and corresponds to j in (6.1). For the single actuator case the source position is simply a quantised version of this parameter, but a more complex relation exists for two actuators. In both cases it is seen that the initial diversity of the actuator position representation in the initial generations (each of 300 chromosomes evaluations) is lost in the later stages. Here a small number of actuator positions are heavily represented within each generation (as represented by the large number of evaluations using these positions), even though evaluations were still performed at other actuator positions. The index and actuator positions corresponding to the chromosome with the best performance in each generation are also shown. In the overall optimisation six different actuator positions occur in the best structure in each generation for one actuator, and only three different actuator positions occur for the two actuator case. The discrete change of actuator positions can, in effect, cause a discrete change in the objective function. By comparing the best actuator position in each generation history with the history of the objective function in Figures 6.4 and 6.5, it is seen that in most cases the improvement coincides with changes in the actuators positions.

6.2.2.2 COMBINED OPTIMISATION USING THE EXTENDED CHROMOSOME

Ten optimised candidates were produced using the extended chromosome as described in Section 6.2.1, in which the significance of the representation of the actuator position in the chromosome is greater. The optimised designs yielding the best performance using one and two actuators are shown in Figures 6.7 and 6.8. The performance and the total control effort required for all the optimised structures are given in Tables 6.9 and 6.11. Comparing these values with their counterparts for the standard chromosome, it is seen that in terms of the performance of the best structure in each case, that the use of the extended chromosome has not yielded structures with better performance, but similar levels of attenuation have been achieved. This is reflected in the values of the average performances. Comparing the average values of total control effort it is seen that for the one actuator case the average figure is $89.9N^2$ for the standard, and $110N^2$ for the extended chromosome. However for the two actuator case the discrepancy has increased to $610N^2$ and $1173N^2$, the use of the extended chromosome almost doubling the average value of total control effort required compared to the use of the standard chromosome, in this example. The contributions of the attenuation due to the geometry and that

due to the AVC system are also given in Tables 6.9 and 6.10, for both cases. The significance of the geometric attenuation and that achieved by the AVC system appears to be very similar to that for use of the standard chromosome. However, on average it appears that the AVC system appears to have a slightly less significant contribution when using the extended chromosome.

The effect of using the extended chromosome on the diversity of the actuator positions considered during the optimisation is shown in Figure 6.9. The interpretation of the figure was explained previously for Figure 6.6 above. Here it is seen that the use of the extended chromosome has maintained the diversity in the later generations of the optimisation dramatically and there appears to be little difference between the diversity of the actuator positions evaluated in the earlier generations and those in the later generations. However, there still appears to be relatively little change in the best actuator positions in each generation, as before with the standard chromosome. The optimal actuators positions for each candidate are given in Table 6.12. When compared with the results for the standard chromosome the increase in diversity is apparent. Actuator positions further from the structure base are also found in the ten structures, there is only one set of actuator positions which occurs for more than once in the ten structures for the one actuator case.

6.2.2.3 USE OF AN EXTENDED CHROMOSOME WITH BIASING FAVOURING MID-STRUCTURAL ACTUATOR POSITIONS

As detailed in section 6.2.1, the author initially used the extended chromosome with a method of combining the individual source indices to form a single source index, which was (unintentionally) biased, for one-actuator positions, in favour of actuator positions occurring in the middle of the structure. Ten optimised structure using a single actuator were produced using this method, and are briefly presented here.

The structure with the best combined performance is given in Figure 6.10, and the performance of all the ten optimised candidates and the total control effort required is given in Table 6.11. Comparing these two parameters with those for the single-actuator passive-then-active and combined optimised structures it is seen that the performance of the structures using the biased chromosome achieves values of attenuation that are comparable to the single-actuator optimised structures using the combined optimisation scheme, using both the standard and extended chromosomes. The total control effort is in general smaller, however, for the biased chromosome case than for all the other cases. The value of the average total control effort is almost half the value for the combined optimised structures using the standard chromosome (which is slightly smaller than for the extended chromosome). Compared to the effective

primary force total control effort the range of values of total control effort for the structures is about 1.5 to 4.5 times.

Figure 6.11 shows the convergence history of the genetic algorithm optimisation for the optimised structure shown in Figure 6.10. The format of the figure has been explained above for the combined optimisation scheme above for Figure 6.6. The biasing of actuator positions considered towards positions in the middle of the structure is apparent. No actuator positions occurring in the two leftmost structure bays (*i.e.*, beam numbers 1 to 8) or the two rightmost structure bays have been considered during optimisation.

The optimised structures produced using this optimisation scheme are not considered further in this thesis. It was not originally intended to bias actuator positions in this way. However from the results presented a few interesting comments can be made. Restricting the freedom of the optimisation, by providing a bias for the actuator positions, has still yielded optimisation designs which still have comparable performance to structures produced without such a bias. Thus if a practical constraint exists (so that mid-structural actuator positions are preferred), this has been shown not to be detrimental the to the performance of the resulting optimised structures. Also, in this case the total control effort (which is an accidental consequence of the optimisation: it is not considered by the optimisation) is actually smaller than for the non-biased cases, which is obviously a practical advantage.

6.3 ANALYSIS OF POWER FLOW IN OPTIMISED STRUCTURES

In order to gain an insight into the mechanisms by which the power dissipation reduction in Beam 40 has been achieved, and to understand the role of the AVC system in the structures resulting from the passive and active optimisation strategies, power in the optimised structures and the contribution of the AVC system was studied. Power analyses are only presented for the structures resulting from the passive-then-active optimisation strategy, and those from the combined optimisation strategy using the standard chromosome. An explanation of the power components used in the analysis of power in a structure using AVC was given in Chapter 5, and are applicable to the power analyses reported here.

The results for the power analysis of the structures resulting from the passive-then-active optimisation are given in Tables 6.2 and 6.4, for one and two actuators respectively. The power components are given with the AVC system operational, and non-operational, so that the contribution of the geometric optimisation and the AVC system can be determined. For these structures the geometries are the same as the optimised structures achieved by the passive optimisation for the broad band case in Chapter 4, and thus the geometric improvements due to

the geometries are the same. For one actuator it is seen that the AVC control has no effect on the input power, and only a slight increase is seen for two actuators. The main effect of the AVC in each case is to provide an additional redistribution of the structural power, which on average is 10.6dB and 31.6dB greater than that achieved by the structure alone, for one and two actuators respectively. Figures 6.12 and 6.13 show the power analysis results, and for the two actuator case the individual actuator power contributions for the actuators can now be seen. In general the actuator contributions are small compared with the other power components except for a few structures, for example PTA1_H and PTA2_J.

The results for the power analysis for the structures resulting from the combined optimisation using the standard chromosome are given in Tables 6.6 and 6.8, for one and two actuators respectively. Again, the power components are given with the AVC system operational, and non-operational, so that the contribution of the geometric redesign and the AVC system can be determined. In this case the structure geometries are those resulting from each individual optimisation. It is seen that the geometric improvement achieved, on average, is slightly less reduction in the input power than for the passive-then-active case. The one and two actuator cases have average reductions of 9.7dB and 10.0dB, compared to 10.7dB for the passive-then-active optimisation. There is a much greater discrepancy between the reductions achieved for the power distribution. Here the values are 14.4dB and 8.5dB for one and two actuators compared with 22.3dB for the passive-then-active case.

The structures achieved using the passive-then-active optimisation strategy, have undergone optimisation, first, solely concerning the geometry. Whereas using the combined strategy the optimisation effort is shared between the geometry and the actuator positions. Thus it is not surprising that the geometric improvements achieved from the combined optimisation are not as large as those in which the optimisation of the geometry was initially the sole aim. However the values of attenuation resulting from an AVC system using the optimally placed actuators resulting from the combined optimisation are greater than those achieved from the passive-then-active optimisation, by about 6dB and 16dB greater on average for one and two actuators respectively. Overall the values of total attenuation achieved are slightly greater than for those achieved from the passive-then-active optimisation. The power analysis results are also shown in Figures 6.14 and 6.15, for the optimised structures using one and two actuators, showing the individual actuator contributions. In general, for the one actuator case the power contributions are relatively very small, as with that for the passive-then-active structures, however for two actuators the individual actuator contributions are larger than for the passive-then-active structures.

The power distributions within the optimised structures PTA1_B and PTA2_C, resulting from the passive-then-active optimisation are shown in Figures 6.16 and 6.17, and also for structures CO1_I and CO2_G resulting from the combined optimisation, in Figures 6.18 and 6.19. The position of the actuator is denoted by a symbol which additionally indicates whether the actuator is absorbing or sourcing power, as explained in the figure captions. The geometric optimisation has achieved a small reduction in power transmission along the structure, to which the use of AVC reduces the transmission even further. For structure PTA2_C (Figure 6.17) the actuator in Beam 1 is seen to increase the power dissipation in this beam. With reference to Figure 6.13 it is seen that this actuator is acting as an energy absorber, the other actuator is acting as an energy source (although its value is not clearly visible in the figure). As well as achieving a reduction of the power dissipated in Beam 40 the input power is slightly decreased.

For both optimisation cases using one actuator power reductions due to the AVC are seen at the far end of the structure but these occur a number of structure bays past the final actuator (actuator nearest Beam 40). The success with one actuator is greater for the combined optimisation. For two actuators a marked reduction in the power transmission past the final actuator is seen to occur from the bay containing the final actuator, and the reduction is greater, again, for the combined optimisation. This is similar to the effect seen in Chapter 5 for the operation of the AVC in the active-only optimised structures, but the amount of power reduction using two actuators is greatest for the combined optimisation (comparing Figures 6.17 and 6.19 with Figure 5.10). Although this effect is not as immediate as for active-only optimisation using three actuators (see Figure 5.11). This suggests that there is an advantage in optimising the structure geometry simultaneously with the actuator positions. The interaction between the two effects in the optimisation process allows AVC with a given number of actuators to have a much greater effect. The apparent strategy adopted by the optimised structures shown here is also the same for those for the active-only optimised structures; a strategy of reducing the power transmission along the structure past the final actuator. This effect is especially apparent for structure CO2_G in Figure 6.19. As discussed in Chapter 5, this implies that the performance of the system is less sensitive to the impedance of the structure and, and thus less sensitive to changes to the mass of Beam 40.

6.4 COMPARISON OF ROBUSTNESS OF OPTIMISED DESIGNS

The robustness of all the structures produced under combined optimisation schemes presented in this chapter was analysed (with the exception of the use of the biased extended chromosome). This was achieved in the same way as for the perturbation analyses presented in

Chapters 4 and 5. Full details are given in Chapter 4. As discussed above, linear superposition is used to calculate the net average energy level in the face of each applied perturbation. A perturbation scaling of 0.01 was used, defining a perturbation range of ±10mm, and the same set of 300 random perturbations were used as before. The results of the perturbation analyses are shown, in terms of both performance and total control effort, in: Figures 6.20 to 6.23 for the structures produced under the passive-then-active optimisation scheme; Figures 6.24 to 6.27 for the structures produced under the combined optimisation using the standard chromosome; and Figures 6.28 to 6.31 for the structures produced under the combined optimisation scheme using the extended chromosome. The 95% probability limits are also shown on all the graphs, which indicate the values for which 95% of the evaluated perturbations, the performance is better or the total control effort smaller. Robustness has been discussed in Chapter 4, and also the 95% probability limit has been defined in more detail in that chapter.

The results of the perturbation analyses are also summarised in Tables 6.1, 6.3, 6.5, 6.7, 6.9 and 6.10. First, considering the robustness of the performance for the optimised structures using one actuator, it is seen that, in general, the average robustness is the same for all the methods: passive-then-active and combined optimisation with the standard and extended chromosome. The ranges are confined to a range of about one order of magnitude. Whilst the best optimised one actuator structure is CO1_I, the one with the smallest 95% probability limit and the best practical performance is seen to be CEX1_B. For optimised actuator positions with two actuators, the general spread of values of performances is similar and is generally confined to two orders of magnitude. Structure CO2_D appears to be extremely unrobust in this respect, but using the 95% probability limit it is seen that, on average, the performance of this structure is expected to be better than for structures CO2_I and CO2_C. For two actuators, the performance for the combined optimised structures using the standard chromosome is the best, the best structure in all respects being CO2_G

As with the active optimised structures a large variation in control effect is seen for all structures. There appears to be no relation between the optimisation strategy and the control effort robustness as the range of values is from a little over one order of magnitude for the CO2 structures and about three orders of magnitude for the PTA1 and CEX2 structures. Again, it is emphasised that control effort is often perceived in linear terms and thus in practice these differences are significant. The best single-actuator structure on nominal performance CO1_I has a relatively high control effort requirement, although CEX1_B the most practical single-actuator structure has a control effort requirement that is almost two orders of magnitude

smaller and more robust. Similarly for structure CO2_G the best two-actuator structure, the control effort is relatively small and robust.

6.5 COMPARISON OF OPTIMISED DESIGNS

Four optimisation strategies have been presented in this thesis: passive optimisation, in which the geometry of the structure is optimised: active optimisation, in which the optimal actuator positions for an Active Vibration Control system applied to the regular structure were sought; passive-then-active optimisation, in which the optimal actuator positions on the previously passively optimised structures were sought; and combined optimisation in which the structure geometry and the optimal actuator positions for an AVC system are optimised simultaneously. For the latter strategy, two versions of genetic algorithm chromosome were used, giving different significance between the geometry and the actuator positions in the optimisation. A comparison of the success of using all the techniques can now be presented.

6.5.1 NOMINAL PERFORMANCE

Figure 6.32 shows the representation of the attenuation of the all the optimised structures produced by each of the optimisation strategies, along with their respective values of total control effort. The values of attenuation for the passively optimised structures are shown on a separate axis as control effort is not applicable for this case. The average performance against average total control effort for each of the ten structure resulting from the different optimisation strategies is also shown in Figure 6.33.

The structures achieved using active optimisation using two actuators, produce similar levels of attenuation as the passively optimised structures. The structures achieved using optimisation strategies involving both passive and active optimisation, using one actuator, yield values of attenuation similar to structures optimised by active optimisation using three actuators. Thus the application of AVC for the former case is more effective. However, as well as using only one actuator in place of three, the structures achieved using both passive and active optimisation use much less control effort. The range from the smallest values for the latter to the largest for the active optimisation structure is over 100,000. The larger control effort is not due to the number of actuators, since for active-only optimisation using one, and two actuators the average total control effort is still a factor of 100 greater. This indicates that the application of AVC to a structure resulting from passive optimisation (whether combined with active optimisation, or passive optimisation first) is more efficient than that using the regular structure. There is little distinction between the passive-then-active or the combined

optimisation strategies regarding the control effort, but the latter is seen, in general to achieve about 5dB more attenuation. Making the same comparison for the structures with two actuators, there is more variation within the values of attenuation achieved with each strategy. Greater values of attenuation are achieved with the combined optimisation using the standard chromosome, than those using the extended chromosome and lastly the passive-then-active optimisation strategy.

The total attenuation achieved by each optimised structure is comprised of two components, the attenuation due to the geometric redesign and that due to the application of AVC. In Figures 6.34 and 6.35 these two components are shown separately. The first figure shows the geometric attenuation component. Obviously the passive-then-active structures have the same values of attenuation as geometrically they are the same structures. The geometric attenuation achieved by the other structures is smaller and ranges from about 10dB to 30dB. In general it is seen that the structures using two actuators appear to have a smaller level of geometric improvement than for those using one actuator. (The exception is that for using two actuators optimised using the extended chromosome whose values of attenuation almost cover the full 20dB range.) Figure 6.35 shows the contribution of the AVC system for each structure produced under all the optimisation strategies. The AVC contribution from the structures produced using the passive-then-active optimisation strategy achieved similar levels of attenuation per actuator as for the regular structure with optimal actuator positions (but with less total control effort as discussed above). For the structures produced under the combined optimisation strategies the level of attenuation achieved using one actuator is about 15dB more than with that using one optimally placed actuator on the regular structure. When the same comparison is made for the combined optimisation using two actuators it is seen that the levels of AVC attenuation are about 20dB more those attained on the regular structure with two optimally placed actuators. In both cases the combined optimisation strategy using the standard chromosome yields better levels of AVC attenuation, despite the fact that the actuator representation had a smaller significance in the chromosome. Finally, it is noted that some of the AVC attenuation contributions are greater than 60dB, however for an AVC system with a realistic noise floor levels of attenuation are unlikely to be realised.

6.5.2 POWER WITHIN OPTIMISED STRUCTURES AND THE ROLES OF GEOMETRIC REDESIGN AND ACTIVE VIBRATION CONTROL

An analysis of the power within the optimised structures to understand the mechanisms by which the reductions in the power dissipated in Beam 40 are achieved, has been reported for those resulting from the main optimisation strategies. There are three main power components to consider; the input power to the structure, the redistribution of the power dissipation within

the structure and the power contributions of the AVC actuators (if applicable). The power contributions of the actuators is distinct from the total control effort which represents the relative electrical power requirements of a practical system.

The structures achieved by solely optimising the geometry of the structure were seen (in Table 4.6) to achieve a reduction in power dissipation in Beam 40 by both the reduction of the input power and the redistribution of the power within the structure. The latter is the greater effect, and in terms of reductions in decibels accounts, in general, for two-thirds of the reduction. Using the unoptimised structure with an AVC system using optimally placed actuator positions, only slight variations in the input power were seen, as shown in Tables 5.2, 5.4 and 5.6. In some cases the power input to the structure is increased. Thus the reductions in the power dissipation in Beam 40 are wholly achieved by the redistribution of the power dissipation within the structure due to the AVC. In almost all of the cases for optimal actuator positions using one, two and three actuators, at least one of the actuators acts as an energy source to the structure. The magnitude of the power contributions from each is small compared to the power input. When using more than one actuator it is seen that the AVC system adopts a strategy of controlling the power distribution beyond the actuator nearest Beam 40, than rather just controlling the power dissipation in Beam 40 itself.

Power analyses were also performed for structures resulting from optimisation strategies involving both geometric and actuator position optimisation. First the passive-then-active structures, which use optimal actuator positions on previously optimised geometries (those resulting from the passive optimisation). It is seen that the AVC system does not affect the power input to the structure beyond those reductions achieved by the geometry optimisation. The AVC system provides further reduction to the redistribution of the structural power. It achieves similar improvements per actuator as for the active-only optimisation, however the addition of the geometric improvement results in better values of total attenuation. With structures resulting from the simultaneous optimisation of both geometry and actuator positions, similar results were obtained. Again, the AVC system does not play a role in reducing the power input to the structure, but provides further reduction to the structural power redistribution. In this case the reductions in input power are smaller than those using the passively optimised structures. However, the values of attenuation achieved per actuator are greater than those for the active-only or passive-then-active optimisation strategies. Overall, in terms of total attenuation, the combined optimisation structures achieve values of attenuation which are comparable to those with the other two strategies using AVC above, but when using one additional actuator. In all cases for optimisation strategies using geometric optimisation the

control effort required by the AVC system is significantly lower, making the application of AVC more efficient.

Analyses of the power distribution within the optimised structures revealed that for the active-only optimisation strategy using two actuators the role of the AVC appears to be to reduce the power transmission beyond the final actuator, Figure 5.11, whereas using one actuator the role of the AVC appears to rely on the reflection of the vibration from the structure end, see Figure 5.9. Reductions in power transmission are also apparent to a lesser extent for the passive-then-active and combined optimisation strategies. This strategy is thought to make the reductions in Beam 40 less sensitive to any impedance changes at the end of the structure which may result from masses being added to Beam 40, for example. Thus the application of AVC is seen to be more efficient, and in some cases more successful, when some form of geometric optimisation has been performed on the structure. This reduces the power input to the structure, which is not achieved using AVC, and also provides a further redistribution of structural power dissipation. This is readily apparent from comparing the power analyses in Figure 4.20 for the passive optimisation, Figures 5.6 to 5.8 for the active-only optimisation and Figures 6.12 to 6.15 for methods using both passive and active optimisation. Noting the reduced scale where applicable, and that this also applies to the individual actuator contributions. This is also reflected in the total control effort required for structures resulting from each optimisation strategy, as discussed earlier in this section.

Finally, a summary of the average values of attenuation achieved by the passive-only, active-only, passive-then-active and combined optimisation (using standard chromosome) strategies is given in Table 6.13, where two actuators are used for AVC in each case, where applicable. Also given are the average values of attenuation resulting from the geometric redesign and from AVC. This emphasises that the application of AVC is more effective using combined optimisation. The average AVC attenuation achieved resulting from this strategy is approximately double the level achieved for the active-only and passive-then-active. The combined optimisation strategy has resulted in the highest average overall vibration reduction, despite that the geometric redesign has only responsible for half of the attenuation achieved with the passive-only and passive-then-active strategies.

6.5.3 PERTURBED PERFORMANCE AND ROBUSTNESS

The 95% probability limits for the performance and the total control effort are shown in Figures 6.35 to 6.38 as vectors emanating from the symbols representing the nominal values. The westward extent thus indicates the 95% performance probability limit, and indirectly provides an indication of the robustness. Similarly the northward extent represents the total

control effort 95% probability limit. The comparison is made using four figures one for each optimisation strategy, so that the vectors for each can be clearly seen. In general it is seen that the robustness of many of the structures are very much comparable, although a few of the two-actuator structures achieved by using the combined optimisation with the standard chromosome exhibit less robustness. In general the robustness of the passively optimised structures is the best, followed by those achieved using the active-only optimisation.

All the optimisation processes detailed in this chapter and Chapters 4 and 5, have not considered robustness within the optimisation process. Hence the robustness of the performance of the resulting design solutions is a consequence of the optimisation process. In the next chapter, optimisation incorporating a measure of robustness is performed. Thus the optimisation aim is to provide *optimal and robust* design solutions.

6.6 CONCLUSIONS

6.6.1 COMBINED PASSIVE AND ACTIVE OPTIMISATION METHODS

The optimisation of the average vibration transmission of a two-dimensional lightweight regular structure was performed over a frequency band of 150Hz to 250Hz. This is measured by evaluating the average energy level in the end beam, Beam 40. Here both passive and active optimisation strategies were used, whereas in the two previous chapters each of these have been used alone. Thus both the structure geometry and the optimal positions of actuators for an Active Vibration Control (AVC) were the subject of optimisation. The first strategy, passive-then-active optimisation, used structure geometries that were the result of passive-only optimisations from Chapter 4. Optimal actuator positions were found for these structures for one to three actuators, although the use of three actuators was not pursued as the attenuation from the AVC system would not be achievable in a practical system. The second strategy, combined optimisation, optimised the structure geometry and optimal actuator positions (for one and two actuators) simultaneously. Different types of genetic algorithm chromosome were used giving different levels of significance between the geometry and the actuator positions. However it was found that the chromosome which had an extended actuator position representation produced solutions with slightly worse performance and required more control effort. This suggests that it is better to adapt the geometry around actuator positions than vice versa. The passive-then-active optimisation strategy was slightly more successful for one actuator, although larger control system efforts were required, and for two actuators the combined optimisation was more successful, but again, larger control effort were required. A

comparison of the performance compared with other optimisation strategies used is discussed below.

Also briefly reported was the use of the combined optimisation with a chromosome which was (unintentionally) biased towards single actuator positions occurring in the middle of the structure. Despite this, the resulting structures had comparable performances to those above, with low control effort. Hence the actuator position bias has not been detrimental to the success of the optimisation.

A power analysis was performed to investigate the mechanisms by which the reductions in vibration transmission of the structures have been achieved. This is distinct from the total control effort, which represents a practical system requirement. It was found that the geometric optimisation reduces the power input to the structure, and also redistributes the power dissipation within the structure so as to reduce the vibration in Beam 40. The AVC has little effect on the input power to the structure, but it provides additional power redistribution within the structure to further decrease the power dissipation in Beam 40. In most of the cases the net power supplied by the actuators is much less than the input power to the structure, and in most cases at least one actuator acts as an energy source. Thus the role of the AVC is not to simply absorb power. Studies of the distribution of power within the structure show that for one actuator the aim appears to be to reduce the power dissipation in Beam 40. However, with two actuators the AVC seems to act to reduce the power transmission along the structure.

Perturbation analyses were performed for structures resulting from the passive-then-active optimisation and the combined optimisation (with both standard and extended chromosome) strategies, to see how the performance and the total control effort change in response to small geometric changes such as might occur through manufacturing tolerances, for example. Some structures appear to be more robust than others in terms of either, or both, performance robustness and control effort robustness. Using the average 95% probability limits, for which the performance or control effort is better for 95% of all perturbations applied, for each case, the average practical performance and practical control effort can be found. For one actuator there is little difference in performance between the three optimisation strategies, also the practical control effort for the passive-then-active is twice as large as for both the combined optimisation strategies. For two actuators the average practical performances are similar, but the combined optimisation strategy with the standard chromosome has the best average practical performance, but the average practical total control effort is eight times greater than for the strategy with the lowest.

Another consideration of the robust performance of the optimised structures might be due to AVC control systems failure. Because both optimisation strategies incorporate geometric optimisation, both have obvious advantages over the active-only optimisation strategy. The passive-then-active strategy has produced the better reductions in vibration transmission due to the geometric redesign, and thus is more robust to AVC system failure.

6.6.2 COMPARISON OF OPTIMISATION STRATEGIES

At this stage in the thesis four different optimisation strategies have been presented in this and the two preceding chapters. A comparison of the results obtained from all the strategies was presented in Section 6.5. In terms of nominal performance, the use of two optimally placed actuators on the regular, unoptimised structure is approximately equivalent to the values of attenuation achieved by the passive optimisation. When using optimally placed actuator positions on geometrically optimised structures the use of one actuator achieves similar levels of attenuation to that using three actuators on the regular, unoptimised structure. Also the total control effort required is much less, by about two orders of magnitude. In general the structures resulting from the combined optimisation produce better performance per actuator, than for the passive-then-active optimisation, especially so for two actuators (although similar levels of control effort are required as for one actuator).

The values of attenuation achieved were split into their two component parts; the attenuation achieved from the geometric optimisation, and that achieved by the AVC system. The former is found to be best with the structures resulting from the passive optimisation, where the structure geometry was the sole optimisation aim. These structure geometries are also used for the passive-then-active optimisation. For the combined optimisation it is found that for two actuators the geometric improvement was smaller than for one actuator. For the passive-then-active optimisation it is found that the levels of attenuation achieved per actuator by the AVC are similar to those achieved for active-only optimisation. However, for the combined optimisation it is seen that the attenuation achieved per actuator is comparable to that for the active-only optimisation when using one additional actuator.

All the optimised structures that are geometrically optimised have significant reductions in the power input to the structure and also show a favourable redistribution of power dissipation within the structure. The application of AVC does not significantly affect the power input, but does have the effect of providing an additional power redistribution within the structure. The net power input from the actuators is, in most cases, much smaller than the input power, and in most cases at least one of the actuators acts as an energy source. Thus the contribution of AVC is more than simply absorbing structural power. Studying the power distribution within the

optimised structures it is seen that the interaction between actuators, for actuator configurations with more than one actuator, act to reduce the power transmitted along the structure, and not just mainly the power in Beam 40. It is thought this makes the application of AVC much more robust to changing the mass of Beam 40.

Finally, considering the robustness of the performance and control effort of all the resulting structures, little distinguishes one optimisation strategy from another in this respect. Although within a set of structures achieved with each strategy there are structures that are more robust on grounds of either, or both, performance or control effort. Thus the robustness of the solutions is important is selecting *practical* optimal solutions. As before, the 95% probability limits enable the practical performance achieved or control effort required to be estimated.

Rank	Structure	Geometric attenuation (dB)	AVC attenuation (dB)	Overall nominal attenuation (dB)	95% probability limit attenuation (dB)	Control effort (N^2)	95% probability limit control effort (N^2)
1	PTA1_B	33.3	12.7	46.0	43.0	291	467
2	PTA1_G	32.0	12.6	44.6	41.6	12.8	23.9
3	PTA1_J	32.3	12.2	44.5	41.5	22.8	30.3
4	PTA1_D	31.6	12.6	44.2	42.6	52.5	84.5
5	PTA1_H	33.9	10.1	44.0	39.6	1.52	2.46
6	PTA1_A	32.3	11.5	43.8	39.1	12.8	31.9
7	PTA1_C	32.8	10.3	43.1	38.2	345	956
8	PTA1_I	31.0	11.9	42.9	39.3	770	1850
9	PTA1_F	34.1	8.3	42.4	37.3	14.7	36.9
10	PTA1_E	34.5	5.9	40.4	38.4	24.0	46.1
average		32.6	11.2	43.2[1]	39.7	155	353

TABLE 6.1. Results summary for single-actuator passive-then-active optimised structures, ranked in order of performance.

Structure	Primary force input power reduction, α_{INPUT} (dB)		Redistribution of power within passive beams of structure, α'_{REDIST} (dB)		Net actuator contribution α_{ACF} (dB)	Net power dissipated in actuators ($x10^{-7}$ W)
	w/o AVC	AVC	w/o AVC	AVC		
PTA1_B	10.7	10.9	22.7	35.0	0.08	5.68
PTA1_G	11.6	11.8	20.4	32.8	0.003	0.169
PTA1_J	9.9	9.8	22.4	34.8	-0.02	-1.63
PTA1_D	10.0	9.6	21.6	34.1	0.4	35.8
PTA1_H	11.0	11.1	22.9	29.1	3.8	168
PTA1_A	11.6	11.6	20.7	32.1	0.006	0.350
PTA1_C	9.0	9.0	23.8	34.1	-0.02	-1.86
PTA1_I	10.1	10.0	20.8	32.6	0.4	28.5
PTA1_F	11.1	11.1	23.0	31.3	-0.03	-2.17
PTA1_E	11.0	11.0	23.4	29.4	-0.01	-0.966
average	10.7	10.7	22.3	32.9	-	-

TABLE 6.2. Power components for single-actuator passive-then-active optimised structures.

[1] See footnote on page 191.

Rank	Structure	Geometric attenuation (dB)	AVC attenuation (dB)	Overall nominal attenuation (dB)	95% probability limit attenuation (dB)	Control effort (N^2)	95% probability limit control effort (N^2)
1	PTA2_C	32.8	35.0	67.8	64.4	223	387
2	PTA2_A	32.3	34.7	67.0	60.2	108	387
3	PTA2_F	34.1	32.2	66.3	62.0	262	552
4	PTA2_B	33.3	32.4	65.7	62.7	25.6	32.9
5	PTA2_G	32.0	33.5	65.5	59.9	83.5	310
6	PTA2_D	31.6	31.8	63.4	58.0	79.6	119
7	PTA2_E	34.5	28.8	63.3	60.1	88.1	178
8	PTA2_H	33.9	29.0	62.9	58.3	44.5	63.7
9	PTA2_I	31.0	29.7	60.7	54.6	1060	1920
10	PTA2_J	32.3	28.3	60.6	56.7	37.3	106
average		32.6	32.2	63.6[1]	58.8	201	406

TABLE 6.3. Results summary for two-actuator passive-then-active optimised structures, ranked in order of performance.

Structure	Primary force input power reduction, α_{INPUT} (dB)		Redistribution of power within passive beams of structure, α'_{REDIST} (dB)		Net actuator contribution α_{ACF} (dB)	Net power dissipated in actuators ($x10^{-7}$ W)
	w/o AVC	AVC	w/o AVC	AVC		
PTA2_C	9.0	9.0	23.8	55.5	3.2	2.41
PTA2_A	11.6	11.4	20.7	57.7	-2.0	-1.59
PTA2_F	11.1	10.5	23.0	55.5	0.4	0.268
PTA2_B	10.7	11.2	22.7	51.3	3.2	1.44
PTA2_G	11.6	11.3	20.4	52.1	2.1	1.05
PTA2_D	10.0	10.0	21.6	53.4	-0.02	-0.0196
PTA2_E	11.0	11.0	23.4	52.4	-0.2	-0.106
PTA2_H	11.0	11.1	22.9	51.7	0.05	0.0348
PTA2_I	10.1	9.2	20.8	50.6	0.9	0.807
PTA2_J	9.9	9.8	22.4	53.3	-2.5	-2.92
average	10.7	10.5	22.3	53.9	-	-

TABLE 6.4. Power components for two-actuator passive-then-active optimised structures.

[1] See footnote on page 191.

Rank	Structure	Geometric attenuation (dB)	AVC attenuation (dB)	Overall nominal attenuation (dB)	95% probability limit attenuation (dB)	Control effort (N^2)	95% probability limit control effort (N^2)
1	CO1_I	23.0	28.0	51.0	44.2	306	572
2	CO1_E	25.3	25.3	50.6	48.1	144	340
3	CO1_C	28.4	22.2	50.6	47.3	9.18	15.0
4	CO1_B	20.4	29.0	49.4	47.0	34.4	39.7
5	CO1_A	19.7	29.6	49.3	45.0	152	378
6	CO1_J	25.4	23.1	48.5	41.0	56.7	77.4
7	CO1_D	19.6	28.5	48.1	45.0	26.0	70.6
8	CO1_H	17.7	29.9	47.6	45.8	54.3	65.8
9	CO1_F	27.0	20.6	47.6	44.8	65.8	83.1
10	CO1_G	17.5	28.9	46.4	43.3	50.6	58.2
average		21.0	27.5	48.7[1]	44.7	89.9	170

TABLE 6.5. Results summary for single-actuator combined optimised structures using the standard chromosome, ranked in order of performance.

Structure	Primary force input power reduction, α_{INPUT} (dB)		Redistribution of power within passive beams of structure, α'_{REDIST} (dB)		Net actuator contribution α_{ACF} (dB)	Net power dissipated in actuators ($x10^{-7}$ W)
	w/o AVC	AVC	w/o AVC	AVC		
CO1_I	10.0	9.3	13.0	42.1	-0.4	-44.3
CO1_E	9.2	8.9	16.1	40.8	1.0	93.1
CO1_C	9.4	9.4	19.0	41.1	0.02	1.77
CO1_B	9.7	10.0	10.7	39.3	0.2	14.4
CO1_A	10.8	10.9	8.9	38.5	-0.07	-4.75
CO1_J	9.0	9.2	16.3	39.4	-0.05	-4.93
CO1_D	10.8	10.9	8.8	37.2	0.01	0.646
CO1_H	9.4	9.7	8.3	37.9	-0.02	-1.93
CO1_F	9.9	10.1	17.1	37.4	-0.002	-0.138
CO1_G	8.5	8.5	9.0	37.9	-0.006	-0.762
average	9.7	9.8	14.4	39.5	-	-

TABLE 6.6. Power components for single-actuator combined optimised structures using standard chromosome.

[1] See footnote on page 191.

Rank	Structure	Geometric attenuation (dB)	AVC attenuation (dB)	Overall nominal attenuation (dB)	95% probability limit attenuation (dB)	Control effort (N^2)	95% probability limit control effort (N^2)
1	CO2_G	22.8	61.2	84.0	80.5	149	210
2	CO2_D	19.8	62.4	82.2	73.2	286	380
3	CO2_E	17.8	60.2	78.0	75.4	271	333
4	CO2_B	12.4	64.9	77.3	73.8	460	590
5	CO2_H	19.0	57.6	76.6	72.4	57.4	91.0
6	CO2_A	15.3	60.0	75.3	71.9	1310	2050
7	CO2_I	15.6	58.1	73.7	67.8	255	454
8	CO2_C	16.0	57.6	73.6	68.5	1770	3320
9	CO2_J	17.0	56.5	73.5	71.6	1410	1860
10	CO2_F	19.9	52.3	72.2	68.6	133	184
average		16.7	60.3	78.4[1]	71.2	610	947

TABLE 6.7. Results summary for two-actuator combined optimised structures using the standard chromosome, ranked in order of performance.

Structure	Primary force input power reduction, α_{INPUT} (dB)		Redistribution of power within passive beams of structure, α'_{REDIST} (dB)		Net actuator contribution α_{ACF} (dB)	Net power dissipated in actuators ($x10^{-7}$ W)
	w/o AVC	AVC	w/o AVC	AVC		
CO2_G	11.0	11.8	11.8	74.2	-2.0	-1.37
CO2_D	8.9	8.9	10.9	75.3	-2.1	-2.92
CO2_E	10.1	10.8	7.7	68.9	-1.8	-1.56
CO2_B	10.2	12.0	2.2	67.0	-1.7	-1.10
CO2_H	9.7	10.1	9.2	66.9	-0.5	-0.405
CO2_A	9.7	9.7	5.7	65.0	0.5	0.460
CO2_I	10.2	10.0	5.4	65.9	-2.2	-2.46
CO2_C	8.2	7.8	7.9	67.9	-2.2	-3.88
CO2_J	11.2	10.6	5.8	65.0	-2.1	-1.97
CO2_F	9.7	10.4	10.2	63.7	-1.9	-1.85
average	10.0	10.4	8.5	69.9	-	-

TABLE 6.8. Power components for two-actuator combined optimised structures using standard chromosome.

[1] See footnote on page 191.

Rank	Structure	Geometric attenuation (dB)	AVC attenuation (dB)	Overall nominal attenuation (dB)	95% probability limit attenuation (dB)	Control effort (N^2)	95% probability limit control effort (N^2)
1	CEX1_B	31.5	18.8	50.3	46.8	6.83	10.3
2	CEX1_G	23.5	25.9	49.4	45.3	21.2	47.0
3	CEX1_I	25.8	23.2	49.0	46.8	53.2	70.5
4	CEX1_E	24.2	23.4	47.6	44.7	17.2	49.1
5	CEX1_J	26.2	20.9	47.1	43.0	140	375
6	CEX1_A	25.3	21.8	47.1	44.8	21.3	36.5
7	CEX1_F	22.4	24.4	46.8	43.5	10.9	35.4
8	CEX1_C	20.0	26.8	46.8	44.2	625	988
9	CEX1_H	22.2	24.2	46.4	43.6	137	169
10	CEX1_D	23.1	22.5	45.6	43.4	64.2	81.6
average		23.6	23.7	47.4[1]	44.4	110	186

TABLE 6.9. Results summary for single-actuator combined optimised structures using the extended chromosome, ranked in order of performance.

Rank	Structure	Geometric attenuation (dB)	AVC attenuation (dB)	Overall nominal attenuation (dB)	95% probability limit attenuation (dB)	Control effort (N^2)	95% probability limit control effort (N^2)
1	CEX2_B	18.9	54.4	73.3	69.8	1510	1650
2	CEX2_I	22.7	48.7	71.4	66.9	29.8	67.1
3	CEX2_D	10.6	59.9	70.5	65.0	6270	8820
4	CEX2_A	19.9	50.3	70.2	66.5	1610	2030
5	CEX2_H	17.2	53.0	70.2	63.4	791	5400
6	CEX2_C	26.7	42.5	69.2	63.8	27.8	35.7
7	CEX2_G	25.3	43.7	69.0	63.2	48.5	83.2
8	CEX2_F	17.9	51.1	69.0	67.3	1280	2450
9	CEX2_E	21.7	46.7	68.4	60.3	115	182
10	CEX2_J	16.1	51.4	67.5	62.0	43.5	82.8
average		17.3	53.0	69.6[1]	64.1	1173	2080

TABLE 6.10. Results summary for two-actuator combined optimised structures using the extended chromosome, ranked in order of performance.

[1] See footnote on page 191.

Rank	Structure	Geometric attenuation (dB)	AVC attenuation (dB)	Nominal attenuation (dB)	95% probability limit attenuation (dB)	Control effort (N^2)	95% probability limit control effort (N^2)
1	E_B	19.2	31.8	51.0	*(not*	35.7	*(not*
2	E_F	24.4	24.0	48.4	*evaluated)*	14.5	*evaluated)*
3	E_G	21.0	26.6	47.6		39.4	
4	E_H	18.3	28.9	47.2		55.2	
5	E_J	23.9	23.1	47.0		87.2	
6	E_C	28.6	17.6	46.2		31.3	
7	E_D	20.3	25.8	46.1		97.9	
8	E_I	20.2	25.3	45.5		13.4	
9	E_E	22.1	23.3	45.4		12.7	
10	E_A	25.0	19.4	44.4		65.9	
average		21.4	26.3	46.6[1]		45.3	

TABLE 6.11. Results summary for single-actuator combined optimised structures using the extended chromosome with bias for mid-structure positions, ranked in order of performance.

Rank	Passive-then-active		Combined		Combined extended chromosome		Combined extended chromosome (biased)
	PTA1_	PTA2_	CO1_	CO2_	CEX1_	CEX2_	E1_
1	12	2, 11	6	1, 9	13	1, 5	19
2	18	1, 4	4	1, 4	3	10, 11	21
3	9	4, 5	11	1, 4	15	4, 5	21
4	4	2, 10	7	1, 5	21	1, 5	14
5	2	2, 13	8	1, 2	12	2, 6	12
6	24	11, 14	4	4, 5	19	8, 12	15
7	24	8, 14	7	1, 5	14	1, 10	17
8	6	5, 17	14	1, 5	12	2, 4	14
9	18	6, 12	9	1, 5	6	11, 14	22
10	21	1, 10	10	1, 4	11	2, 3	13

TABLE 6.12. Summary of actuator positions for all the optimisation strategies considered in this chapter.

[1] See footnote on page 191.

Optimisation strategy	Average attenuation (dB)		
	Geometric	AVC	Total
Passive-only	32.6	0	32.6
Active-only	0	27.7	27.2
Passive-then-active	32.6	32.2	63.3[1]
Combined (CO)	16.7	60.3	75.4[1]

TABLE 6.13. Summary of the average attenuation achieved by the geometric redesign and application of AVC with two actuators for the main optimisation strategies considered.

[1] As a consequence of the logarithmic scaling, the addition of the two average components of the nominal total attenuation does not result in the average total attenuation, as with the individual cases.

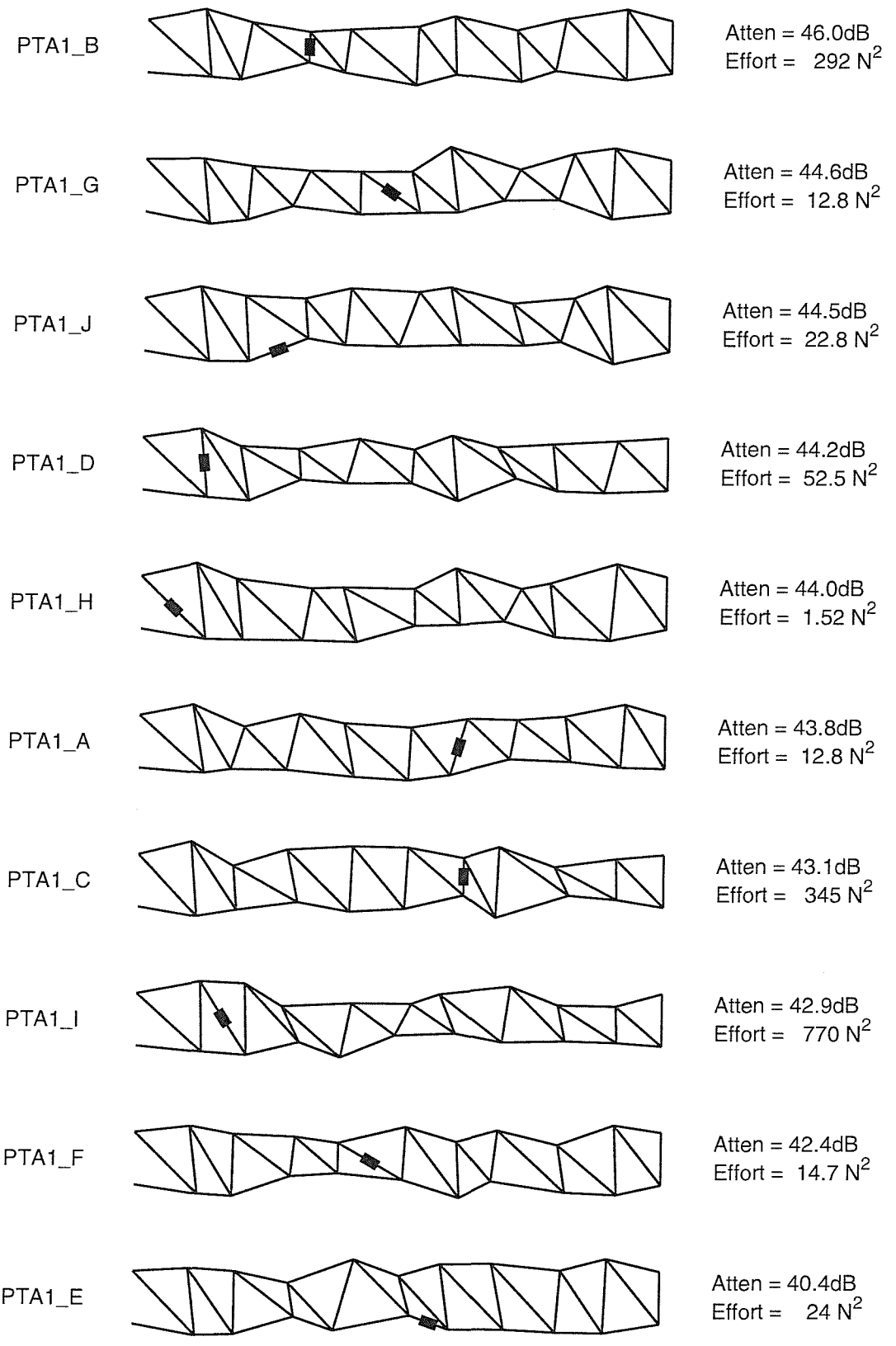

Figure 6.1: The ten best performance ranked single-actuator positions for the previously geometrically optimised structures, for the frequency band 150Hz to 250Hz.

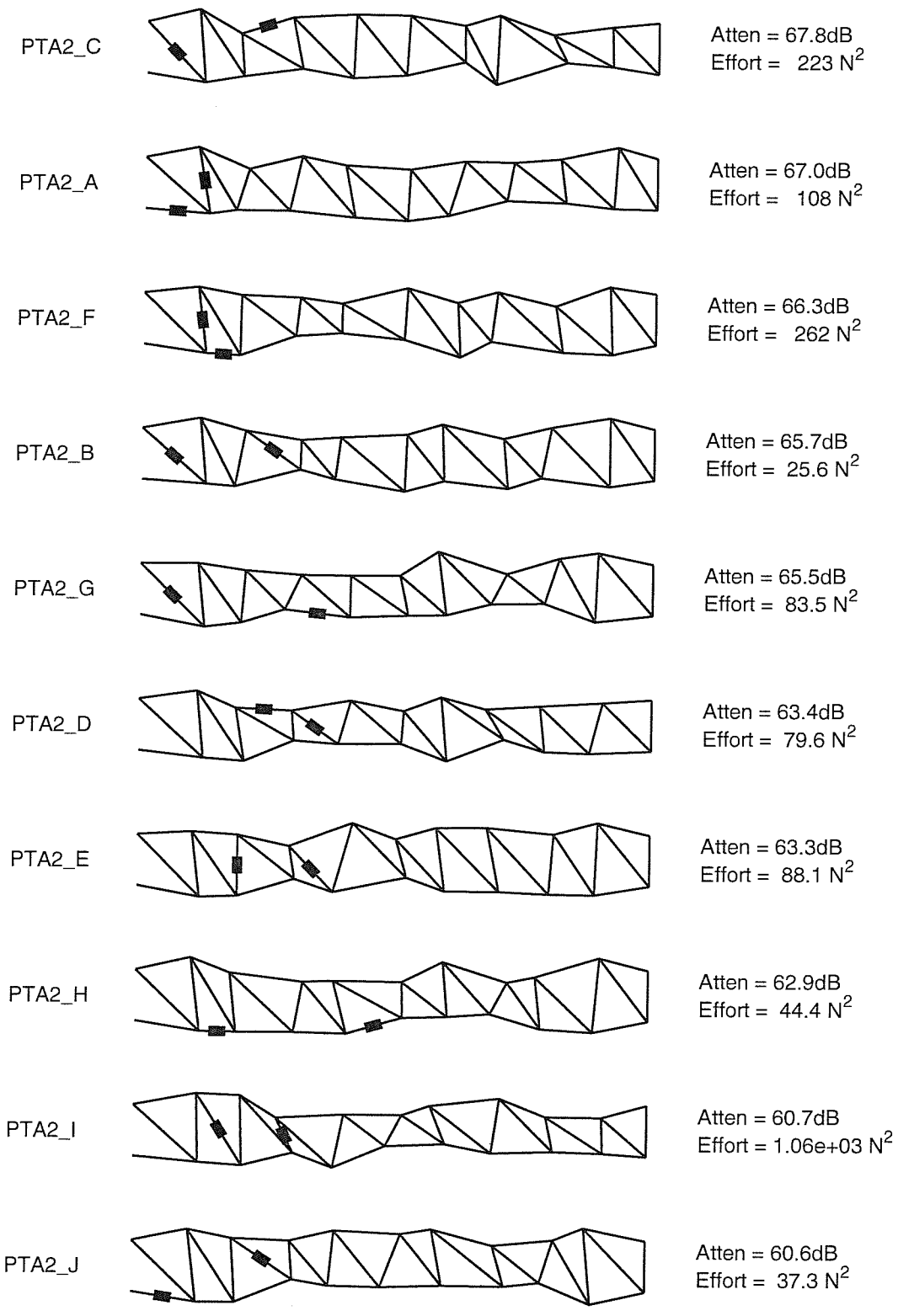

Figure 6.2: The ten best performance ranked two-actuator positions for the previously geometrically optimised structures, for the frequency band 150Hz to 250Hz.

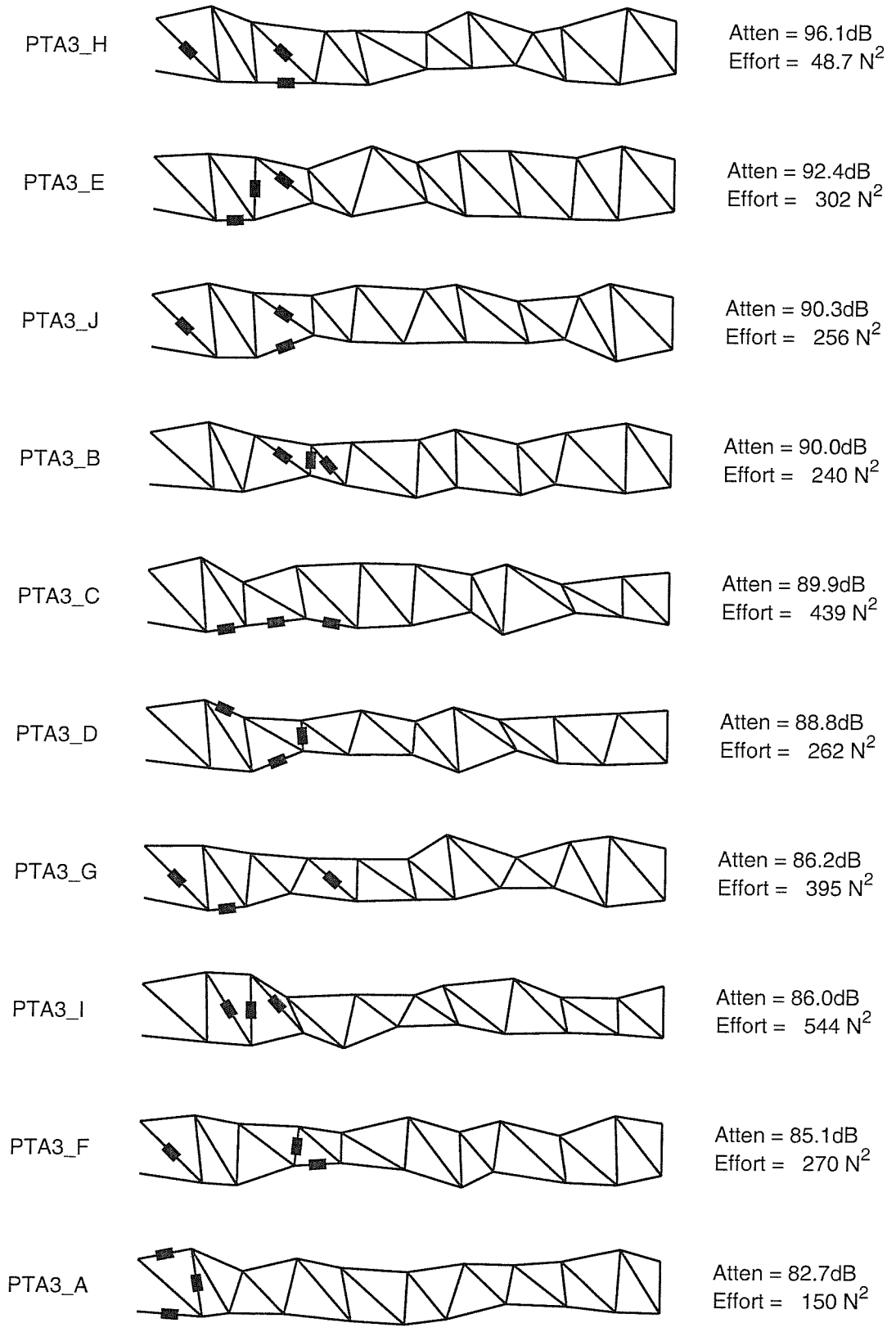

Figure 6.3: The ten best performance ranked three-actuator positions for the previously geometrically optimised structures, for the frequency band 150Hz to 250Hz.

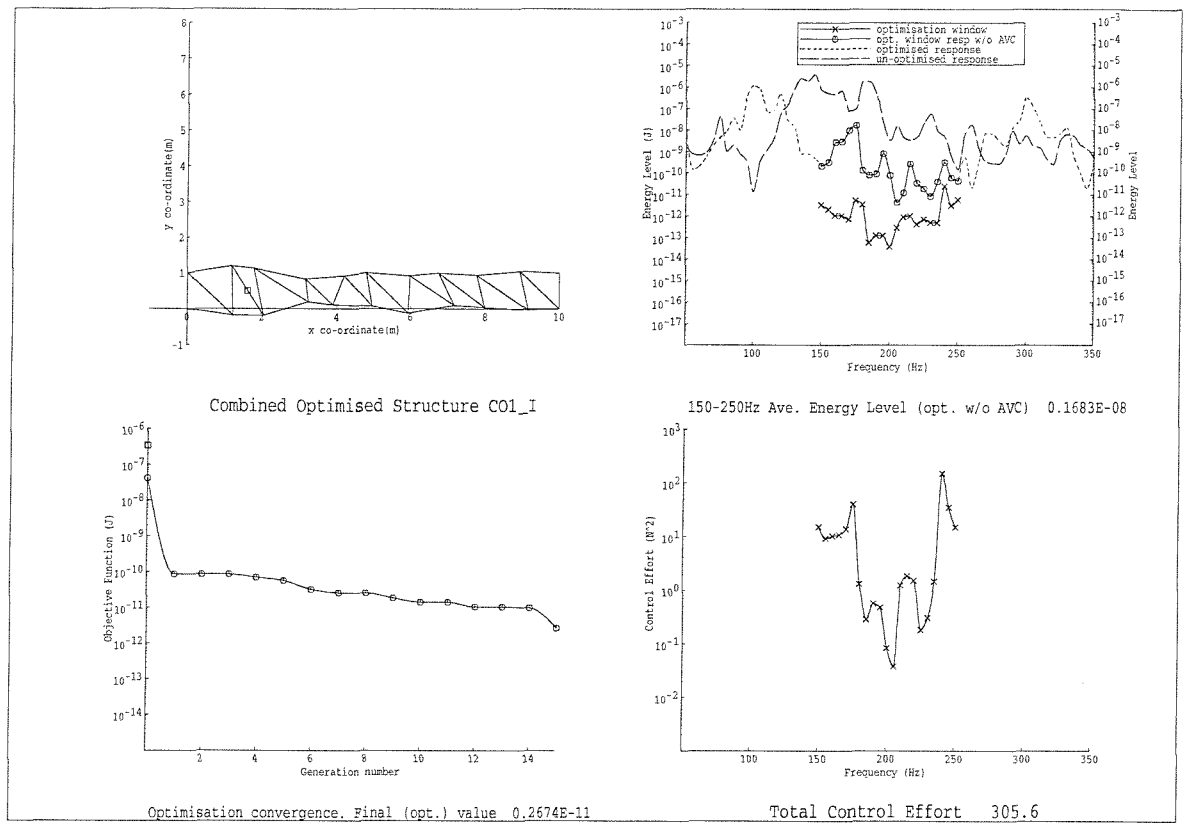

Figure 6.4: Structure with best optimised average performance over 150Hz to 250Hz using a single actuator (□), CO1_I. Both structure geometry and actuator position were optimised simultaneously.

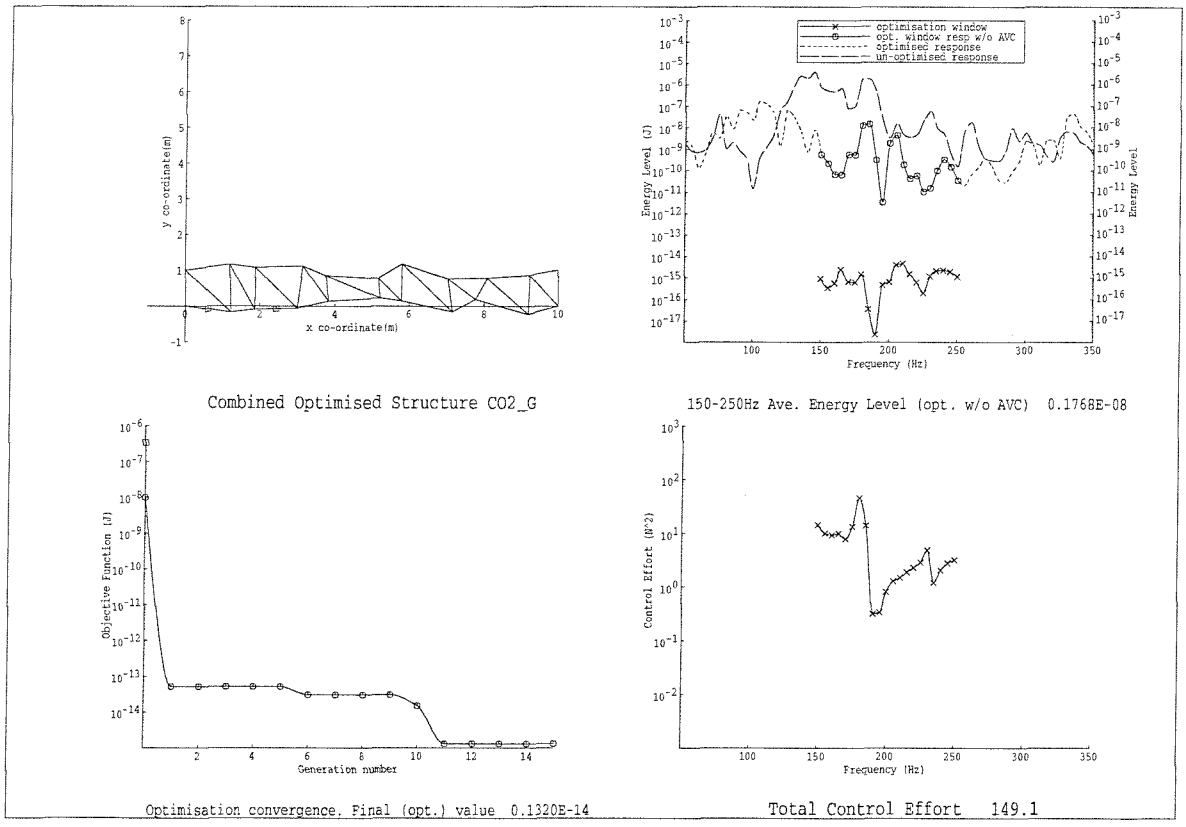

Figure 6.5: Structure with best optimised average performance over 150Hz to 250Hz using two actuators (□), CO2_G. Both structure geometry and actuator position were optimised simultaneously.

a)

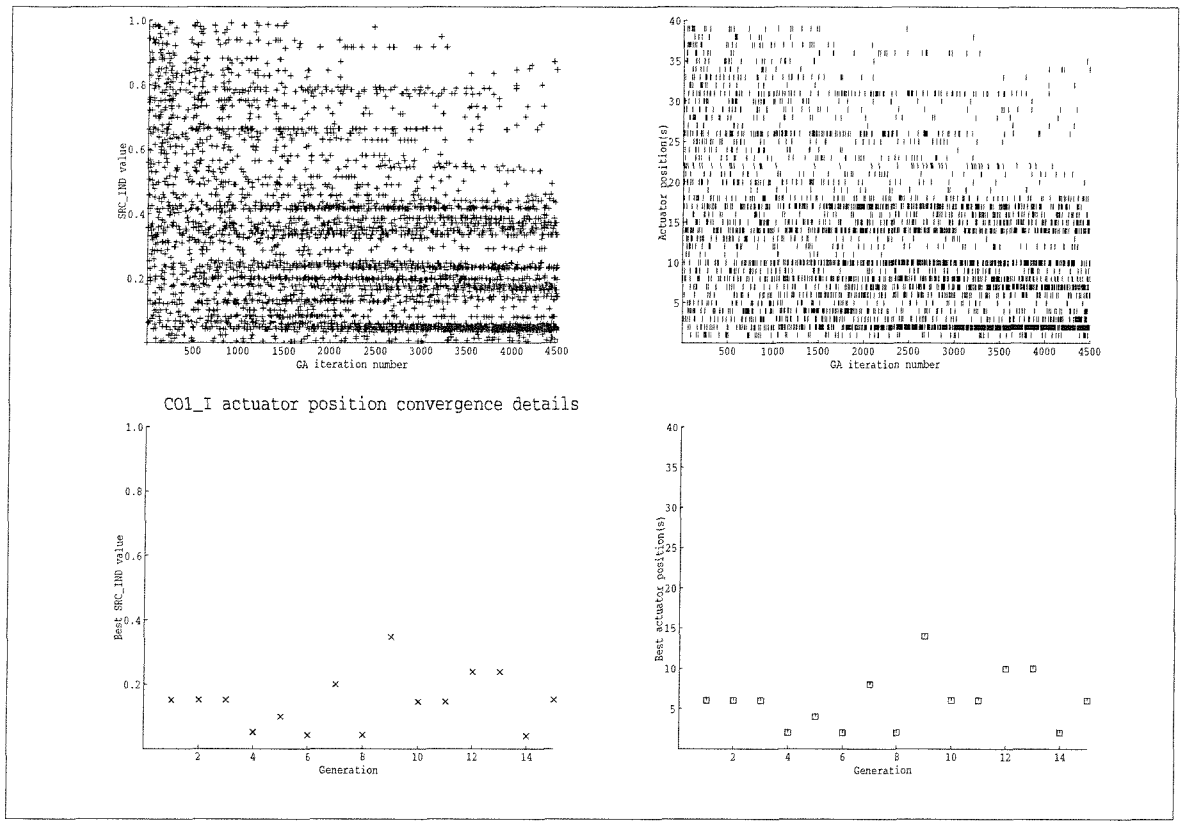

b)

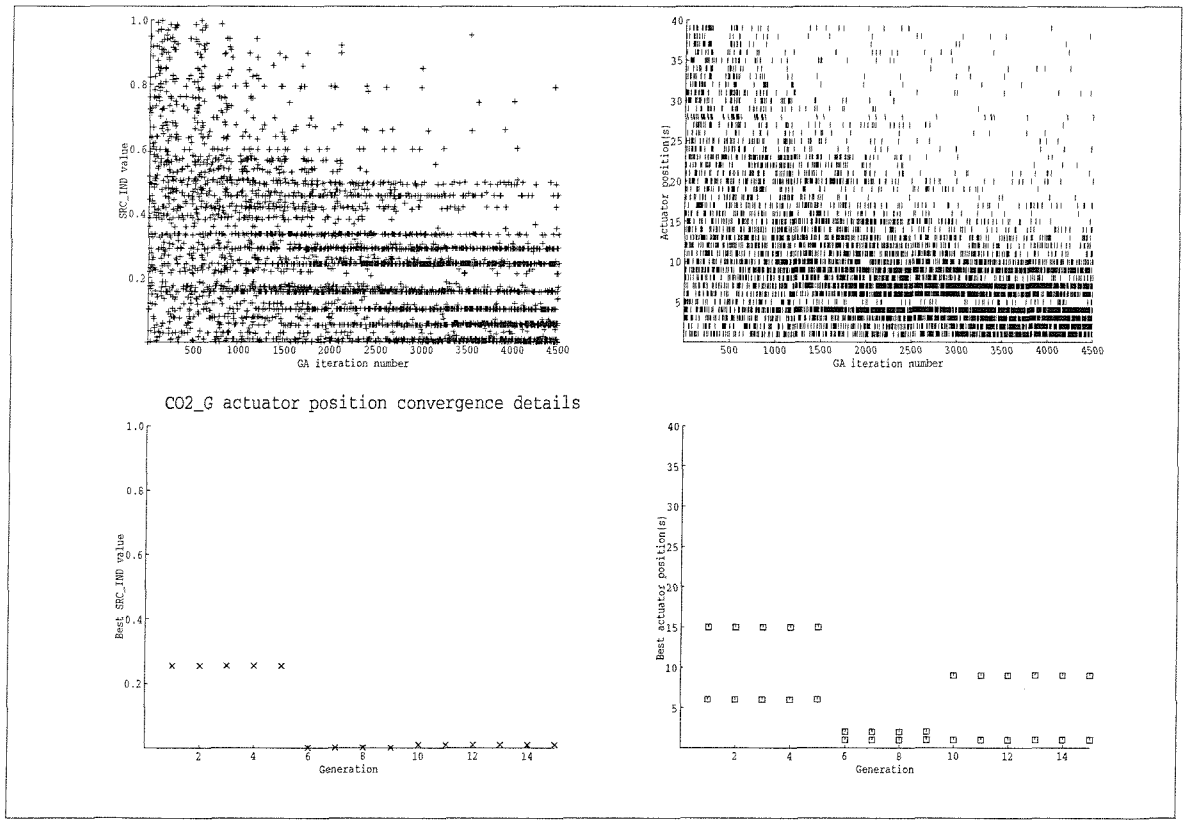

Figure 6.6: The performance of the genetic algorithm optimisation, with respect to actuator positions, resulting in structures CO1_I(a) and CO2_G(b), shown in Figures 6.4 and 6.5. The source position index is given for each evaluation (top left), and the corresponding actuator positions (top right), the best source position index and corresponding actuator position after each generation are also shown (bottom left and right).

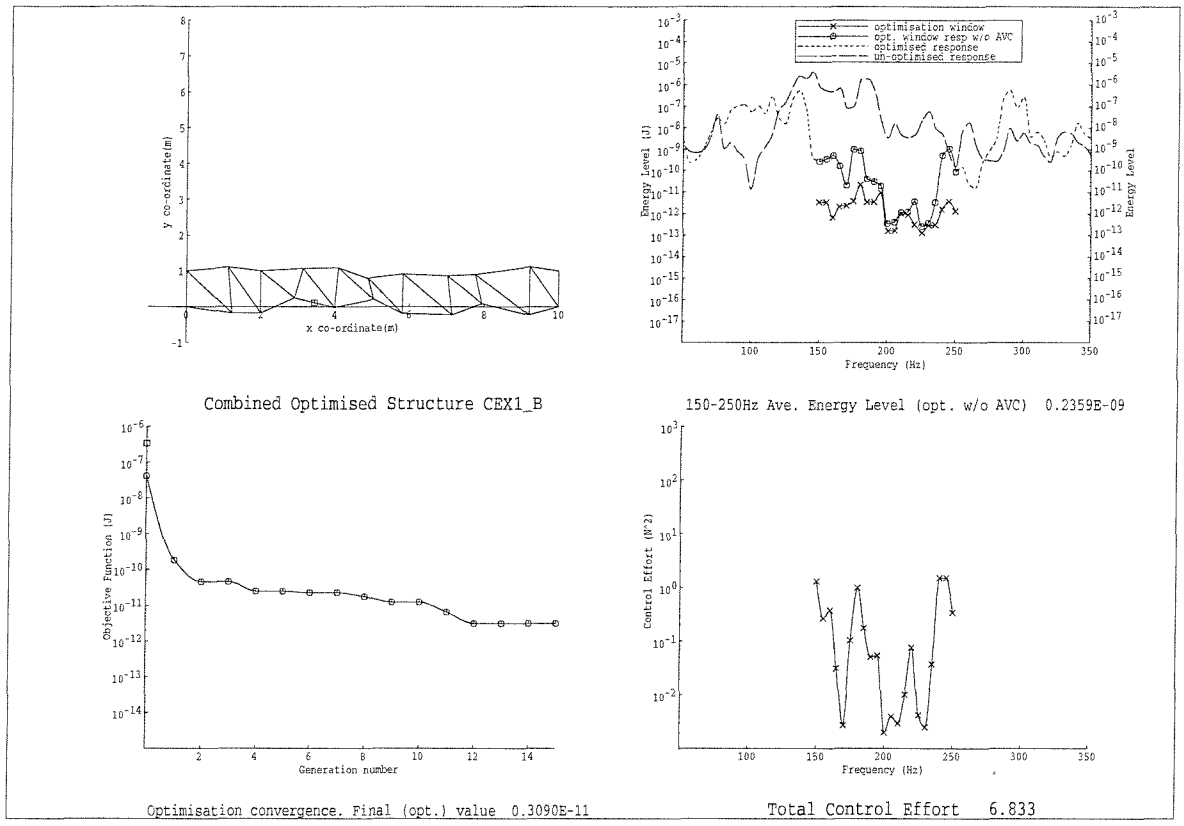

Figure 6.7: Structure with best optimised average performance over 150Hz to 250Hz using a single actuator (□), CEX1_B. Both structure geometry and actuator position were optimised simultaneously using the extended chromosome.

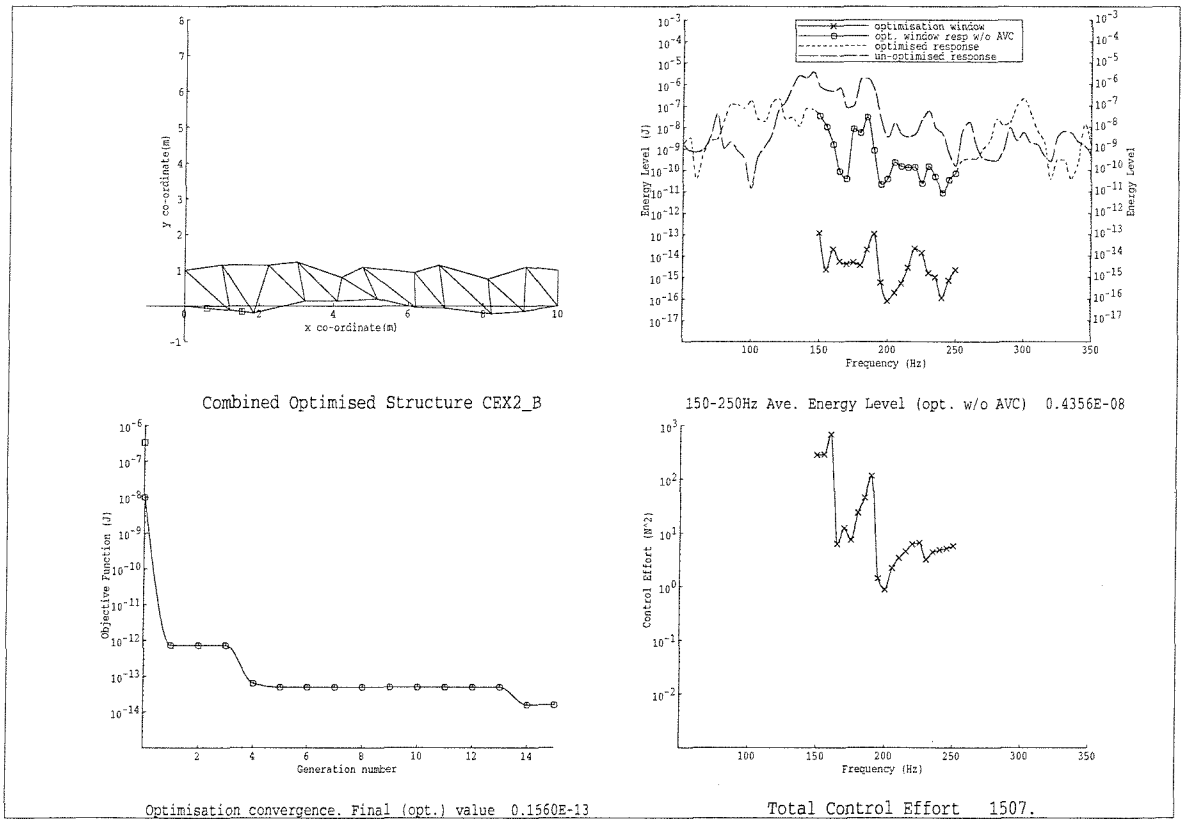

Figure 6.8: Structure with best optimised average performance over 150Hz to 250Hz using two actuators (□), CEX2_B. Both structure geometry and actuator position were optimised simultaneously using the extended chromosome.

a)

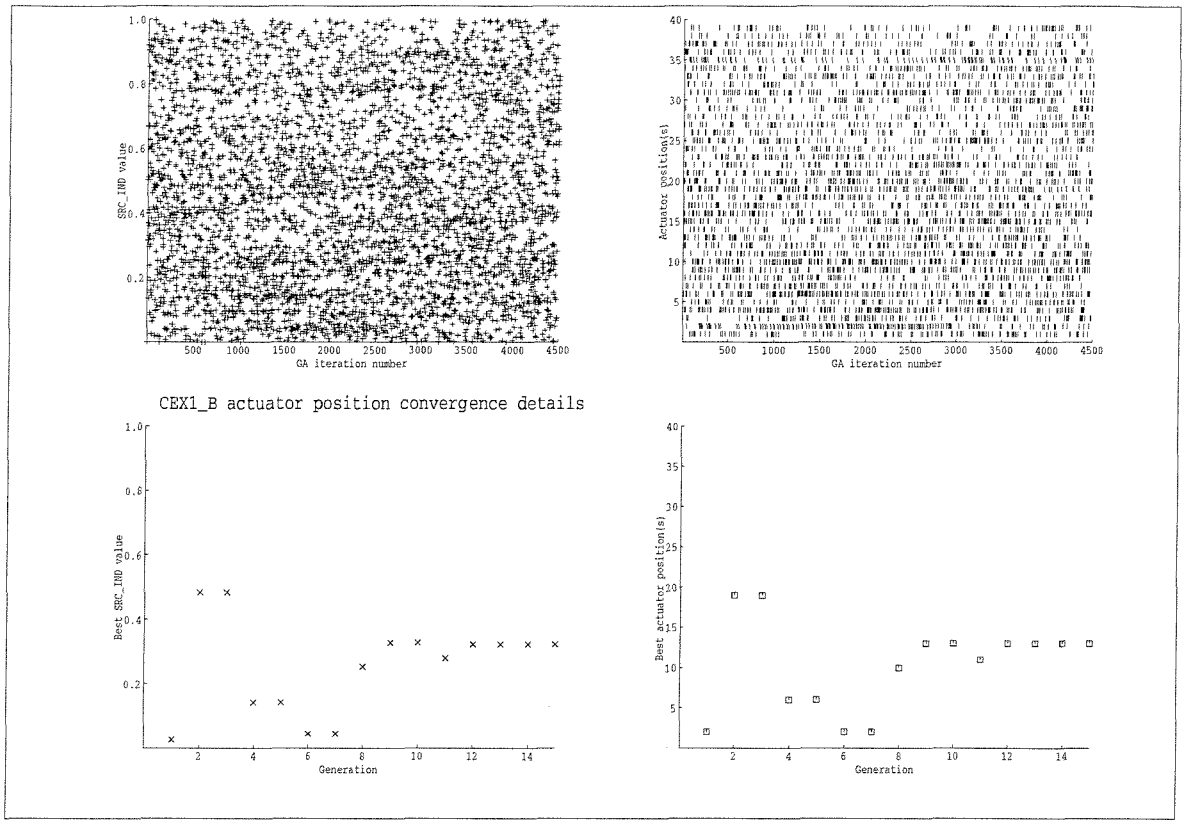

b)

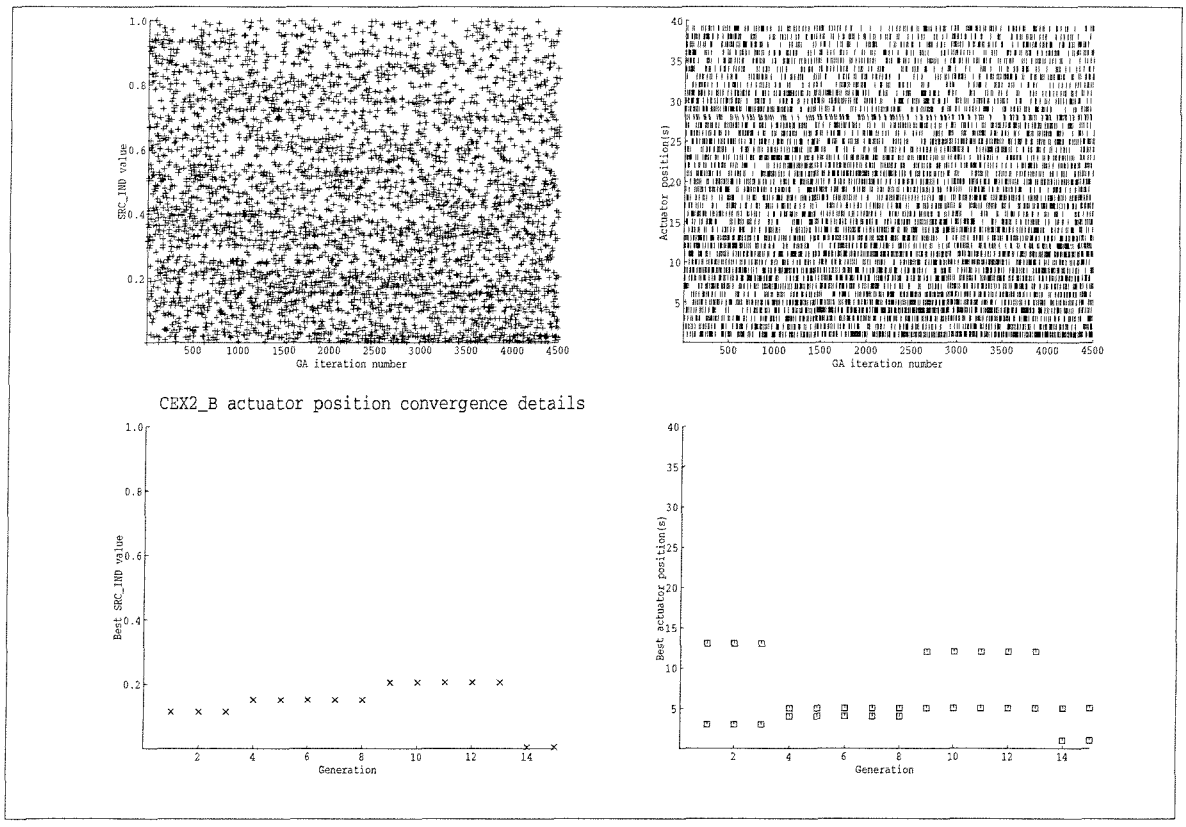

Figure 6.9: The performance of the genetic algorithm optimisation, with respect to actuator positions, resulting in structures CEX1_B(a) and CEX2_B(b), shown in Figures 6.7 and 6.8. The source position index is given for each evaluation (top left), and the corresponding actuator positions (top right), the best source position index and corresponding actuator position after each generation are also shown (bottom left and right).

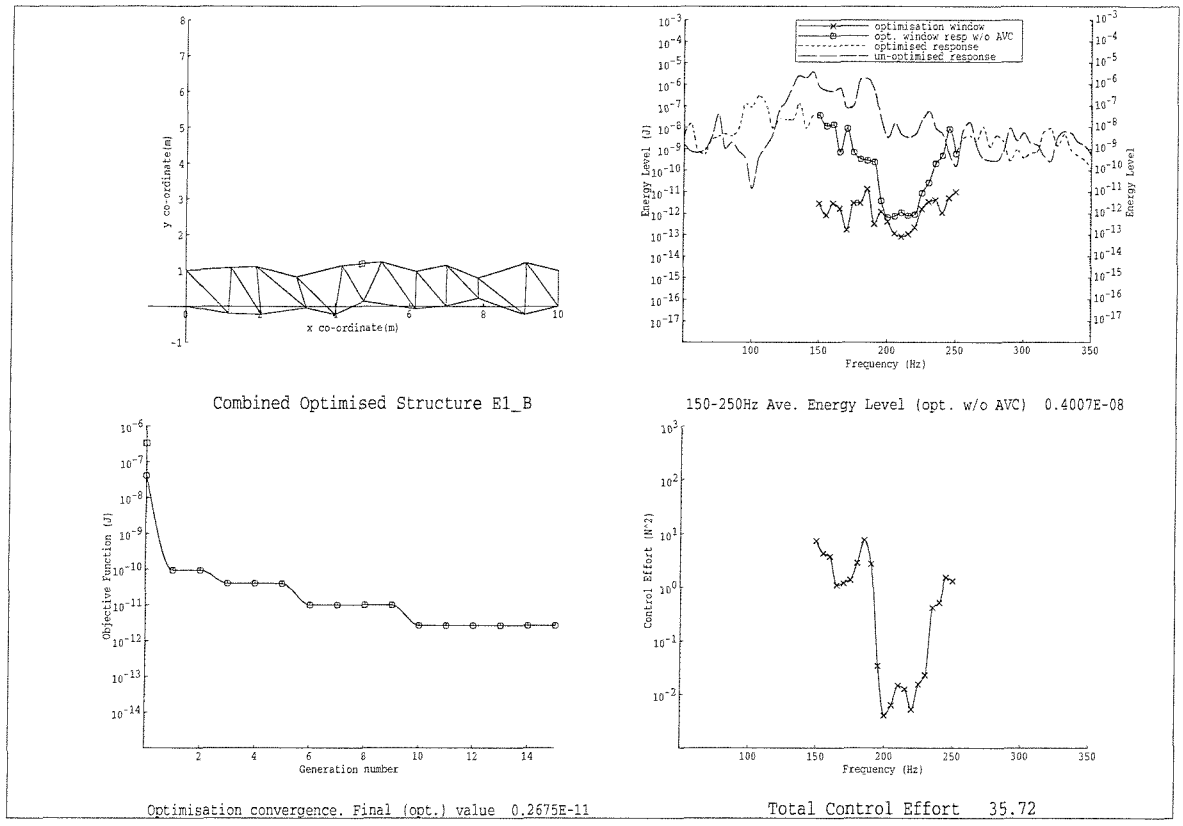

Figure 6.10: Structure with best optimised average performance over 150Hz to 250Hz using a single actuator (□), E1_B. Both structure geometry and actuator position were optimised simultaneously, using an extended chromosome, but biased towards mid-structure positions.

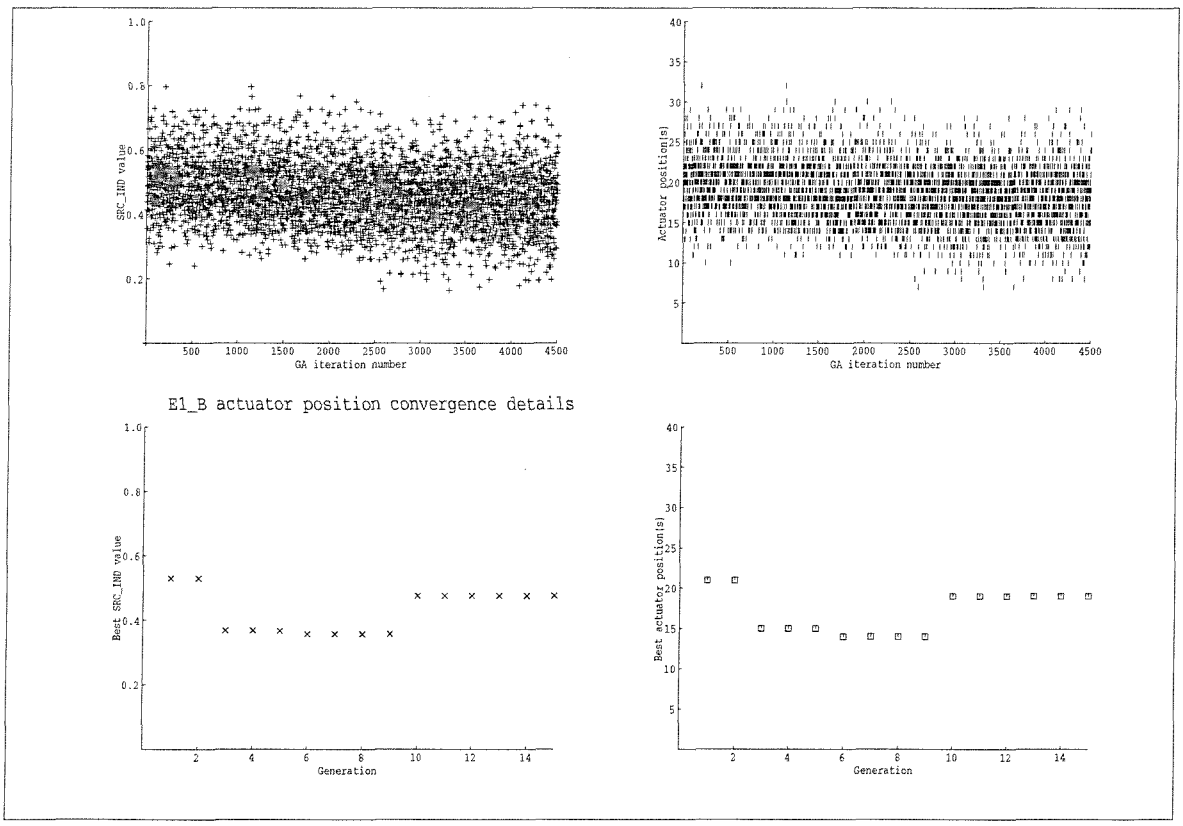

Figure 6.11: The performance of the genetic algorithm optimisation resulting in structure E1_B, shown in Figure 6.10. Figure layout is as for Figure 6.9.

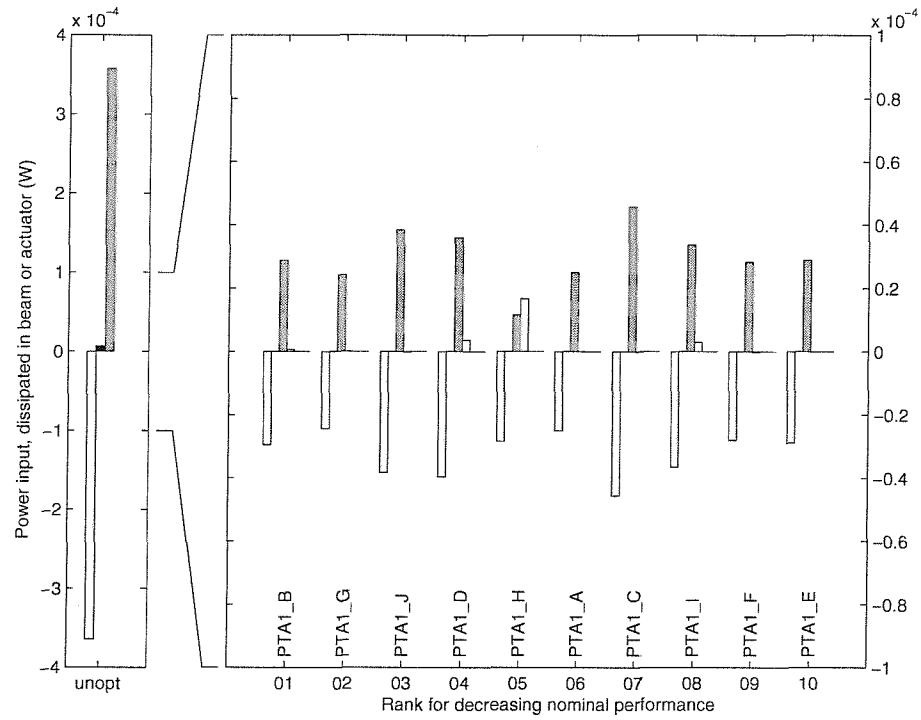

Figure 6.12: Power components in optimised structures PTA1_A to PTA1_J. Negative values of dissipation indicate power supplied to the structure. Light grey: Power input to structure, Dark grey: Power dissipated in Beams 1 to 39 without actuators, Black: Power dissipated in Beam 40, White: Power contributions from actuator. (N.B. Power dissipated in Beam 40 is only distinguishable for unoptimised structure without AVC. For optimised structures the range is 1.67×10^{-10} to 6.11×10^{-10} W.)

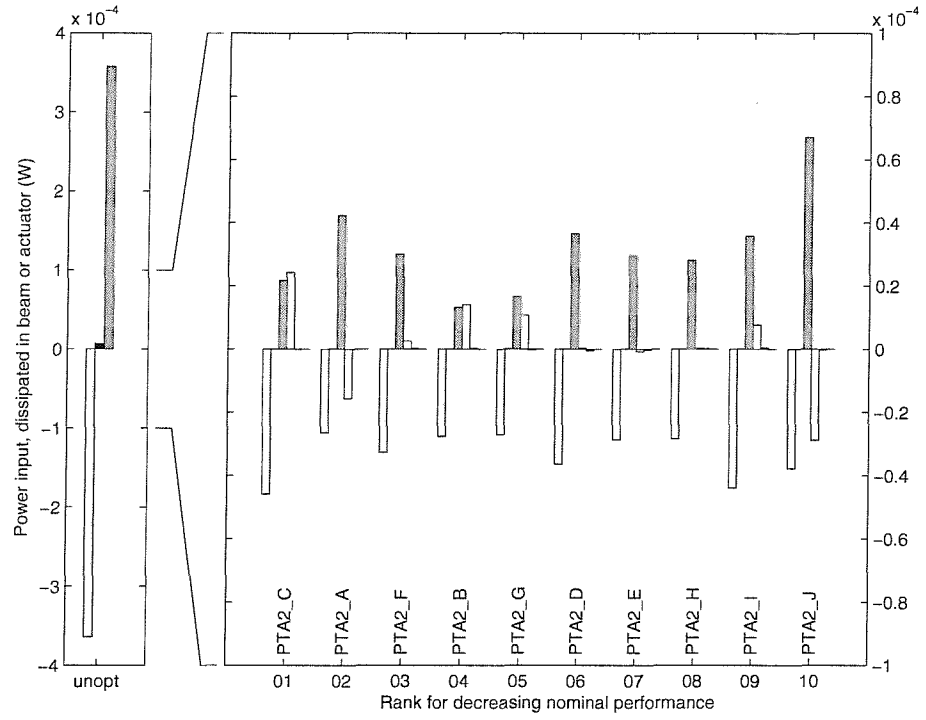

Figure 6.13: Power components in optimised structures PTA2_A to PTA2_J. Key as for Figure 6.12. The values of actuator power for each structure is shown from left to right for increasing beam number position. (N.B. Power dissipated in Beam 40 is only distinguishable for unoptimised structure. For optimised structures the range is 1.11×10^{-12} to 5.78×10^{-12} W.)

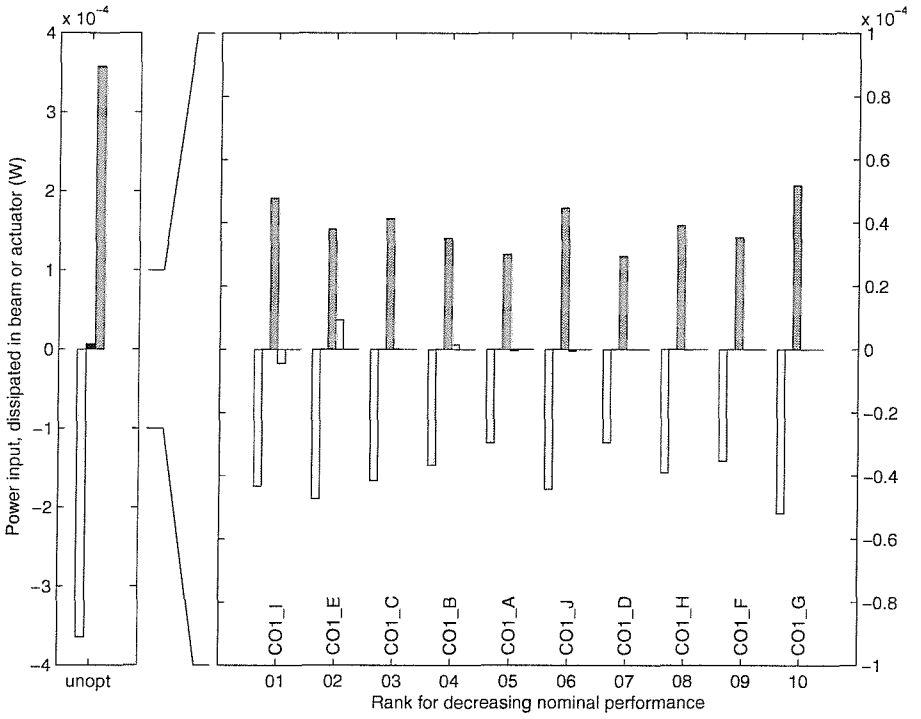

Figure 6.14: Power components in optimised structures CO1_A to CO1_J. Key as for Figure 6.12. (N.B. Power dissipated in Beam 40 is only distinguishable for unoptimised structure. For optimised structures the range is 5.35×10^{-11} to 1.55×10^{-10} W.)

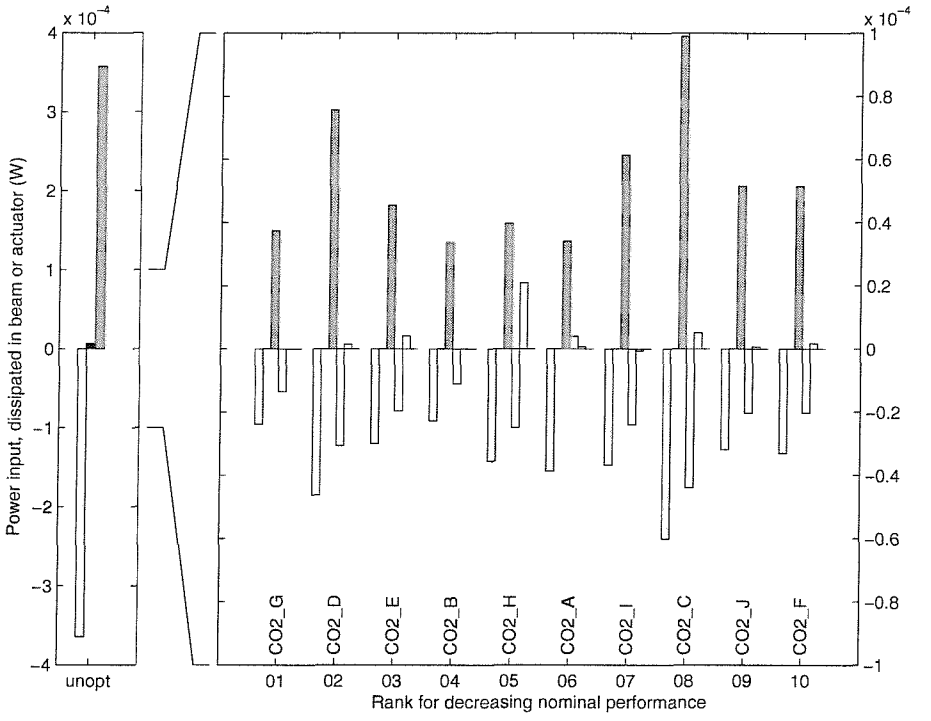

Figure 6.15: Power components in optimised structures CO2_A to CO2_J. Key as for Figure 6.12. The values of actuator power for each structure is shown from left to right for increasing beam number position. (N.B. Power dissipated in Beam 40 is only distinguishable for unoptimised structure. For optimised structures the range is 2.64×10^{-14} to 4.01×10^{-13} W.)

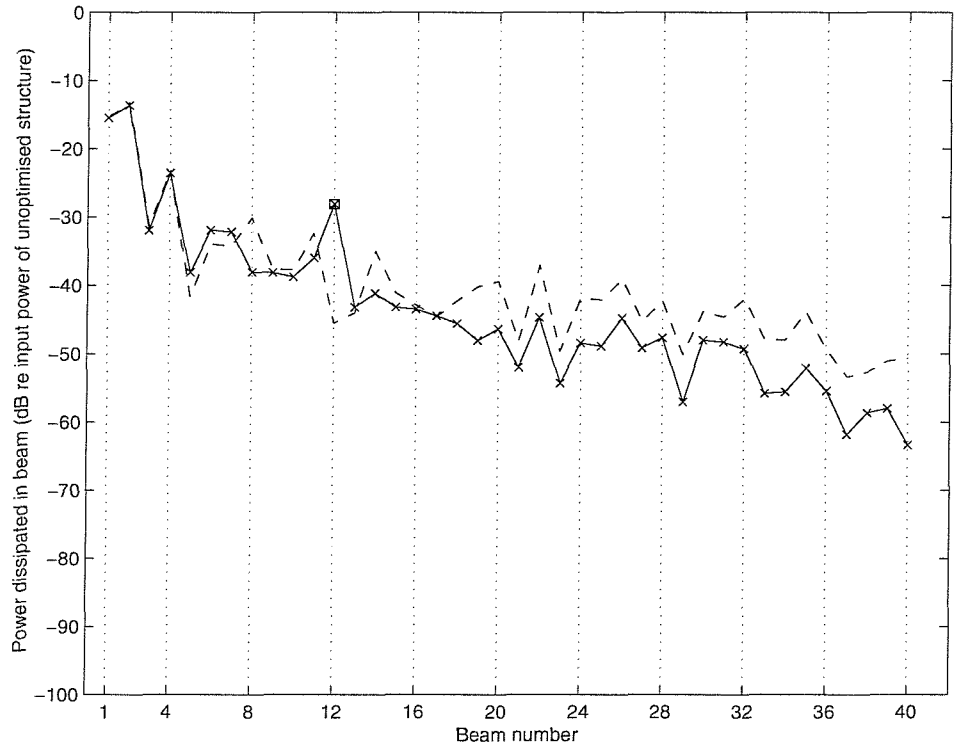

Figure 6.16: Power dissipated in each beam of structure for optimised structure PTA1_B. Vertical gridline represents vertical beam at end of each bay. - - - no AVC, —— with AVC. Actuator position is denoted □.

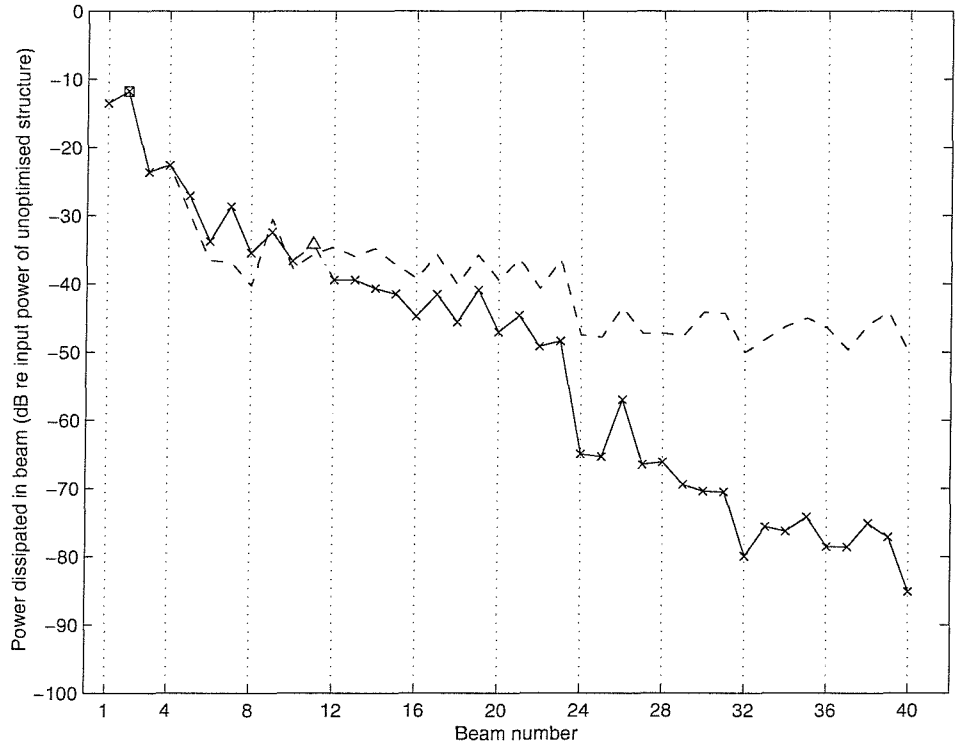

Figure 6.17: Power dissipated in each beam of structure for optimised structure PTA2_C. Vertical gridline represents vertical beam at end of each bay. - - - no AVC, —— with AVC. □ denotes position of actuator dissipating power, △ denotes position of actuator sourcing power (with magnitude shown in the same sense as for dissipation).

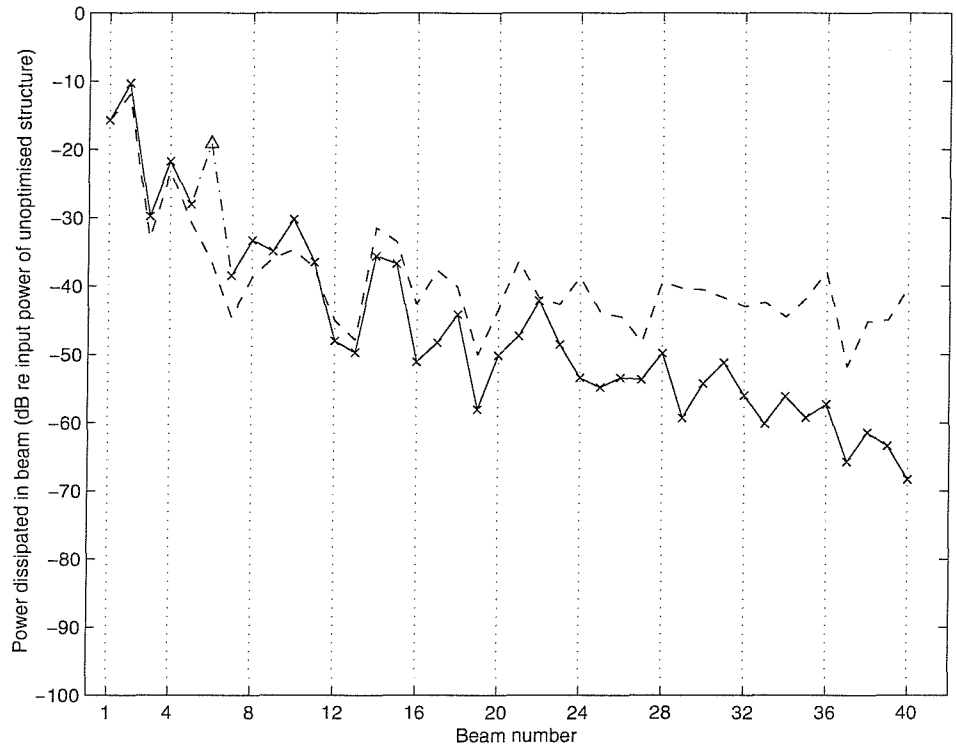

Figure 6.18: Power dissipated in each beam of structure for the combined optimised structure CO1_I. Vertical gridline represents vertical beam at end of each bay. - - - no AVC, —— with AVC. Actuator position is denoted △ and is sourcing power to the structure. It is shown with correct magnitude but in the same sense as for dissipation.

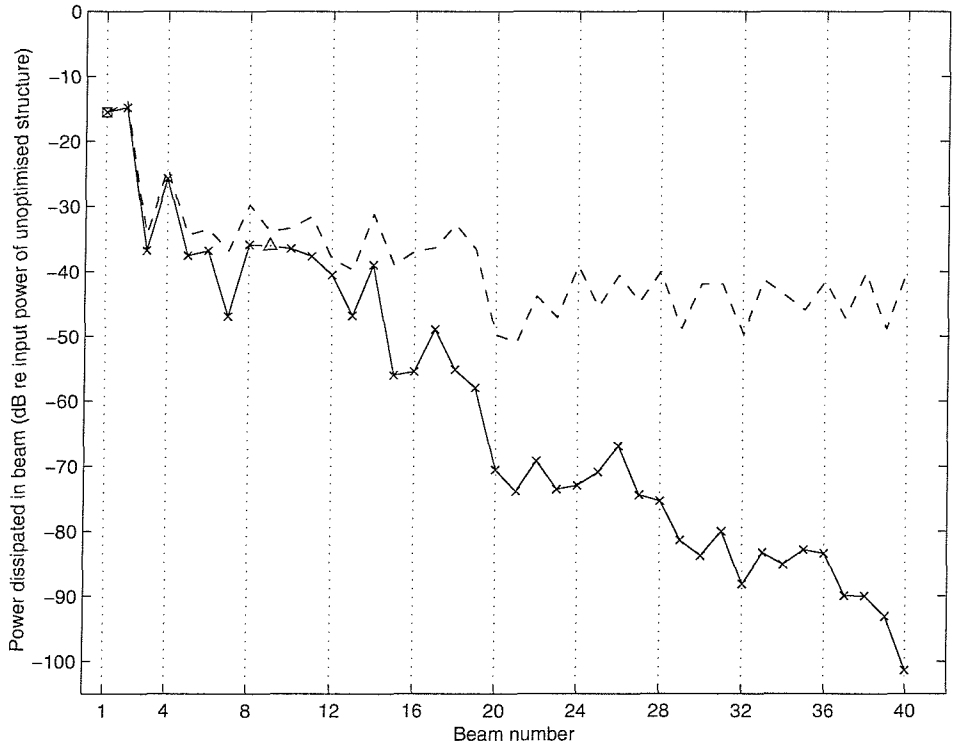

Figure 6.19: Power dissipated in each beam of structure for the combined optimised structure CO2_G. Vertical gridline represents vertical beam at end of each bay. - - - no AVC, —— with AVC. □ denotes position of actuator dissipating power, △ denotes position of actuator sourcing power (with magnitude shown in the same sense as for dissipation).

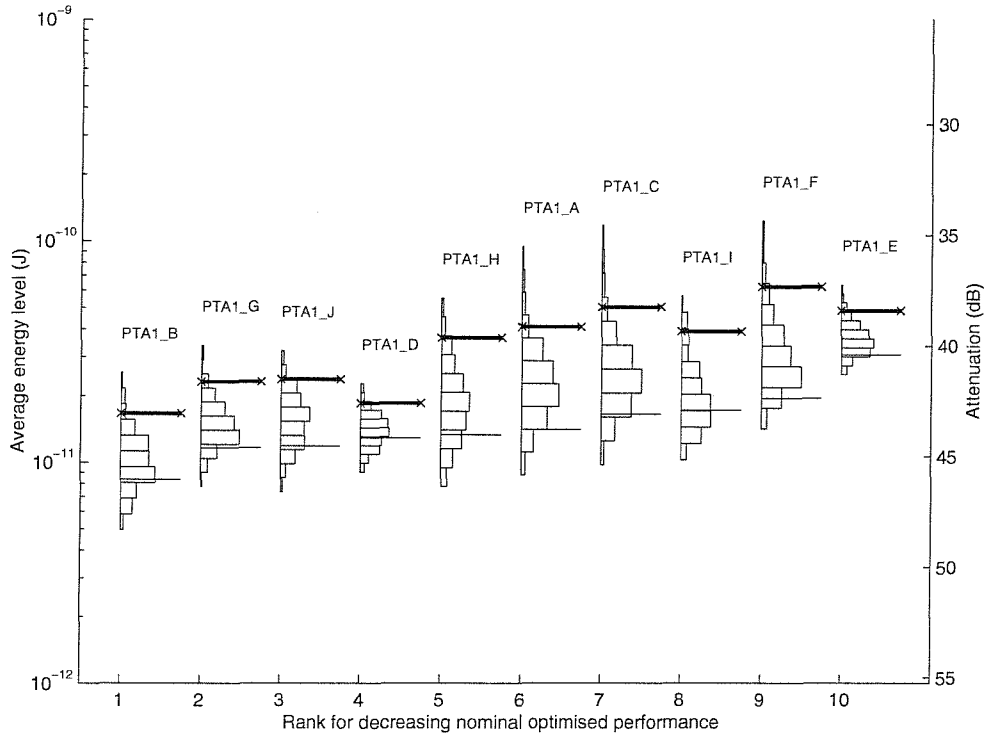

Figure 6.20: Statistical distribution and 95% probability limits (bold lines) for the overall performance of the passive-then-active optimised structures using one actuator, for frequency band 150Hz to 250Hz. Values of nominal performance are shown by thin lines.

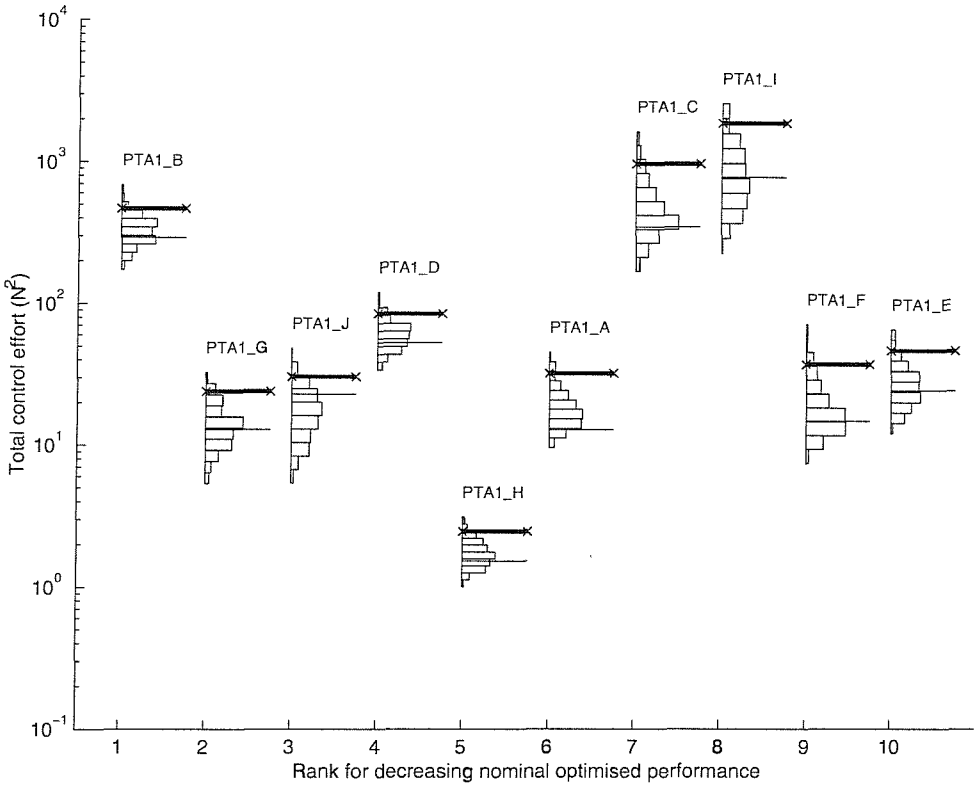

Figure 6.21: Statistical distribution and 95% probability limits (bold lines) for the AVC total control effort required by the passive-then-active optimised structures using one actuator, for frequency band 150Hz to 250Hz. Values of nominal control effort are shown by thin lines.

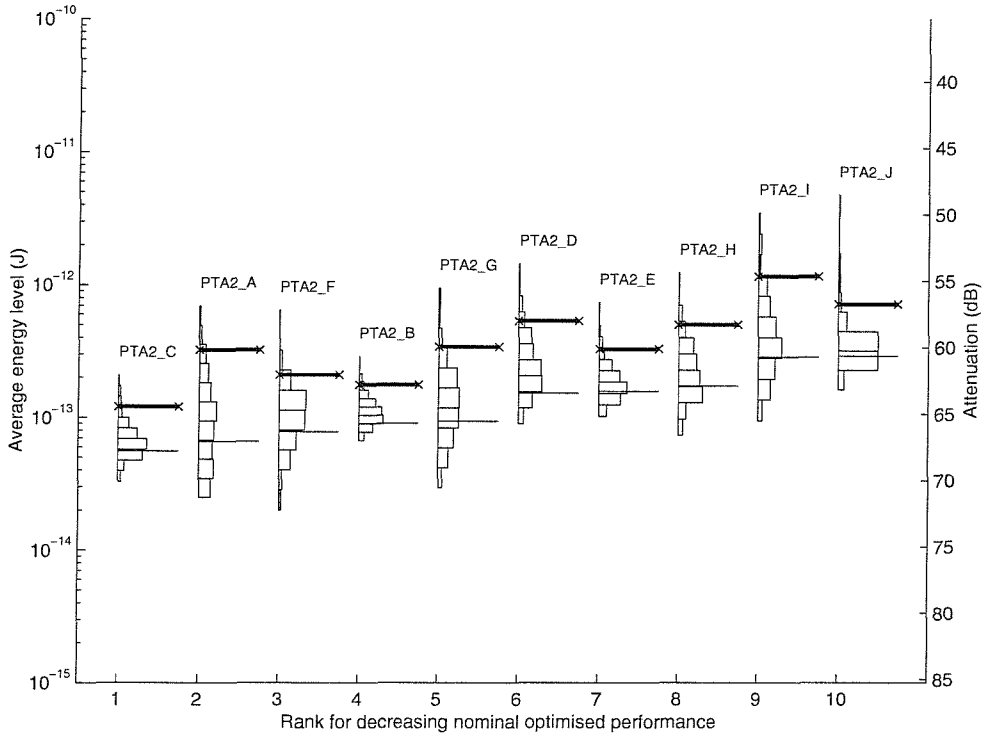

Figure 6.22: Statistical distribution and 95% probability limits (bold lines) for the overall performance of the passive-then-active optimised structures using two actuators, for frequency band 150Hz to 250Hz. Values of nominal performance are shown by thin lines.

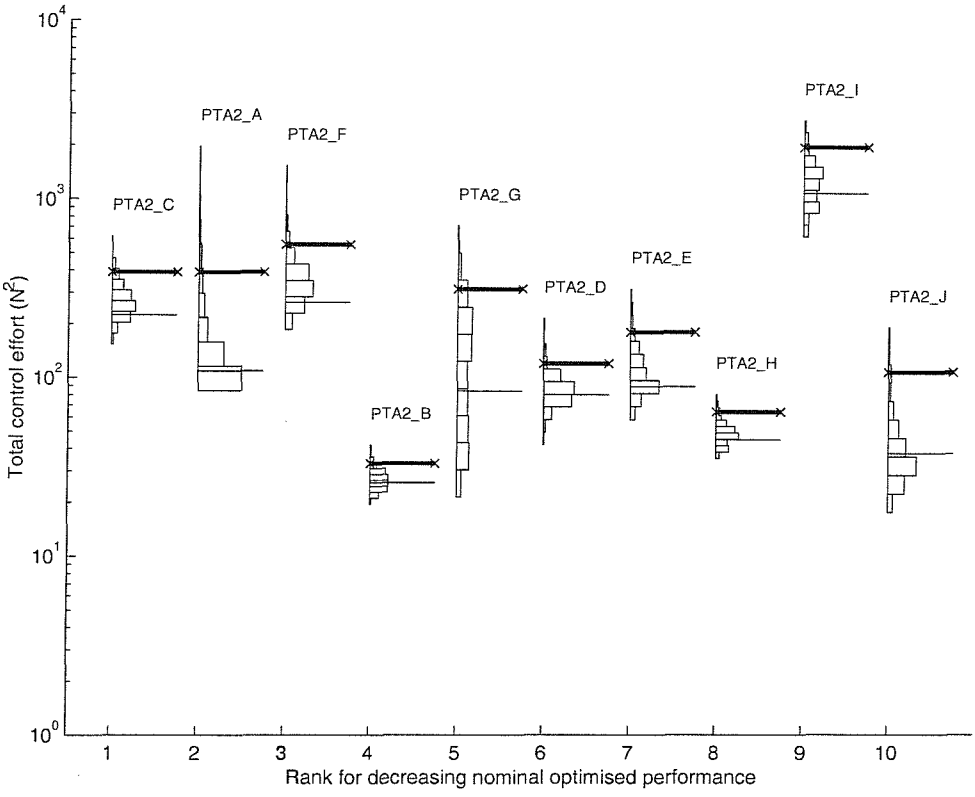

Figure 6.23: Statistical distribution and 95% probability limits (bold lines) for the AVC total control effort required by the passive-then-active optimised structures using two actuators, for frequency band 150Hz to 250Hz. Values of nominal control effort are shown by thin lines.

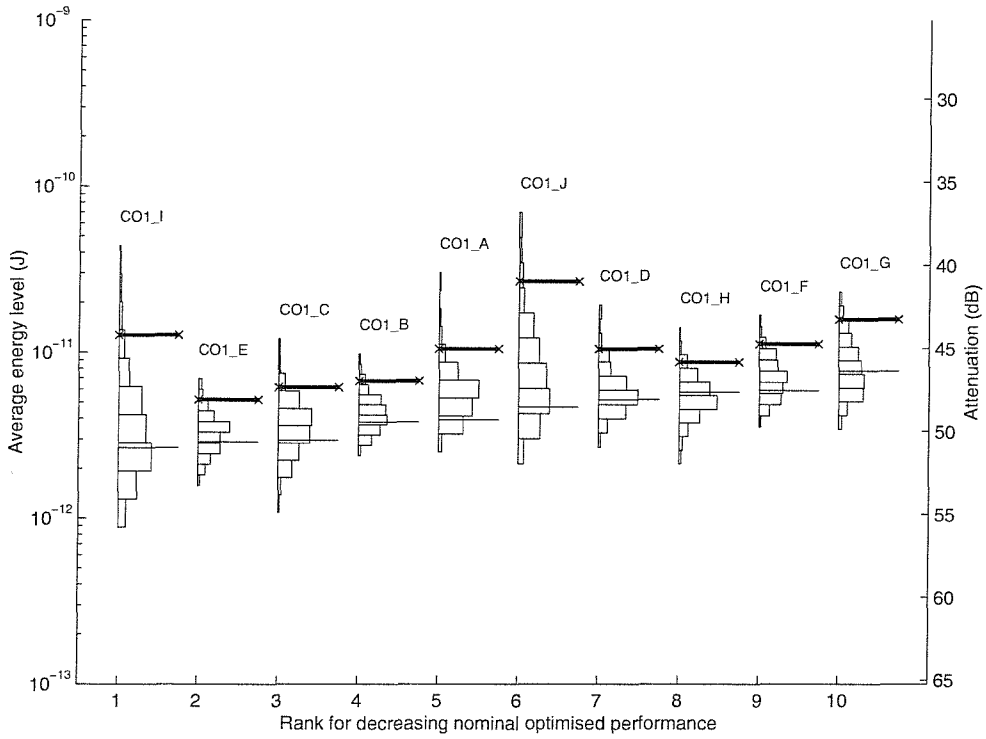

Figure 6.24: Statistical distribution and 95% probability limits (bold lines) for the overall performance of the combined optimised structures using one actuator, for frequency band 150Hz to 250Hz. Values of nominal performance are shown by thin lines.

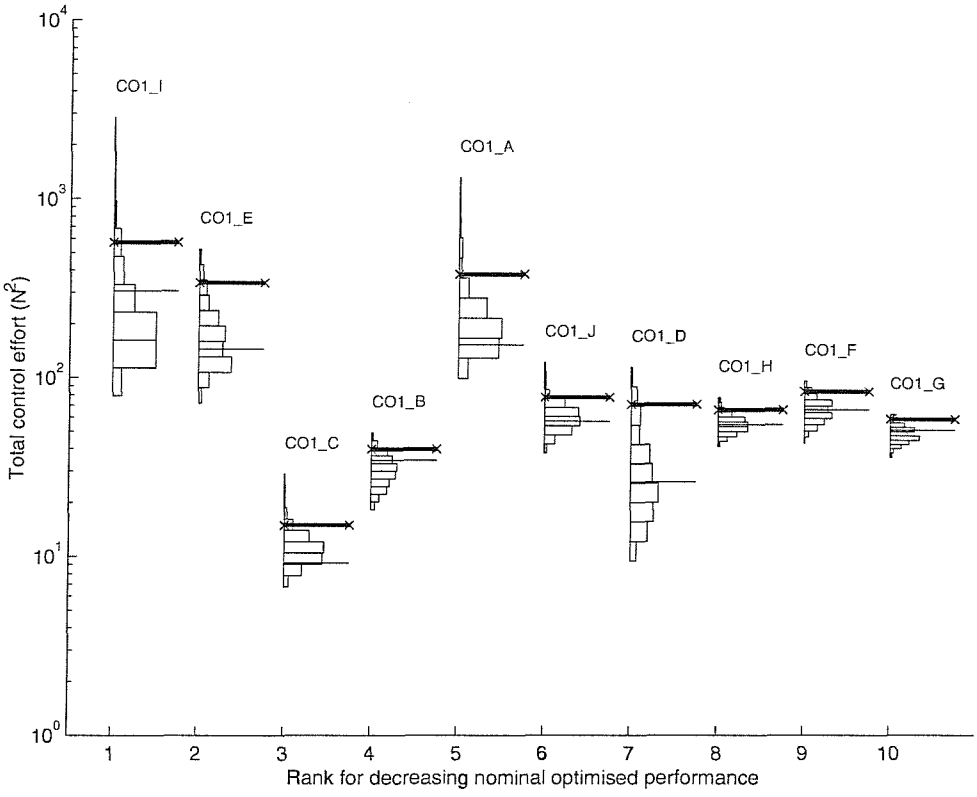

Figure 6.25: Statistical distribution and 95% probability limits (bold lines) for the AVC total control effort required by the combined optimised structures using one actuator, for frequency band 150Hz to 250Hz. Values of nominal control effort are shown by thin lines.

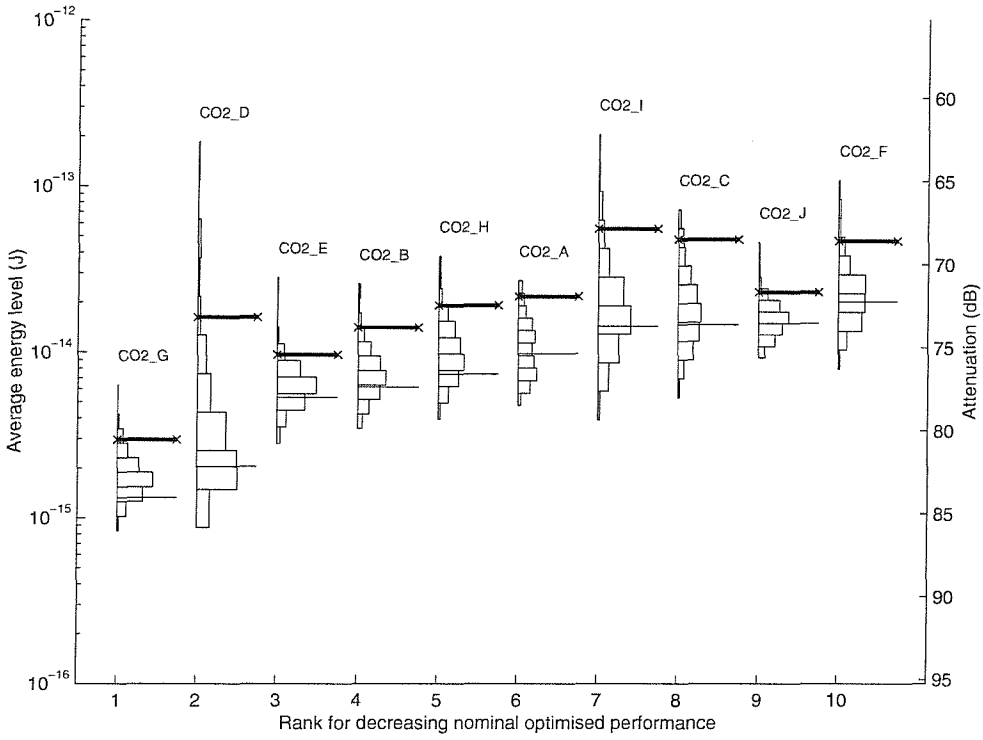

Figure 6.26: Statistical distribution and 95% probability limits (bold lines) for the overall performance of the combined optimised structures using two actuators, for frequency band 150Hz to 250Hz. Values of nominal performance are shown by thin lines.

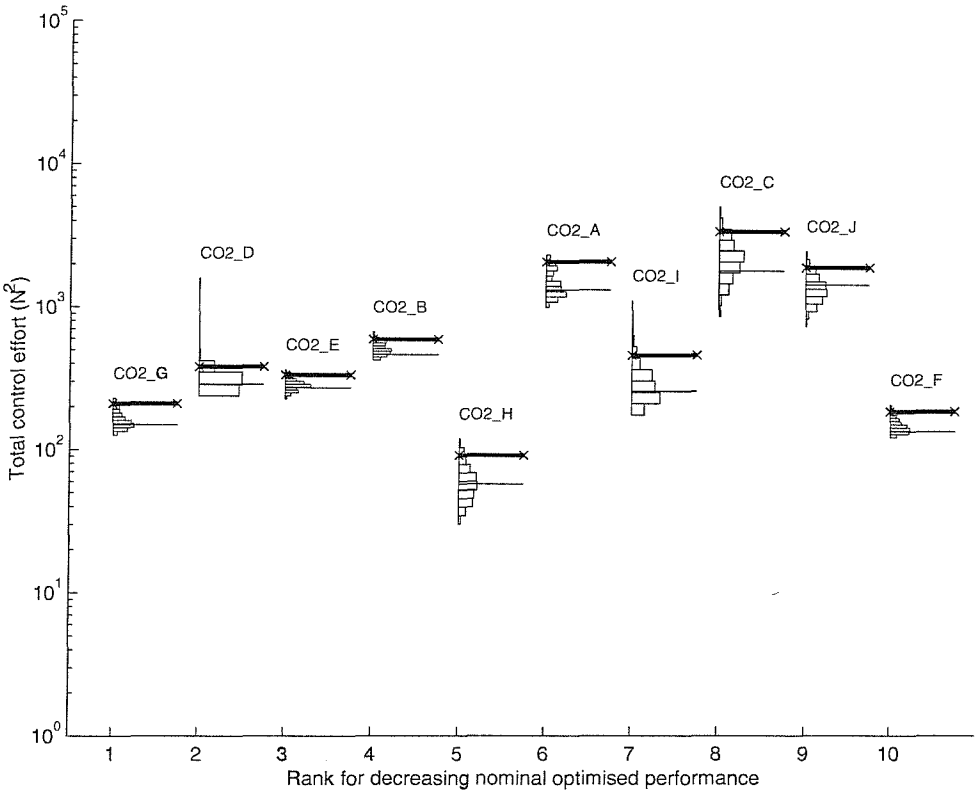

Figure 6.27: Statistical distribution and 95% probability limits (bold lines) for the AVC total control effort required by the combined optimised structures using two actuators, for frequency band 150Hz to 250Hz. Values of nominal control effort are shown by thin lines.

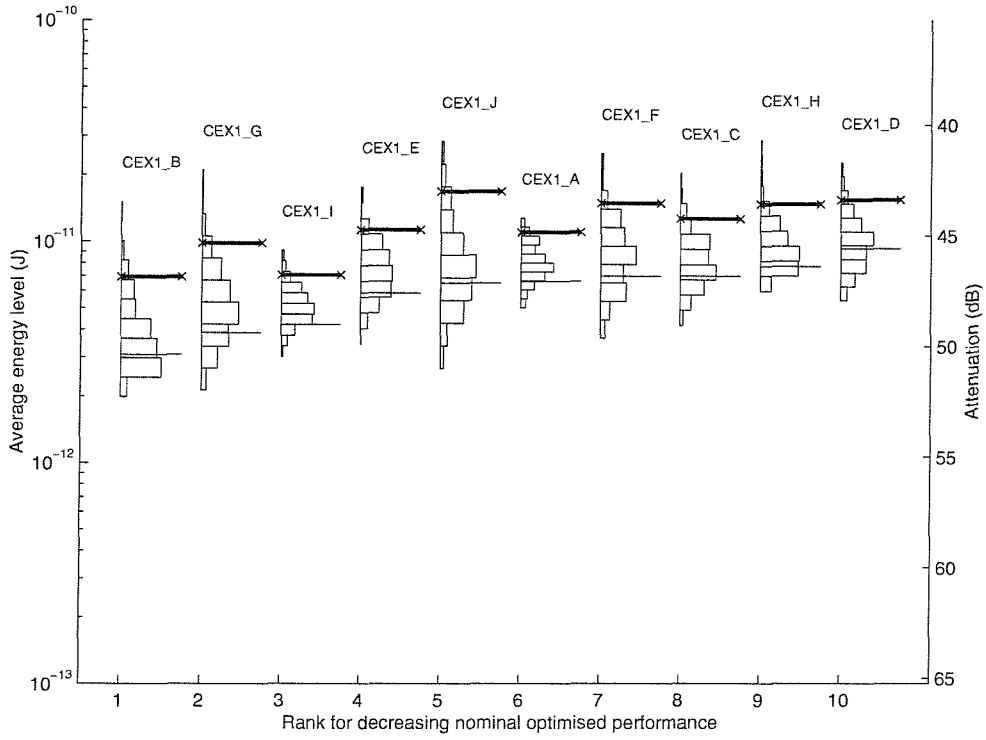

Figure 6.28: Statistical distribution and 95% probability limits (bold lines) for the overall performance of the combined optimised structures using an extended chromosome for one actuator, for frequency band 150Hz to 250Hz. Values of nominal performance are shown by thin lines.

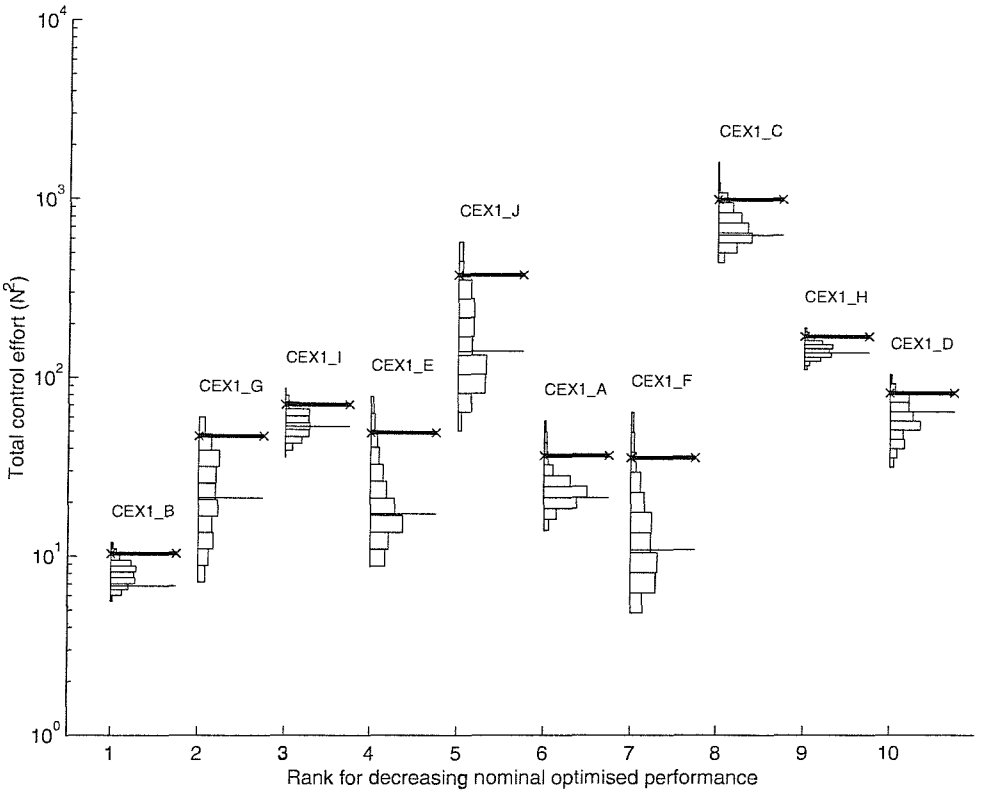

Figure 6.29: Statistical distribution and 95% probability limits (bold lines) for the AVC total control effort required by the combined optimised structures using an extended chromosome for one actuator, for frequency band 150Hz to 250Hz. Values of nominal control effort are shown by thin lines.

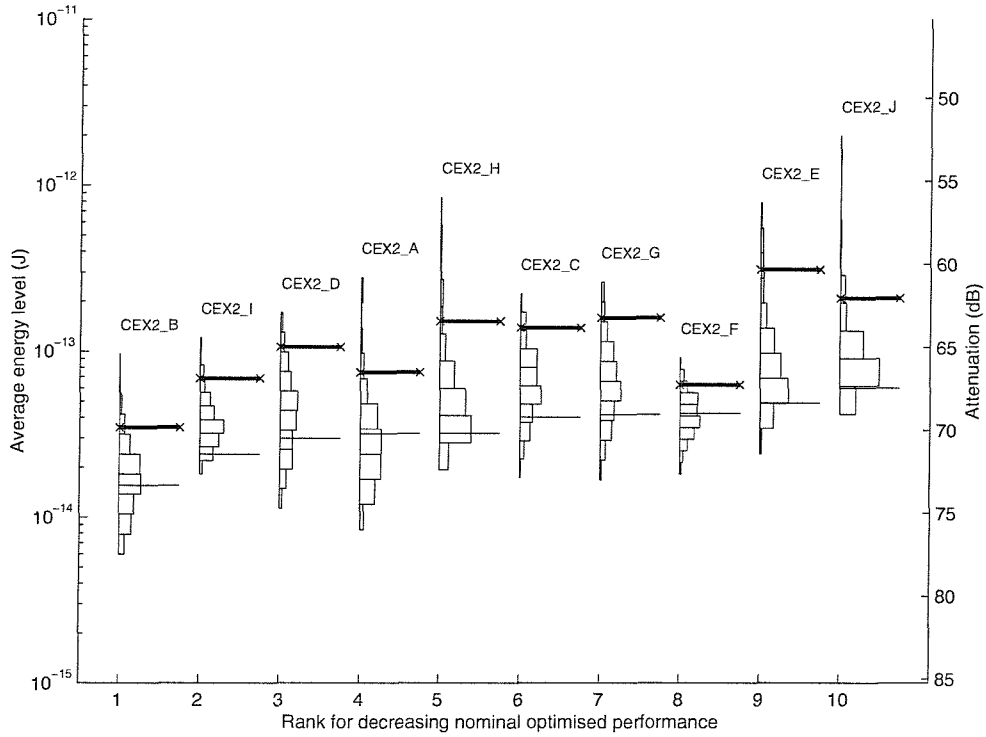

Figure 6.30: Statistical distribution and 95% probability limits (bold lines) for the overall performance of the combined optimised structures using an extended chromosome for two actuators, for frequency band 150Hz to 250Hz. Values of nominal performance are shown by thin lines.

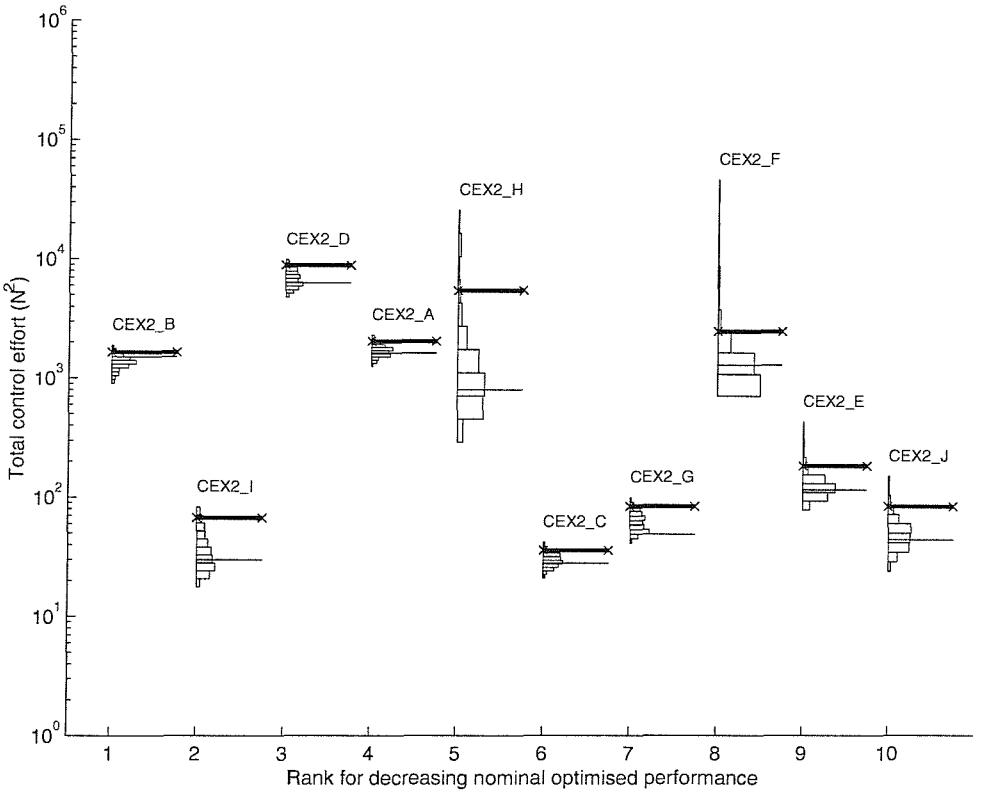

Figure 6.31: Statistical distribution and 95% probability limits (bold lines) for the AVC total control effort required by the combined optimised structures using an extended chromosome for two actuators, for frequency band 150Hz to 250Hz. Values of nominal control effort are shown by thin lines.

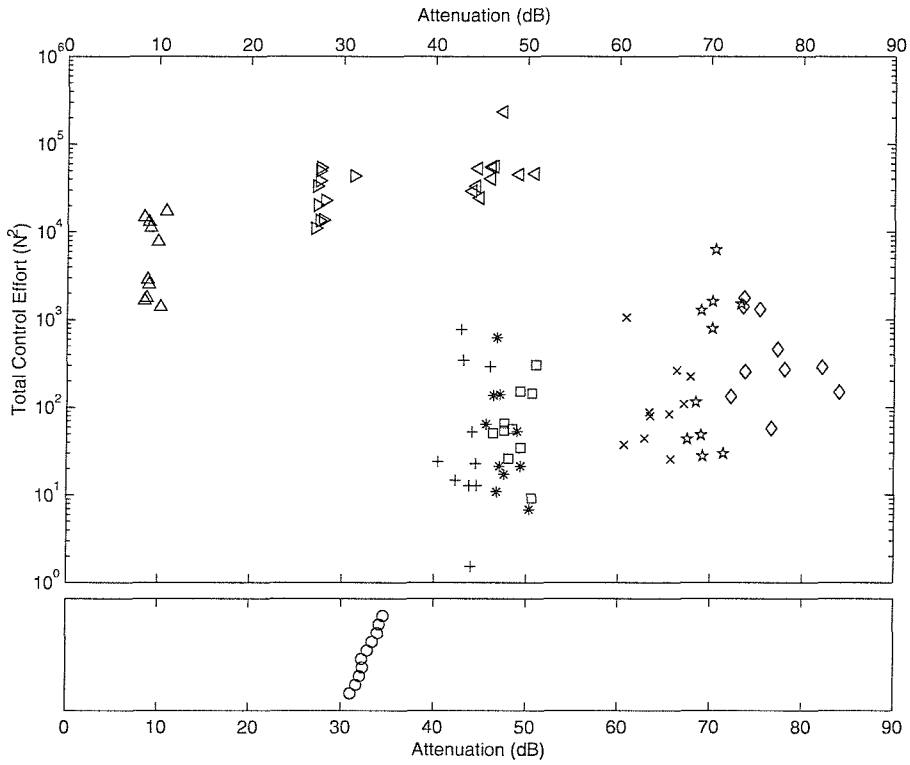

Figure 6.32: Comparison of nominal optimised overall performance and total control effort for all optimised structures considered in Chapters 4, 5 and 6. Key: passive only optimisation ○; active only optimisation △, ▷, ◁ (1,2,3 actuators); passive-then-active optimisation +, × (1,2 actuators); combined optimisation □, ◇ (1,2 actuators); combined optimisation with extended chromosome ∗, ⋆ (1,2 actuators).

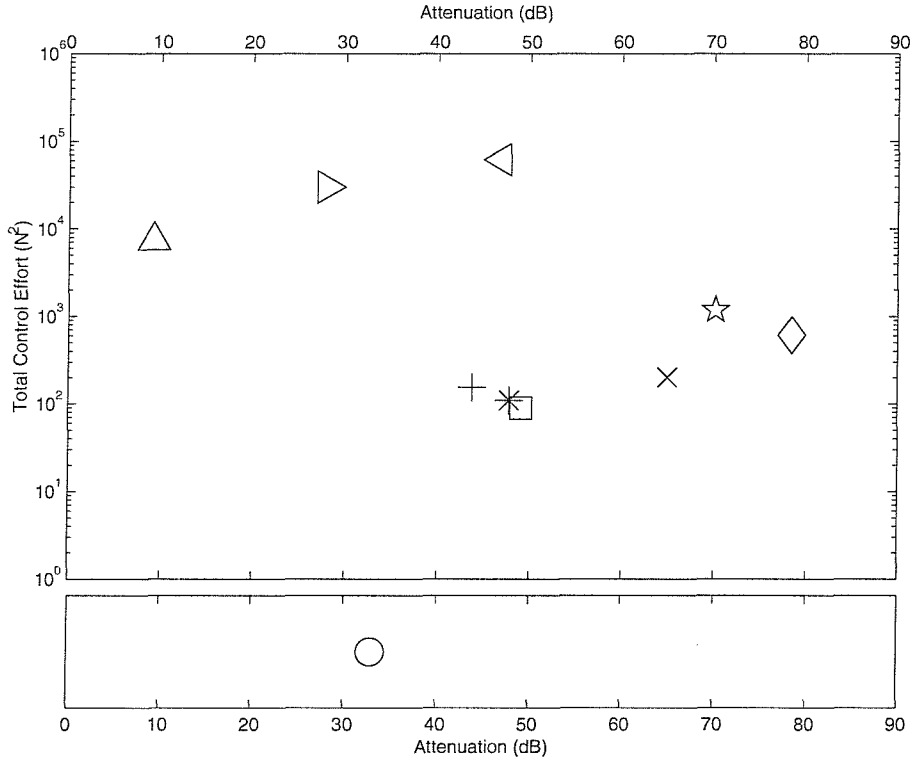

Figure 6.33: Comparison of average nominal optimised overall performance and average total control effort for all optimised structures considered in Chapters 4, 5 and 6. Key as Figure 6.32

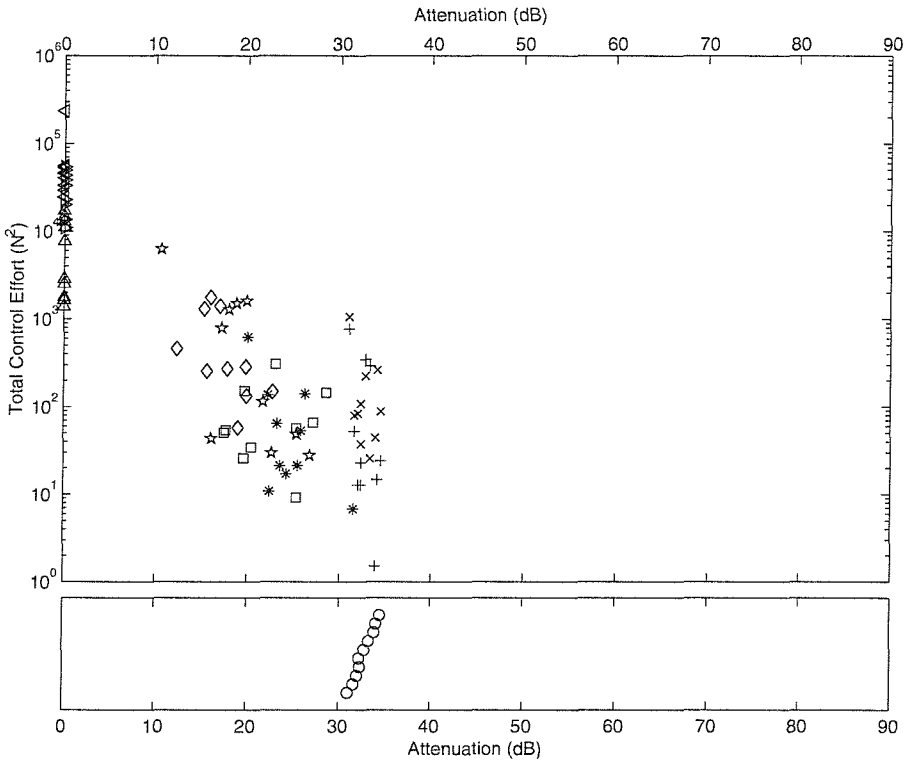

Figure 6.34: Comparison of nominal optimised structure performance for all optimised structures considered in Chapters 4, 5 and 6, with no AVC system operating, such that the contribution of any geometric optimisation can be seen. The total control effort values in Figure 6.32 are maintained to aid reference to this figure, for which the graph key also applies.

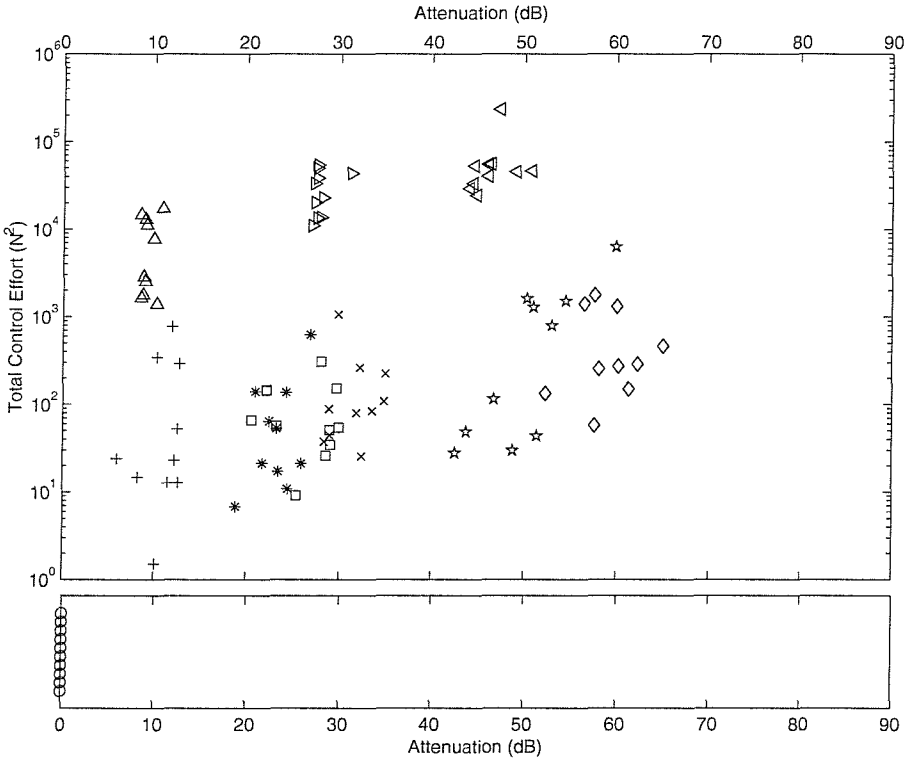

Figure 6.35: Comparison of the values of nominal AVC attenuation contributions from all the optimised structures considered in Chapters 4, 5 and 6. The graph key from Figure 6.32 applies.

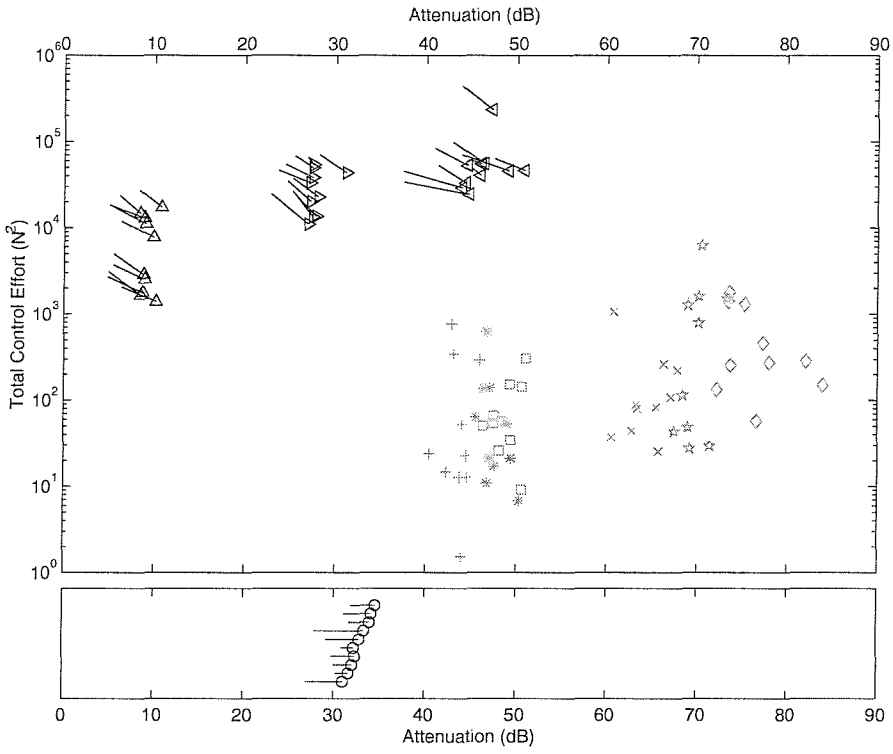

Figure 6.36: The robustness of the performance of the geometrically optimised structures and those using the optimal actuator positions on the regular structure. Vectors denoting both the 95% limits for performance and total control effort are shown, the nominal operational values are denoted by the symbol at the base of each vector. Other nominal results are shown faint. The graph key to Figure 6.32 applies.

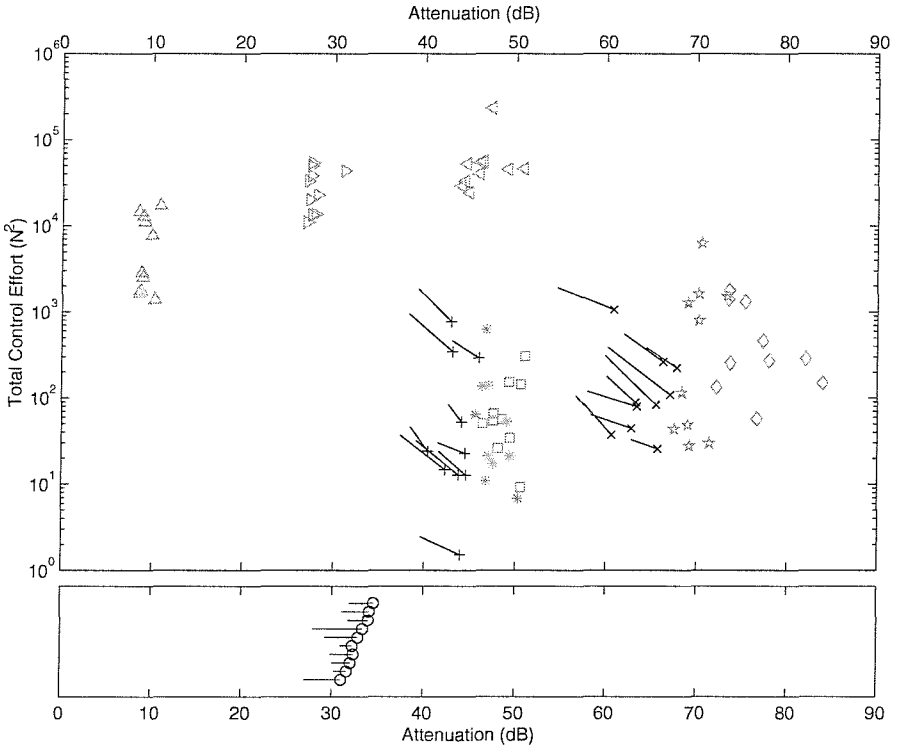

Figure 6.37: The robustness of the performance of the geometrically optimised structures and those using the optimal actuator positions on these geometries. The graph key to Figure 6.32 applies.

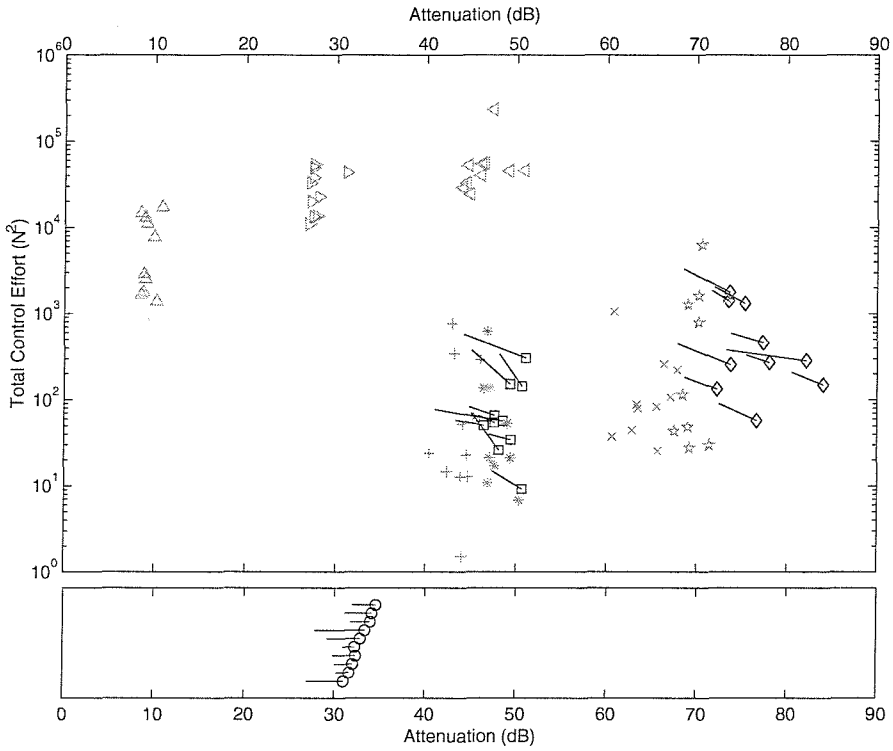

Figure 6.38: The robustness of the performance of the geometrically optimised structures and those using combined optimisation of the structure geometry and actuator positions simultaneously. The graph key to Figure 6.32 applies.

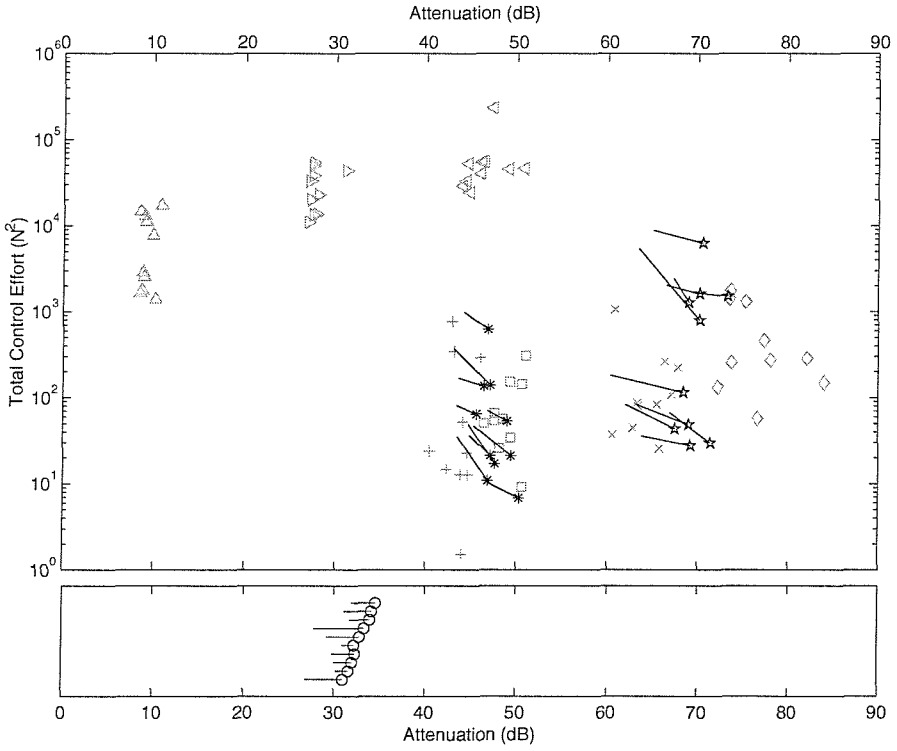

Figure 6.39: As Figure 6.38, but using the extended chromosome detailed in the text. The graph key to Figure 6.32 applies.

CHAPTER 7

Optimisation for Structures with Robust Optimal Performance

7.0 INTRODUCTION

In the preceding three chapters structures were optimised, with respect to vibration transmission, using different combinations of optimisation strategies where performance was evaluated solely on nominal performance. For all of the structures produced, the robustness was assessed to see how sensitive the performance (the amount of vibration transmission) of each structure was to the application of small geometric perturbations to the structures. The structures that are less sensitive (more robust) can then be selected (if robustness is of primary importance). Alternatively, a 95% probability limit was developed which predicts the probable worst performance likely to occur in the face of such small geometric perturbations with the uniform probability distribution used.

For these optimised structures the robustness of the performance is merely an 'accidental' consequence of the optimisation. The objective function used in the optimisation represented the nominal performance and contained no representation of the sensitivity of the performance to the optimisation variables. Thus the range of values of robustness given by the chosen structures is fixed and the structure whose performance is best in respect of robustness must be selected. A remaining question is whether it is possible to improve the 95% probability limits or the robustness and whether this would compromise the absolute value of performance. Recalling the optimised structures presented using classical techniques in Chapter 4, the perturbed performance was found to deviate greatly from the nominal performance. It was discovered, however, that the optimised structures found using genetic algorithm optimisation resulted in more robust designs than those found using the gradient search techniques. It may be possible to improve the robustness further by incorporating a measure of robustness or perturbed performance into the objective function and thus obtain a strategy to deliberately design for robust optimal structures.

This chapter describes a preliminary attempt to design for structures that have optimal nominal performance and that are, in addition, robust. Due to limitations on the time available the only optimisation case studied is that for passive optimisation (using solely geometric redesign) for

the average performance over a narrow frequency band. Different measures of robustness or perturbed performance are employed, with differing levels of additional computational expense.

This chapter is structured as follows: Section 7.1 details the perturbed performance and robustness measures used. Section 7.2 evaluates the success of using the reduced-expense perturbed performance estimates against the existing measure. Section 7.3 presents the results achieved in using the robustness and perturbed performance measures as the objective function to optimise for robust designs. The results are discussed in Section 7.4 and conclusions drawn in Section 7.5.

7.1 MEASURES OF PERTURBED PERFORMANCE AND ROBUSTNESS

In this chapter the distinction is made between robustness and perturbed performance. In preceding chapters the terms have been used interchangeably. *Perturbed performance* is represented by the 95% probability limit given in (3.23). This does not represent the range of the variability of the performance but the probable worst performance expected for 95% of perturbations. *Robustness* is defined as a measure of the variability of the performance of structure, which is represented by the spread of the histogram used in the robustness analysis results in Chapters 4, 5 and 6 (see Figures 4.25 and 4.26, for example). This could be calculated from the 5% and 95% probability limits, but the measure of robustness, r, used here is that simply defined by the difference between the 95% probability limit and value of the nominal performance, and is given by,

$$r = \left| f_{95} - f(\mathbf{x}_o) \right|, \tag{7.1}$$

where $f(\mathbf{x}_o)$ is the nominal value of the objective function in an optimal design solution and f_{95} the limit which defined that the perturbed performance of the structure is better for 95% of applied perturbations. The absolute value operator ensures that r is always positive, as it is possible that the 95% probability limit could be less than the nominal value.

7.1.1 MEASURES OF PERTURBED PERFORMANCE

The robustness analysis was performed in the preceding three chapters by applying 300 random perturbations with a uniform probability distribution to the structure. The 95% probability limit was used as a measure of the expected worst performance. This was calculated from the observed probability distribution of the performance. This number of perturbations was found to be sufficient to estimate the distribution and little improvement on

the shape of the performance distribution histograms were found when 1000 perturbations were used. The 95% probability limit was calculated for the optimised structures N_A to N_J, which were obtained using passive optimisation over a narrow band of frequencies (175Hz to 195Hz, in 5Hz steps), as reported in Chapter 4. These probability limits are denoted here by $f_{95,300}$ to be distinguish between probability limits derived by other methods in this chapter. It would be possible to use this measure of expected performance directly as the objective function in the optimisation. However, this would require 300 additional frequency-averaged performance evaluations for each objective function, and the computational expense would increase severely. To apply this to the broad band passive optimisation presented in Chapter 4 using hardware platform B (the fastest, detailed in Appendix E) would require 13 months to produce each optimal design. For the narrow band optimisation case (with a smaller number of total iterations), as considered in this chapter, this would still require over 20 days. However, it should also be remembered that due to the stochastic nature of the operation of genetic algorithms it is recommended that a number of optimised structures are normally evaluated, and one of these selected.

Thus more efficient measures of assessing perturbed performance are sought. Three alternatives are studied here, all based on computer experiments. In these the average performance of the structure is re-evaluated under a smaller, defined set of perturbations, which were scaled accordingly. Firstly a measure of perturbed performance was investigated which is based on the *one-at-a-time* (OAT) experimental method, detailed in Chapter 3. In this method 37 experiments are performed. One with the unperturbed structure, and then one for each of the optimisation variables perturbed in a positive sense (with relation to the global coordinates, see Figure 2.1), whilst the other coordinates remain unaltered. The other two perturbed performance measures use the orthogonal arrays L64 and L81, detailed in Chapter 3, and given explicitly in Appendix C. In the first, the L64 method, each row of the L64 array is used to define perturbation sets for the optimisation variables (joint coordinates). Each column is assigned to a joint coordinate, and the array defines perturbations only in the positive sense with respect to the global coordinates. The mapping between the table values and the joint perturbation is given in Table 7.1. The variable ν defines the size of the perturbations (defined by the perturbation scaling). Only the first 36 columns of the array are used, although all the experiments (as defined by each row in the tables) must still be performed to achieve the properties of the array. In the same way the L81 method uses the L81 orthogonal array. Both positive and negative sense perturbations are used in this scheme, the mapping between the table values and the perturbations are given in Table 7.2. It is noted that for both L64 and L81 arrays with the mappings used, that the first experiment (row 1) is an evaluation of the nominal

structure (with no joint perturbations). Thus the nominal performance evaluation is included in each scheme.

7.1.2 MEASURES OF ROBUSTNESS

A measure of robustness can also be incorporated into the optimisations performed here by using the noisy phenotype genetic algorithm described in Chapter 3. In this method uniformly distributed noise is applied to the phenotype before the objective function evaluation. However, the noise is only added for the evaluation and the chromosomes in the population are not permanently altered by this action. Thus, the noise only effects the objective function evaluation. This algorithm is given the label NP for identification purposes within this chapter. Weismann *et al* (1998) showed that the NP method can provide misleading results, and that the minimum of the expectation of the noisy phenotype evaluation may not coincide with a minimum in the function. This was demonstrated in Chapter 3. However with reference to Figure 4.1, in which the shape of a two-dimensional slice of the search space is given, it is seen to be relatively smooth. Here the search space represents the variation of the average performance over a broad band of frequencies and it is expected that the search space would lose its 'smoothness' as the bandwidth was decreased to the narrower frequency band considered here. This was *not* found to be so, and the appearance of the search space does not change dramatically when the narrow frequency band is studied, as shown in Figure 7.1, for the same joint. In Chapter 3 it is seen that only certain types of 'spiky' search spaces can yield misleading results. This simple investigation (of one joint variation, with all others fixed) gives some confidence that these special conditions are unlikely to occur.

An alternative noisy phenotype genetic algorithm is proposed by the author, and has also been investigated. In this optimisation algorithm both the noisy phenotype and the nominal phenotype are evaluated. The value of objective function which is the worse of the two (the maximum) is taken. As with the NP algorithm, the noise only effects the evaluation. This algorithm is labelled NP2. Thus, formally the objective function value used for the NP2 algorithm is given,

$$f_{NP2}(\mathbf{x}) = \max\left(f(\mathbf{x}), f(\mathbf{x}+\Delta)\right) \tag{7.2}$$

where $\mathbf{x}$ and Δ are the optimisation variable and perturbation vectors respectively, as defined in (3.1) and (3.7).

When implementing a genetic algorithm with an elitist strategy in OPTIONS, the best chromosome is passed directly into the subsequent population but the objective function value itself is not transferred. Instead the objective function is re-evaluated in the next generation.

When using the ordinary genetic algorithm the same objective function value results. However, with the NP and NP2 methods when the best chromosome is re-evaluated a different noise vector is added to the phenotype and a different value of objective function is likely to result. Due to the nature of the operation of the noisy phenotype genetic algorithm, this effect in the re-evaluation was not thought to affect the implementation of the algorithm.

7.2 EVALUATING DIFFERENT MEASURES OF PERTURBED PERFORMANCE

First the accuracy of the three 95% probability limits measures OAT, L64 and L81 were evaluated for the perturbed performance of existing optimised structures, described above. These limits are denoted $\hat{f}_{95,OAT}$, $\hat{f}_{95,L64}$ and $\hat{f}_{95,L81}$ respectively. The 95% probability limit, $f_{95,300}$, was used as the reference measure, allowing the average performance of the other methods to be evaluated across the ten structures. However, how the perturbation scaling compares between each method must be first considered. The probability distributions for the optimisation variables p_{OAT} , p_{L64} and p_{L81} are shown in Figure 7.2. The L81 and L64 methods have an equal number of each state for each column of the arrays and so the probabilities for each state are one-third and one-half respectively. However this is not the case for the OAT, in which each joint coordinate is only perturbed once in the 37 experiments. As the uniformly distributed perturbation measure is a continuous function, p_{300}, the perturbations may assume any value between the limits, whereas for the other methods the probability function is only defined at a discrete number of values. It is clear that if each of the perturbation functions were used with the same value of maximum amplitude that different 'strengths' of perturbations would result. For example, comparing p_{300} and p_{L81}, both have the same average perturbation of zero, but every non-zero perturbation for L81 is at the extremes of the positive and negative values of the maximum perturbations for p_{300}. Thus the variance of the perturbations would be different. Some method of defining the strength of the perturbations must be used to ensure similar strengths are used between all the perturbed performance methods. One such measure is the mean absolute deviation, *mad*. The *mad* is defined for continuous distributions as,

$$mad = \int_{x=-\infty}^{\infty} |x| \mathrm{p}_{\langle \mathrm{mtd} \rangle}(x) \mathrm{dx} , \tag{7.3}$$

and for discrete distributions as,

$$mad = \sum_i |x_i| p_{\langle mtd \rangle}(x_i), \tag{7.4}$$

both for the independent variable x, where $p_{\langle mtd \rangle}$ is the probability distribution function or probability function for the continuous and discrete cases respectively. $\langle mtd \rangle$ defines the method used to achieve the probability limit and is one of the three methods OAT, L64 or L81. i is the index for the values in the discrete distribution. The values for the average, *mad* and the variance are given in Table 7.3 for all the probability distributions considered here. It is seen that for the *mad* all the methods except OAT have the same value. Second order statistics may also be considered to define the variability of the perturbation strengths. These all have different values as also shown in Table 7.3. To make the variance for all the methods the same, a correction to v could be made. The correction factor required (to v^2) to equalise all the variances of the probability functions is shown on the bottom row of the table. Thus it would be possible to apply perturbation functions with the equal variances, although due to the one-sided nature of the L64 and OAT methods the average perturbations would not be zero (although the average value of the OAT method is small). However to normalise the variance of the OAT method would require increasing the size of the maximum amplitude of the perturbation, v, by a factor of about 3.5. With reference to Chapter 4, in which the effect of the size of the perturbations on the results of perturbation analysis was studied, it is possible that this could mean that the OAT method would no longer be operating in the linear region in this case (where the performance degradation falls off linearly with perturbation amplitude). This is an area that requires further investigation, especially with respect to how perturbations with discrete distributions can represent a uniformly distributed one. With the time available to the author it was decided to use a common value of v for all the perturbation functions so that, except for the OAT method, all the functions have the same *mad*. No further consideration was given to any higher order measure. The amplitude of the OAT function was not increased in order to have the same *mad* as this would require an increase in its amplitude by over 15 times, on grounds of maintaining operation within the linear region, as discussed above.

The values of the three 95% probability estimates when used to evaluate the perturbed performance of the 10 optimised structures N_A to N_J, first presented in Chapter 4, using a perturbation scaling of 0.01 are shown in Figure 7.3. Similar findings resulted from using a scaling factor of 0.005. The nominal value of the performance is shown by the solid circle, and the value of $f_{95,300}$ shown by an intersecting line. It is apparent that the value of $f_{95,L64}$ is the most accurate estimator when compared with $f_{95,300}$ and for some structures the agreement is very good. A more general measure of the success of using the three methods is achieved by

comparing the average performance of the estimators. This was achieved by again comparing the limits achieved using $f_{95,300}$ which uses 300 random perturbations as a reference measure. An index was used to allow comparison, the *average normalised deviation*, m, which is defined,

$$m = \frac{1}{n}\sum\left(\frac{\left|f^i_{95,300} - \hat{f}^i_{95,\langle mtd\rangle}\right|}{f^i_{95,300}}\right), \tag{7.5}$$

where $f^i_{95,300}$ is the reference 95% probability limit for structure i and $\hat{f}^i_{95,\langle mtd\rangle}$ is the 95% probability estimate determined by the method $\langle mtd\rangle$, as above. The average here was performed over 10 structures (n = 10).

The results of the comparison for two values of perturbation scaling factors are presented in Figure 7.4. The use of the L64 orthogonal array has yielded the least average error in the 95% probability limit, equivalent to roughly 10% for values of perturbation scaling of both 0.005 and 0.01 (corresponding to maximum perturbations of 5mm and 10mm). This has been achieved at about one-fifth of the computational expense of evaluating the performance of 300 perturbed structures. This is to be compared with the average errors of about 30% and 60% for 5mm and 10mm perturbation sizes respectively, for the other two methods. It is not clear why $f_{95,L64}$ should provide the best estimate. In particular, why it is better than $f_{95,L81}$ which uses positive and negative perturbations, and not just positive perturbation as for $f_{95,L64}$. Finally, it should be noted that these comparisons have been made with uniformly distributed perturbations. The results are likely to depend on the nature of the distribution and, for example, using normal probability distribution may not yield the same results.

7.3 OPTIMISATION FOR ROBUSTNESS AND PERTURBED PERFORMANCE

The measures of robustness and perturbed performance described above were then used as the basis to find design solutions that have good nominal and robust performance. Ten optimised structures were produced using each of the above methods: NP, NP2, OAT, L64 and L81. The noise added to the phenotype in the NP and NP2 methods was uniformly distributed, as that shown in Figure 7.2 a) with v equal to 0.005. For all of the methods the performance of the structure was optimised over a narrow band of frequencies; 175Hz to 195Hz in five 5Hz steps, as in Chapter 4. The genetic algorithm used was also the same; 1000 evaluations consisting of

5 generations each of population size 200. The remaining genetic algorithm parameters are detailed in Table D.6 in Appendix D.

Using hardware platform B (detailed in Appendix E) the approximate time taken to evaluate each candidate is given in Table 7.4. The best structures resulting from each optimisation method are shown in Figures 7.5 to 7.9. Each is figure shows the optimised structure geometry, the frequency response of the optimised structure against that of the unoptimised structure, and the history of the objective function after each generation. For the optimisation methods OAT, L64 and L81 the objective function is the 95% probability limit, the nominal performance is also shown at the end of each generation as a dotted line. For the NP and NP2 methods the value of the objective function shown is that for the evaluation of the phenotype *without* added noise.

For the ten optimised structures produced using each of the robust and perturbed performance optimisation methods, the perturbed performance was accurately evaluated using the more accurate parameter $f_{95,300}$. To show the effect on the perturbed performance of structures produced using such methods, as compared to those using an objective function consisting of purely nominal performance, the results are compared against the limit $f_{95,300}$ for the structures N_A to N_J generated in Chapter 4. The performance of the best structure (evaluated by the value of the objective function used) for each robust and nominal optimisation method is shown in Table 7.4. A negative value of change in the value of the performance parameters given in this table indicates an improvement in performance. The 95% probability limit was calculated using a perturbation scaling of 0.005 (corresponding to a maximum joint coordinate perturbation of 5mm).

The nominal performance has worsened slightly for the L64 and L81 methods. The maximum improvement in nominal performance was achieved by the OAT method where the best structure has had its nominal performance improved by almost 6dB. However, as discussed, the nominal performance is not necessarily practicably realisable, and the 95% probability limit is a better parameter by which to assess performance. It is seen that this structure also has the largest increase in 95% probability limit of 5dB, this improvement is followed closely by that for the NP2 method. For the best structures for each optimisation case, it is seen that both the values of nominal and perturbed performance are very similar for the L64 and L81 methods, compared with those produced from the nominal optimisation.

The average performances for structures produced using these methods (evaluated over ten structures) are given in Table 7.5 and are also shown in Figure 7.10. These have been assessed using perturbation scalings of 0.005 and 0.01. Values are shown for the nominal performance,

the 95% probability limit and the robustness (7.1). It is seen that only for the L81 optimisation method has the nominal performance been worsened. There is little change for the NP method, but a reduction of almost 2dB for the OAT method. Although as discussed above, the use of the nominal performance is not recommended as a measure of practical performance. Similar relative success is found for the average 95% probability limits, for both the 0.005 and 0.01 perturbation size, although in each case improvements are seen over the average performance of the nominal performance optimised structures. Since this parameter is the best gauge of expected practical performance, it is seen that the best average improvement in performance has been achieved with the OAT method and the NP2 method. The change in average robustness is also shown, and a similar trend exists between the results for the two perturbation sizes. The best reductions are found for the OAT and then the NP2 methods, for both perturbation sizes.

It is not obvious how the irregular geometries of these structures lead to a performance that is more robust, when compared with the best structure optimised on nominal performance (see Figure 4.17). It is also interesting to note that in Figure 7.9 the frequency region where the minimum vibration level occurs is not actually within the narrow frequency band using for the objective function.

The above results suggest that the OAT method has provided the better average results on grounds of nominal performance and 95% probability limit. However the computational expense required to achieve the optimised structures can be important and the results are also shown normalised by the evaluation time in Figure 7.11. This provides a 'figure of merit', and compensates any gain in performance for the expense required. With this consideration, the optimisation method NP2 is seen to be the most successful method (better than the OAT method) providing the best improvement per additional computational expense.

7.4 DISCUSSION OF RESULTS

Two optimisation methods designed to produce structures with robust performance have been investigated. Their optimisation strategies differ. The robustness measures, used in the noisy phenotype methods, NP and NP2, bias the search away from areas where the performance is sensitive to small changes in the optimisation variables. The absolute performance is still minimised, but only in areas of the search space where performance is robust. The perturbed performance method evaluates the performance due to perturbations, and provides a measure of the expected performance. The improvement in the perturbed performance may arise by the optimisation finding regions in the search space that are very optimal, but relatively unrobust,

or regions that are (less) optimal but more robust. The perturbed performance measure cannot distinguish between the two. Thus it is possible to produce a structure with a good perturbed performance that is still very sensitive to geometric changes. In some cases, a large variation in the performance, if so extreme, would not be a good design solution, even though the expected perturbed performance yields an optimal nominal value. Although in the results presented here no such instances occurred. In general the L64 and L81 methods resulted in the smallest improvement in robustness, but the OAT method produced the best improvements.

The measures of perturbed performance estimates show that the L64 method is the best reduced-expense method for evaluating the 95% probability limits, for both sizes of perturbations studied. However, this measure was not found to be the best to use for the objective function when optimising for structures with improved perturbed performance. In this case the OAT method is better. Therefore, a good measure of evaluating perturbed performance, when used as a less-expensive estimate in place of a more accurate method, does not imply it is the best measure to use for the objective function of an optimisation. It is also surprising that the simple OAT method has performed so well, given its simple construction compared to the other designed methods, L64 and L81. When there is a high level of interaction between variables, the benefit of the design of orthogonal array is to provide good estimates of a full factorial experiment, however this does not seem to be borne out here. Although the OAT method strictly relies on little interactions between the variables, the optimisation task here obviously has strong interactions between the variables. Only the small perturbation size can justify the application of such methods. However, the simplest experimental array is seen to be superior over the L64 and L81 arrays. One reason may be because is has a small value of *mad* and variance. Thus its perturbation strength is actually less, and thus the effect of variable interactions may be less on these grounds. Thus, the comparison between the OAT method and the L64 and the L81 methods with the amplitudes used may not be strictly valid. This is also suggested with reference to the optimisation histories for each of the best structures, in Figures 7.7 to 7.9. It is seen that for the OAT method the 95% probability limit (estimate) of the best structure candidate in each generation is virtually indistinguishable from the nominal performance. Further investigation is required in this area.

The NP2 method in this instance is shown to be a better technique than the NP method. It uses a noisy evaluation of the phenotype but only uses this result if it is worse than the nominal evaluation. In the NP2 method only the addition of noise to the phenotype which diminishes the true chromosome's objective function value is allowed to affect the natural operation of the genetic algorithm. This reduces the probability of the chromosome being subsequently selected from the current population. The other effect of the noise, which would normally augment the

true objective function value, and grant the chromosome a higher probability of selection from the current population is ignored, whenever it occurs, in the NP2 method. In this case, if the increase of the true value is large, then the chromosome does not represent a robust solution, but it relies on further subsequent noisy evaluations (in subsequent generations), such that the true objective function is not augmented by the action of the noise. Then the true or diminished value results and the chromosome is given a low probability of subsequent selection. The NP2 method distinguishes against this scenario immediately. Therefore it reduces the number of unrobust genotypes which might normally survive with the NP method. Even though these genotype represent unrobust solutions it is possible that through the crossover and mutation operators, good, robust genotypes might result. However, the better success of the NP2 method implies that this is not significant. As with the NP method, if a chromosome represents a relatively robust solution, the addition of noise to the phenotype will have little affect on the chromosome survival.

It is also noted that using a scaling of v=0.05 for the noise added to the phenotype, the effective 'perturbation strength' applied to each chromosome evaluated during the genetic algorithm had a *mad* of only $v/4$. This is a half of that used for the L81 and L64 methods, and thus better success achieved with the NP and NP2 methods may also be partly attributed to the perturbation strength, as with the OAT method as discussed above.

Considering computational expense, the NP2 method is seen to be better than the OAT method. The relevance of the computational expense is reinforced with reference to Table 7.4, which shows the time required to produce each optimised structure. Only a small frequency band average was used here, mainly because the computational time available in the latter stages of the work presented in this thesis. The author also had access to high performance computational facilities. In many instances with a more realistic problem (for example the broad band frequency average, used in Chapters 4, 5 and 6) and more modest computational facilities, that is might not be feasible to execute the more expensive robust optimal measures. Thus the additional performance achieved using the OAT method is small with relation to the extra cost required. Thus the NP2 method is deemed to be the best optimisation method in this study. It has only required a factor of two increase in the computational expense for a 5dB improvement in practical performance.

7.5 CONCLUSIONS

At the end of this study of robust, optimised structures a preliminary attempt was made to produce optimised structures with optimal and robust performance using genetic algorithm

optimisation. This was achieved by the geometric redesign of the structure to optimise the performance of the structure over a narrow frequency band. The same optimisation was reported in Chapter 4, optimised only on the nominal performance of the structure. Two classes of objective function were used, one that optimises the performance using only regions of robust performance on the search space (robustness methods) and one that optimised the expected perturbed performance value.

In the first robustness method noise is added to the phenotype of each chromosome before evaluation of the objective function (NP). The author proposed a variation to this method in which the objective function was evaluated with and without noise added to the phenotype. The worst performance between the two is taken (NP2). These methods require only one and two evaluations respectively. Three reduced-expense perturbed performance were studied: one based on a simple perturbation of each optimisation variable at a time (OAT, using 37 evaluations), and two based on fractional factorial experimental design (L64 and L81, using 64 and 81 evaluations). The L64 only uses positive perturbations, while the L81 incorporates both positive and negative perturbations. The accuracy of these three methods over an existing and more accurate, but more computationally expensive method (using 300 random evaluations) was performed. For two sizes of perturbation the L64 method was found to be the best estimate with approximately 10% error in the 95% probability limit.

Ten optimised structures were then achieved using each of the five measures as the value of the objective function. Their robust performance was evaluated using the existing more accurate, but more computationally expensive, perturbed performance measure. The optimisation success was made by a comparison with optimised structure achieved by only using the nominal performance as the objective function. The performance for the best structure and the average of the performance of ten optimised structures resulting from each optimisation were studied. All the methods, except one, were found to have improved the average nominal performance although, as discussed, this measure is of dubious significance. The best structure produced by the OAT method had an improvement on the nominal performance by almost 6dB. The same structure also had an improved 95% probability limit by 5dB. On average, improvements in the 95% probability limit were found for all methods. The OAT method had the best average improvement in the 95% probability limit by about 3dB and also the best average improvement in the robustness by about 4dB. The average perturbed performance improvements were similar for both sizes of perturbation used.

When considering the improvements achieved using the optimisation methods, the range of additional computational expense was considered. Normalising the improvements with the computational expense enables the most effective method to be identified. On these grounds the

NP2 method is the best method outright for all performance considerations. Any small improvements on this accredited to more expensive methods, including the OAT, are outweighed by the additional computational expense required. The most efficient, NP2 method requires an increase in the computational expense of only a factor of 2.

L64 Value	Perturbation
1	0
2	+v

Table 7.1. The mapping between the L64 orthogonal array values and the joint perturbation sizes.

L81 Value	Perturbation
1	0
2	+v
3	-v

Table 7.2. The mapping between the L81 orthogonal array values and the joint perturbation sizes.

Statistical property	Perturbation method			
	p_{300}	p_{L81}	p_{L64}	p_{OAT}
Average	0	0	v/2	v/37
mad	v/2	v/2	v/2	v/37
σ^2	$v^2/3$	$2v^2/3$	$v^2/4$	$0.026v^2$
correction to v^2 to equalise σ^2	1	1/2	4/3	13

Table 7.3. The statistical properties of perturbation methods studied.

Optimisation method	Change in objective function value for the best optimised structure performance, compared with that using the nominal objective function (dB).		Approximate evaluation time per structure (hours)
	Nominal performance	$f_{95,300}$ ν= 0.005	
nominal	0	0	1.6
NP	-1.3	-0.2	1.6
NP2	-3.2	-4.4	3.3
OAT	-5.7	-5.0	62
L64	0.8	0.1	110
L81	0.4	0.1	140

Table 7.4. A comparison of the performance of the best structures using different optimisation methods and structure evaluation times. A negative change in performance indicates an improvement.

Optimisation method	Average structural performance compared with those for the structures obtained using nominal objective function (dB).				
	Nominal performance	$f_{95,300}$		r	
		ν= 0.005	ν= 0.01	ν= 0.005	ν= 0.01
nominal	0	0	0	0	0
NP	-0.1	-0.5	-0.6	-1.0	-0.8
NP2	-0.8	-1.8	-2.1	-3.2	-2.8
OAT	-1.9	-2.8	-3.1	-4.2	-3.8
L64	-0.9	-1.5	-1.4	-2.3	-1.7
L81	2.5	-0.3	-1.0	-1.5	-1.9

Table 7.5. A comparison of the average nominal performance, 95% probability limits and robustness of optimised structures using different optimisation methods, evaluated using two maximum perturbation sizes, ν. A negative change in performance indicates an improvement.

GLOSSARY OF SYMBOLS FOR CHAPTER 7

The major notation used in this chapter is listed below. Other symbols are defined locally.

f_{95}	Value of 95% probability limit
$f_{95,<mtd>}$	Value of 95% probability limit achieved using method <*mtd*>
f_{NP2}	Value of NP2 noisy phenotype objective function
m	Average normalised deviation
mad	Mean absolute deviation
$p_{<mtd>}$	Probability (density) function for method <*mtd*>
r	Robustness
v	Joint perturbation size
σ^2	Variance

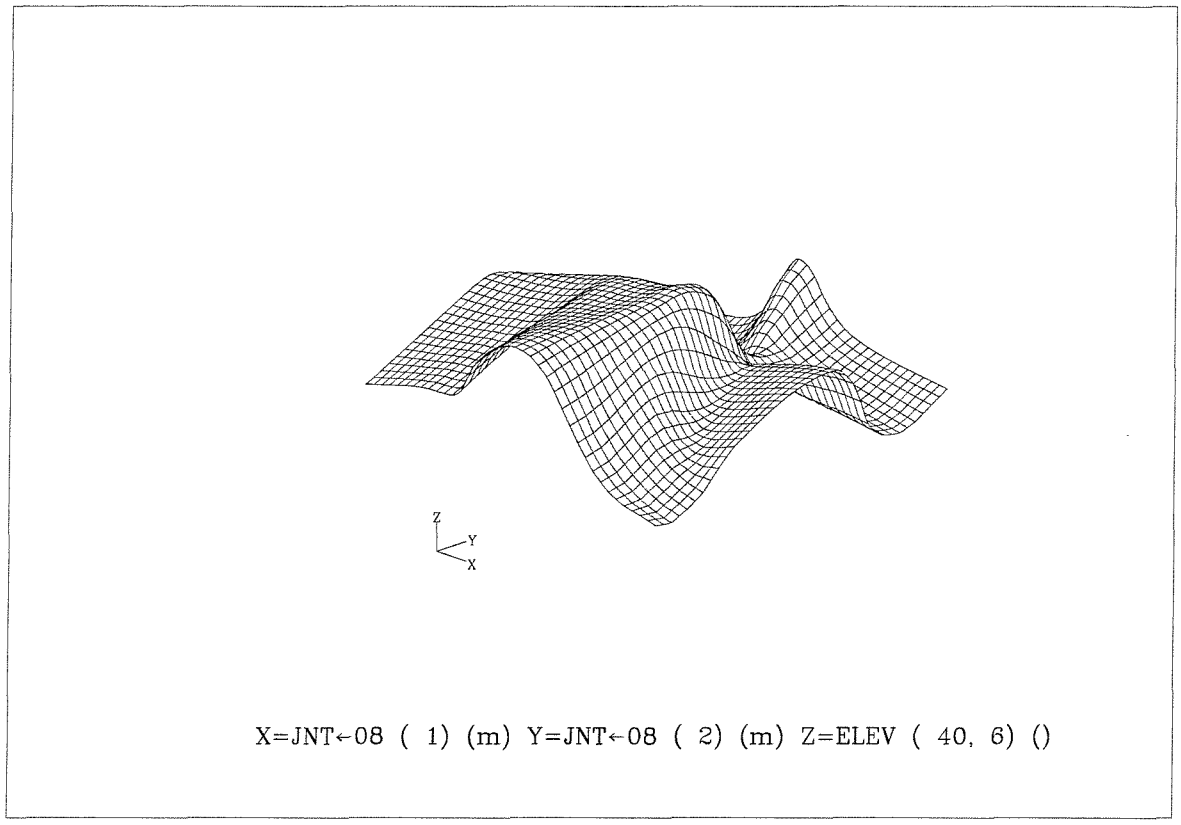

Figure 7.1: Contour plot of the narrow band objective function against x and y coordinates for joint 8 within the optimisation limits.

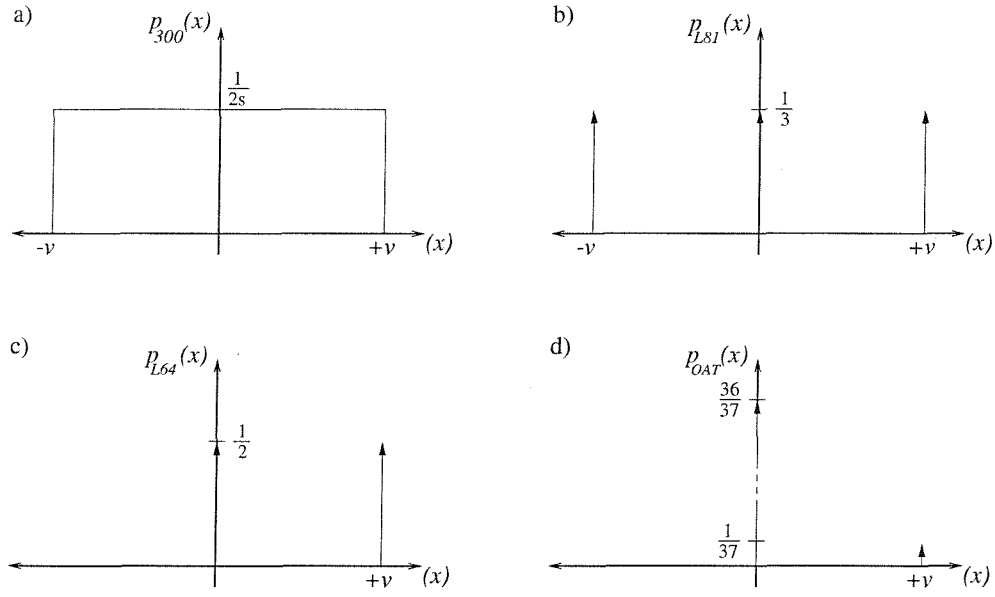

Figure 7.2: a) The probability density function p_{300}, and the probability functions b) p_{L81}, c) p_{L64} and d) p_{OAT}.

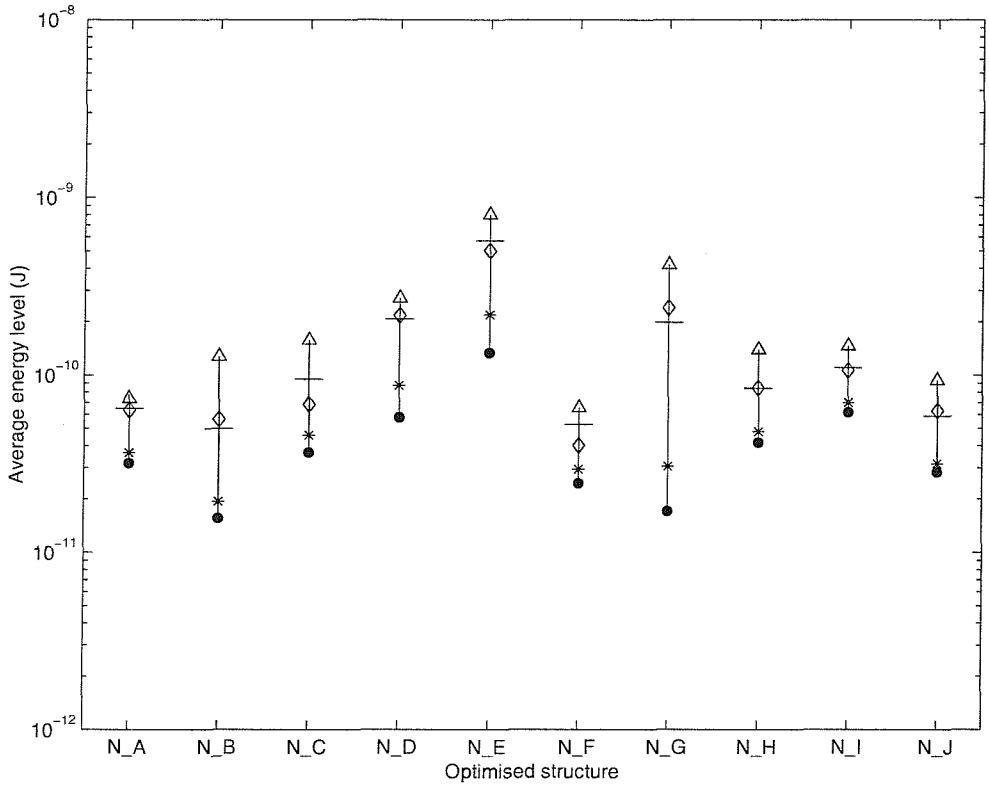

Figure 7.3: A comparision of the 95% probability limits evaluated by different methods, using a perturbation scaling of 0.01, for the ten optimised structures N_A to N_J. The nominal performance is shown by • and the existing 95% probability limit p_{300} by the horizontal intersecting line. Other methods shown are: p_{OAT} *; p_{L64} ◇; p_{L81} △.

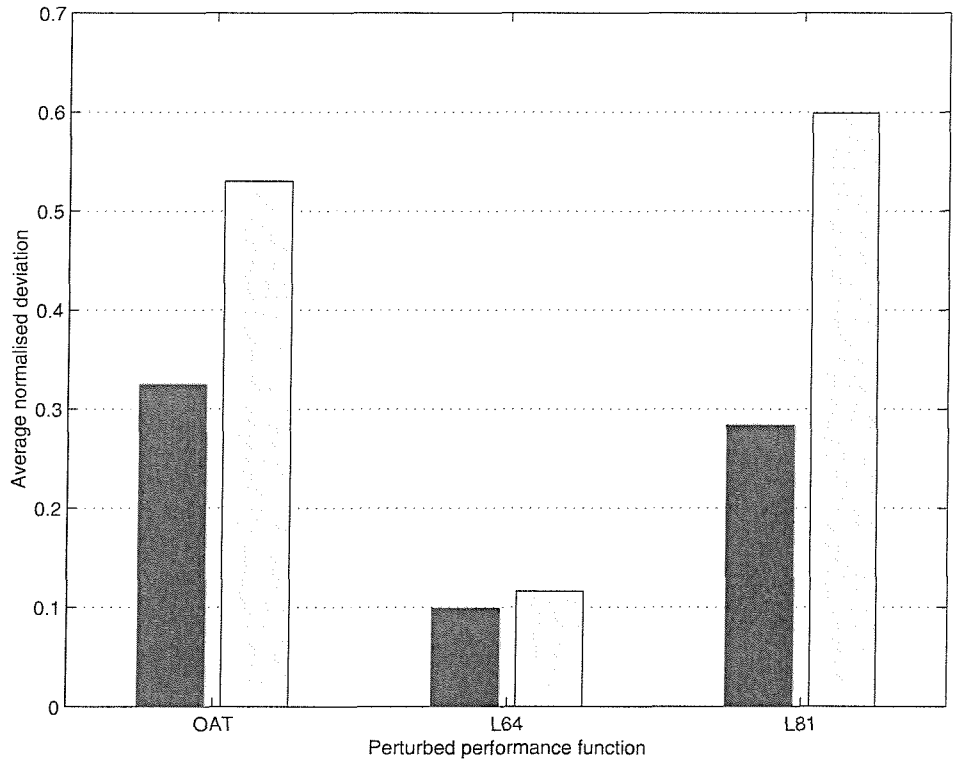

Figure 7.4: A comparison of the accuracy of the reduced-expense probability limit estimate methods against using 300 random perturbations, for a perturbation scaling of 0.005 (dark) and 0.01 (light).

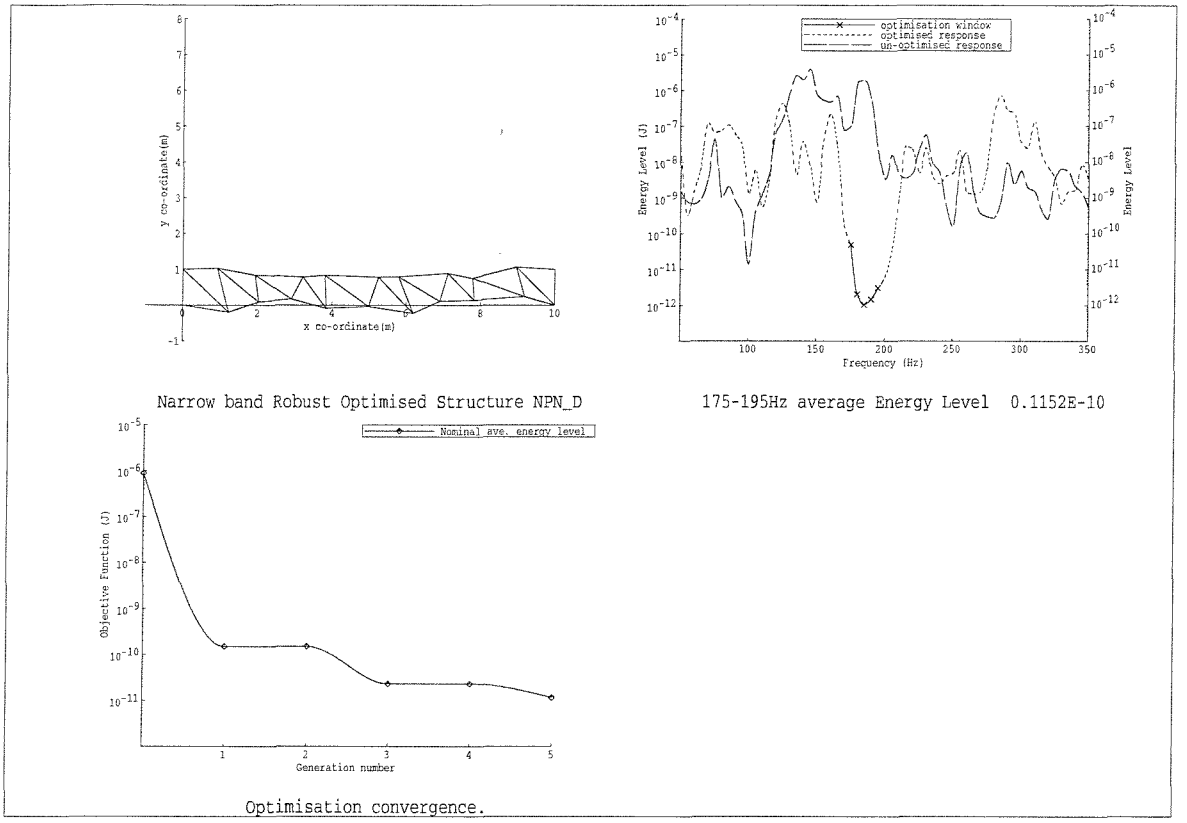

Figure 7.5: The best optimised structure produced using the noisy phenotype genetic algorithm, NP, showing the structure geometry, frequency response, optimisation history and robustness of each evaluation. See text for details.

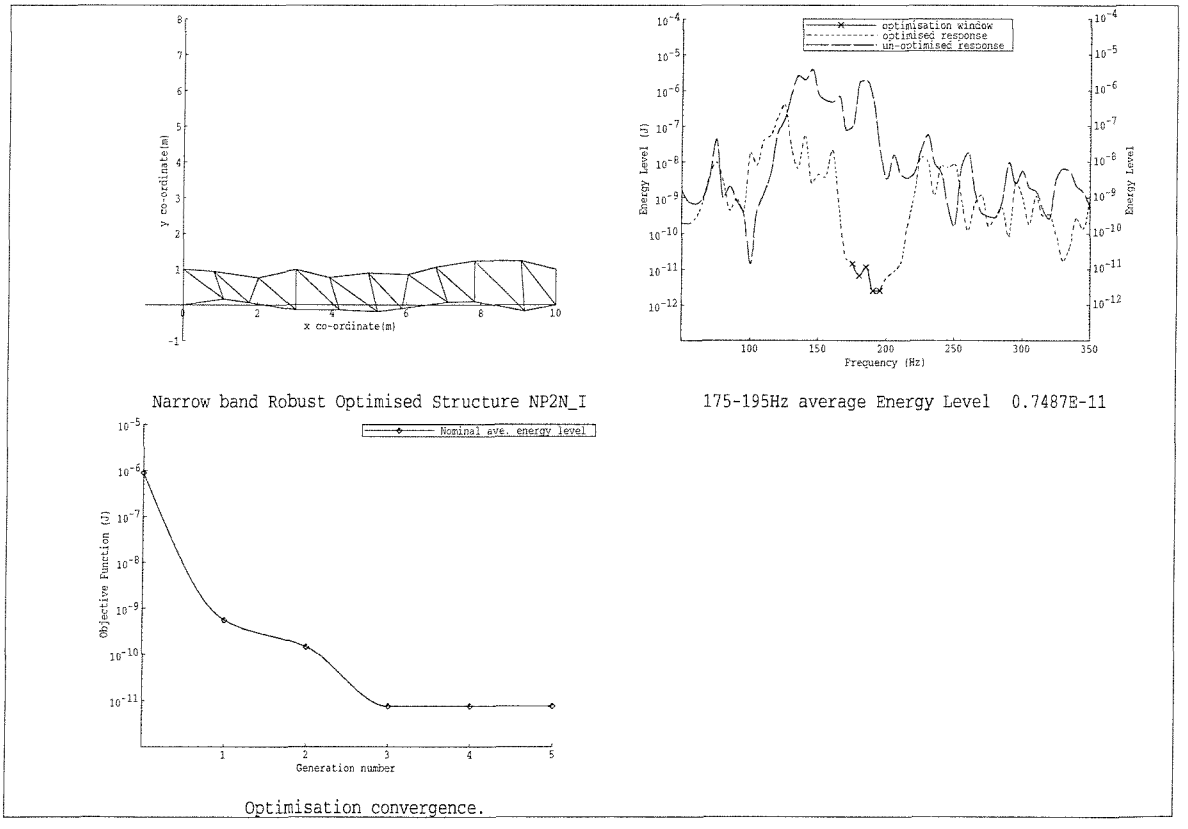

Figure 7.6: The best optimised structure produced using the author's variation on the noisy phenotype genetic algorithm, NP2, showing the structure geometry, frequency response, optimisation history and robustness of each evaluation. See text for details.

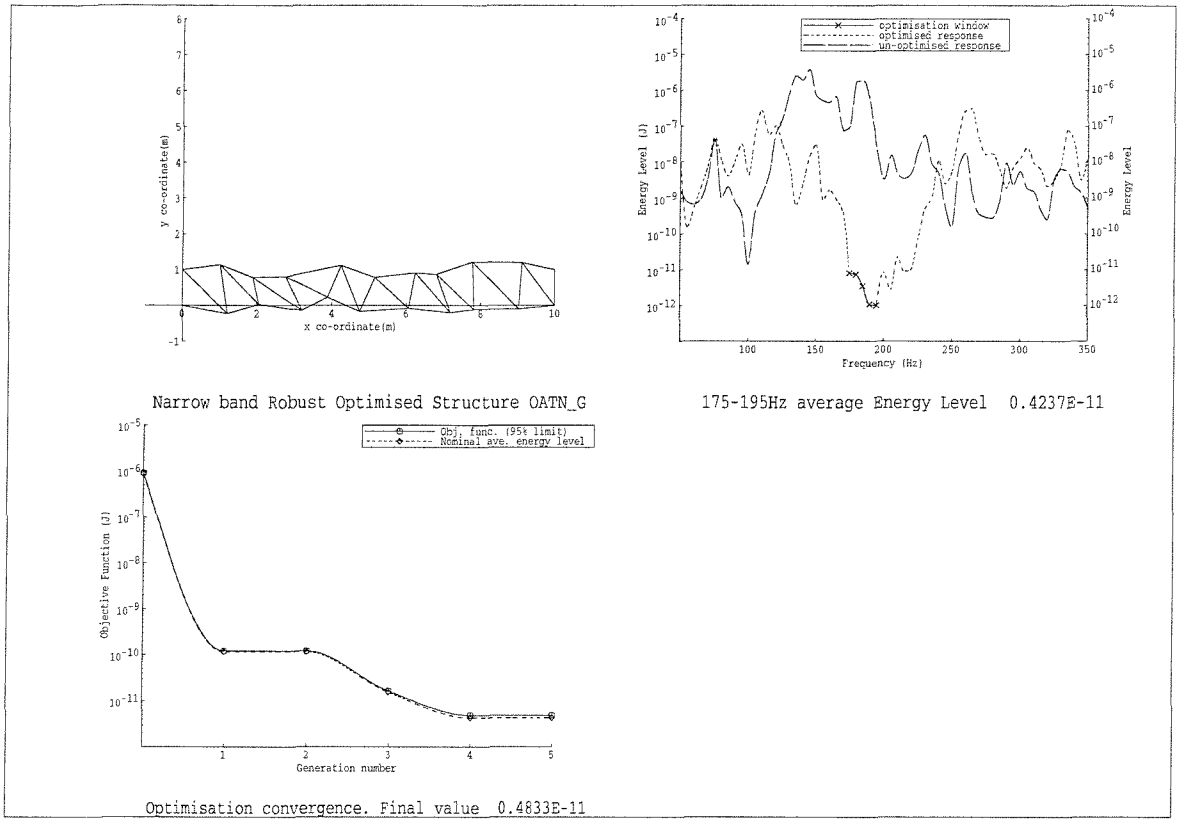

Figure 7.7: The best optimised structure produced using the OAT estimate of the 95% probability limit as the objective function, showing the structure geometry, frequency response, optimisation history and robustness of each evaluation. See text for details.

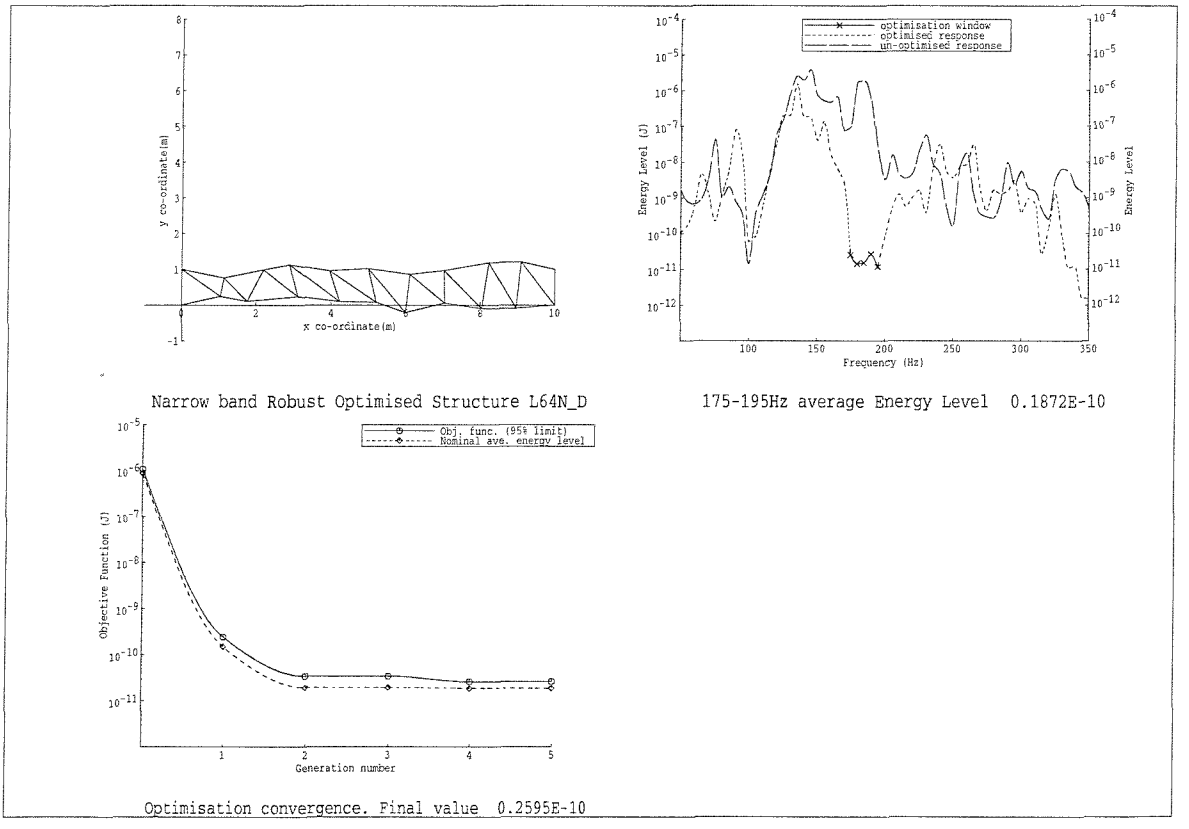

Figure 7.8: The best optimised structure produced using the 95% probability limit, estimated by the L64 method, as the objective function, showing the structure geometry, frequency response, optimisation history and robustness of each evaluation. See text for details.

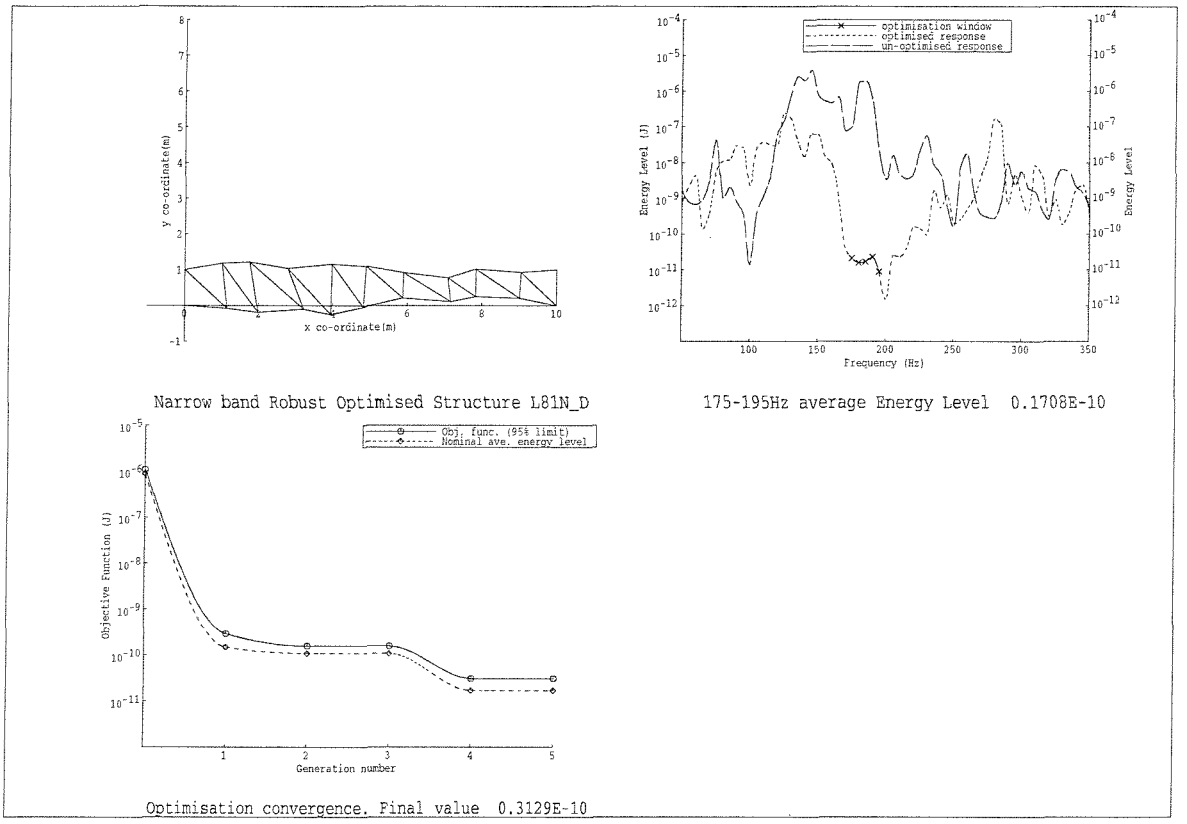

Figure 7.9: The best optimised structure produced using the 95% probability limit, estimated by the L81 method, as the objective function, showing the structure geometry, frequency response, optimisation history and robustness of each evaluation. See text for details.

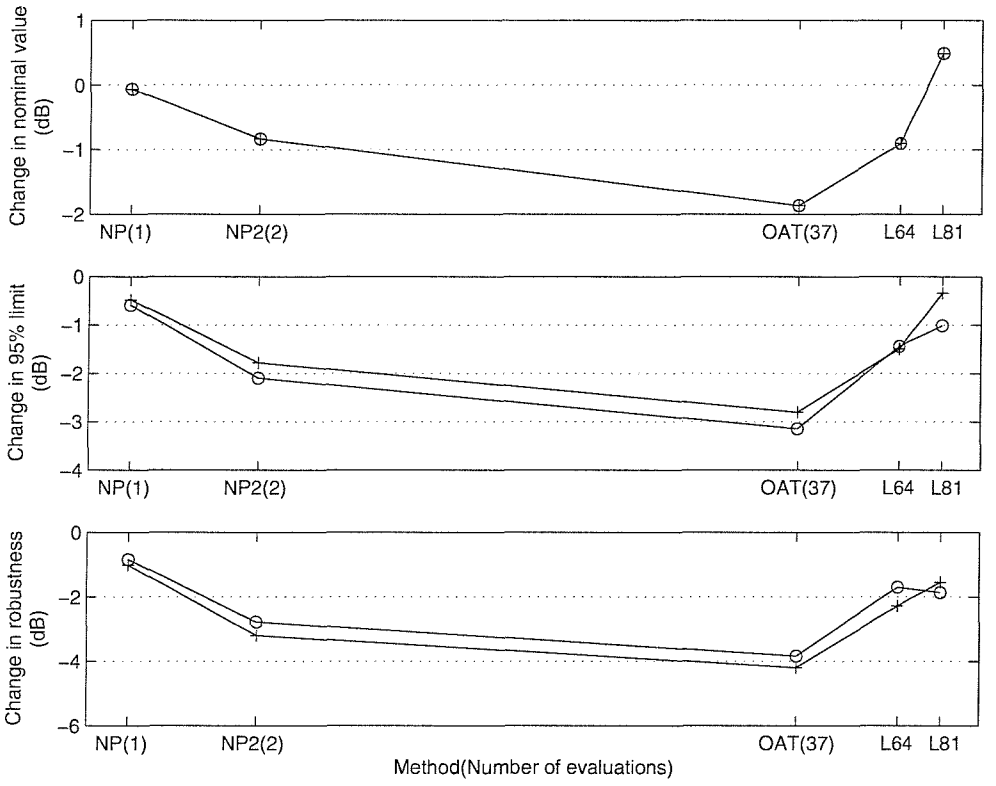

Figure 7.10: The average change in nominal performance, 95% probability limit and the robustness for the optimised structures achieved using robust or perturbed measures of performance as the objective function, against structures produced using a nominal performance objective function. For perturbation scaling 0.005 +, and 0.01 ◯.

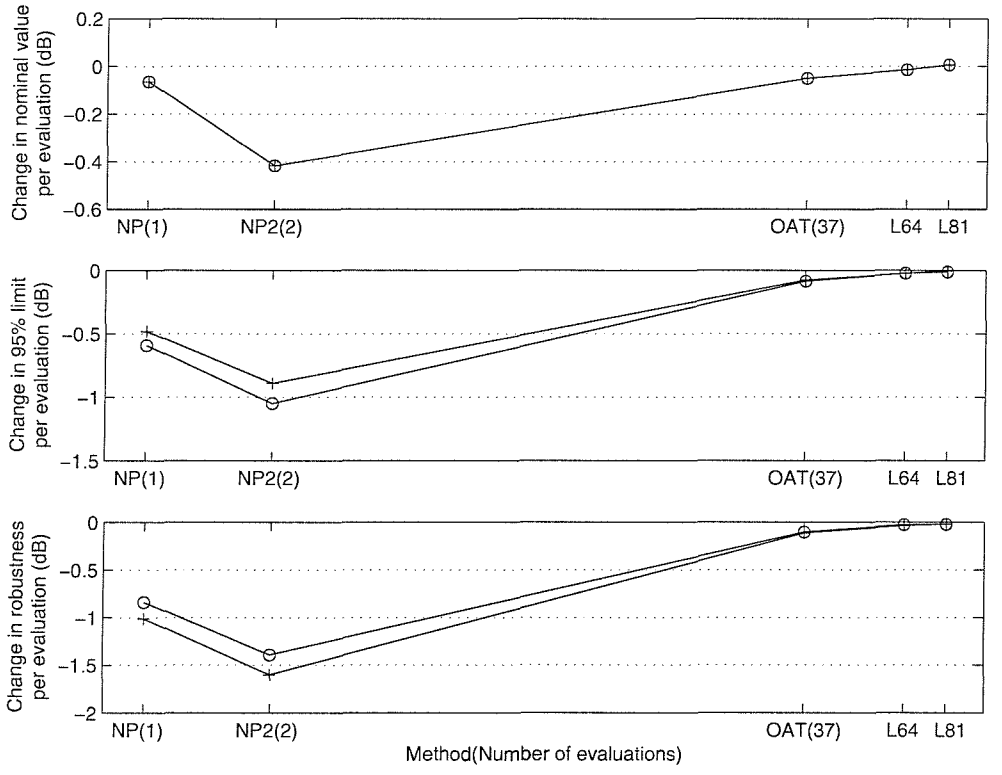

Figure 7.11: The results given in Figure 7.10, when normalised against the computational expense required.

CHAPTER 8

Conclusions and Suggestions for Further Work

8.0 INTRODUCTION

The work presented in this thesis has reported a study of the optimisation of a two-dimensional cantilever structure so as to reduce the vibration transmission from the base to the end. This aim was achieved by two methods: geometric redesign and the application of feedforward Active Vibration Control (AVC) techniques using optimal actuators positions. These methods were each employed alone, and then in combination, to produce optimal structure designs. The robustness of the performance (and the total control effort required by the AVC system, where applicable) was studied. It was then possible to distinguish between those optimised structures whose performance is sensitive to small geometric perturbations (which might occur due to manufacturing tolerances, for example) and those structures which were *robust* to such effects, and thus are more practical. Finally, a measure of robustness was incorporated into the optimisation algorithm so the optimisation process sought structures whose performance was both nominally optimal and robust. The major conclusions from the work are summarised below. Then, suggestions for further areas of study resulting from the work presented are given.

8.1 CONCLUSIONS

The geometric (or passive) optimisation of the structure was performed using both classical optimisation methods (*e.g.*, those using gradient based search methods) and genetic algorithm optimisation in order to reduce the vibration transmission. The genetic algorithm has advantages over the classical optimisation methods due to the multi-modal nature of the search space for these problems. The vibration was reduced at a single frequency, and the average vibration was also reduced over narrow and broad frequency bands. Good success in reducing the vibration was found using all optimisation methods. The best reductions in nominal performance were seen for some of the classical methods. However, when the performance was studied in the face of small geometric changes the optimised designs produced by the classical methods were found to be unrobust, in some cases to such an extent that it is highly unlikely

that the nominal performance would be realised in practice. When the robustness of the ten structures produced from the genetic algorithm optimisation was studied, variation in the values of robustness was found. The best practical structure could then be selected for an application encountering similar geometric perturbations in practice. This is often different to the 'best' structure selected by nominal performance alone. It was also found that, in general, the wider the frequency band over which the average vibration was evaluated, the more robust the performance of the structures. A brief study of the transmission response of the optimised structure using modal analysis showed that the reductions were achieved by a modal redistribution, such that modal frequency clusters, often relating to peaks in the vibration response, were dispersed. Although the dispersion of the modal clusters was found to be due primarily to the irregularity of the structure. In the subsequent optimisation studies reported below the performance was only that averaged over the broad frequency band, and genetic algorithm optimisation was used, unless otherwise stated.

The next optimisation strategy investigated was to use AVC techniques (active optimisation) to reduce the vibration transmission. The first optimisation task considered here is to find the optimal actuator positions on the unoptimised structure so as to achieve the best value of reduction. This was achieved for one, two and three actuators using an exhaustive search of all possible actuator configurations. The robustness of the performance of the ten best actuator positions for each case was evaluated to find systems with good nominal performances that were the most practically realisable. The robustness of the control effort required by the AVC also needs to be considered, to ensure that the highest expected value of control effort can be met in practice. At this stage the parameter used to represent the vibration transmission, which is the energy level in a beam due to its flexural vibration, was briefly compared against other alternatives; one representing the overall vibrational energy (including rigid body motion) and two only using velocity measurements. It was found that the parameter used up until this point in the thesis, even though not the most comprehensive measure, was sufficient. Especially when used for such a system comprised of thin, flexible beams. It was also found that if only velocity measurements were to be used (in an experimental system, for example) that the rotational velocity is important in providing a good estimate of the overall vibrational energy.

The two final optimisation strategies were based on combinations of both passive and active optimisation. The first was to find the best actuator positions for the structures with geometries which had first been passively optimised, the second was to perform the optimisation of both geometry and actuator positions simultaneously. Both strategies achieved designs that produced better reductions per actuator than those produced by the active optimisation using the unoptimised, regular structure. Additionally the control effort required was found to be much

smaller. So, it can be concluded that more effective and efficient use of AVC results from both geometric and actuator position optimisation, the simultaneous optimisation of both producing the best results. Robustness analysis, again, was used to identify the most practical optimal structures, and is discussed below. The results for the passive and active optimised structures with two actuators are summarised in Table 8.1.

For structures designed using the different optimisation schemes, analyses were performed to gain an insight into the mechanisms by which the reductions in vibration had been achieved, and also the role of the AVC system, where applicable. It was found that the geometric optimisation produced a reduction of power input to the structure from the vibration source and also a redistribution of structural power dissipation around the structure so as to reduce the vibration of the end beam. The application of AVC was also found to provide a similar reduction by power redistribution but had no real effect on the power input to the structure by the unwanted vibration source. Less actuator power was found to be required by an AVC system to achieve a set level of reduction where geometric optimisation had also been used. For the application of AVC with two or three actuators, the AVC system was seen to act to block the power transmission along the structure past the structure bay containing the actuator furthermost from the vibration source. This means that the vibration reduction would be less sensitive to changing conditions at the end of the structure, for example, by additional mass loading.

For all the candidate structures produced using the above optimisation strategies (except classical optimisation) their variation in robustness was directly compared but no one strategy was found to be superior in terms of the robustness of the optimised structures produced. For each structure a 95% probably limit was evaluated (using 300 random geometric perturbations) to predict the minimum performance which could be expected for 95% of similar perturbations encountered in practice. In general, no one optimisation technique was seen to be superior with respect to the overall robustness of the structures produced. Although between individual structures the use of the robustness analysis enabled the more practical structures to be selected.

All the optimisations detailed above have sought to optimise the nominal performance of the structures, and then the most practical structure has been selected using a post-optimisation robustness analysis. An attempt was then made to incorporate a measure of perturbed performance into the optimised performance parameter to optimise for both optimal and robust solutions. This was studied to reduce the vibration transmission over the narrow frequency band using geometric redesign. More efficient estimators of the 95% probability limit were required, and firstly these were evaluated against the existing measure. Then the estimators

were used as the parameter that was optimised in order to produce optimised structures. Additionally two versions of noisy-phenotype genetic algorithm were also employed, one previously reported and a variant suggested by the author. The perturbed performance of the resulting structures was then re-evaluated using the original, more accurate 95% probability limit. It was found that the best estimator of the more accurate 95% probability limit did not yield the structures which had the best practical performance when used as the optimised parameter. After considering the extra computational expense required for the optimisation, the optimisation method which gave structures with the best improvement in perturbed performance required only twice the computational expense of the that required for nominal performance optimisation.

8.2 SUGGESTIONS FOR FURTHER WORK

The structure used as the focus of this thesis is a simplified model of a typical structure. The most significant simplifications that have been made are that the structure is two-dimensional, and where active control of vibration has been applied the actuators were considered not to effect the properties of the beam on which they are placed (*e.g.*, actuators were assumed mass-less). Whilst these simplifications do not affect the validity of the methods developed and the overall findings presented, the actual results are not directly applicable in practice. A three-dimensional structure should be therefore be studied, and additional modelling refinements applied to improve the models accuracy. Although practical verification has been performed for an geometrically optimised two-dimensional structure (Keane and Bright, 1995), the optimisation methods need to be applied to an actual physical structure design. At the time of completion of this thesis, an industrially funded research project has recently commenced in the Computational Engineering and Design Centre at the University of Southampton. The objective is to design, build and test three optimised structures using three optimisation strategies: geometric optimisation, application of active control and the use of both optimisation techniques. (Keane *et al*, 1998).

Feedforward control methods have been assumed in this thesis as a way in which the AVC system would be implemented. Further work clearly needs to be done on the practical implementation of such systems for various kinds of disturbance, and in the relative performance of global feedforward control systems compared to local feedback systems (Preumont, 1997). Also, it has been assumed that sufficient 'time-advance' exists in the reference signal in order that no causality constraints on a controller exist. If the broadband vibration source is near the structure base then this may limit the effectiveness of the AVC at

high frequencies. Thus, in practice, this may also need to be considered when finding the optimal actuator positions. The consideration of such issues here would have unnecessarily uncomplicated the optimisation problem, such issues are specific to the application and there is no merit in including them on an arbitrary basis.

The research presented here has covered much ground, investigating a number of different optimisation strategies and an analysis of the robustness of the performance in each case, so that a comparison of the success of using each strategy could be presented. Because of this schedule, however, little time was available for any in-depth analysis of the mechanisms by which the optimisation process had achieved better dynamic performance. Power analyses were performed to show the power changes on a macro level, *i.e.* changes in input power, actuator power and power in Beam 40. However, to gain a further understanding a full modal analysis of the optimised structures needs to be performed, including the evaluation of the modeshapes of the structure. How these modeshapes change, due to optimisation, at the positions of power input and output to the structure is probably the key to a full understanding of the mechanism of the optimal control achieved. In particular, with active control the interaction between the active control system and the structure geometry could then be investigated. This would help to explain why, when using active control on a geometrically optimised structure, the active control is more effective and efficient than when using a geometrically unoptimised structure. The analysis of the modeshapes might also help explain the reasons why some structures are more robust than others, even though a clue to this lies in the modal frequency distribution for the optimised structures presented.

The perturbation analysis performed here is based on a uniform distribution of joint position perturbations might be appropriate to represent manufacturing tolerances. It is difficult due to the multi-modal nature of the search space to predict the effect of changing the perturbation distribution, but the success of the analysis would be improved if the distribution used was similar to that encountered in practice. The perturbations used here are *unstructured*, that is, each joint coordinate perturbation was independent, and therefore provide a reasonable representation of those that arise from manufacturing tolerances. Other types of geometric distribution, such as that due to thermal expansion and contraction, are *structured* perturbations. This has not been addressed here, although such a study has been reported for the static case on a truss structure (Farmer *et al*, 1992). Lastly, the requirements on the robustness of a system might not only refer to the robustness due to geometric uncertainties. Another consideration might be to reduce the sensitivity of the performance of a system due to the failure of any one of the active control actuators or sensors. The results presented here suggest that a structure, which has first undergone geometric optimisation and then the

determination of the optimal actuator positions, may perform almost as well as structure whose geometry and actuator positions were simultaneously optimised. However, the performance if the active control system failed would be better in the former case, as the significance of the reductions achieved by the geometric redesign is greater. Further work is required to investigate this aspect of robustness.

Finally, only an initial study on the design of structures to optimise their robust performance has been conducted. It has been shown that improvements in both robustness (change in performance) and absolute performance in the face of small geometric perturbations can be achieved, with little additional computational expense. This optimisation was only considered for the performance over a narrow frequency band, due to time available. Further investigation is required to optimise the performance over the broad frequency band that was used for the majority of the optimisations performed in this thesis, in order to see whether improvements would also found in this case. Also, it is not clear why the simplest measure of perturbed performance, which was not expected to produce a good estimate of the average perturbed performance, is better than one based on a full factorial experimental design. One possible reason is that the magnitude of perturbations used for each method did not represent equal 'strengths'. The use of a discrete probability distribution to represent a continuous one in this application needs further consideration. Perhaps a perturbed performance measure requiring only a few random perturbation experiments could be used with similar success.

Optimisation type	Reduction in average energy level of vibration (dB)	AVC control effort (normalised to primary control effort)
Passive (geometric redesign)	33	0
Active (application of AVC)	28	1,400
Passive-then-active	64	10
Combined (passive and active)	78	29

Table 8.1 Summary of average results of the four main optimisation methods over the frequency band 150Hz to 250Hz. The results for those methods using active vibration control are given for using two actuators.

APPENDIX A

Minimisation of a Hermitian Quadratic Form with Positive Definite Quadratic Coefficient Matrix

The object of this appendix is to show the derivation of the minimum of the cost function used in the main text, in the case where the quadratic coefficient matrix is always positive definite. This assumption avoids the complexities of using differential calculus (as discussed by Nelson and Elliott, 1992, and Haykin, 1996, for example) which would normally be required to show a solution for a general case where no such assumptions can be made. All symbols used apply locally to this appendix.

The cost function J is defined in quadratic form with the complex column vector $\mathbf{x}$ containing l complex independent variables,

$$J(\mathbf{x}) = \mathbf{x}^{\mathrm{H}}\mathbf{A}\mathbf{x} + \mathbf{x}^{\mathrm{H}}\mathbf{b} + \mathbf{b}^{\mathrm{H}}\mathbf{x} + c, \tag{A.1}$$

where $\mathbf{A}$ is a square matrix of dimension l x l, $\mathbf{b}$ is a complex vector of length l, and c is a positive scalar. If $\mathbf{A}$ is Hermitian and also positive definite, then (Datta, 1995),

$$\mathbf{x}^{\mathrm{H}}\mathbf{A}\mathbf{x} = y > 0 \quad \text{for all} \quad \mathbf{x} \neq \mathbf{0}, \tag{A.2}$$

and y will always be a positive scalar, if $\mathbf{x} \neq \mathbf{0}$. The positive definiteness of $\mathbf{A}$ is ensured in practice (see Chapter 5) and is verified by testing that all the eigenvalues of $\mathbf{A}$ are positive (Datta, 1995). Assuming that a solution that minimises J exists, (A.1) may be written as,

$$J(\mathbf{x}) = \left(\mathbf{x} - \mathbf{x}_0\right)^{\mathrm{H}} \mathbf{A}\left(\mathbf{x} - \mathbf{x}_0\right) + d, \tag{A.3}$$

where d is a real scalar, and $\mathbf{x}_0$ is the optimum value of vector $\mathbf{x}$. Expanding (A.3), so

$$J(\mathbf{x}) = \mathbf{x}^{\mathrm{H}}\mathbf{A}\mathbf{x} - \mathbf{x}^{\mathrm{H}}\mathbf{A}\mathbf{x}_0 - \mathbf{x}_0^{\mathrm{H}}\mathbf{A}\mathbf{x} + c, \tag{A.4}$$

which allows, firstly, the scalar relation between c and d to be defined as,

$$c = \mathbf{x}_0^{\mathrm{H}}\mathbf{A}\mathbf{x}_0 + d. \tag{A.5}$$

Secondly, equating the coefficients between (A.1) and (A.4), gives

$$-\mathbf{x}_0\mathbf{A} = \mathbf{b} \quad , \quad -\mathbf{x}_0^{\mathrm{H}}\mathbf{A} = \mathbf{b}^{\mathrm{H}}, \tag{A.6a,b}$$

which are two forms of the same solution. The solution to (A.3), which minimises J, is clearly given when $\mathbf{x} = \mathbf{x}_0$, and thus,

$$J(\mathbf{x}_0) = d = c - \mathbf{x}_0^{\mathrm{H}}\mathbf{A}\mathbf{x}_0 . \tag{A.7}$$

The optimum values of $\mathbf{x}$ are obtained from (A.6a,b),

$$\mathbf{x}_0 = -\mathbf{A}^{-1}\mathbf{b} \quad , \quad \mathbf{x}_0^{\mathrm{H}} = -\mathbf{b}^{\mathrm{H}}\mathbf{A}^{-1} . \tag{A.8a,b}$$

As $\mathbf{A}$ is positive definite it is also of full rank (Datta, 1995), and hence its inverse exists. As in (A.6), the two forms given in (A.8) are not different solutions but equivalent forms of the same solution, as for a Hermitian matrix $\mathbf{A}^{-1} = \mathbf{A}^{-\mathrm{H}}$. The minimum value of the cost function (A.7) can be expressed in terms of the coefficients from the quadratic form (A.1) using (A.8),

$$J(\mathbf{x}_0) = c - \mathbf{b}^{\mathrm{H}}\mathbf{A}^{-1}\mathbf{b} . \tag{A.9}$$

Because the vector-matrix term in (A.9) results in a positive scalar, the solution is a minimum as the value of $J(\mathbf{x}_0)$ is less than $J(\mathbf{x})$ when $\mathbf{x} = \mathbf{0}$.

APPENDIX B

Background to Optimisation Techniques

B.0 INTRODUCTION

The purpose of this Appendix is to provide full details of the optimisation techniques used in Chapter 3 for readers who are unfamiliar with the background to these techniques. Variable definitions, not explicitly given here, are defined in Chapter 3. All symbols used apply locally to this appendix, unless otherwise stated.

B.1 DAVIDON-FLETCHER-POWELL & BROYDEN-FLETCHER-GOLDFARB-SHANNO VARIABLE METRIC METHODS.

If a function f is differentiable it can be represented as a Taylor series expansion about the position of its minimum value, $\mathbf{x}_0$, and the vector offset to the start point of the search, $\mathbf{x}_e$,

$$f(\mathbf{x}_0 + \mathbf{x}_e) = f(\mathbf{x}_0) + \mathbf{g}^{\mathrm{T}}\mathbf{x}_e + \frac{1}{2}\mathbf{x}_e^{\mathrm{T}}\mathbf{H}\mathbf{x}_e + \ldots , \tag{B.1}$$

where $\mathbf{g}$ is the *Jacobian gradient vector* of first order partial derivatives defined,

$$\mathbf{g}^{\mathrm{T}} = \nabla f = \left[\frac{\partial f}{\partial x_1} \quad \frac{\partial f}{\partial x_2} \quad \ldots \quad \frac{\partial f}{\partial x_n} \right], \tag{B.2}$$

and $\mathbf{H}$ is the *Hessian matrix* of second order partial derivatives, defined:

$$\mathbf{H} = \begin{bmatrix} \frac{\partial^2 f}{\partial x_1^2} & \frac{\partial^2 f}{\partial x_1 \partial x_2} & \cdots & \frac{\partial^2 f}{\partial x_1 \partial x_n} \\ \frac{\partial^2 f}{\partial x_2 \partial x_1} & \frac{\partial^2 f}{\partial x_2^2} & & \vdots \\ \vdots & & & \vdots \\ \frac{\partial^2 f}{\partial x_n \partial x_1} & \cdots & \cdots & \frac{\partial^2 f}{\partial x_n^2} \end{bmatrix}. \tag{B.3}$$

The minimum value of the function can be written, to a second order approximation, as the evaluation at a point in search space which is a distance $\mathbf{x}_e$ away from the optimum vector $\mathbf{x}_0$. An estimate of the Jacobian gradient vector is attainable by evaluating locally over a finite difference (an estimate of the Hessian matrix is not easily achieved but is assumed for now),

$$f(\mathbf{x}_0 + \mathbf{x}_e) = f(\mathbf{x}_0) + \hat{\mathbf{g}}^{\mathrm{T}}\mathbf{x}_e + \frac{1}{2}\mathbf{x}_e^{\mathrm{T}}\hat{\mathbf{H}}\mathbf{x}_e . \tag{B.4}$$

If $\mathbf{x}_e$ can thus be evaluated a single step of $-\mathbf{x}_e$ can be made to reach the optimum position in the search space. Taking the derivative of (B.4) with respect to $\mathbf{x}_e$, the current position,

$$\nabla f(\mathbf{x}_0 + \mathbf{x}_e) = \hat{\mathbf{g}} + \hat{\mathbf{H}}\mathbf{x}_e . \tag{B.5}$$

$\nabla f(\mathbf{x}_0 + \mathbf{x}_e)$ is then set to zero to find $\mathbf{x}_e$,

$$\mathbf{x}_e = -\hat{\mathbf{H}}^{-1}\hat{\mathbf{g}} . \tag{B.6}$$

Hence the move to the minimum could be made in one move (assuming the search space has no non-zero derivatives above second order), however, it is obtaining a good estimate of $\mathbf{H}$ which normally presents the main problem. An estimate of $\mathbf{H}$ is formed from an initial starting point which is usually the identity matrix, and is updated every time an iterative step is made nearer the minimum. The process of finding the minimum becomes iterative as steps are made nearer using the current and increasing better estimate of the inverse of the Hessian matrix. So two successive iterations of (B.6), using index i, are given explicitly,

$$\mathbf{x}_i = -\hat{\mathbf{H}}_i^{-1}\hat{\mathbf{g}}_i \quad , \quad \mathbf{x}_{i+1} = -\hat{\mathbf{H}}_i^{-1}\hat{\mathbf{g}}_{i+1} , \tag{B.7}$$

and the iterative step is thus,

$$\Delta\mathbf{x}_{i+1} = \mathbf{x}_{i+1} - \mathbf{x}_i = -\hat{\mathbf{H}}_i^{-1}\Delta\hat{\mathbf{g}}_{i+1} , \tag{B.8}$$

where,

$$\Delta\hat{\mathbf{g}}_{i+1} = \hat{\mathbf{g}}_{i+1} - \hat{\mathbf{g}}_i . \tag{B.9}$$

Then, the estimate of $\mathbf{H}$ is updated. For the Davidon-Fletcher-Powell algorithm, the current estimate is updated,

$$\hat{\mathbf{H}}_{i+1}^{-1} = \hat{\mathbf{H}}_i^{-1} + \Delta\hat{\mathbf{H}}_{FDP} , \tag{B.10}$$

where the update term is defined,

$$\Delta\hat{\mathbf{H}}_{FDP} = \frac{\Delta\mathbf{x}_{i+1} \otimes \Delta\mathbf{x}_{i+1}}{\Delta\mathbf{x}_{i+1} \cdot \Delta\hat{\mathbf{g}}_{i+1}} - \frac{\left(\hat{\mathbf{H}}_i \cdot \Delta\hat{\mathbf{g}}_{i+1}\right) \otimes \left(\hat{\mathbf{H}}_i \cdot \Delta\hat{\mathbf{g}}_{i+1}\right)}{\Delta\hat{\mathbf{g}}_{i+1} \cdot \hat{\mathbf{H}}_i \cdot \Delta\hat{\mathbf{g}}_{i+1}} \tag{B.11}$$

where $\otimes$ denotes the outer product of two vectors. The Broyden-Fletcher-Goldfarb-Shanno algorithm uses an additional update term,

$$\hat{\mathbf{H}}_{i+1}^{-1} = \hat{\mathbf{H}}_{ii}^{-1} + \Delta\hat{\mathbf{H}}_{FDP} + \Delta\hat{\mathbf{H}}_{BFGS}, \tag{B.12}$$

which is defined,

$$\Delta\hat{\mathbf{H}}_{BFGS} = \left(\Delta\hat{\mathbf{g}}_{i+1} \cdot \hat{\mathbf{H}}_i \cdot \Delta\hat{\mathbf{g}}_{i+1}\right)\mathbf{u} \otimes \mathbf{u}, \tag{B.13}$$

where, $\mathbf{u}$ is given,

$$\mathbf{u} = \frac{\Delta\mathbf{x}_{i+1}}{\Delta\mathbf{x}_{i+1} \cdot \Delta\hat{\mathbf{g}}_{i+1}} - \frac{\hat{\mathbf{H}}_i \cdot \Delta\hat{\mathbf{g}}_{i+1}}{\Delta\hat{\mathbf{g}}_{i+1} \cdot \hat{\mathbf{H}}_i \cdot \Delta\hat{\mathbf{g}}_{i+1}}. \tag{B.14}$$

It can be shown (Press *et al*, 1992) that the Hessian matrix does converge to the actual Hessian matrix for a quadratic problem.

B.2 FUNDAMENTAL THEOREM OF GENETIC ALGORITHMS

(The main symbols used in this section are listed in the glossary of symbols for Chapter 3).

The most commonly used alphabet with genetic algorithms is a binary alphabet which is used for the coding of the chromosome strings, as used in this work, the alphabet of the chromosomes V is thus

$$V = \{0 \quad 1\}. \tag{B.15}$$

An augmented alphabet V^+ is required for the schemata, formed by the addition of a wild card character *,

$$V^+ = \{0 \quad 1 \quad *\}. \tag{B.16}$$

Thus, for example, a schema H (normally denoted thus because it represents a hyperplane in the search space) may be given as 1011*0*1. This schema then represents the four chromosome strings which, explicitly, are 10110001, 10110011, 10111001 and 10111011. Each of these are termed *instances* of H. Using schemata the evolution may be studied in a macro level. The probability, p_i, that a chromosome i , with fitness f_i, will be selected into the pool of n chromosome strings which will be available to form the next generation is given by,

$$p_i = \frac{f_i}{\sum_{j=1}^{n} f_j}. \tag{B.17}$$

So np_i is the expectation of the number of chromosomes i which survive. The number of chromosome strings represented by a particular schema H in a population at the evolutionary

generation time step t is $m(H,t)$. For a non-overlapping population (the entire population is replaced at the same time) the expected number of chromosomes represented by the schema in the next generation is given by,

$$m'(H,t+1) = m(H,t)n\frac{f(H)}{\sum_{j=1}^{n} f_j}, \tag{B.18}$$

where $f(H)$ is the average fitness value of the schema (average fitness values of all the chromosomes represented by schema H). The average fitness of the entire population can be expressed,

$$\bar{f} = \frac{\sum_{j=1}^{n} f_j}{n}, \tag{B.19}$$

which allows (B.18) to be expressed as,

$$m'(H,t+1) = m(H,t)\frac{f(H)}{\bar{f}}. \tag{B.20}$$

It is re-iterated that this represents the expected number of chromosome strings represented by schema H in the next generation *by selection alone*. The effects of the crossover and mutation operators will be discussed below. However from (B.20) it can be seen that for schemata that have average fitnesses above the average fitness of the population are expected to represent an increased number of chromosome strings in the next generation.

The effects of the crossover and mutation operators on the survival rate of each schema are now studied. Both of these operators serve to change the chromosomes on which they operate. Therefore the effect on the expected rate of survival of chromosomes represented by a particular schema is the expectation that schemata remain unaffected by these two operators.

The crossover operator swaps genetic information between two paired chromosomes. This will result in two altered chromosomes, unless the crossover operation has no effect due to similarities between the two chromosomes with the elected crossover site. This probability is not easily defined, especially with on-going evolution. Additional algorithm operations which prevent 'crowding', where the situation of the population converging to only a few 'good' positions in the search space, also act to keep this probability small. To analyse the effect of crossover succinctly, the parameter 'defining length' is used. The defining length of a schema is the length (in gene positions) between the two outer-most fixed values. In the schemata in Figure 3.5 the defining length of schema A, denoted $d(A)$ is five and for $d(B)$ is zero. The

probability that a schema will be changed by a crossover point is the ratio of the number of crossover sites between the extremes of the defined part of the schema, which is the defining length, and the total number of crossover sites on the chromosomes string. If the chromosome is of length l then the number of such borders is l-1. The probability that the schema, H will survive crossover is then,

$$p_{s_{cross}} \geq 1 - p_c \frac{d(H)}{l-1}. \tag{B.21}$$

The inequality defines the minimum probability of survival since, depending on similarities between the two schemata, the schema may remain unchanged despite the interchange of fixed allele positions.

The effect of the mutation operator is facilitated by the definition of the order of a schema. This is the number of positions that are assigned to particular values, and not the 'wildcard' value *. Figure 3.5 show two schemata, the order of schema A, denoted *O(A)*, is 4, whereas *O(B)* is 1. If p_m is the probability that each *allele* (unit of information for each chromosome) undergoes mutation. The probability that each fixed allele survives is therefore (1- p_m). The probability that the schema survives is the probability that all of the fixed allele values within the schema survive. The survival of each fixed allele is statistically independent, and thus for a schema with *O(H)* fixed value the probability of survival is,

$$p_{s_{mut}} = (1 - p_m)^{O(H)}. \tag{B.22}$$

Since p_m is usually a small value, such that $p_m << 1$, the survival of the schema is then for most cases adequately approximated by,

$$1 - O(H)p_m. \tag{B.23}$$

The expected number of chromosomes represented by schema H in the next generation is therefore given by (B.20) multiplied with the probability that the schema survives both crossover and mutation. This probability is the product of (B.21) and (B.23), of which a first order approximation is accepted to yield the Schema Theorem or the Fundamental Theorem of Genetic Algorithms (Goldberg, 1989),

$$m(H, t+1) \geq m(H, t) \frac{f(H,t)}{\overline{f(t)}} \left(1 - p_c \frac{d(H)}{l-1} - O(H)p_m \right). \tag{B.24}$$

APPENDIX C

Standard Orthogonal Arrays

C.1 TAGUCHI'S L64 ORTHOGONAL ARRAY

	1	2	3	4	5	6	7	8	9	10	11	12	13	14	15
1	1	1	1	1	1	1	1	1	1	1	1	1	1	1	1
2	1	1	1	1	1	1	1	1	1	1	1	1	1	1	1
3	1	1	1	1	1	1	1	1	1	1	1	1	1	1	1
4	1	1	1	1	1	1	1	1	1	1	1	1	1	1	1
5	1	1	1	1	1	1	1	2	2	2	2	2	2	2	2
6	1	1	1	1	1	1	1	2	2	2	2	2	2	2	2
7	1	1	1	1	1	1	1	2	2	2	2	2	2	2	2
8	1	1	1	1	1	1	1	2	2	2	2	2	2	2	2
9	1	1	1	2	2	2	2	1	1	1	1	2	2	2	2
10	1	1	1	2	2	2	2	1	1	1	1	2	2	2	2
11	1	1	1	2	2	2	2	1	1	1	1	2	2	2	2
12	1	1	1	2	2	2	2	1	1	1	1	2	2	2	2
13	1	1	1	2	2	2	2	2	2	2	2	1	1	1	1
14	1	1	1	2	2	2	2	2	2	2	2	1	1	1	1
15	1	1	1	2	2	2	2	2	2	2	2	1	1	1	1
16	1	1	1	2	2	2	2	2	2	2	2	1	1	1	1
17	1	2	2	1	1	2	2	1	1	2	2	1	1	2	2
18	1	2	2	1	1	2	2	1	1	2	2	1	1	2	2
19	1	2	2	1	1	2	2	1	1	2	2	1	1	2	2
20	1	2	2	1	1	2	2	1	1	2	2	1	1	2	2
21	1	2	2	1	1	2	2	2	2	1	1	2	2	1	1
22	1	2	2	1	1	2	2	2	2	1	1	2	2	1	1
23	1	2	2	1	1	2	2	2	2	1	1	2	2	1	1
24	1	2	2	1	1	2	2	2	2	1	1	2	2	1	1
25	1	2	2	2	2	1	1	1	1	2	2	2	2	1	1
26	1	2	2	2	2	1	1	1	1	2	2	2	2	1	1
27	1	2	2	2	2	1	1	1	1	2	2	2	2	1	1
28	1	2	2	2	2	1	1	1	1	2	2	2	2	1	1
29	1	2	2	2	2	1	1	2	2	1	1	1	1	2	2
30	1	2	2	2	2	1	1	2	2	1	1	1	1	2	2
31	1	2	2	2	2	1	1	2	2	1	1	1	1	2	2
32	1	2	2	2	2	1	1	2	2	1	1	1	1	2	2
33	2	1	2	1	2	1	2	1	2	1	2	1	2	1	2
34	2	1	2	1	2	1	2	1	2	1	2	1	2	1	2
35	2	1	2	1	2	1	2	1	2	1	2	1	2	1	2
36	2	1	2	1	2	1	2	1	2	1	2	1	2	1	2
37	2	1	2	1	2	1	2	2	1	2	1	2	1	2	1
38	2	1	2	1	2	1	2	2	1	2	1	2	1	2	1
39	2	1	2	1	2	1	2	2	1	2	1	2	1	2	1
40	2	1	2	1	2	1	2	2	1	2	1	2	1	2	1
41	2	1	2	2	1	2	1	1	2	1	2	2	1	2	1
42	2	1	2	2	1	2	1	1	2	1	2	2	1	2	1
43	2	1	2	2	1	2	1	1	2	1	2	2	1	2	1
44	2	1	2	2	1	2	1	1	2	1	2	2	1	2	1
45	2	1	2	2	1	2	1	2	1	2	1	1	2	1	2
46	2	1	2	2	1	2	1	2	1	2	1	1	2	1	2
47	2	1	2	2	1	2	1	2	1	2	1	1	2	1	2
48	2	1	2	2	1	2	1	2	1	2	1	1	2	1	2
49	2	2	1	1	2	2	1	1	2	2	1	1	2	2	1
50	2	2	1	1	2	2	1	1	2	2	1	1	2	2	1
51	2	2	1	1	2	2	1	1	2	2	1	1	2	2	1
52	2	2	1	1	2	2	1	1	2	2	1	1	2	2	1
53	2	2	1	1	2	2	1	2	1	1	2	2	1	1	2
54	2	2	1	1	2	2	1	2	1	1	2	2	1	1	2
55	2	2	1	1	2	2	1	2	1	1	2	2	1	1	2
56	2	2	1	1	2	2	1	2	1	1	2	2	1	1	2
57	2	2	1	2	1	1	2	1	2	2	1	2	1	1	2
58	2	2	1	2	1	1	2	1	2	2	1	2	1	1	2
59	2	2	1	2	1	1	2	1	2	2	1	2	1	1	2
60	2	2	1	2	1	1	2	1	2	2	1	2	1	1	2
61	2	2	1	2	1	1	2	2	1	1	2	1	2	2	1
62	2	2	1	2	1	1	2	2	1	1	2	1	2	2	1
63	2	2	1	2	1	1	2	2	1	1	2	1	2	2	1
64	2	2	1	2	1	1	2	2	1	1	2	1	2	2	1

Table C.1. *(part 1 of 4)*. Taguchi's L64 orthogonal array (after Taguchi, 1987 as cited by Phadke, 1989). Corrected by author (see main text). Each row defines an experiment of 63 two-level factors.

	16	17	18	19	20	21	22	23	24	25	26	27	28	29	30	31
1	1	1	1	1	1	1	1	1	1	1	1	1	1	1	1	1
2	1	1	1	1	1	1	1	1	1	1	1	1	1	1	1	1
3	2	2	2	2	2	2	2	2	2	2	2	2	2	2	2	2
4	2	2	2	2	2	2	2	2	2	2	2	2	2	2	2	2
5	1	1	1	1	1	1	1	1	2	2	2	2	2	2	2	2
6	1	1	1	1	1	1	1	1	2	2	2	2	2	2	2	2
7	2	2	2	2	2	2	2	2	1	1	1	1	1	1	1	1
8	2	2	2	2	2	2	2	2	1	1	1	1	1	1	1	1
9	1	1	1	1	2	2	2	2	1	1	1	1	2	2	2	2
10	1	1	1	1	2	2	2	2	1	1	1	1	2	2	2	2
11	2	2	2	2	1	1	1	1	2	2	2	2	1	1	1	1
12	2	2	2	2	1	1	1	1	2	2	2	2	1	1	1	1
13	1	1	1	1	2	2	2	2	2	2	2	2	1	1	1	1
14	1	1	1	1	2	2	2	2	2	2	2	2	1	1	1	1
15	2	2	2	2	1	1	1	1	1	1	1	1	2	2	2	2
16	2	2	2	2	1	1	1	1	1	1	1	1	2	2	2	2
17	1	1	2	2	1	1	2	2	1	1	2	2	1	1	2	2
18	1	1	2	2	1	1	2	2	1	1	2	2	1	1	2	2
19	2	2	1	1	2	2	1	1	2	2	1	1	2	2	1	1
20	2	2	1	1	2	2	1	1	2	2	1	1	2	2	1	1
21	1	1	2	2	1	1	2	2	2	2	1	1	2	2	1	1
22	1	1	2	2	1	1	2	2	2	2	1	1	2	2	1	1
23	2	2	1	1	2	2	1	1	1	1	2	2	1	1	2	2
24	2	2	1	1	2	2	1	1	1	1	2	2	1	1	2	2
25	1	1	2	2	2	2	1	1	1	1	2	2	2	2	1	1
26	1	1	2	2	2	2	1	1	1	1	2	2	2	2	1	1
27	2	2	1	1	1	1	2	2	2	2	1	1	1	1	2	2
28	2	2	1	1	1	1	2	2	2	2	1	1	1	1	2	2
29	1	1	2	2	2	2	1	1	2	2	1	1	1	1	2	2
30	1	1	2	2	2	2	1	1	2	2	1	1	1	1	2	2
31	2	2	1	1	1	1	2	2	1	1	2	2	2	2	1	1
32	2	2	1	1	1	1	2	2	1	1	2	2	2	2	1	1
33	1	2	1	2	1	2	1	2	1	2	1	2	1	2	1	2
34	1	2	1	2	1	2	1	2	1	2	1	2	1	2	1	2
35	2	1	2	1	2	1	2	1	2	1	2	1	2	1	2	1
36	2	1	2	1	2	1	2	1	2	1	2	1	2	1	2	1
37	1	2	1	2	1	2	1	2	2	1	2	1	2	1	2	1
38	1	2	1	2	1	2	1	2	2	1	2	1	2	1	2	1
39	2	1	2	1	2	1	2	1	1	2	1	2	1	2	1	2
40	2	1	2	1	2	1	2	1	1	2	1	2	1	2	1	2
41	1	2	1	2	2	1	2	1	1	2	1	2	2	1	2	1
42	1	2	1	2	2	1	2	1	1	2	1	2	2	1	2	1
43	2	1	2	1	1	2	1	2	2	1	2	1	1	2	1	2
44	2	1	2	1	1	2	1	2	2	1	2	1	1	2	1	2
45	1	2	1	2	2	1	2	1	2	1	2	1	1	2	1	2
46	1	2	1	2	2	1	2	1	2	1	2	1	1	2	1	2
47	2	1	2	1	1	2	1	2	1	2	1	2	2	1	2	1
48	2	1	2	1	1	2	1	2	1	2	1	2	2	1	2	1
49	1	2	2	1	1	2	2	1	1	2	2	1	1	2	2	1
50	1	2	2	1	1	2	2	1	1	2	2	1	1	2	2	1
51	2	1	1	2	2	1	1	2	2	1	1	2	2	1	1	2
52	2	1	1	2	2	1	1	2	2	1	1	2	2	1	1	2
53	1	2	2	1	1	2	2	1	2	1	1	2	2	1	1	2
54	1	2	2	1	1	2	2	1	2	1	1	2	2	1	1	2
55	2	1	1	2	2	1	1	2	1	2	2	1	1	2	2	1
56	2	1	1	2	2	1	1	2	1	2	2	1	1	2	2	1
57	1	2	2	1	2	1	1	2	1	2	2	1	2	1	1	2
58	1	2	2	1	2	1	1	2	1	2	2	1	2	1	1	2
59	2	1	1	2	1	2	2	1	2	1	1	2	1	2	2	1
60	2	1	1	2	1	2	2	1	2	1	1	2	1	2	2	1
61	1	2	2	1	2	1	1	2	2	1	1	2	1	2	2	1
62	1	2	2	1	2	1	1	2	2	1	1	2	1	2	2	1
63	2	1	1	2	1	2	2	1	1	2	2	1	2	1	1	2
64	2	1	1	2	1	2	2	1	1	2	2	1	2	1	1	2

Table C.1. *(part 2 of 4).* Taguchi's L64 orthogonal array (after Taguchi, 1987 as cited by Phadke, 1989). Corrected by author (see main text). Each row defines an experiment of 63 two-level factors.

	32	33	34	35	36	37	38	39	40	41	42	43	44	45	46	47
1	1	1	1	1	1	1	1	1	1	1	1	1	1	1	1	1
2	2	2	2	2	2	2	2	2	2	2	2	2	2	2	2	2
3	1	1	1	1	1	1	1	1	1	1	1	1	1	1	1	1
4	2	2	2	2	2	2	2	2	2	2	2	2	2	2	2	2
5	1	1	1	1	1	1	1	1	2	2	2	2	2	2	2	2
6	2	2	2	2	2	2	2	2	1	1	1	1	1	1	1	1
7	1	1	1	1	1	1	1	1	2	2	2	2	2	2	2	2
8	2	2	2	2	2	2	2	2	1	1	1	1	1	1	1	1
9	1	1	1	1	2	2	2	2	1	1	1	1	2	2	2	2
10	2	2	2	2	1	1	1	1	2	2	2	2	1	1	1	1
11	1	1	1	1	2	2	2	2	1	1	1	1	2	2	2	2
12	2	2	2	2	1	1	1	1	2	2	2	2	1	1	1	1
13	1	1	1	1	2	2	2	2	2	2	2	2	1	1	1	1
14	2	2	2	2	1	1	1	1	1	1	1	1	2	2	2	2
15	1	1	1	1	2	2	2	2	2	2	2	2	1	1	1	1
16	2	2	2	2	1	1	1	1	1	1	1	1	2	2	2	2
17	1	1	2	2	1	1	2	2	1	1	2	2	1	1	2	2
18	2	2	1	1	2	2	1	1	2	2	1	1	2	2	1	1
19	1	1	2	2	1	1	2	2	1	1	2	2	1	1	2	2
20	2	2	1	1	2	2	1	1	2	2	1	1	2	2	1	1
21	1	1	2	2	1	1	2	2	2	2	1	1	2	2	1	1
22	2	2	1	1	2	2	1	1	1	1	2	2	1	1	2	2
23	1	1	2	2	1	1	2	2	2	2	1	1	2	2	1	1
24	2	2	1	1	2	2	1	1	1	1	2	2	1	1	2	2
25	1	1	2	2	2	2	1	1	1	1	2	2	2	2	1	1
26	2	2	1	1	1	1	2	2	2	2	1	1	1	1	2	2
27	1	1	2	2	2	2	1	1	1	1	2	2	2	2	1	1
28	2	2	1	1	1	1	2	2	2	2	1	1	1	1	2	2
29	1	1	2	2	2	2	1	1	2	2	1	1	1	1	2	2
30	2	2	1	1	1	1	2	2	1	1	2	2	2	2	1	1
31	1	1	2	2	2	2	1	1	2	2	1	1	1	1	2	2
32	2	2	1	1	1	1	2	2	1	1	2	2	2	2	1	1
33	1	2	1	2	1	2	1	2	1	2	1	2	1	2	1	2
34	2	1	2	1	2	1	2	1	2	1	2	1	2	1	2	1
35	1	2	1	2	1	2	1	2	1	2	1	2	1	2	1	2
36	2	1	2	1	2	1	2	1	2	1	2	1	2	1	2	1
37	1	2	1	2	1	2	1	2	2	1	2	1	2	1	2	1
38	2	1	2	1	2	1	2	1	1	2	1	2	1	2	1	2
39	1	2	1	2	1	2	1	2	2	1	2	1	2	1	2	1
40	2	1	2	1	2	1	2	1	1	2	1	2	1	2	1	2
41	1	2	1	2	2	1	2	1	1	2	1	2	2	1	2	1
42	2	1	2	1	1	2	1	2	2	1	2	1	1	2	1	2
43	1	2	1	2	2	1	2	1	1	2	1	2	2	1	2	1
44	2	1	2	1	1	2	1	2	2	1	2	1	1	2	1	2
45	1	2	1	2	2	1	2	1	2	1	2	1	1	2	1	2
46	2	1	2	1	1	2	1	2	1	2	1	2	2	1	2	1
47	1	2	1	2	2	1	2	1	2	1	2	1	1	2	1	2
48	2	1	2	1	1	2	1	2	1	2	1	2	2	1	2	1
49	1	2	2	1	1	2	2	1	1	2	2	1	1	2	2	1
50	2	1	1	2	2	1	1	2	2	1	1	2	2	1	1	2
51	1	2	2	1	1	2	2	1	1	2	2	1	1	2	2	1
52	2	1	1	2	2	1	1	2	2	1	1	2	2	1	1	2
53	1	2	2	1	1	2	2	1	2	1	1	2	2	1	1	2
54	2	1	1	2	2	1	1	2	1	2	2	1	1	2	2	1
55	1	2	2	1	1	2	2	1	2	1	1	2	2	1	1	2
56	2	1	1	2	2	1	1	2	1	2	2	1	1	2	2	1
57	1	2	2	1	2	1	1	2	1	2	2	1	2	1	1	2
58	2	1	1	2	1	2	2	1	2	1	1	2	1	2	2	1
59	1	2	2	1	2	1	1	2	1	2	2	1	2	1	1	2
60	2	1	1	2	1	2	2	1	2	1	1	2	1	2	2	1
61	1	2	2	1	2	1	1	2	2	1	1	2	1	2	2	1
62	2	1	1	2	1	2	2	1	1	2	2	1	2	1	1	2
63	1	2	2	1	2	1	1	2	2	1	1	2	1	2	2	1
64	2	1	1	2	1	2	2	1	1	2	2	1	2	1	1	2

Table C.1. *(part 3 of 4).* Taguchi's L64 orthogonal array (after Taguchi, 1987 as cited by Phadke, 1989). Corrected by author (see main text). Each row defines an experiment of 63 two-level factors.

	48	49	50	51	52	53	54	55	56	57	58	59	60	61	62	63
1	1	1	1	1	1	1	1	1	1	1	1	1	1	1	1	1
2	2	2	2	2	2	2	2	2	2	2	2	2	2	2	2	2
3	2	2	2	2	2	2	2	2	2	2	2	2	2	2	2	2
4	1	1	1	1	1	1	1	1	1	1	1	1	1	1	1	1
5	1	1	1	1	1	1	1	1	2	2	2	2	2	2	2	2
6	2	2	2	2	2	2	2	2	1	1	1	1	1	1	1	1
7	2	2	2	2	2	2	2	2	1	1	1	1	1	1	1	1
8	1	1	1	1	1	1	1	1	2	2	2	2	2	2	2	2
9	1	1	1	1	2	2	2	2	1	1	1	1	2	2	2	2
10	2	2	2	2	1	1	1	1	2	2	2	2	1	1	1	1
11	2	2	2	2	1	1	1	1	2	2	2	2	1	1	1	1
12	1	1	1	1	2	2	2	2	1	1	1	1	2	2	2	2
13	1	1	1	1	2	2	2	2	2	2	2	2	1	1	1	1
14	2	2	2	2	1	1	1	1	1	1	1	1	2	2	2	2
15	2	2	2	2	1	1	1	1	1	1	1	1	2	2	2	2
16	1	1	1	1	2	2	2	2	2	2	2	2	1	1	1	1
17	1	1	2	2	1	1	2	2	1	1	2	2	1	1	2	2
18	2	2	1	1	2	2	1	1	2	2	1	1	2	2	1	1
19	2	2	1	1	2	2	1	1	2	2	1	1	2	2	1	1
20	1	1	2	2	1	1	2	2	1	1	2	2	1	1	2	2
21	1	1	2	2	1	1	2	2	2	2	1	1	2	2	1	1
22	2	2	1	1	2	2	1	1	1	1	2	2	1	1	2	2
23	2	2	1	1	2	2	1	1	1	1	2	2	1	1	2	2
24	1	1	2	2	1	1	2	2	2	2	1	1	2	2	1	1
25	1	1	2	2	2	2	1	1	1	1	2	2	2	2	1	1
26	2	2	1	1	1	1	2	2	2	2	1	1	1	1	2	2
27	2	2	1	1	1	1	2	2	2	2	1	1	1	1	2	2
28	1	1	2	2	2	2	1	1	1	1	2	2	2	2	1	1
29	1	1	2	2	2	2	1	1	2	2	1	1	1	1	2	2
30	2	2	1	1	1	1	2	2	1	1	2	2	2	2	1	1
31	2	2	1	1	1	1	2	2	1	1	2	2	2	2	1	1
32	1	1	2	2	2	2	1	1	2	2	1	1	1	1	2	2
33	1	2	1	2	1	2	1	2	1	2	1	2	1	2	1	2
34	2	1	2	1	2	1	2	1	2	1	2	1	2	1	2	1
35	2	1	2	1	2	1	2	1	2	1	2	1	2	1	2	1
36	1	2	1	2	1	2	1	2	1	2	1	2	1	2	1	2
37	1	2	1	2	1	2	1	2	2	1	2	1	2	1	2	1
38	2	1	2	1	2	1	2	1	1	2	1	2	1	2	1	2
39	2	1	2	1	2	1	2	1	1	2	1	2	1	2	1	2
40	1	2	1	2	1	2	1	2	2	1	2	1	2	1	2	1
41	1	2	1	2	2	1	2	1	1	2	1	2	2	1	2	1
42	2	1	2	1	1	2	1	2	2	1	2	1	1	2	1	2
43	2	1	2	1	1	2	1	2	2	1	2	1	1	2	1	2
44	1	2	1	2	2	1	2	1	1	2	1	2	2	1	2	1
45	1	2	1	2	2	1	2	1	2	1	2	1	1	2	1	2
46	2	1	2	1	1	2	1	2	1	2	1	2	2	1	2	1
47	2	1	2	1	1	2	1	2	1	2	1	2	2	1	2	1
48	1	2	1	2	2	1	2	1	2	1	2	1	1	2	1	2
49	1	2	2	1	1	2	2	1	1	2	2	1	1	2	2	1
50	2	1	1	2	2	1	1	2	2	1	1	2	2	1	1	2
51	2	1	1	2	2	1	1	2	2	1	1	2	2	1	1	2
52	1	2	2	1	1	2	2	1	1	2	2	1	1	2	2	1
53	1	2	2	1	1	2	2	1	2	1	1	2	2	1	1	2
54	2	1	1	2	2	1	1	2	1	2	2	1	1	2	2	1
55	2	1	1	2	2	1	1	2	1	2	2	1	1	2	2	1
56	1	2	2	1	1	2	2	1	2	1	1	2	2	1	1	2
57	1	2	2	1	2	1	1	2	1	2	2	1	2	1	1	2
58	2	1	1	2	1	2	2	1	2	1	1	2	1	2	2	1
59	2	1	1	2	1	2	2	1	2	1	1	2	1	2	2	1
60	1	2	2	1	2	1	1	2	1	2	2	1	2	1	1	2
61	1	2	2	1	2	1	1	2	2	1	1	2	1	2	2	1
62	2	1	1	2	1	2	2	1	1	2	2	1	2	1	1	2
63	2	1	1	2	1	2	2	1	1	2	2	1	2	1	1	2
64	1	2	2	1	2	1	1	2	2	1	1	2	1	2	2	1

Table C.1. (*part 4 of 4*). Taguchi's L64 orthogonal array (after Taguchi, 1987 as cited by Phadke, 1989). Corrected by author (see main text). Each row defines an experiment of 63 two-level factors.

C.2 TAGUCHI'S L81 ORTHOGONAL ARRAY

	1	2	3	4	5	6	7	8	9	10	11	12	13	14	15	16	17	18	19	20	21	22
1	1	1	1	1	1	1	1	1	1	1	1	1	1	1	1	1	1	1	1	1	1	1
2	1	1	1	1	1	1	1	1	1	1	1	1	1	2	2	2	2	2	2	2	2	2
3	1	1	1	1	1	1	1	1	1	1	1	1	1	3	3	3	3	3	3	3	3	3
4	1	1	1	1	2	2	2	2	2	2	2	2	2	1	1	1	1	1	1	1	1	1
5	1	1	1	1	2	2	2	2	2	2	2	2	2	2	2	2	2	2	2	2	2	2
6	1	1	1	1	2	2	2	2	2	2	2	2	2	3	3	3	3	3	3	3	3	3
7	1	1	1	1	3	3	3	3	3	3	3	3	3	1	1	1	1	1	1	1	1	1
8	1	1	1	1	3	3	3	3	3	3	3	3	3	2	2	2	2	2	2	2	2	2
9	1	1	1	1	3	3	3	3	3	3	3	3	3	3	3	3	3	3	3	3	3	3
10	1	2	2	2	1	1	1	2	2	2	3	3	3	1	1	1	2	2	2	3	3	3
11	1	2	2	2	1	1	1	2	2	2	3	3	3	2	2	2	3	3	3	1	1	1
12	1	2	2	2	1	1	1	2	2	2	3	3	3	3	3	3	1	1	1	2	2	2
13	1	2	2	2	2	2	2	3	3	3	1	1	1	1	1	1	2	2	2	3	3	3
14	1	2	2	2	2	2	2	3	3	3	1	1	1	2	2	2	3	3	3	1	1	1
15	1	2	2	2	2	2	2	3	3	3	1	1	1	3	3	3	1	1	1	2	2	2
16	1	2	2	2	3	3	3	1	1	1	2	2	2	1	1	1	2	2	2	3	3	3
17	1	2	2	2	3	3	3	1	1	1	2	2	2	2	2	2	3	3	3	1	1	1
18	1	2	2	2	3	3	3	1	1	1	2	2	2	3	3	3	1	1	1	2	2	2
19	1	3	3	3	1	1	1	3	3	3	2	2	2	1	1	1	3	3	3	2	2	2
20	1	3	3	3	1	1	1	3	3	3	2	2	2	2	2	2	1	1	1	3	3	3
21	1	3	3	3	1	1	1	3	3	3	2	2	2	3	3	3	2	2	2	1	1	1
22	1	3	3	3	2	2	2	1	1	1	3	3	3	1	1	1	3	3	3	2	2	2
23	1	3	3	3	2	2	2	1	1	1	3	3	3	2	2	2	1	1	1	3	3	3
24	1	3	3	3	2	2	2	1	1	1	3	3	3	3	3	3	2	2	2	1	1	1
25	1	3	3	3	3	3	3	2	2	2	1	1	1	1	1	1	3	3	3	2	2	2
26	1	3	3	3	3	3	3	2	2	2	1	1	1	2	2	2	1	1	1	3	3	3
27	1	3	3	3	3	3	3	2	2	2	1	1	1	3	3	3	2	2	2	1	1	1
28	2	1	2	3	1	2	3	1	2	3	1	2	3	1	2	3	1	2	3	1	2	3
29	2	1	2	3	1	2	3	1	2	3	1	2	3	2	3	1	2	3	1	2	3	1
30	2	1	2	3	1	2	3	1	2	3	1	2	3	3	1	2	3	1	2	3	1	2
31	2	1	2	3	2	3	1	2	3	1	2	3	1	1	2	3	1	2	3	1	2	3
32	2	1	2	3	2	3	1	2	3	1	2	3	1	2	3	1	2	3	1	2	3	1
33	2	1	2	3	2	3	1	2	3	1	2	3	1	3	1	2	3	1	2	3	1	2
34	2	1	2	3	3	1	2	3	1	2	3	1	2	1	2	3	1	2	3	1	2	3
35	2	1	2	3	3	1	2	3	1	2	3	1	2	2	3	1	2	3	1	2	3	1
36	2	1	2	3	3	1	2	3	1	2	3	1	2	3	1	2	3	1	2	3	1	2
37	2	2	3	1	1	2	3	2	3	1	3	1	2	1	2	3	2	3	1	3	1	2
38	2	2	3	1	1	2	3	2	3	1	3	1	2	2	3	1	3	1	2	1	2	3
39	2	2	3	1	1	2	3	2	3	1	3	1	2	3	1	2	1	2	3	2	3	1
40	2	2	3	1	2	3	1	3	1	2	1	2	3	1	2	3	2	3	1	3	1	2
41	2	2	3	1	2	3	1	3	1	2	1	2	3	2	3	1	3	1	2	1	2	3
42	2	2	3	1	2	3	1	3	1	2	1	2	3	3	1	2	1	2	3	2	3	1
43	2	2	3	1	3	1	2	1	2	3	2	3	1	1	2	3	2	3	1	3	1	2
44	2	2	3	1	3	1	2	1	2	3	2	3	1	2	3	1	3	1	2	1	2	3
45	2	2	3	1	3	1	2	1	2	3	2	3	1	3	1	2	1	2	3	2	3	1
46	2	3	1	2	1	2	3	3	1	2	2	3	1	1	2	3	3	1	2	2	3	1
47	2	3	1	2	1	2	3	3	1	2	2	3	1	2	3	1	1	2	3	3	1	2
48	2	3	1	2	1	2	3	3	1	2	2	3	1	3	1	2	2	3	1	1	2	3
49	2	3	1	2	2	3	1	1	2	3	3	1	2	1	2	3	3	1	2	2	3	1
50	2	3	1	2	2	3	1	1	2	3	3	1	2	2	3	1	1	2	3	3	1	2
51	2	3	1	2	2	3	1	1	2	3	3	1	2	3	1	2	2	3	1	1	2	3
52	2	3	1	2	3	1	2	2	3	1	1	2	3	1	2	3	3	1	2	2	3	1
53	2	3	1	2	3	1	2	2	3	1	1	2	3	2	3	1	1	2	3	3	1	2
54	2	3	1	2	3	1	2	2	3	1	1	2	3	3	1	2	2	3	1	1	2	3
55	3	1	3	2	1	3	2	1	3	2	1	3	2	1	3	2	1	3	2	1	3	2
56	3	1	3	2	1	3	2	1	3	2	1	3	2	2	1	3	2	1	3	2	1	3
57	3	1	3	2	1	3	2	1	3	2	1	3	2	3	2	1	3	2	1	3	2	1
58	3	1	3	2	2	1	3	2	1	3	2	1	3	1	3	2	1	3	2	1	3	2
59	3	1	3	2	2	1	3	2	1	3	2	1	3	2	1	3	2	1	3	2	1	3
60	3	1	3	2	2	1	3	2	1	3	2	1	3	3	2	1	3	2	1	3	2	1
61	3	1	3	2	3	2	1	3	2	1	3	2	1	1	3	2	1	3	2	1	3	2
62	3	1	3	2	3	2	1	3	2	1	3	2	1	2	1	3	2	1	3	2	1	3
63	3	1	3	2	3	2	1	3	2	1	3	2	1	3	2	1	3	2	1	3	2	1

Table C.2. (*part 1 of 4*). Taguchi's L81 orthogonal array (after Taguchi, 1987 as cited by Phadke, 1989). Each row defines an experiment of 40 three-level factors.

	23	24	25	26	27	28	29	30	31	32	33	34	35	36	37	38	39	40
1	1	1	1	1	1	1	1	1	1	1	1	1	1	1	1	1	1	1
2	2	2	2	2	2	2	2	2	2	2	2	2	2	2	2	2	2	2
3	3	3	3	3	3	3	3	3	3	3	3	3	3	3	3	3	3	3
4	2	2	2	2	2	2	2	2	2	3	3	3	3	3	3	3	3	3
5	3	3	3	3	3	3	3	3	3	1	1	1	1	1	1	1	1	1
6	1	1	1	1	1	1	1	1	1	2	2	2	2	2	2	2	2	2
7	3	3	3	3	3	3	3	3	3	2	2	2	2	2	2	2	2	2
8	1	1	1	1	1	1	1	1	1	3	3	3	3	3	3	3	3	3
9	2	2	2	2	2	2	2	2	2	1	1	1	1	1	1	1	1	1
10	1	1	1	2	2	2	3	3	3	1	1	1	2	2	2	3	3	3
11	2	2	2	3	3	3	1	1	1	2	2	2	3	3	3	1	1	1
12	3	3	3	1	1	1	2	2	2	3	3	3	1	1	1	2	2	2
13	2	2	2	3	3	3	1	1	1	3	3	3	1	1	1	2	2	2
14	3	3	3	1	1	1	2	2	2	1	1	1	2	2	2	3	3	3
15	1	1	1	2	2	2	3	3	3	2	2	2	3	3	3	1	1	1
16	3	3	3	1	1	1	2	2	2	2	2	2	3	3	3	1	1	1
17	1	1	1	2	2	2	3	3	3	3	3	3	1	1	1	2	2	2
18	2	2	2	3	3	3	1	1	1	1	1	1	2	2	2	3	3	3
19	1	1	1	3	3	3	2	2	2	1	1	1	3	3	3	2	2	2
20	2	2	2	1	1	1	3	3	3	2	2	2	1	1	1	3	3	3
21	3	3	3	2	2	2	1	1	1	3	3	3	2	2	2	1	1	1
22	2	2	2	1	1	1	3	3	3	3	3	3	2	2	2	1	1	1
23	3	3	3	2	2	2	1	1	1	1	1	1	3	3	3	2	2	2
24	1	1	1	3	3	3	2	2	2	2	2	2	1	1	1	3	3	3
25	3	3	3	2	2	2	1	1	1	2	2	2	1	1	1	3	3	3
26	1	1	1	3	3	3	2	2	2	3	3	3	2	2	2	1	1	1
27	2	2	2	1	1	1	3	3	3	1	1	1	3	3	3	2	2	2
28	1	2	3	1	2	3	1	2	3	1	2	3	1	2	3	1	2	3
29	2	3	1	2	3	1	2	3	1	2	3	1	2	3	1	2	3	1
30	3	1	2	3	1	2	3	1	2	3	1	2	3	1	2	3	1	2
31	2	3	1	2	3	1	2	3	1	3	1	2	3	1	2	3	1	2
32	3	1	2	3	1	2	3	1	2	1	2	3	1	2	3	1	2	3
33	1	2	3	1	2	3	1	2	3	2	3	1	2	3	1	2	3	1
34	3	1	2	3	1	2	3	1	2	2	3	1	2	3	1	2	3	1
35	1	2	3	1	2	3	1	2	3	3	1	2	3	1	2	3	1	2
36	2	3	1	2	3	1	2	3	1	1	2	3	1	2	3	1	2	3
37	1	2	3	2	3	1	3	1	2	1	2	3	2	3	1	3	1	2
38	2	3	1	3	1	2	1	2	3	2	3	1	3	1	2	1	2	3
39	3	1	2	1	2	3	2	3	1	3	1	2	1	2	3	2	3	1
40	2	3	1	3	1	2	1	2	3	3	1	2	1	2	3	2	3	1
41	3	1	2	1	2	3	2	3	1	1	2	3	2	3	1	3	1	2
42	1	2	3	2	3	1	3	1	2	2	3	1	3	1	2	1	2	3
43	3	1	2	1	2	3	2	3	1	2	3	1	3	1	2	1	2	3
44	1	2	3	2	3	1	3	1	2	3	1	2	1	2	3	2	3	1
45	2	3	1	3	1	2	1	2	3	1	2	3	2	3	1	3	1	2
46	1	2	3	3	1	2	2	3	1	1	2	3	3	1	2	2	3	1
47	2	3	1	1	2	3	3	1	2	2	3	1	1	2	3	3	1	2
48	3	1	2	2	3	1	1	2	3	3	1	2	2	3	1	1	2	3
49	2	3	1	1	2	3	3	1	2	3	1	2	2	3	1	1	2	3
50	3	1	2	2	3	1	1	2	3	1	2	3	3	1	2	2	3	1
51	1	2	3	3	1	2	2	3	1	2	3	1	1	2	3	3	1	2
52	3	1	2	2	3	1	1	2	3	2	3	1	1	2	3	3	1	2
53	1	2	3	3	1	2	2	3	1	3	1	2	2	3	1	1	2	3
54	2	3	1	1	2	3	3	1	2	1	2	3	3	1	2	2	3	1
55	1	3	2	1	3	2	1	3	2	1	3	2	1	3	2	1	3	2
56	2	1	3	2	1	3	2	1	3	2	1	3	2	1	3	2	1	3
57	3	2	1	3	2	1	3	2	1	3	2	1	3	2	1	3	2	1
58	2	1	3	2	1	3	2	1	3	3	2	1	3	2	1	3	2	1
59	3	2	1	3	2	1	3	2	1	1	3	2	1	3	2	1	3	2
60	1	3	2	1	3	2	1	3	2	2	1	3	2	1	3	2	1	3
61	3	2	1	3	2	1	3	2	1	2	1	3	2	1	3	2	1	3
62	1	3	2	1	3	2	1	3	2	3	2	1	3	2	1	3	2	1
63	2	1	3	2	1	3	2	1	3	1	3	2	1	3	2	1	3	2

Table C.2. *(part 2 of 4).* Taguchi's L81 orthogonal array (after Taguchi, 1987 as cited by Phadke, 1989). Each row defines an experiment of 40 three-level factors.

	1	2	3	4	5	6	7	8	9	10	11	12	13	14	15	16	17	18	19	20	21	22
64	3	2	1	3	1	3	2	2	1	3	3	2	1	1	3	2	2	1	3	3	2	1
65	3	2	1	3	1	3	2	2	1	3	3	2	1	2	1	3	3	2	1	1	3	2
66	3	2	1	3	1	3	2	2	1	3	3	2	1	3	2	1	1	3	2	2	1	3
67	3	2	1	3	2	1	3	3	2	1	1	3	2	1	3	2	2	1	3	3	2	1
68	3	2	1	3	2	1	3	3	2	1	1	3	2	2	1	3	3	2	1	1	3	2
69	3	2	1	3	2	1	3	3	2	1	1	3	2	3	2	1	1	3	2	2	1	3
70	3	2	1	3	3	2	1	1	3	2	2	1	3	1	3	2	2	1	3	3	2	1
71	3	2	1	3	3	2	1	1	3	2	2	1	3	2	1	3	3	2	1	1	3	2
72	3	2	1	3	3	2	1	1	3	2	2	1	3	3	2	1	1	3	2	2	1	3
73	3	3	2	1	1	3	2	3	2	1	2	1	3	1	3	2	3	2	1	2	1	3
74	3	3	2	1	1	3	2	3	2	1	2	1	3	2	1	3	1	3	2	3	2	1
75	3	3	2	1	1	3	2	3	2	1	2	1	3	3	2	1	2	1	3	1	3	2
76	3	3	2	1	2	1	3	1	3	2	3	2	1	1	3	2	3	2	1	2	1	3
77	3	3	2	1	2	1	3	1	3	2	3	2	1	2	1	3	1	3	2	3	2	1
78	3	3	2	1	2	1	3	1	3	2	3	2	1	3	2	1	2	1	3	1	3	2
79	3	3	2	1	3	2	1	2	1	3	1	3	2	1	3	2	3	2	1	2	1	3
80	3	3	2	1	3	2	1	2	1	3	1	3	2	2	1	3	1	3	2	3	2	1
81	3	3	2	1	3	2	1	2	1	3	1	3	2	3	2	1	2	1	3	1	3	2

Table C.2. *(part 3 of 4).* Taguchi's L81 orthogonal array (after Taguchi, 1987 as cited by Phadke, 1989). Each row defines an experiment of 40 three-level factors.

	23	24	25	26	27	28	29	30	31	32	33	34	35	36	37	38	39	40
64	1	3	2	2	1	3	3	2	1	1	3	2	2	1	3	3	2	1
65	2	1	3	3	2	1	1	3	2	2	1	3	3	2	1	1	3	2
66	3	2	1	1	3	2	2	1	3	3	2	1	1	3	2	2	1	3
67	2	1	3	3	2	1	1	3	2	3	2	1	1	3	2	2	1	3
68	3	2	1	1	3	2	2	1	3	1	3	2	2	1	3	3	2	1
69	1	3	2	2	1	3	3	2	1	2	1	3	3	2	1	1	3	2
70	3	2	1	1	3	2	2	1	3	2	1	3	3	2	1	1	3	2
71	1	3	2	2	1	3	3	2	1	3	2	1	1	3	2	2	1	3
72	2	1	3	3	2	1	1	3	2	1	3	2	2	1	3	3	2	1
73	1	3	2	3	2	1	2	1	3	1	3	2	3	2	1	2	1	3
74	2	1	3	1	3	2	3	2	1	2	1	3	1	3	2	3	2	1
75	3	2	1	2	1	3	1	3	2	3	2	1	2	1	3	1	3	2
76	2	1	3	1	3	2	3	2	1	3	2	1	2	1	3	1	3	2
77	3	2	1	2	1	3	1	3	2	1	3	2	3	2	1	2	1	3
78	1	3	2	3	2	1	2	1	3	2	1	3	1	3	2	3	2	1
79	3	2	1	2	1	3	1	3	2	2	1	3	1	3	2	3	2	1
80	1	3	2	3	2	1	2	1	3	3	2	1	2	1	3	1	3	2
81	2	1	3	1	3	2	3	2	1	1	3	2	3	2	1	2	1	3

Table C.2. *(part 4 of 4).* Taguchi's L81 orthogonal array (after Taguchi, 1987 as cited by Phadke, 1989). Each row defines an experiment of 40 three-level factors.

APPENDIX D

Optimisation Algorithm Parameters

KEY: OPTIONS: Design Exploration System used (Dynamics Modelling Ltd, 1996)
Siddall: Optimisation software suite implemented in OPTIONS (Siddall, 1982)
BFGS: Broyden-Fletcher-Goldfarb-Shanno
DFP: Davidon-Fletcher-Powell

N.B. Where no OPTIONS variable shown, parameter is not variable by user.

OPTIONS variable	Siddall variable	Description	Value
OPT_TOL	TOL	Tolerance for penalty function	1e-10
OPT_STEP	F	fraction of each variable range used to calculate variable derivative	1e-5
function argument	G	convergence criterion: minimum fractional change between successive objective function result	1e-5 (Broad) 1e-3(Narrow) 1e-3(Single)

Table D.1. Optimisation parameters used for the Davidon-Fletcher-Powell method.

OPTIONS variable	Siddall variable	Description	Value
OPT_TOL	TOL	Tolerance for penalty function	1e-10
OPT_STEP	F	fraction of each variable range used as initial step size	0.1
function argument	G	convergence criterion: minimum step size specified as fraction of initial step size	0.01
	NSHOT	Number of search/shotgun cycles	2
	NTEST	Number of points in shotgun search at end of search phase	100

Table D.2. Optimisation parameters used for the Hooke and Jeeves method.

OPTIONS variable	Siddall variable	Description	Value
C_TOL	ZERO	Amount constraint functions may be infeasible	1e-8
_PENAL		Violated constraint multiplier r in (3.4)	1e20

Table D.3. One Pass penalty function parameters used for the FDP, BFGS and, Hooke and Jeeves methods.

OPTIONS variable	Siddall variable	Description	Value
C_TOL	ZERO	Amount constraint functions may be infeasible	1e-8
OPT_TOL	TOL	Tolerance for penalty function	1e-10
	R	Initial penalty function multiplier r in (3.A.5)	1
	REDUCE	Reduction factor for R	0.04

Table D.4. Fiacco-McCormick penalty function parameters used for the FDP, BFGS and, Hooke and Jeeves methods.

OPTIONS variable	Description	Value
DHC_INITZ	Initial step size specified as fraction of variable range	0.05
DHC_THRESH	Covergence critereon: minimum step size as fractional of variable range	1e-9
DHC_PENAL	Penalty function. (One Pass External)	1e20
DHC_NRANDM	Random number seed	(see text)
function argument	Maximum number of iterations, after which no new searches are started	2000

Table D.5. Optimisation parameters used for the Dynamic Hill Climbing method.

OPTIONS variable / Common notation	Description	Value
N_{gen}	maximum no. of generations allowed	(see main text)
GA_NPOP, N_{pop}	size of each population	(see main text)
GA_PBEST, P_{best}	proportion of population surviving to next generation	0.8
GA_PCROSS, P_{cross}	proportion of surviving population allowed to breed	0.8
GA_PINVRT, P_{invert}	proportion of breeding population that have genetic material re-ordered	0.5
GA_PMUTNT, $P_{mutation}$	proportion of generation's new material randomly changed	0.005
GA_PRPTNL	flag which sets whether either new generation's genetic material is biased in favour of better members of previous population (TRUE), or all P_{best} is scaled to prevent dominance (FALSE)	TRUE
GA_DMIN, D_{min}	minimum non-dimensional Euclidean distance between clusters (those closer are collapsed)	0.05
GA_DMAX, D_{max}	maximum non-dimensional Euclidean radius of a cluster (beyond which clusters sub-divide)	0.1
GA_NCLUST, N_{clust}	the initial number of clusters in which a generation is divided	25
GA_NBREED, N_{breed}	minimum number of members in a cluster before exclusive breeding within cluster takes place	5
GA_ALPHA, α	a penalising index used in the management of clusters (see Yin and Germay, 1993)	0.5
GA_NBIN	number of binary bits used to represent each optimisation variable	16
GA_RANDM	number of samples of random number generation discarded before first sample is used	(see main text)

Table D.6. Optimisation parameters used for the genetic algorithm optimisation.

APPENDIX E

Computational System Details

E.0 COMPUTING HARDWARE PLATFORM DETAILS

The specifications of the computing systems used to perform the results presented in the main text are given below. Only the specifications required to given an indication of the computing system power are given, the system is a shared resource and the performance is thus dependent upon the computing load of the machine. The computing times quoted in the main text are approximate, and relate to the system operating at less than 100% of full capacity (so that no computing job-sharing occurs).

E.1 DETAILS OF HARDWARE PLATFORM A

Hardware platform A was used for work presented in the earlier part of the thesis, and is detailed in Table E.1. This system contains two processor types and it can not be assured which specific processors were used within the system management scheme. It is feasible to assume that the computing effort was shared equally by all the processors, resulting in an average processor speed is 80MHz.

System	Silicon Graphics Inc. Power Challenge (6 processors)
Processor details	Processors 0 to 3: 90MHz IP21 CPU: MIPS R8000 Processor Chip Revision: 3.0 FPU: MIPS R8010 Floating Point Chip Revision: 0.2 Processors 4 and 5: 75MHz IP21 CPU: MIPS R8000 Processor Chip Revision: 2.2 FPU: MIPS R8010 Floating Point Chip Revision: 0.1
Memory	Main memory size: 512Mbytes

Table E.1. Brief summary of the specification of computing hardware platform A.

E.2 DETAILS OF HARDWARE PLATFORM B

Hardware platform B was used for the work presented in the latter part of the thesis, and is detailed in Table E.2.

System	Silicon Graphics Inc. Origin 2000 (14 processors)
Processor details	Processors 0 to 13: 250MHz IP27 CPU: MIPS R10010 Processor Chip Revision: 0.0 FPU: MIPS R10000 Floating Point Chip Revision: 3.4
Memory	Main memory size: 4068Mbytes

Table E.2. Brief summary of the specification of computing hardware platform B.

REFERENCES

ADELMAN H.M and HAFTKA R.T. 1986. *AIAA Journal.* **24**(5), 823-832. Sensitivity Analysis of Discrete Structural Systems.

ANTHONY D.K. and ELLIOTT S.J. 2000a. *Journal of Sound and Vibration.* Robustness of Optimal Design Solutions to Reduce Vibration Transmission in a Lightweight 2-D Structure. Part II: Application of Active Vibration Control Techniques. (Proposed publication date, January 2000)

ANTHONY D.K. and ELLIOTT S.J. 2000b. *Journal of Sound and Vibration.* Comparison of the Effectiveness of Cost Function Parameters for Minimisation by Active Control of Vibrational Energy Transmission in a Lightly Damped Structure. (Provisionally accepted for publication.)

ANTHONY D.K., ELLIOTT S.J. and KEANE A.J. 2000. *Journal of Sound and Vibration.* Robustness of Optimal Design Solutions to Reduce Vibration Transmission in a Lightweight 2-D Structure. Part I: Geometric Redesign. (Proposed publication date, January 2000)

BÄCK T. 1996 *Evolutionary Algorithms in Theory and Practice.* Oxford: Oxford University Press.

BÄCK T., HAMMEL U. and SCHWEFEL H. 1997a. Evolutionary Computation: Comments on the History and Current State. *IEEE Transaction on Evolutionary Computation.* **1**(1), 3-17.

BÄCK T., FOGEL D.B and MICHALEWICZ Z (editors) 1997b. *Handbook of Evolutionary Computation.* Bristol: IOP Publishing Ltd and Oxford: Oxford University Press.

BAEK H.K. and ELLIOTT S.J. 1995. *Journal of Sound and Vibration* **186**(2), 245-267. Natural Algorithms for choosing Source Locations in Active Control Systems.

BARDOU O., GARDONIO P., ELLIOTT S.J. and PINNINGTON R.J. 1997 *Journal of Sound and Vibration* **208**(1), 111-151. Active Power Minimisation and Power Absorption in a Plate with Force and Moment Excitation.

BENZARIA E. and MARTIN V. 1994. *Journal of Sound and Vibration* **173**(1), 137-144. Secondary Source Locations in Active Noise Control: Selection or Optimization?

BISHOP R.E.D. and JOHNSON D.B. 1960. *The Mechanics of Vibration.* Cambridge: Cambridge University Press.

BONDARYK J.E. 1997. *Journal of the Acoustical Society of America* **102**(4), 2167-2175. Vibration of truss structures.

BRENNAN M.J., ELLIOTT S.J. and PINNINGTON R.J. 1995. *Journal of Sound and Vibration* **186**(4), 657-688. Strategies for the Active Control of Flexural Vibration on a Beam.

CHEN G., BRUNO R. and SALAMA M. 1991. *AIAA Journal.* **29**(8), 1327-1334. Optimal Placement of Active/Passive Members in Truss Structures Using Simulated Annealing.

DATTA B.N. 1995. *Numerical Linear Algebra and Applications.* California: Brooks/Cole Publishing Co.

DE FONSECA P., SAS P. and VAN BRUSSEL H. 1999. *Journal of Sound & Vibration* **221**(4), 651-679. A Comparative Study of Methods for Optimising Sensor and Actuator Locations in Active Control Applications.

DYNAMICS MODELLING LTD., 1996. *THE OPTIONS DESIGN EXPLORATION SYSTEM: Reference Manual and User Guide - Version B1.1.* (for more information see: http://www.soton.ac.uk/~ajk/options.ps).

EL-BELTAGY M.A. and KEANE A.J. 1998. *Optimization for multilevel problems: A Comparison of Various Algorithms.* 111-120. Proceedings of the Third International conference on Adaptive Computing in Design and Manufacture (ADCM '98). ed. Parmee I., Springer, London.

ELLIOTT S.J. and BILLET L. 1993. *Journal of Sound and Vibration* **163**(2), 295-310. Adaptive Control of Flexural Waves Propagating in a Beam.

ERIKSTAD S.O. *et al.* 1995. *Journal of Guidance, Control and Dynamics.* **18**(5), 1163-1168. Integrating Robustness into Multiobjective Space Vehicle Design Process.

FARAG N.H. and PAN J. 1997. *Journal of the Acoustical Society of America* **102**(1), 315-325. Dynamic response and power flow in three-dimensional coupled beam structures. Part I: Analytical modeling.

FARMER *et al.* 1992. *Journal of Spacecraft and Rockets.* **29**(3), 386-393. Thermal Distortion of an Antenna-Support Truss in Geosynchronous Orbit.

FIACCO A.V. and McCORMICK G.P, 1968. *Nonlinear programming: sequential unconstrained minimization techniques.* Wiley

FISHER Sir R.A. 1925. *Statistical methods for Research Workers.* Hafner Press/Macmillan Publishing Co. Inc., New York.

FORGRAVE J.C., MAN K.F. and NEWELL J.M. 1999. *Sound and Vibration.* March, 28-31. Spacecraft Acoustic and Random Vibration Test Optimization.

FULLER C.R., ELLIOTT S.J. and NELSON P.A. 1996. *Active Control of Vibration.* Academic Press.

FURUYA H. 1995. *AIAA/ASME/ASCE/AHS Structures, Structural Dynamics & Materials Conference Collection of Technical Papers.* **5**, 3500-3505. Simultaneous Design for Configurations and Actuator Locations of Space Truss Structures.

FURUYA H. and HAFTKA R.T. 1993. *Structures and Controls Optimization, ASME 1993.* **38**, 1-11. Locating Actuators for Vibration Suppression on Space Trusses by Genetic Algorithms.

FURUYA H. and HAFTKA R.T. 1995. *Journal of Spacecraft and Rockets.* **32**(5), 856-865. Static Shape Control of Space Trusses with Partial Measurements.

FURUYA H. and HAFTKA R.T. 1996. *Journal of Spacecraft and Rockets.* **33**(3), 422-427. Combining Genetic and Deterministic Algorithms for Locating Actuators on Space Structures.

GOLDBERG D.E. 1989. *Genetic Algorithms in Search, Optimisation and Machine Learning.* Cambridge MA: Addison-Wesley.

HAFTKA R.T. and ADELMAN H.M. 1985. *AIAA Journal.* **23**(3), 450-457. An Analytical Investigation of Shape Control of Large Space Structures by Applied Temperatures.

HAHN S.R. and FERRI A.A. 1997. *Journal of the Acoustical Society of America* **101**(2), 918-924. Sensitivity analysis of coupled structural-acoustic problems using perturbation techniques.

HANSEN C.H. and SNYDER S.D. 1997. *Active Control of Noise and Vibration.* E & FN Spon, London UK.

HAYKIN S. 1996. *Adaptive Filter Theory.* New Jersey: Prentice-Hall Inc.

HOEL P.G. 1984. *Introduction to Mathematical Statistics.* John Wiley and Sons, U.S.A.

HOLLAND J.H. 1975 *Adaptation in Natural and Artificial Systems : An Introductory Analysis with Applications to Biology, Control and Artificial Intelligence.* Ann Arbour MI: The University of Michigan Press.

HOOKE R. and JEEVES T.A. 1961. *Journal of Ass. Comp. Mach.* **8**, 212-221. Direct search solution of numerical and statistical problems.

HOSSAIN M.A. *et al.* 1995. *Genetic Algorithms in Engineering Systems: Innovations and Applications. IEE Conference Publication.* 175-180. Adaptive Active Vibration Control using Genetic Algorithms.

HOWARD C.Q. and HANSEN C.H. 1997. *Acoustics Australia* **25**(2), 65-67. Active Isolation of a Vibrating Mass

IBARAKI T. 1997. *Handbook of Evolutionary Computation.* IOP Publishing Ltd & Oxford University Press. Section D3.2: Combination with local search.

KEANE A.J. 1993. *Artificial Neural Networks and Genetic Algorithms (ANNGA), Innsbruck.* Structural Design for Enhanced Noise Performance using Genetic Algorithm and other Optimization Techniques. Albrecht, Reeves & Steele (eds.). Springer-Verlag. 536-543.

KEANE A.J. 1994. *Adaptive Computing in Engineering Design and Control, Plymouth UK.* Experiences with Optimizers in Structural Design.

KEANE A.J. 1995a. *Artificial Intelligence in Engineering* **9**(2), 75 - 83. Genetic Algorithm Optimisation of Multi-Peak Problems - Studies in convergence and Robustness.

KEANE A.J. 1995b. *Journal of Sound & Vibration* **185**(3), 441-453. Passive Vibration Control via Unusual Geometries - The Application of Genetic Algorithm Optimisation to Structural Design.

KEANE A.J. 1998. *Personal communication.*

KEANE A.J. 1999. *Personal Communication.*

KEANE A.J. and BRIGHT A.P. 1995. *Journal of Sound & Vibration* **190**(4), 713-719. Passive Vibration Control via Unusual Geometries: Experiments on Model Aerospace Structures.

KEANE A.J. and BROWN S.M. 1996. *Proceedings of ACEDC, Plymouth UK.* 107-113. The Design of a satellite Boom with Enhanced vibration performance using Genetic Algorithm Techniques.

KEANE A.J. and MANOHAR C.S. 1993. *Journal of Sound & Vibration* **168**(2), 253-284. Energy Flow Variability in a Pair of Coupled Stochastic Rods.

KEANE A.J. *et al.* 1998. Grant No. GR/MMS 33624. EPSRC/Matra Marconi Space: Integration of Advanced Active and Passive Noise Control methods. (June 1998). The University of Southampton, UK.

KEMPTHORNE O. 1952. *Design and Analysis of Experiments.* John Wiley & Sons, Inc. United States of America.

KIM Y., KUM D. and NAM C. 1997. *Journal of Guidance, Control and Dynamics.* **20**(6), 1111-1117. Simultaneous Structural/Control Optimum Design of Composite Plate with Piezoelectric Actuators.

KIRKPATRICK S., GELATT C.D. and VECCHI M.P. 1983. *Science.* **220**, 671-680. Optimization by Simulated Annealing.

LANGLEY R.S. 1990. *Journal of Sound & Vibration* **136**(3), 439-452. Analysis of Power Flow in Beams and Frameworks using the Direct-Dynamic Stiffness Method.

LAUTENSCHLAGER U. *et al.* 1995. *Journal of Guidance, Control and Dynamics.* **18**(5), 1126-1132. Experimental Satellite Trajectory Analysis using Decision-Based Robust Design.

LIU X., BEGG D.W. and FISHWICK R.J. 1998. *International Journal for Numerical Methods in Engineering.* **40**, 815-830. Genetic Approach to Optimal Topology/Controller Design of Adaptive Structures.

LIU X., BEGG D.W. and MATRAVERS D.R. 1997. *Journal of Aerospace Engineering.* July, 119-125. Optimal Topology/Actuator Placement Design of Structures using SA.

LYON R.H. 1975. *Statistical Energy Analysis of Dynamical Systems: Theory and Applications.* MA: MIT Press.

MANOHAR C.S. and ADHIKAR S. 1998. *Journal of Sound & Vibration* **217**(1), 43-74. Statistics of Vibration Energy Flow in Randomly Parametered Trusses.

MATHWORKS, INC., 1997. *MATLAB 5. (Ver 5.1).* The MathWorks, Inc., Natick MA. 01760-1500

MITCHELL M. 1996. *An Introduction to Genetic Algorithms.* United States of America. CIP.

MONTGOMERY D.C. 1983. *Design and Analysis of Experiments.* 3rd ed. United States of America. John Wiley & Sons, Inc.

MONTGOMERY D.C. 1996. *Design and Analysis of Experiments.* 4th ed. United States of America. John Wiley & Sons, Inc.

NAIR P.B., KEANE A.J. and LANGLEY R.S. 1998. *AIAA Journal.* **36**(9), 1721-1727. Improved First-Order Approximation of Eigenvalues and Eigenvectors.

NELSON P.A. and ELLIOTT S.J. 1992. *Active Control of Sound.* London: Academic Press.

OMOTO A. and ELLIOTT S.J. 1996. *Proceedings ICASSP-96, Atlanta, GA.* The Effect of Structured Uncertainty in Multichannel Feedforward Control Systems.

ONODO J. and HAFTKA R.T. 1987. *AIAA Journal.* **25**(8), 1133-1138. An Approach to Structure/Control Simultaneous Optimization for Large Flexible Spacecraft.

PADULA S.L. and KINCAID R.K. 1999. *NASA/TM-1999-209126.* Optimization Strategies for Sensor and Actuator Placement.

PAN X. and HANSEN C.H. 1993. *Journal of Sound and Vibration* **165**(3), 497-510. The Effect of Error Sensor Location and Type on Active Control of Beam Vibration.

PHADKE M.S. 1989. *Quality Engineering Using Robust Design.* London. Prentice-Hall International.

PHADKE M.S. 1998. *Personal Communication.*

PRESS W.H., TEUKOLSKY S.A. and VETTERLING W.T. 1992. *Numerical Recipes in Fortran 77: The Art of Scientific Computing.* Cambridge University Press.

PREUMONT A. 1997. *Vibration Control of Active Structures.* Kluwer Academic Publishers.

RAO S., TZONG-SHII P. and VENKAYYA V. 1990. *AIAA Journal.* **28**(2), 353-361. Robustness Improvement of Actively Controlled structures through Structural Modifications.

RAO, C.R. 1947. *Journal of Royal Statistical Society, Series B.* **9**, 128-139. Factorial Experiments Derivable from Combinatorial Arrangements of Arrays.

RAYLEIGH Lord. 1894. *The Theory of Sound.* Macmillan. London

REDMAN-WHITE W., NELSON P.A. and CURTIS A.R.D. 1987 *Journal of Sound and Vibration* **112**(1), 187-191. Experiments on the Active Control of Flexural Wave Power Flow.

SHANKAR K. and KEANE A.J. 1995. *Journal of Sound & Vibration* **185**(5), 867-890. Energy Flow Predictions in a Structure of Rigidly Joined Beams using Receptance Theory.

SHANKAR K. and KEANE A.J. 1997. *Journal of Sound & Vibration* **201**(4), 491-513. Vibrational Energy Flow Analysis using a Substructure Approach: The Application of Receptance Theory to FEA and SEA.

SIDDALL J.N, 1982. *Optimal Engineering Design; Principles and Applications.* Marcel Dekker, Inc., New York.

SIMPSON M. T. and HANSEN C.H. 1996. *Noise Control Engineering Journal.* **44**(4), 169-184. Use of genetic algorithms to optimize vibration actuator placement for active control of harmonic interior noise in a cylinder with floor structure.

STRUCTURAL DYNAMICS RESEARCH CORPORATION. 1997. *IDEAS Master Series 5.* Structural Dynamics Research Corporation, Ohio 45150.

TAGUCHI G. 1987. *System of Experimental Design.* (Vol. 1 & 2). English translation. UNIPUB/Kraus International Publications. New York. (Translated from Japanese).

TANG K.S., MAN K.F., KWONG S. and CHAN C.Y. 1996. *Real-Time Systems.* **11**, 289-302. Application of the genetic Algorithm to Real-Time Active Noise Control.

TIMOSHENKO S.P. 1955. *Vibration Problems in Engineering.* 3rd ed. Van Nostrand.

TSE F.S., MORSE I.E. and HINKLE R.T. 1978. *Mechanical Vibrations. Theory and Applications.* Boston MA: Allyn and Bacon, Inc.

TSUTSUI S. and GHOSH A. 1997. Genetic Algorithms with a Robust Solution Searching Scheme. *IEEE Transactions on Evolutionary Computation.* **1**(3), September 1997. 201-208.

VIPPERMANN J.S., BURDISSO R.A. and FULLER C.R. 1993. *Journal of Sound & Vibration* **166**(2), 283-299. Active Control of Broadband Structural Vibration using the LMS Adaptive Algorithm.

VON FLOTOW A.H. 1988. *Large Space Structures: Dynamics and Control* (S.N Atluri and A.K Amos, eds.). Springer-Verlag, Heidelberg. 213-238. The acoustic limit of control in structural dynamics.

WIESMANN D., HAMMEL U. and BÄCK T. 1998. *IEEE Transactions on Evolutionary Computation.* **2**(4) 162-167. Robust Design of Multilayer Optical Coatings by Means of Evolutionary Algorithms.

YIN X. and GERMAY N. 1993. *Proceedings of the International Conference on Artificial Neural Nets and Genetic Algorithms* (editors E.R.F Albrecht, C.R. Reeves and N.C. Steele), Innsbruck, Springer-Verlag, 450-457. A Fast Genetic Algorithm with Sharing Scheme using Cluster Methods in Multimodal Function Optimization.

YURET D. 1994. *From Genetic Algorithms to Efficient Optimization.* M.Sc, Thesis, Massachusetts Institute of Technology.

YURET D. and DE LA MAZA M. 1993. *Proceedings of the 2nd Turkish Symposium on AI and ANN.* 254-260. Dynamic Hill Climbing: Overcoming the limitations of Optimization Techniques.

ZHU Y. *et al.* 1999. *Journal of Vibration and Acoustics.* **121**, 237-243. Simultaneous Optimization of Structure and Control for Vibration Suppression.

ZIENKIEWICZ O.C. 1965. *The Finite Element Method.* 3rd ed. McGraw-Hill.

ZIMMERMAN D.C. 1993. *Journal of Sound and Vibration* **7**(4), 363-374. A Darwinian Approach to the Actuator Number and Placement Problem with Non-negligible Actuator Mass.